N O T I C E

THIS DOCUMENT HAS BEEN REPRODUCED FROM MICROFICHE. ALTHOUGH IT IS RECOGNIZED THAT CERTAIN PORTIONS ARE ILLEGIBLE, IT IS BEING RELEASED IN THE INTEREST OF MAKING AVAILABLE AS MUCH INFORMATION AS POSSIBLE

NASA

AIRESEARCH QCGAT PROGRAM
FINAL REPORT

by R. Heldenbrand, and W. M. Norgren

AIRESEARCH MANUFACTURING COMPANY OF ARIZONA
A DIVISION OF THE GARRETT CORPORATION
P. O. BOX 5217
PHOENIX, ARIZONA 85010

Prepared for

NATIONAL AERONAUTICS AND SPACE ADMINISTRATION

NASA Lewis Research Center
Cleveland, Ohio 44135

Contract NAS3-20585

FOREWORD

Design and analysis of the AiResearch QCGAT engine and engine/nacelle system were conducted at the AiResearch Engineering facilities at Phoenix, Arizona. Fabrication, testing, data reduction and analysis were also conducted at the AiResearch facilities.

Testing was also performed on the 35-percent scale model exhaust nozzles for the QCGAT program at the FluiDyne Engineering Corporation's facilities at the FluiDyne Medicine Lake Aerodynamic Laboratory, Minneapolis, Minnesota.

The authors wish to acknowledge the technical contribution of the following members of the Garrett-AiResearch organizations without whose efforts the QCGAT program would not have been completed successfully:

W. M. Gipson and L. S. Kisner, Acoustics; F. Davis, Emissions; Mark Steele and Pat Hale, Engine Performance; Walt Blackmore, M. H. Willmore and G. Paden, Nacelle Design and Fabrication; S. Huo, Turbine Aerodynamics.

This is, of necessity, only a partial list; space does not permit including a complete list.

PRECEDING PAGE BLANK NOT FILMED

v/vi

TABLE OF CONTENTS

TABLE OF CONTENTS (Contd)

TABLE OF CONTENTS (Contd)

TABLE OF CONTENTS (Contd)

LIST OF FIGURES

LIST OF FIGURES (Contd)

xiii

LIST OF FIGURES (Contd)

LIST OF FIGURES (Contd)

LIS. OF FIGURES (Contd)

LIST OF TABLES

LIST OF TABLES (Contd)

LIST OF TABLES (Contd)

SECTION I

SUMMARY

1.0 SUMMARY

1.1 Objectives

The objectives of the NASA QCGAT (Quiet Clean General Aviation Turbofan) engine and the engine/nacelle system program were to demonstrate the applicability of large turbofan engine technology to small general aviation turbofan engines, and to obtain significant reductions in noise and pollutant emissions while reducing or maintaining fuel consumption levels.

1.2 Scope

An AiResearch Model TFE731-3 Engine was used as a base-line engine for the QCGAT program. All new-technology designs for rotating parts and all items in the engine and nacelle that contributed to improvement of the acoustic and pollution characteristics of the engine system were of flight design, weight, and construction. These changes were limited to those that made the engine quiet or clean or reduced fuel consumption.

1.3 Goals and Results

The QCGAT program goals and the test results are listed in Table 1-1. As shown, the major noise, emissions and performance goals were met. Noise levels, estimated for the three FAR Part 36 conditions, are 10 to 15 EPNdB below FAA requirements; emissions values are considerably reduced below those of current technology engines; and the engine performance represents a TSFC improvement of approximately 9 percent over other turbofan engines.

ν

TABLE 1-1. QCGAT PROGRAM GOALS AND RESULTS.

Condition	Goal				Results			
	Thrust		TSFC		Thrust		TSFC	
	N	(lb)	Kg/hr/N	(lb hr/lb)	N	(lb)	kg/hr/N	(lb hr/lb)
Takeoff, Sea-Level Static Standard Day								
(1) Uninstalled	17,513	(3937)	0.0431	(0.418)	17,513	(3937)	0.0439	(0.431)
(2) With ground test nacelle and acoustic treatment and mixer nozzle**	17,313	(3892)	0.0431	(0.423)	17,313	(3892)	0.0437	(0.429)
Design Cruise* 12,192m (40,000 ft) Altitude, 0.8m								
(1) Uninstalled**	3,955	(889)	0.0775	(0.765)	3,955	(889)	0.0797	(0.782)
(2) With ground test nacelle and acoustic treatment and mixer nozzle***	4,017	(903)	0.07589	(0.744)	4,017	(903)	0.0755	(0.741)

Condition	Goal	Results
Engine Dry Weight	377.4 kg (832 lb)	379.6 (837 lb) (Estimated for Production)
Noise		
(1) Sideline Noise at 457.2m (1500 ft)	82.3 EPNdB	80.3 EPNdB
(2) Takeoff (without cutback)	73.3 EPNdB	73.1 EPNd
(3) Approach	87.3 EPNdB	82.7 EPNdB
Emissions		
(1) Carbon monoxide (CO)	4.26 kg/4,448 N thrust-hr/cycle[+] (9.4 lb/1000 lb thrust-hr/cycle)	3.63 (8.0)
(2) Unburned hydrocarbons (UHC)	0.726 kg/4,448 N thrust-hr/cycle[+] (1.6 lb/1000 lb thrust-hr/cycle)	.726 (1.6)
(3) Nitrogen (NO_x)	1.68 kg/4.448 N thrust-hr/cycle[+] (3.7 lb/1000-lb thrust/hr/cycle)	2.09 (4.6)
(4) Smoke (SAE Smoke Number)	38	42

NOTE: The minimum design life goal for QCGAT development components is 10,000 hours of typical general aviation operation.

 *Extrapolated from static data
 **Reference bellmouth, hardwall bypass duct, reference coannular nozzle
***With nacelle lip
[+]Cycle consists of 33 1/2 minutes of idle, takeoff, climbout and approach power.

SECTION II

INTRODUCTION

2.0 INTRODUCTION

2.1 Background

The turbojet- and turbofan-powered portion of the general aviation fleet is increasing at a greater rate than the rest of the general aviation fleet. Jet-powered general aviation aircraft utilize small airports for a large portion of their flights. These airports are generally located in suburban areas unprotected by industrial or commercial buffer zones. Therefore, the use of small aircraft has the potential to create a more widespread adverse community reaction to the jet noise and pollution than do the transport aircraft.

Engine-quieting and emission-reduction technology and recent developments for improving fuel economy, have been directed principally at large engines used in commercial carriers. It is, therefore, important to determine the applicability of the large engine technology to smaller turbine engines and to develop new and more suitable technology where required.

The QCGAT program seeks to demonstrate that theories, techniques and concepts presently applicable to large turbofan engines can be successfully applied to turbofan engines with sea-level thrust levels below 22.241 kN (5000 pounds). The goals are to improve the environmental characteristics of civil aircraft by alleviating noise as well as pollution near airports, thereby assisting in reducing current growth restraints to civil aviation, and also providing engines with reduced fuel consumption.

2.2 Scope

In order to meet the goals of the QCGAT program, the following tasks were performed:

(1) The engine was defined and its characteristics determined for a quiet, clean, turbofan engine applicable to general aviation aircraft.

(2) New and modified parts were designed and fabricated to be used with an existing gas generator core in the turbofan engine.

(3) Evaluation tests were performed on critical components.

3

(4) Evaluation tests were performed on the QCGAT engine.

(5) An acoustically treated nacelle was designed and fabri-
cated.

(6) Engine noise, pollution, and sea-level static overall
engine performance was measured to establish validity of
predictions prior to engine delivery to NASA.

(7) A quiet, clean turbofan engine, an acoustically treated
nacelle, and engine test support hardware were delivered
to the Government.

2.2.1 Performance Goals

In performing the tasks identified above, the performance,
noise, and emissions goals for the engine and for the engine/
nacelle system were established and are listed in Table 2-1.

2.2.2 Noise Goals

Noise goals for FAR Part 36 sideline, takeoff, and approach
locations and operating procedures are as follows for the twin-
engine aircraft also to be defined during the QCGAT program:

Sideline (457.2m) [1500 ft]:   EPNL = 39.5 + 10 log W

Takeoff (without cutback):   EPNL = 30.5 + 10 log W

Approach: EPNL = 44.5 + 10 log W

where W is the aircraft maximum takeoff gross weight in pounds.

TABLE 2-1.   ENGINE PERFORMANCE GOALS.

| | GOAL | | | |
| | THRUST | | TSFC | |
CONDITION	N	(lb)	kg/hr/N	(lb/hr/lb)
Takeoff, Sea-Level Static, Standard Day				
(1) Uninstalled*	17,513	(3937)	0.0426	(0.416)
(2) With Ground Test Nacelle and Acoustic Treatment and Mixer Nozzle**	17,313	(3892)	0.0431	(0.423)
Design Cruise, 12,192 m (40,000 Ft.) Altitude, 0.8 Mn				
(1) Uninstalled*	3,955	(889)	0.0775	(0.760)
(2) With Ground Test Nacelle and Acoustic Treatment and Mixer Nozzle**	4,017	(903)	0.0759	(0.744)
Engine Dry Weight Goal	377.4	kg	(832 lb)	

NOTE: The minimum design life goal for QCGAT developed components 10,000 hours of typical general aviation operation.

 *Reference bellmouth, hardwall bypass duct, reference
  coannular nozzle.
**With nacelle lip.

2.2.3   Emissions Goals

The emissions goals for carbon monoxide (CO), unburned hydro-carbons (UHC), Oxides of Nitrogen (NO_x), and smoke were as follows:

```
CO  - 4.26 kg per 4,448 N Thrust-hr per cycle*
      (9.4 lb per 1000 lb thrust-hr per cycle*)

UHC - 0.726 kg per 4,448 N Thrust-hr per cycle*
      (1.6 lb per 1000 lb thrust-hr per cycle*)

NO_X - 1.68 kg per 4,448 N Thrust-hr per cycle*
       (3.7 lb per 1000 lb thrust-hr per cycle*)
```

Smoke Number: Allowable SAE Smoke Number value (determined by the procedures set forth by the United States Environmental Protection Agency in the Federal Register Volume 38, No. 136, July 17, 1973, incorporated herein by reference and made a part hereof) was 38.

2.2.4 Hardware Design

Rotating parts, all new technology designs demonstrated, and all items in the engine and nacelle contributing to the acoustic and pollution characteristics of the engine system are of flight design, weight and construction. Stationary structural portions of the engine and nacelle are flight weight except where nonflight type construction resulted in appreciable cost savings with little or no compromise of the technology objectives. All weight estimates, however, are based on flight designs. All hardware is suitable for the testing required by the program and subsequent ground testing by the Government.

Engine core modifications were limited to those changes that made the engine quiet or clean or reduced fuel consumption. No modifications were made to the engine core assemblies or components unless they were shown to contribute directly and substantially to the reduction of noise, pollutant emissions or fuel consumption.

---

*Cycle consists of:

Mode	% Power	Time (minutes)
Taxi-Idle	Ground Idle	19.0
Takeoff	100	0.5
Climbout	90	2.5
Approach	30	4.5
Taxi-Idle	Ground Idle	7.0

6

2.3 Purpose

This report covers the design effort, fabrication and test results of the NASA QCGAT program and compares the analytical techniques and predicted performance to the actual test results.

The test results are then used to predict the altitude performance and the flyover acoustic signature of the engine and the projected aircraft with the QCGAT engine/nacelle system.

The analytical techniques that were successfully employed in the program include the use of a 3D-viscous computer program to define LP turbine vanes, stators and duct contours. The contours that provide the lowest losses and the most uniform radial loss distribution were chosen and proved to be an excellent and efficient design tool for this component.

The 3D-viscous method was also used for the mixer-compound nozzle with significant time and cost savings. The design and optimization was demonstrated on a model test rig and the full-scale design was shown to closely demonstrate the predicted performance and noise reduction due to the mixer-compound nozzle.

Acoustic design and prediction methods were also developed that modified a number of established methods to provide an optimum design for the performance/noise attenuation trade-offs.

SECTION III

ENGINE AND NACELLE DESIGN

3.0 QCGAT ENGINE AND NACELLE DESIGN APPROACH

3.1 Engine Cycle

The QCGAT Engine, as shown in cross section in Figure 3-1, utilizes the core of the AiResearch production Model TFE731-3 Turbofan Engine. A front view is shown in Figure 3-2. The QCGAT flight engine weight is estimated to be 379.6 kilograms (837 pounds). The QCGAT engine is a geared front-fan, twin-spool configuration with a bypass ratio of 3.714 at its design point of 12,192 meters (40,000 feet), and Mach 0.8. The low-pressure (LP) spool consists of a single-stage fan and a four-stage axial LP compressor driven by a three-stage axial LP turbine. The high-pressure (HP) spool consists of a single-stage centrifugal compressor driven by a single-stage axial turbine. The combustor is a reverse-flow, annular design.

The primary changes to the Model TFE731, to improve its performance for QCGAT, consist of replacement of the TFE731 fan with a modified ATF3 fan, incorporation of a new reduction gear, new LP turbine design, and incorporation of a mixer-compound exhaust system in place of the two-nozzle system of the TFE731. A low-smoke combustor is also employed in conjunction with an air-assisted fuel nozzle system for improved exhaust emissions. The unique parts are shown as shaded areas in Figure 3-3.

The noise reduction technology utilized in the QCGAT Engine design was applied to three major noise sources--fan, jet, and core engine. Fan-noise research at AiResearch has produced several major noise reduction techniques for small turbofan engines. Noise reduction features incorporated in the QCGAT Engine design include: elimination of inlet guide vanes, single-stage fan with low fan-tip speed and low-pressure ratio, large rotor-stator spacing, optimum number of vanes and blades, mixer-compound nozzle and acoustical treatment.

3.2 Cycle Selection Criteria

In the aerodynamic cycle selected for the QCGAT Engine, the jet velocity was made as low as possible consistent with the engine design goals. This resulted in exhaust velocities substantially below those used in present medium-bypass-ratio small turbofan engines. In addition to lowering jet velocity, a mixer-compound nozzle was installed because of its potential for thrust coefficient improvement and an anticipated reduction in takeoff and sideline flyover noise levels.

143.15
(56.36)

48.21
(18.98)

94.94
(37.38)

71.65
(28.21)

42.55
(16.75)

91.34
(35.96)

36 BLADES

73 STRUTS

77.47
(30.5)

**10 STRUTS
(5 MAIN)**

8 STRUTS

54.00 (21.26) TO C_L OF ENGINE

**ALL DIMENSIONS
SHOWN IN CM (IN)**

75.84
(29.86)
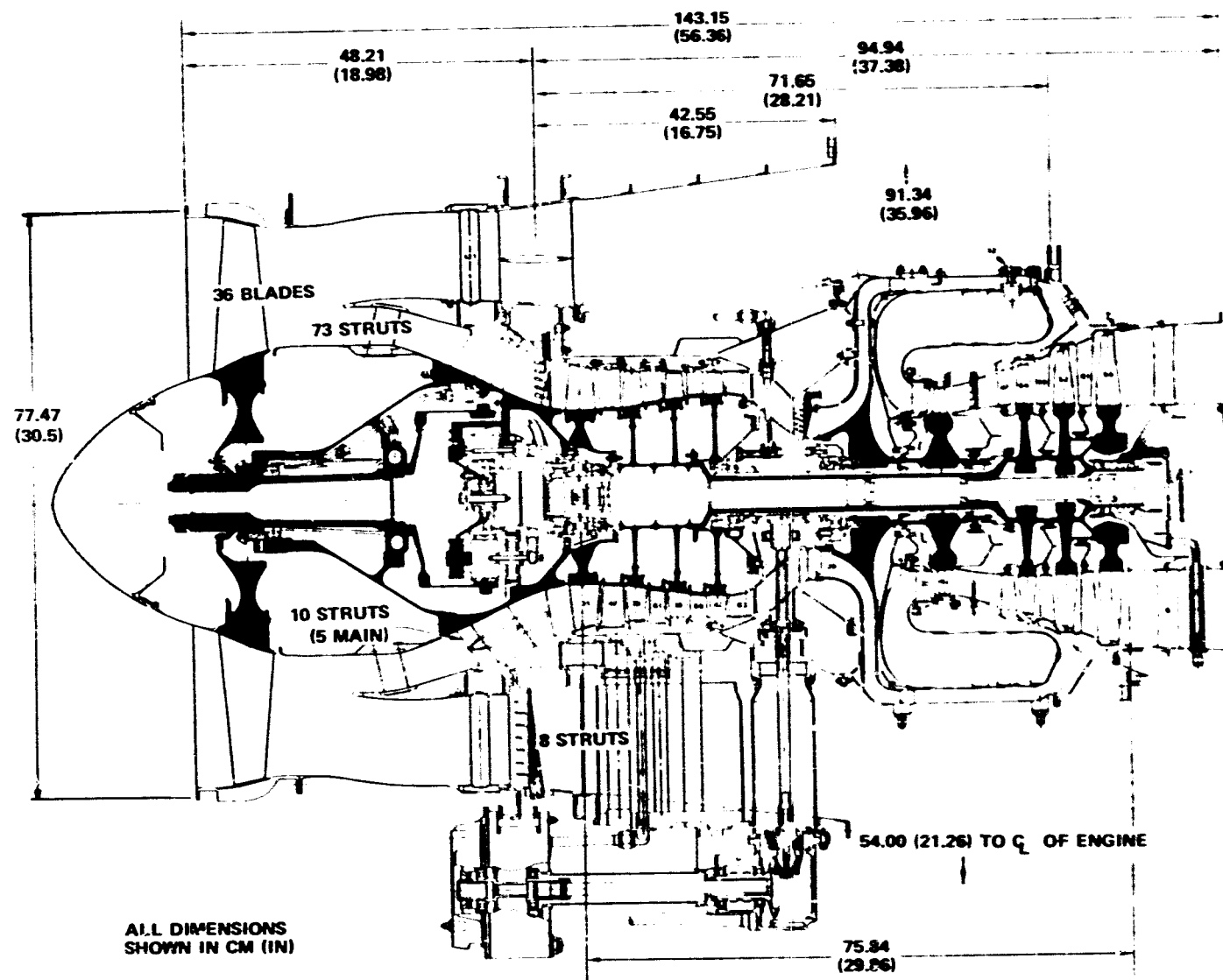
Figure 3-1.   AiResearch QCGAT Engine Cross Section.

7.94
(3.125)

15.65
(6.16)
REF

61.11 R MAX
(24.06 R)
REF

63.65
(25.06)

ACC PAD

ACC PAD
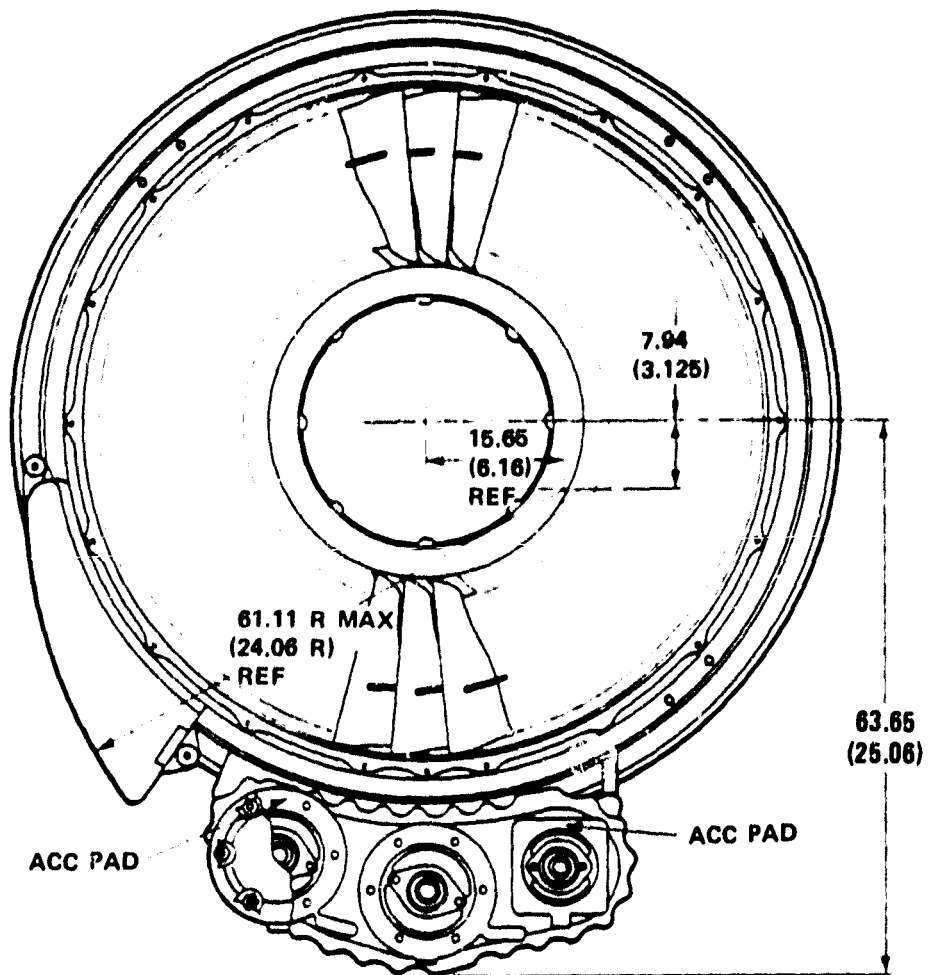
Figure 3-2.   AiResearch QCGAT Engine Front View.

11

143.15
(56.36)

48.21
(18.98)

94.94
(37.38)

71.65
(28.21)

42.55
(16.75)

91.34 DIA.
(35.96)

ALL DIMENSIONS
SHOWN IN CM (IN)

54.00 (21.26) TO ℄ OF ENGINE

75.84
(29.86)
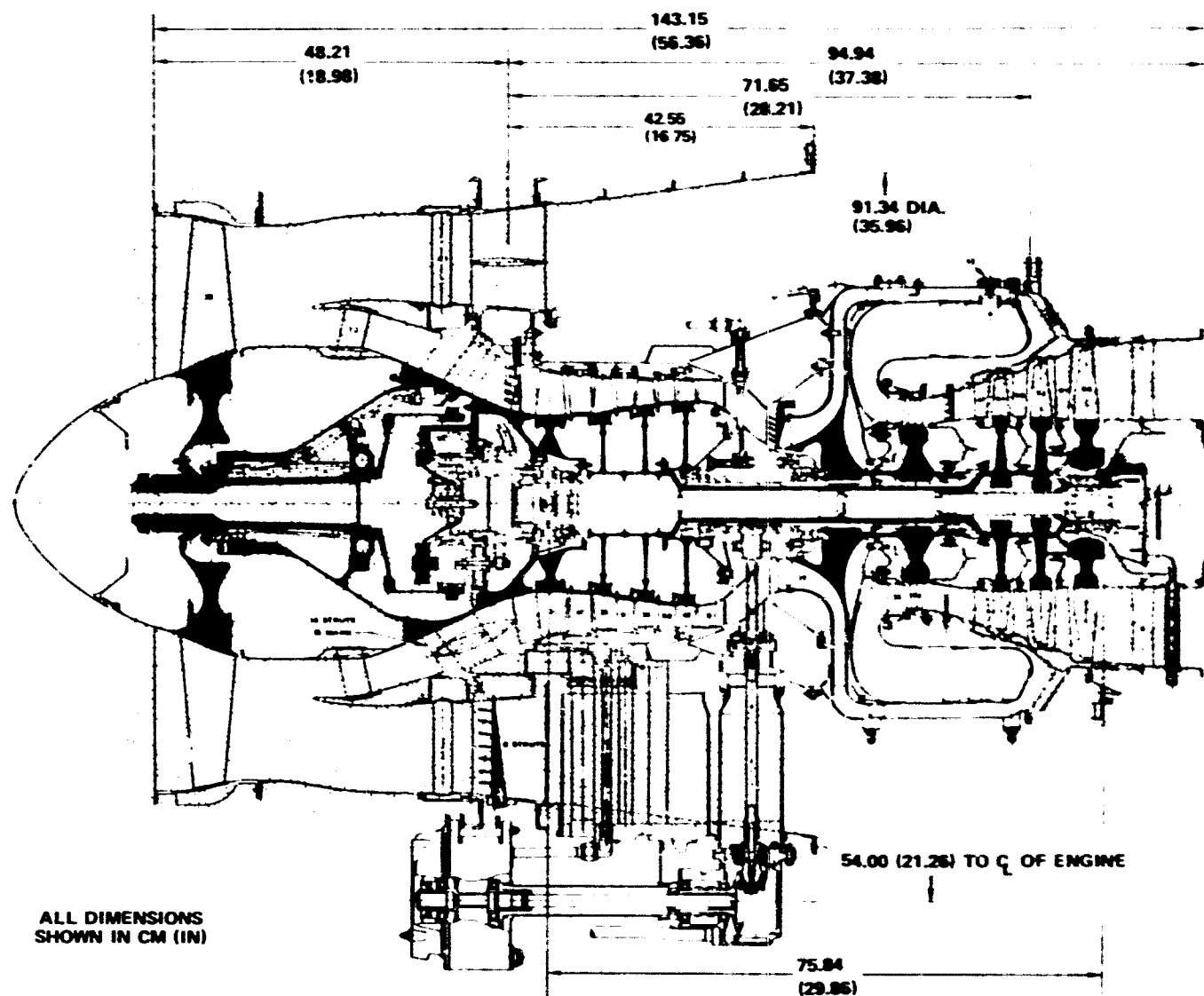
Figure 3-3.   AiResearch QCGAT Engine Unique Parts (Shaded Area).

The dominant core engine noise source in small gas turbines has been shown to be the combustor. The use of large-diameter annular reverse-flow combustors has been very effective in reducing exhaust noise in AiResearch engines compared with straight-through-flow annular or can configurations. Core noise contributed by the three-stage LP turbine occurs at blade passing frequencies well beyond the practical range of concern at all FAR Part 36 conditions, including approach. As a result, turbine tones do not contribute to flyover noise levels.

3.3   Engine Configuration

The basic QCGAT Engine was designed with provisions for both "hardwall" and acoustic treatments for a "workhorse" nacelle. These variations allowed for a base-line calibration for comparison purposes, and for evaluation of the effect of the various acoustical treatments available on the basic engine.

A standard, calibrated bellmouth was designed to obtain basic engine data. The flight-simulator lip was designed to simulate inlet conditions during static tests. A nacelle lip was also designed, fabricated and tested as the final flight design delivered with the engine. Hardwall and attenuated panels for the inlet section, fan duct, bypass duct, inner- and outer-aft ducts we made interchangeable in order to compare the acoustical properties of the panels. A coannular and a mixer-compound exhaust nozzle were also tested to provide a series of combinations of the six basic configurations.

3.3.1   Fan

The QCGAT Engine fan is derived from the fan used on the AiResearch ATF3-6 Turbofan Engine. The stator system has been modified to optimize the rotor-stator spacing and blade-vane counts for minimum rotor-stator noise interaction. The position of the splitter has been modified to accommodate the higher bypass ratio of the QCGAT Engine. The QCGAT fan flow path is shown in Figure 3-4.

The basic fan design parameters of the QCGAT fan that correspond to engine operation at the 12,192 m (40,000 ft.), Mach 0.8, ISA cruise design point are listed in Table 3-1.

BYPASS STATOR

0.63   0.60   0.58   0.46

FAN STAGE AND   BYPASS
DUCTS   STATORS   P/P - 1.628
MACH NUMBERS   (121 VANES)   η - 0.877
(ABSOLUTE)
                     P/P   1.638   (8 STRUTS)
                      η - 0.9003   0.68   0.46

FAN   0.60
(36
BLADES) 0.88   0.41   P/P - 1.586
              0.83   0.61   η - 0.879

0.66   (10
          CORE STATOR   STRUTS)
          (73 VANES)
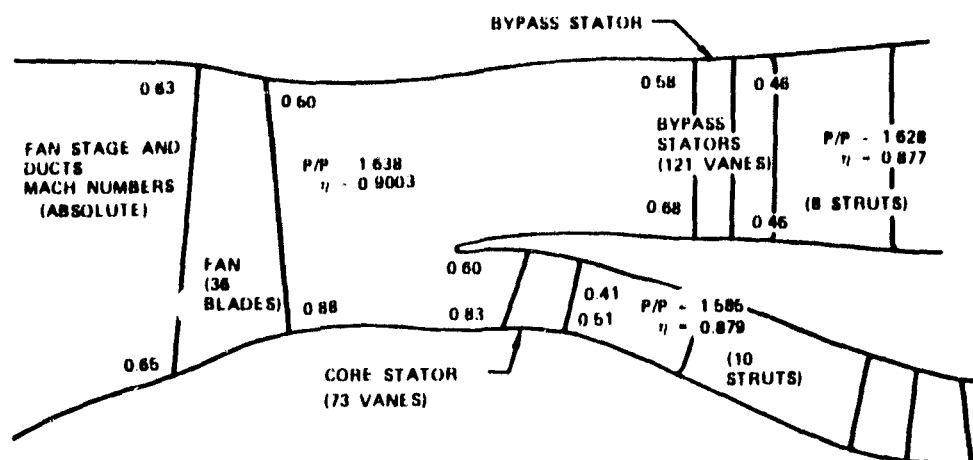
Figure 3-4.   Transition Duct and Fan Stage.

TABLE 3-1.   FAN DESIGN PARAMETERS

Parameters	Fan Design Point	Engine Match Point
$N/\sqrt{\theta}$	1057.67 rad/s (10,100 rpm)	1083.33 rad/s (10,345 rpm)
$W/\sqrt{\theta_{t2.0}/\delta_{2.0}}$ (fan)	76.88 kg/s (169.5 lbm/sec	77.83 kg/s (171.58 lbm/sec)
$M_{1 rel, tip}$	1.40	1.43
Fan inlet tip speed	408.7 m/s (1341 ft/sec)	418.8 m/s 1374 ft/sec)
P/P_{core} (stage)	1.593	1.57
P/P_{bypass} (stage)	1.628	1.62

o   Rotor hub-tip ratio = 0.46
o   Rotor tip diameter = 77.47 cm (30.5 inches)
o   Part-span dampers on rotors
o   Split stator configuration
o   Bypass stator D-factor (mean) = 0.461
o   Core stator D-Factor (mean) = 0.532

The 36-blade fan is a mirror image of a configuration developed in the ATF3 engine program. A series of full-scale rig tests have been conducted in that program to optimize the aerodynamic characteristics of the blade and the structural support of the midspan damper. Core (hub) and bypass (tip) performance maps for the QCGAT fan are shown in Figures 3-5 and 3-6.

Fan blade vibration frequencies are shown in Figure 3-7. The fundamental mode is satisfactorily well removed from excitations at 1 and 2 times shaft speed. The vibration modes shown will not be excited at any speed above idle by passage of the core or bypass stator vanes.

The resonance diagram shown in Figure 3-8 indicates that the fan rotor will be free of critical speed problems in the operating range. The critical speed predicted for fan synchronous excitation is more than 3 times maximum operating speed. The margin for LP spool excitation is much less, and experience with the TFE731 has shown that the squeeze film dampers are effective in preventing this type of coupling.

3.3.2 Fan Gearbox

Figure 3-9 shows the preliminary star gearbox configuration, together with component materials. Table 3-2 presents gearbox design data, including a comparison of calculated and allowable bending and compressive stress.

Figure 3-10 summarizes the star carrier requirements for dynamic considerations. Critical speed calculations (see Figure 3-10) show that the spring rate to be 1.428×10^6 kg/m (80,000 lb/in.) or more to maintain the desired margin of 25 percent. The actual spring rates that exist in the star carrier are many times this value.

The carrier is designed to constrain the star gears to an angular misalignment of 0.0005 cm/cm (0.0002 in./in.) or less. The effective spring rates at the planet gear bearings are approximately equal in order to minimize misalignment, and to minimize the helix correction requirements. Table 3-3 summarizes the fan shaft and star bearing capabilities. These bearings are adequate.

3.3.3 LP Compressor

The LP compressor for the QCGAT Engine is identical with the production TFE731-3 LP compressor.

The compressor achieves excellent surge margin without variable inlet guide vanes.
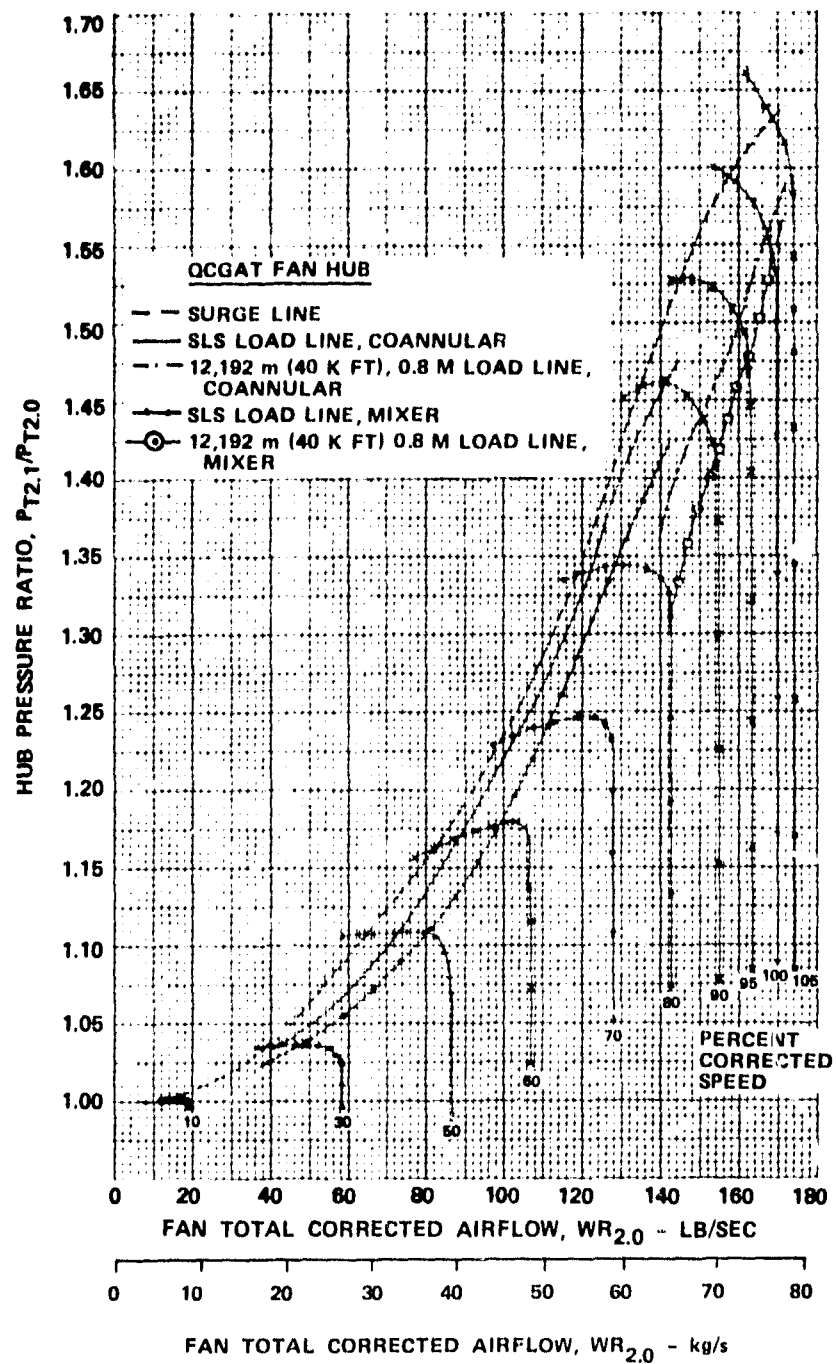
Figure 3-5. Fan Core Performance, AiResearch QCGAT Engine.
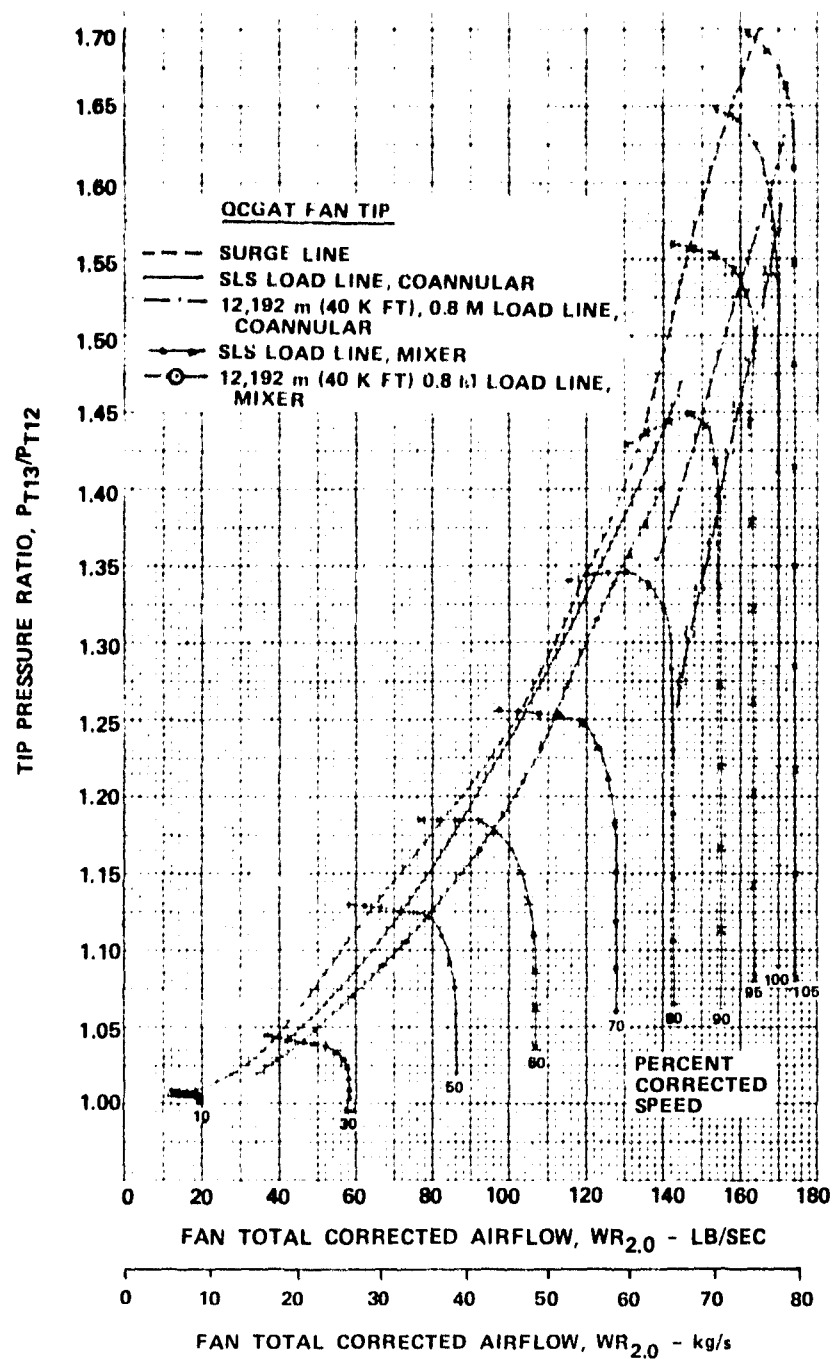
Figure 3-6. Fan Bypass Performance, AiResearch QCGAT Engine.
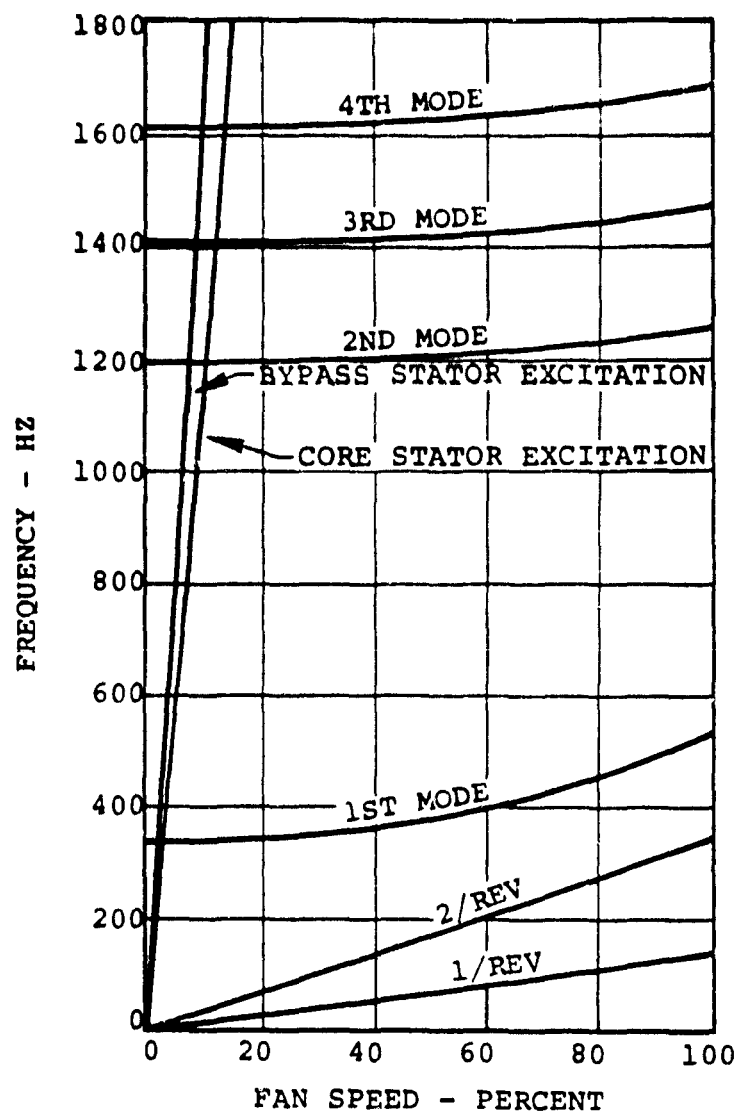
Figure 3-7. Fan Blade Natural Frequencies.

18
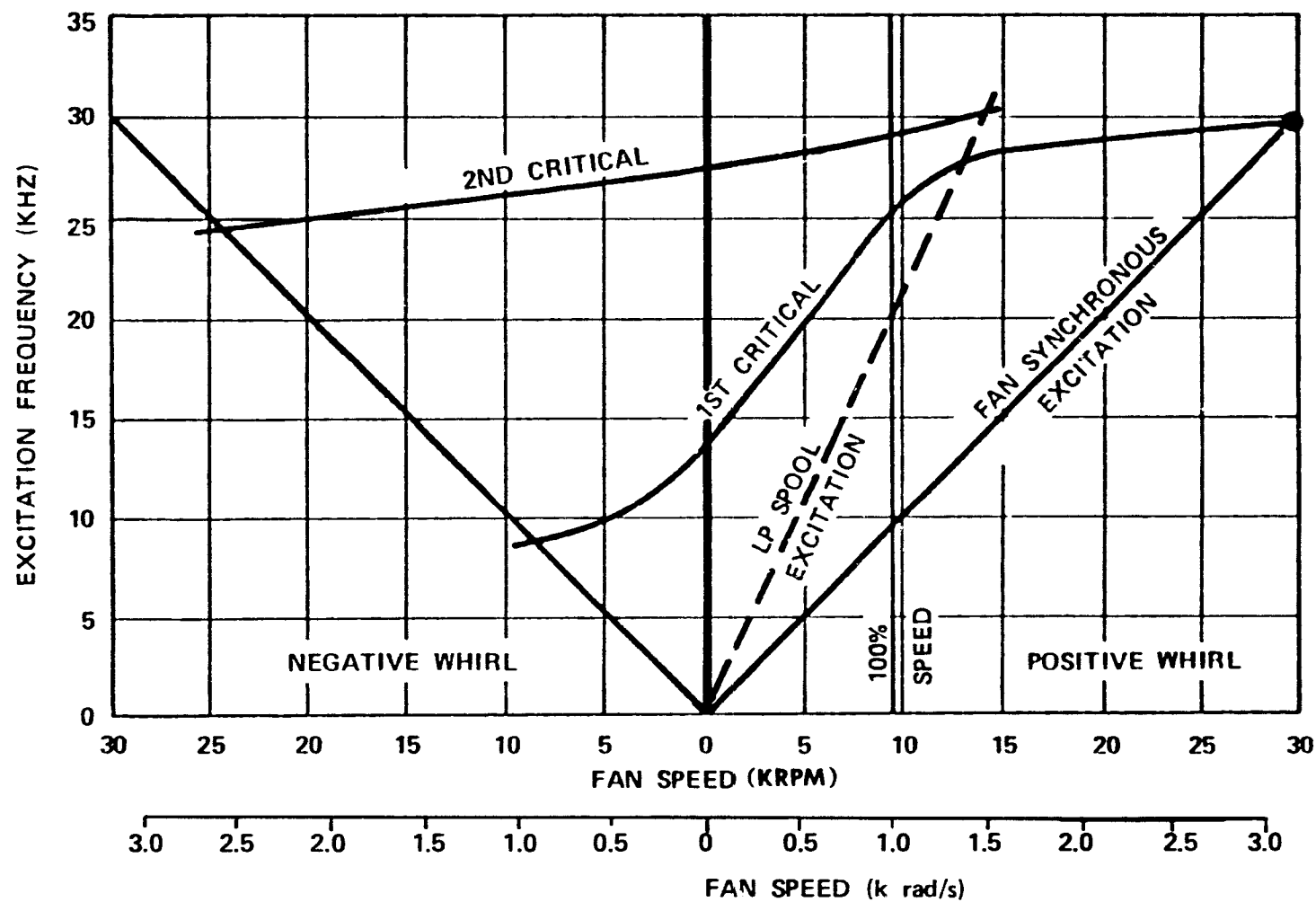
Figure 3-8. QCGAT Fan Critical Speed Summary.
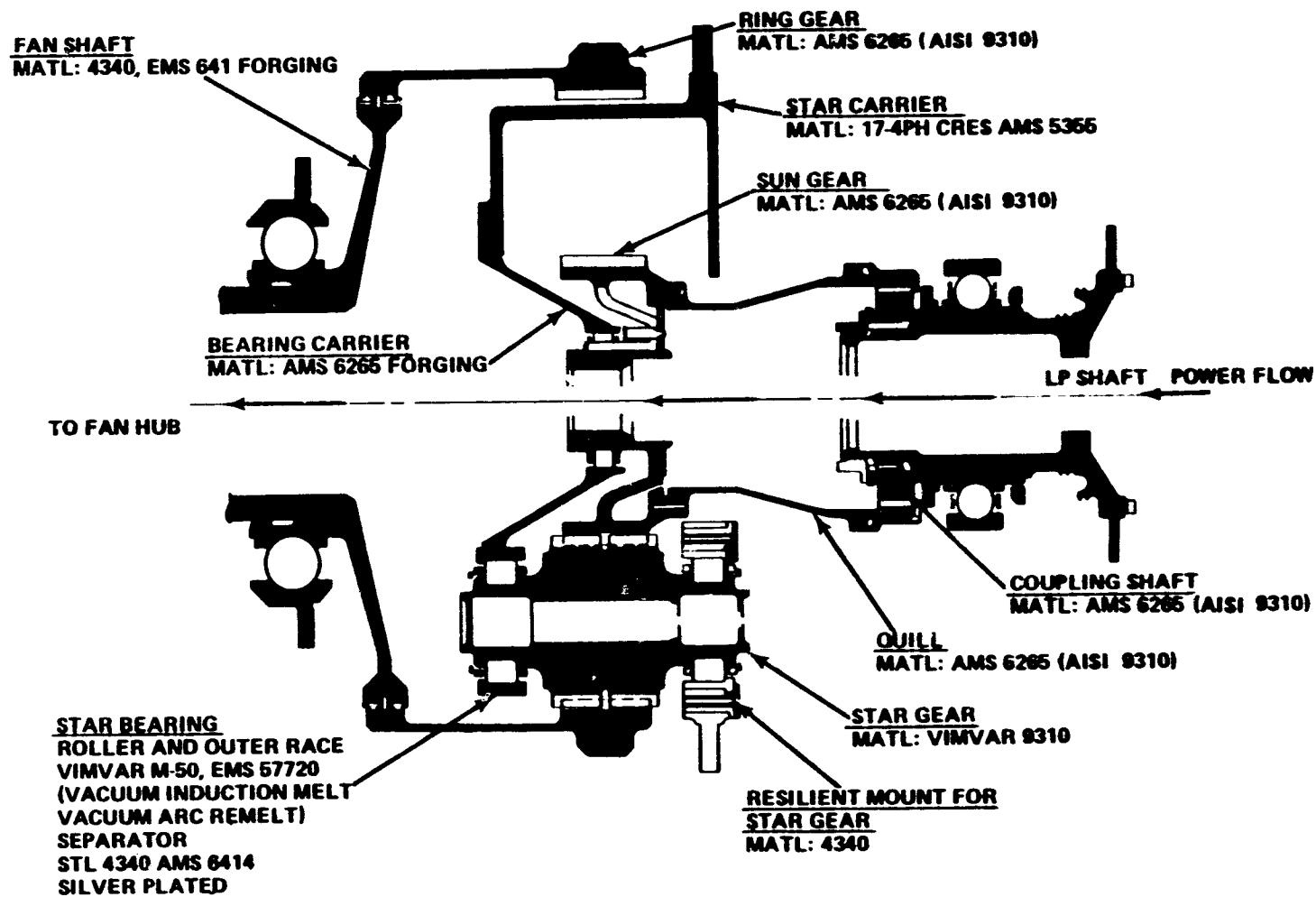
Figure 3-9. QCGAT Planet Gearbox.

TABLE 3-2.   FAN GEARBOX ANALYSIS

PARAMETER	SUN		STAR		RING
Total Facewidth, cm (in.)	2.97 (1.17)		3.56 (1.40)		3.07 (1.21)
Rotational Speed (rad/s) (rpm)	2105.6 (20,111)		3636.9 (34,737)		975.8 (9,320)
Tan. Tooth Load, N (lbf)		6200.8 (1394)		6196.4 (1393)	
Torque, Nm (lbf-in.)	1,602.5 (14,184)				3457.9 (30,607)
Allowable Bending Stress kN/cm^2 (Kpsi)	54.19 (78.6)		46.53 (67.5)		42.13 (61.1)
Calculated Bending stress fillet radius kN/cm^2 (Kpsi)	49.16 (71.3)		44.33 (64.3)		35.23 (51.1)
Allowable Compressive Stress kN/cm^2 (Kpsi)	173.75 (252)	213.74 (310)		211.67 (307)	179.95 (261)
Calculated Compressive Stress kN/cm^2 (Kpsi)		139.27 (202)		96.53 (140)	
Specific Film Thickness, λ		2.422		2.2799	
Minimum Contact Ratio		1.7089		1.7763	
Ring/Sun Reduction		0.4634			

NOTE: 1. 3375 kW at 2105.6 rad/s (4526 HP at 20,111 RPM) with a 1.3 Dynamic Load Factor.

2. 0.349 radian (20°) Pressure Angle, 14 pitch.

3. Tooth Count -- Sun   57
                    Planet 33
                    Ring   123
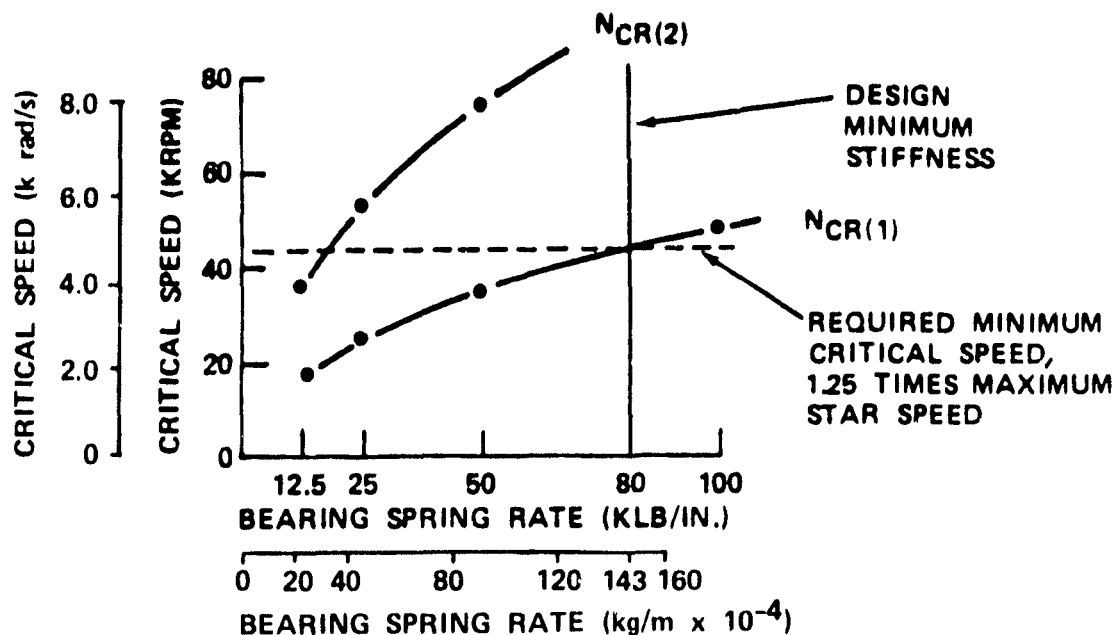
Figure 3-10. Star Carrier Dynamic Requirements.

TABLE 3-3. QCGAT BEARING SUMMARY

BEARING	CONDITION	ANALYSIS
Fan Roller Bearing	1 Blade Out	142.34 kN (32,000 lb) load. 99% probability of survival based on roller fracture stress.
	2 Blades Out	284.69 kN (64,000 lb) load. 90% probability of survival based on roller fracture stress.
Fan Ball Bearing	Duty Cycle Proportioned from TFE731 "Executive Type"	10,200 hours L_1 Life
	Maximum Thrust	770 Hours L_1 Life
Star Roller Bearing	Takeoff rpm and Load	3,200 Hours L_1 Life

22

3.3.4 HP Compressor

The HP compressor for the QCGAT Engine is identical with the HP compressor on the TFE731 Engine. This compressor is a backward curved single-stage centrifugal compressor with a single-vane island diffuser row followed by a 90-degree bend to the axial direction and a row of deswirl vanes.

3.3.5 Combustor

The combustor system selected for the QCGAT Engine consists of a modified version of the TFE731 production burner. The combustor, identified as PAP234342, had a row of 48 holes of 0.459 cm diameter (0.181 in.) added to the dome for the purpose of smoke reduction. The fuel nozzles are standard production TFE731-3 dual orifice assemblies, Part No. 3071101-14. Air-assist was utilized in the secondary circuit of these fuel nozzles at idle conditions only. For the engine test, the fuel flow divider was capped and an air line was connected directly to the secondary fuel manifold. For the production engine configuration, the fuel line would remain connected and a check valve would be put in the air-assist line. (See Figure 3-11 for a schematic of the air-assist nozzle system).

The air supplied to the fuel nozzle tips is an aid in the atomization process. The air supplied during ground test operations is from a laboratory compressed air source with a supply pressure of 206.8 Pa (300 psig) and heated to a temperature range of 366 to 462K (200 to 300°F) by an electric heat exchanger.

3.3.6 HP Turbine

The HP turbine for the QCGAT Engine is identical to the TFE731-3 HP turbine. The TFE731-3 HP turbine is a single-stage axial design with internally cooled vanes and blades.

Characteristics of the QCGAT HP turbine at design condition are:

o $\dfrac{W\sqrt{\theta}_{4.1}}{\delta_{4.1}}$ = 2.129 kgs/s (4.693 lbm/sec)

o P/P = 1.832

o $N/\sqrt{\theta}_{4.1}$ = 1406.2 rad/s (13,431 rpm)

o $\dfrac{\Delta H}{\theta_{4.1}}$ = 39.797 kj/kg (17.11 Btu/lbm)
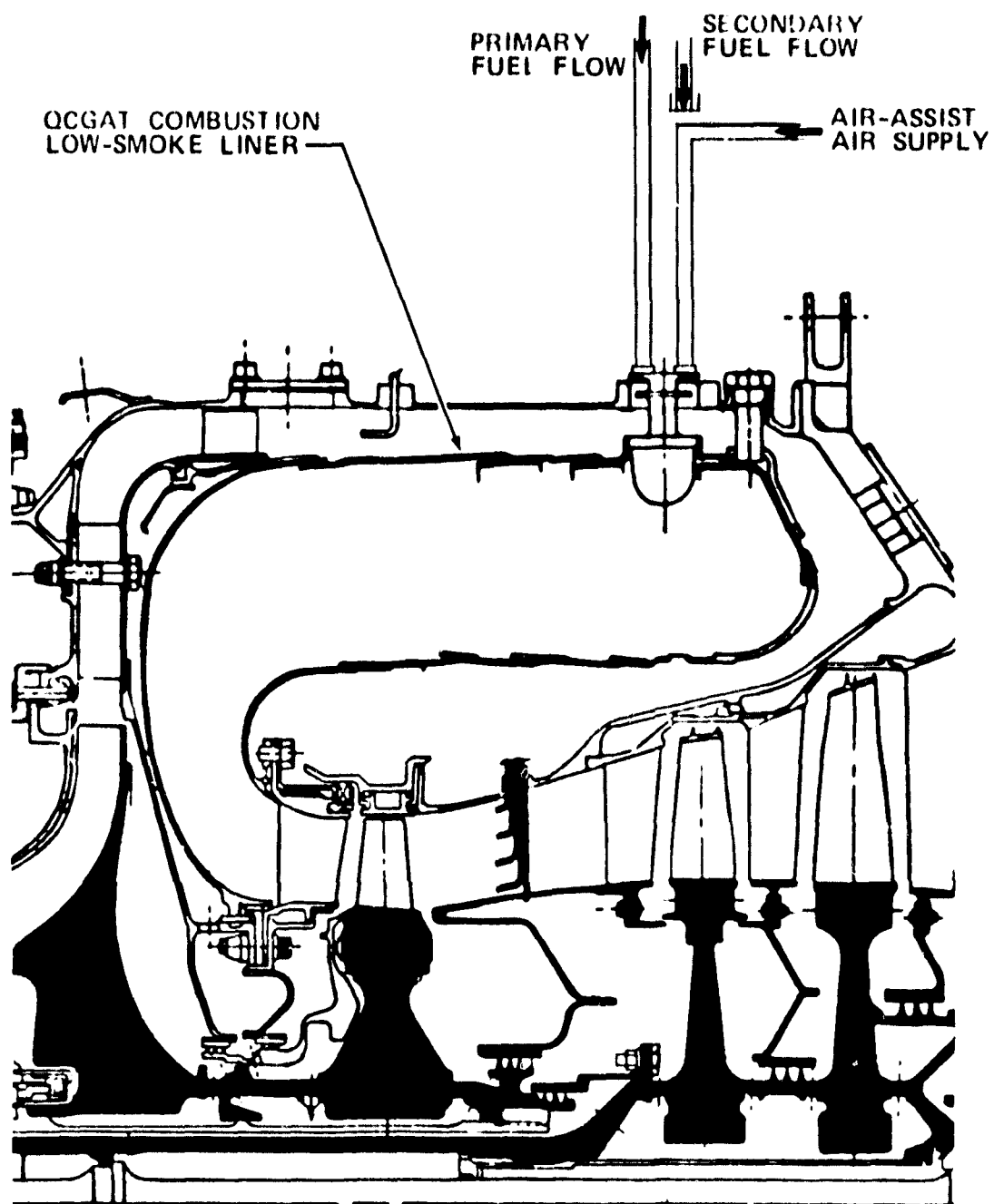
Figure 3-11.   Air Assist Nozzle System for IDLE-Power settings.

o $T_{4.1}$ max = 1352.4 °K (1975°F)

o $T_{4.1}$ QCGAT max = 1329.1 °K (1933°F)

3.3.7 LP Turbine

The LP turbine for the QCGAT Engine is a new design, optimized to maximize turbine performance at the QCGAT cruise design point. This turbine retains the three-stage configuration of the TFE731-3 LP turbine, but has blading optimized for the higher overall pressure ratio required to drive the higher bypass ratio fan. This increased turbine pressure ratio reduces core nozzle pressure ratio, thereby, reducing core jet velocity and noise.

The design point turbine efficiency goal in excess of 90 percent requires the application of large turbine design technology demonstrated in recent NASA and AFAPL fan turbine programs. This technology includes the application of non-free-vortex vector diagram concepts along with advanced profile design techniques to provide superior stage performance.

Figure 3-12 provides the vector diagram nomenclature for the LP stages. Design characteristics of the QCGAT LP turbine are shown in Table 3-5, and 3-6. The flow path for the LP turbine is shown in Figure 3-13 with the predicted off-design LP turbine maps are shown in Figures 3-14 and 3-15.

3.3.7.1 LP Turbine Mechanical Design

The preliminary mechanical design of the LP turbine section is summarized in Figures 3-16, 3-17, and 3-18. Figure 3-16 lists design features and improvements to the turbine rotor. Materials of the major components are shown in Figure 3-17. Figure 3-18 illustrates secondary cooling and leakage flows.

3.3.8 Engine Static Structure

The AiResearch QCGAT Engine design minimizes length and height. The main frame consists of two cylinders--the compressor and turbine plenums--joined by a conical transition structure. This framework takes all inertia and thrust loads, and embodies a "cool-skin" design wherein the entire structure is enveloped by fan and compressor discharge air. The conical compressor-turbine transition structure also supports the accessory drive power shaft and right-angle gearbox. The accessory drive is powered by the HP spool through a bevel gear set.

25
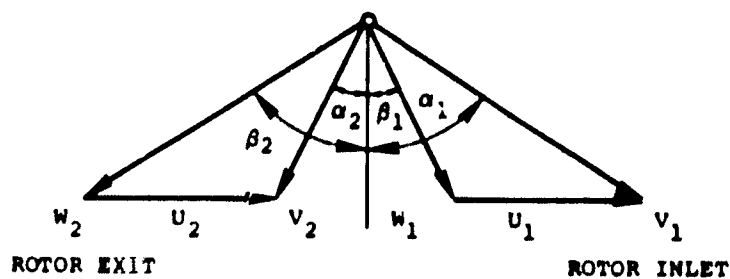
Figure 3-12.   LP Turbine Vector Diagram.
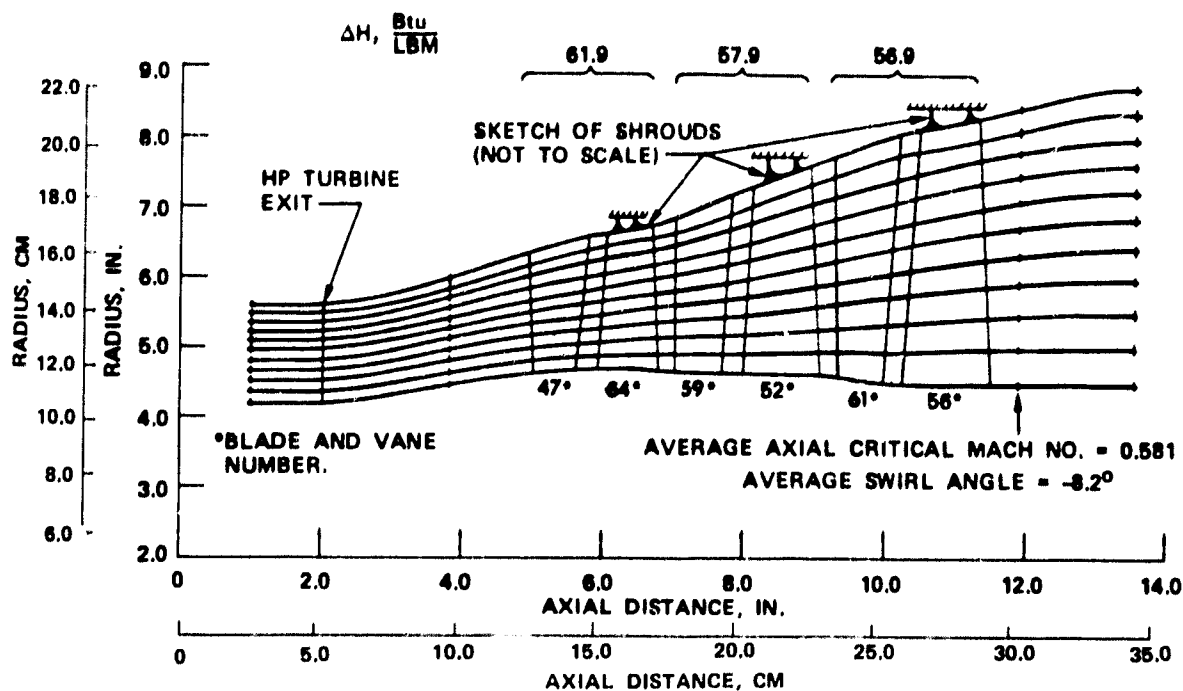
Figure 3-13.   QCGAT Low-Pressure Turbine Flow Path.
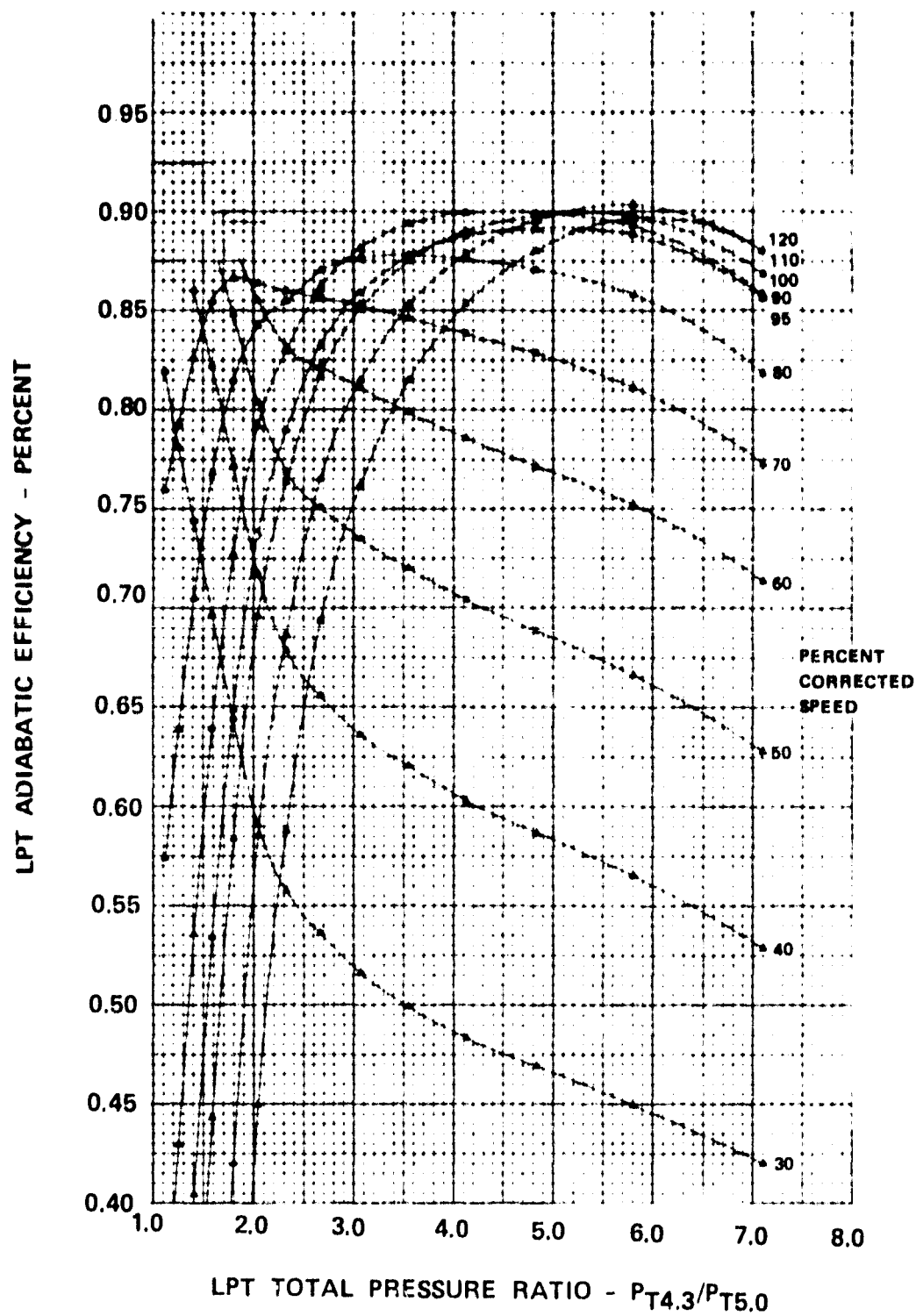
Figure 3-14. Low-Pressure Turbine Efficiency Versus Total Pressure Ratio.
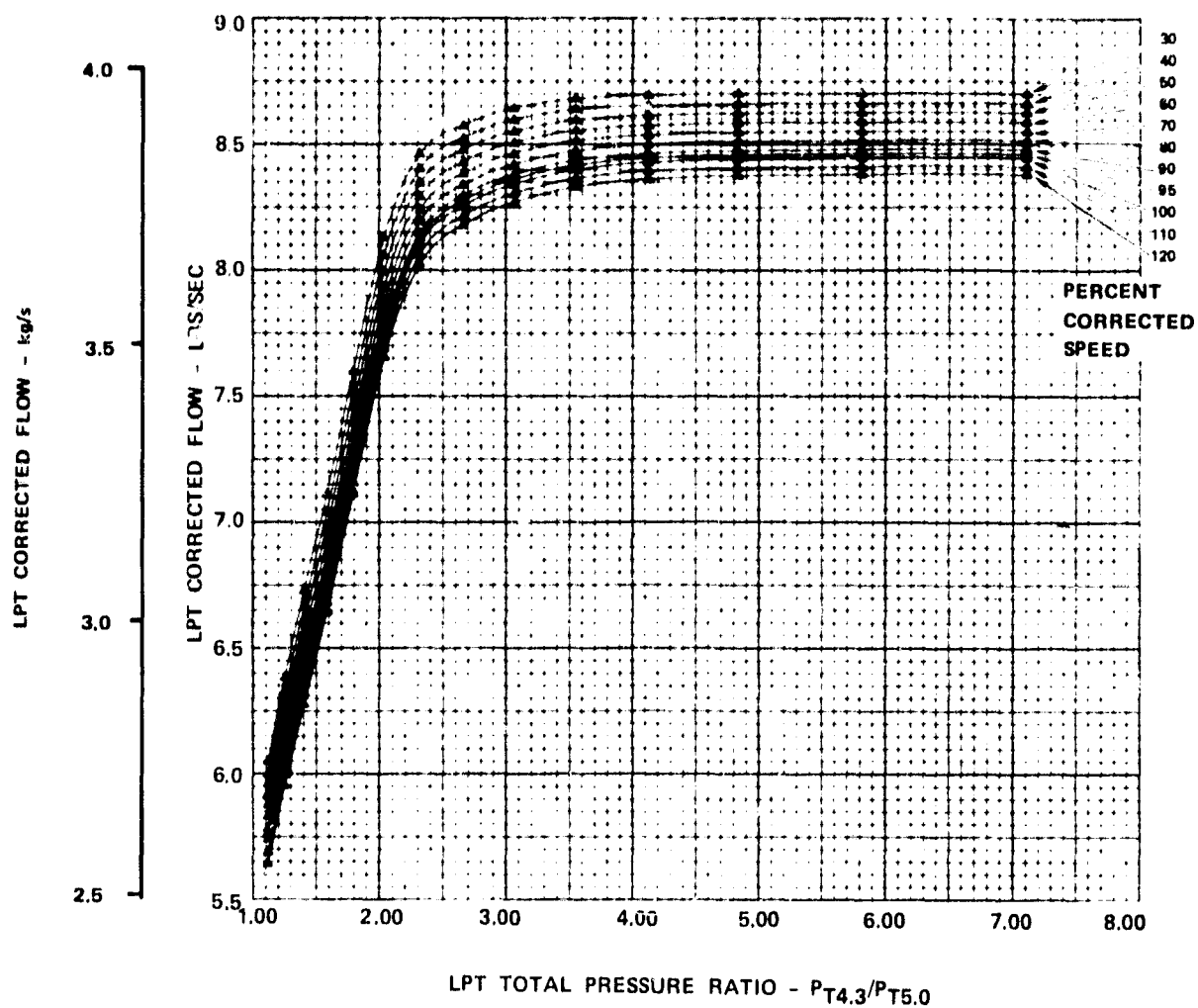
Figure 3-15.   Low-Pressure Turbine Airflow Versus Total
Pressure Ratio.

28

TABLE 3-4. MAIN DESIGN POINT DATA FOR THE QCGAT LP TURBINE.

	Engine Operating Condition	Corrected to Standard Air Condition
Pressure ratio, total to total rating	$PR = 5.707$	$PR_{cor} = 6.555$
Mass flow rate, kg/s (lbm/sec)	5.055 (11.145)	$\dfrac{W\sqrt{\theta}_{CR}}{4.3} = 3.909$ (8.618)
Speed, rad/s (rpm)	2,118 (20,229)	$\dfrac{N}{\sqrt{\theta}_{CR}} = 1,095$ (10,454)
Specific work, J/kg (Btu/lbm)	406,515 (174.77)	$\dfrac{\Delta H}{\theta_{CR}} = 108,554$ (46.67)

Notes:

Number of stages = 3

Efficiency, total to total, rating = 90.2 percent

TABLE 3-5. SUMMARY OF CHARACTERISTIC DATA FOR QCGAT
LP TURBINE STAGES.

	First Stage	Second Stage	Third Stage	Overall
Inlet temperature, K (°R)	1080.1 (1944.1)	983.2 (1769.7)	866.4 (1559.6)	
Inlet total pressure kPa (psia)	262.6 (38.08)	154.4 (22.39)	87.36 (12.67)	
Pressure ratio, total to total	1.705	1.770	1.905	5.747
Specific work, ΔH (for zero clearance kJ/kg (btu/lbm)	144.0 (61.9)	134.7 (57.9)	132.3 (56.9)	411.0 (176.7)
Tip peripheral speed U_{tip} m/s (fps)	362.7 (1190)	409.0 (1342)	445.6 (1462)	
Mean work coefficient $\lambda = \Delta H/U_M^2$	1.523	1.244	1.120	
Mean flow coefficient $\phi = V_X/U_M$	0.669	0.634	0.823	
Efficiency, total to total with zero clearance	0.9102	0.8986	0.8978	0.9096
Efficiency, total to total, with 0.064 cm (0.025 in.) clearance (shrouded)	0.9050	0.8948	0.8947	0.9054

TABLE 3-6. SUMMARY OF VECTOR DIAGRAM DATA
OF THE QCGAT LP TURBINE.

STAGE 1

Parameter	Hub		Mean*		Tip	
	Inlet	Exit	Inlet	Exit	Inlet	Exit
Radius cm (in.)	11.938 (4.700)	11.913 (4.690)	14.399 (5.669)	14.727 (5.798)	16.904 (6.655)	17.120 (6.740)
α rad (Deg)	1.093 (62.6)	-0.412 (-23.6)	1.148 (65.8)	-0.276 (-15.8)	1.183 (67.8)	-0.236 (-13.5)
β rad (Deg)	0.722 (41.4)	-1.019 (-58.4)	0.517 (29.6)	-1.061 (-60.8)	0.028 (1.6)	-1.082 (-62.0)
V/A'_{CR}	0.868	0.745	0.380	0.649	0.384	
U/A''_{CR}	0.435	0.433	0.522	0.534	0.611	0.617
W/A''_{CR}	0.551	0.696	0.363	0.727	0.252	0.791
Reaction (%)		20.5		43.2		59.8

STAGE 2

Parameter	Hub		Mean*		Tip	
	Inlet	Exit	Inlet	Exit	Inlet	Exit
Radius cm (in.)	11.836 (4.660)	11.760 (4.630)	15.232 (5.997)	15.761 (6.205)	18.542 (7.300)	19.304 (7.600)
α rad (Deg)	1.021 (58.5)	-0.305 (-17.5)	1.072 (61.4)	-0.276 (-15.8)	1.094 (62.7)	-0.206 (-11.8)
β rad (Deg)	0.560 (32.1)	-0.915 (-52.4)	0.192 (11.0)	-1.075 (-61.6)	-0.492 (-28.2)	-1.143 (-65.5)
V/A'_{CR}	0.840	0.495	0.724	0.416	0.611	0.397
U/A''_{CR}	0.455	0.453	0.586	0.605	0.708	0.734
W/A''_{CR}	0.535	0.754	0.364	0.811	0.325	0.892
Reaction (%)		32.4		54.8		72.3

STAGE 3

Parameter	Hub		Mean*		Tip	
	Inlet	Exit	Inlet	Exit	Inlet	Exit
Radius cm (in.)	11.43 (4.500)	11.43 (4.500)	16.538 (6.511)	16.947 (6.672)	20.638 (8.125)	21.031 (8.280)
α rad (Deg)	1.052 (60.3)	0.152 (-8.7)	1.005 (57.6)	-0.145 (-8.3)	0.946 (54.2)	-0.122 (-7.0)
β rad (Deg)	0.702 (40.2)	-0.757 (-43.4)	-0.052 (-3.0)	-0.956 (-54.8)	-0.731 (-41.9)	-1.009 (-57.8)
V/A'_{CR}	1.001	0.614	0.754	0.575	0.616	0.621
U/A''_{CR}	0.471	0.471	0.678	0.692	0.832	0.846
W/A''_{CR}	0.678	0.816	0.416	0.945	0.489	1.084
Reaction (%)		19.3		61.6		78.9

*50 Percent Streamline

A — INCREASED BORE TO REDUCE COOLING FLOW PRESSURE DROP

B — REDUCED DIAMETER AND INCREASED NUMBER OF TEETH TO REDUCE LEAKAGE FLOW

C — ALL DISKS WITH 125 MINIMUM BURST SPEED MARGIN

D — ESTIMATED ROOT AVERAGE CENTRIFUGAL STRESSES

STAGE 1 = 219.3 kPa (31.8 KSI)
STAGE 2 = 319.2 kPa (46.3 KSI)
STAGE 3 = 344.7 kPa (50.0 KSI)
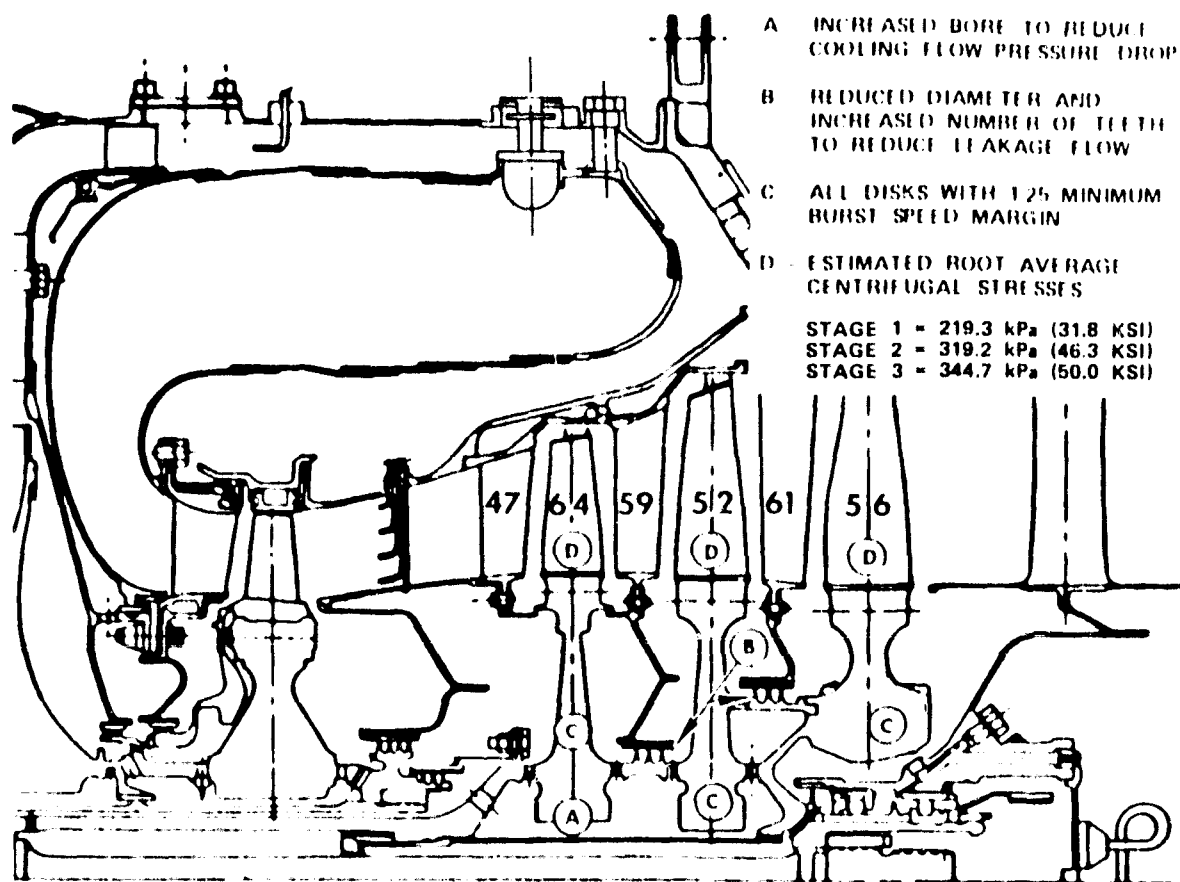
Figure 3-16.   QCGAT LP Turbine Rotor Mechanical Design Features.

The fan rotor is overhung from its bearings, which are supported in a forged steel housing. Thrust and inertia loads pass from the bearing support through the fan strut housing to the engine main-mount ring. The mount ring acts as a flow channel for the fan bypass air and supports the fan-bypass stator, the fan-inlet housing, and the accessory drive gearbox.

The outer-fan duct is made of high-strength materials to accept thrust reverser loading and the loads imposed by the nacelle. In addition to increased strength, integral axial flanges provide for improved engine serviceability. Fan-support structure materials are shown in Figure 3-19. Design loads for the fan-support structure are shown in Table 3-7.

The LP rotor is supported by a forward ball bearing, which takes thrust and inertial loads, and an aft roller bearing that reacts to inertial loads. The aft roller bearing is supported by a housing which consists of an inner conical shell, a radial
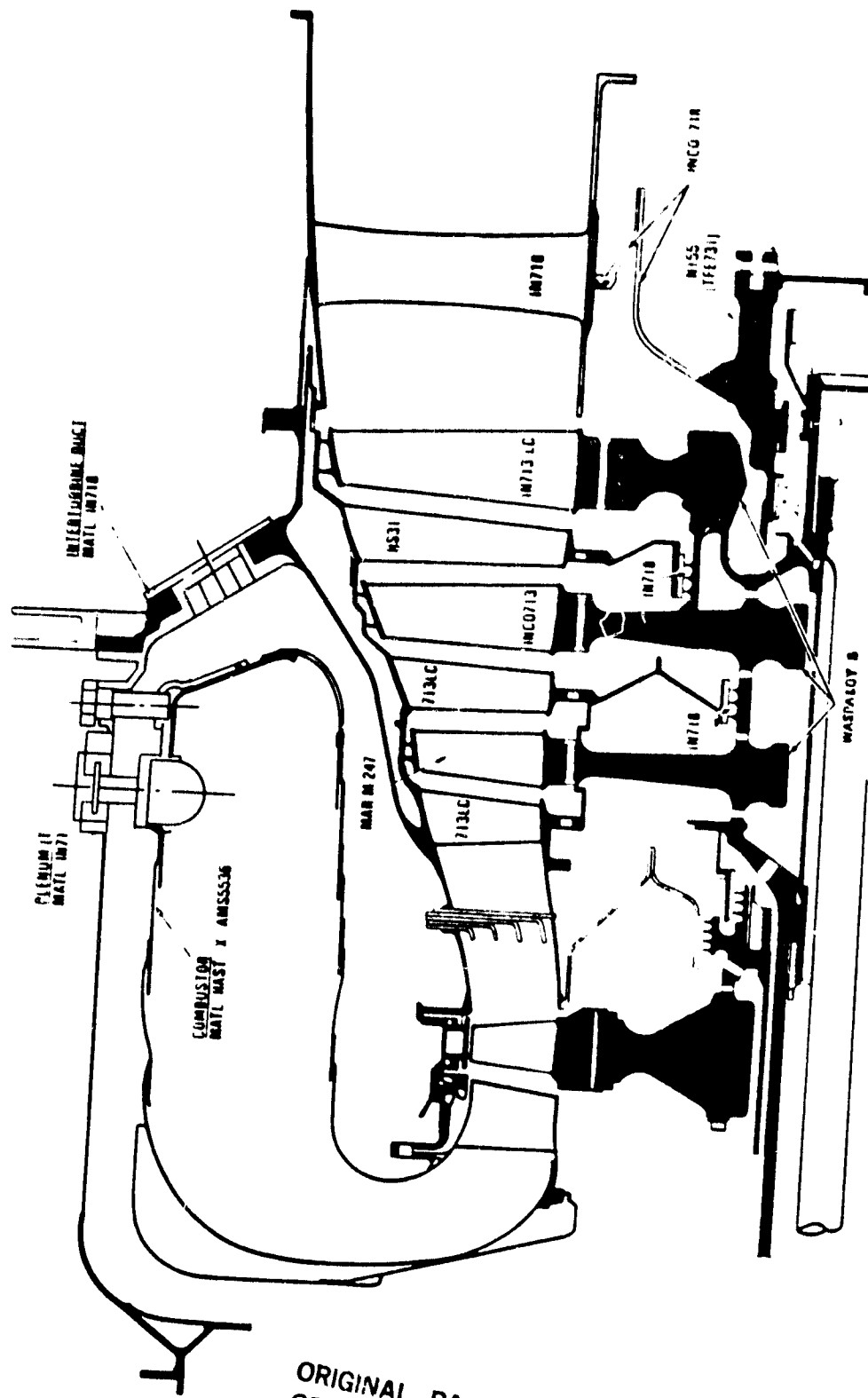
Figure 3-17. 2CGAT Low-Pressure Turbine Materials.

SEA-LEVEL TAKEOFF CONDITIONS

ALL FLOWS ARE SHOWN AS A PERCENT OF THE LP TURBINE CORE FLOW.
THE CIRCLED NUMBERS REPRESENT THE PUMPING REQUIREMENT IN EACH CAVITY.
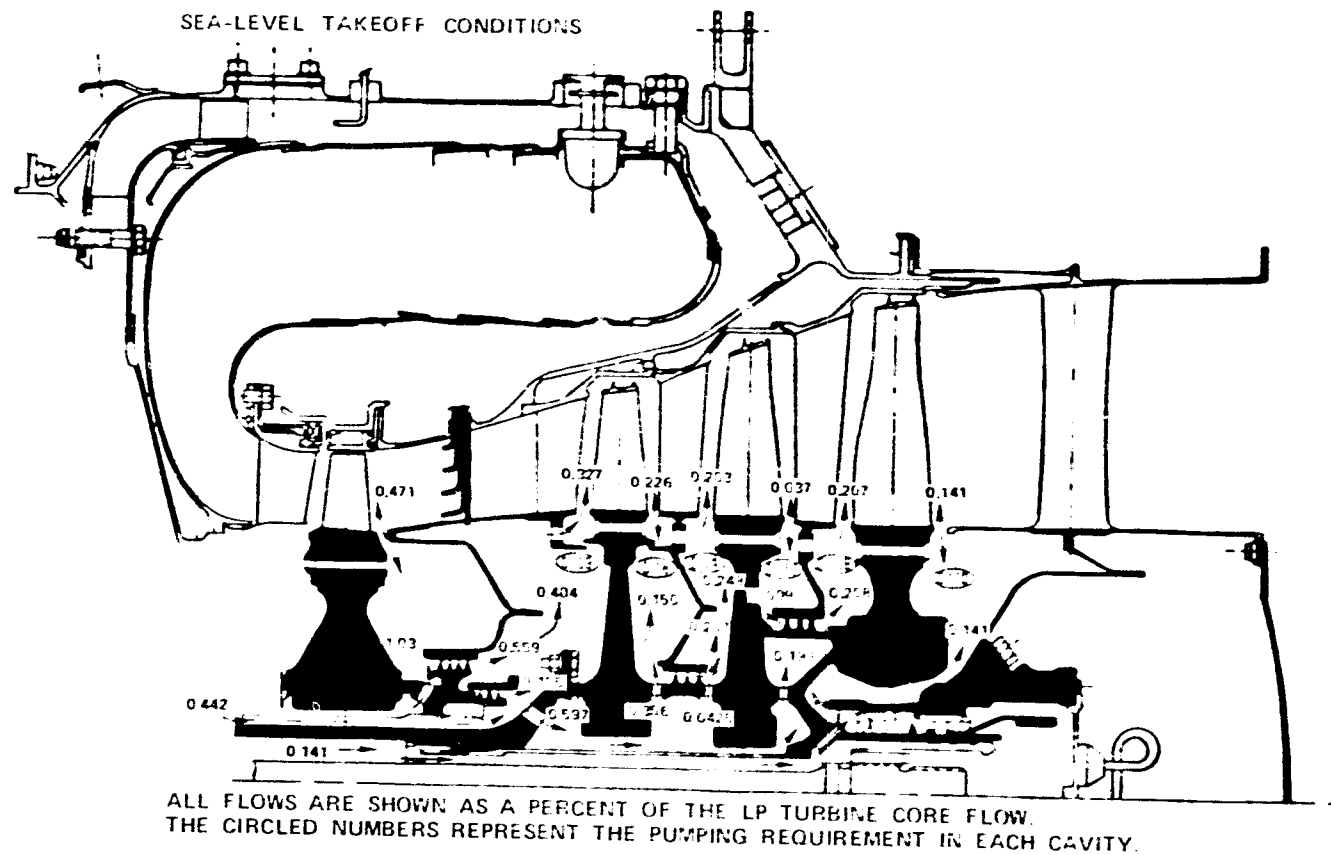
Figure 3-18. QCGAT Low-Pressure Turbine Cooling and Leakage Flows.

STRUT (8 PLACES)

INTERMEDIATE CASE
MATERIAL = K01-T7 CAST ALUMINUM

STRUT
(10 PLACES)

FAN SUPPORT
MATERIAL = 17-4PH CRES

ENGINE SUPPORT HOUSING
MATERIAL = 6 Al-4V TITANIUM
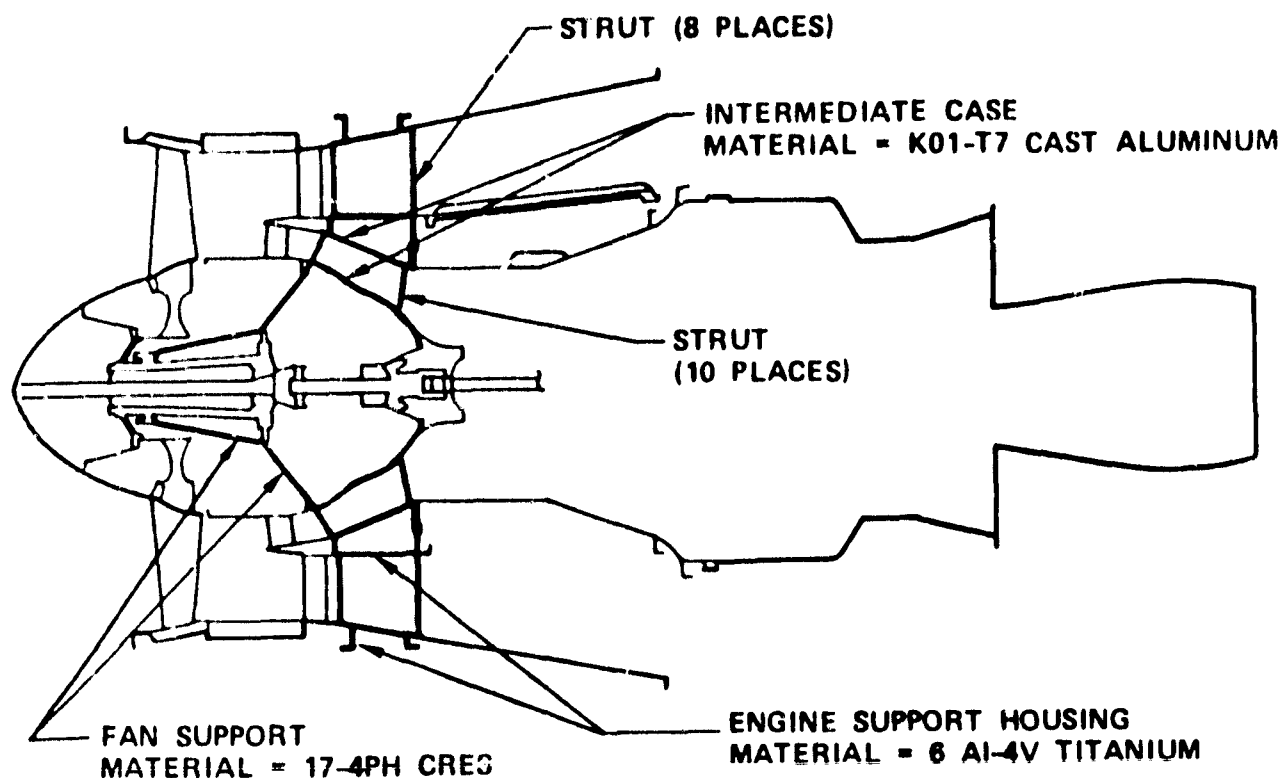
Figure 3-19.   QCGAT Engine Fan Support Structure.

struts, and an outer cylindrical shell which is bolted to the
outer case of the engine. This Rear Bearing Support Housing pro-
vides the load path from the L.P. rotor rear bearing to the outer
case of the engine. The turbine plenum end cone supports the Rear
Bearing Support Housing and the L.P. turbine stators.

The HP rotor is overhung from a forward roller and an aft
ball bearing with the bearing-support structures attached to the
intermediate-strut housing. This overhung arrangement for the
short-coupled HP spool has definite advantages. In addition to
the reduced weight achieved by elimination of a hot sump, oil
delivery is simplified, coking problems are eliminated, and bearing
lives are increased because of cooler oil. The HP compressor-
diffuser housing provides support for the combustor transition
liner and the HP turbine stator, as well as being the pressure
bulkhead between the LP and HP spools.

35

TABLE 3-7. DESIGN LOADS - EXISTING TFE731 VERSUS QCGAT.

	Radial Load kN (lb)		Moment Load Nm (in-lb)		Fan Thurst N (lb)		Bird Strike Nm (in-lb)	
	TFE731	QCGAT	TFE731	QCGAT	TFE731	QCGAT	TFE731	QCGAT
Fan Support	489.304* (110,000*) -84,516** (-19,000**)	156.132* (35,100*) -31,582** (-7,100**)	--	--	13,789.5 (3,100)	14,679.1 (3,300)	--	--
Inter-mediate Case	489.304 (110,000)	124.550 (28,000)	68,242.8 (604,000)	34,234.4 (303,000)	13,789.5 (3,100)	14,679.1 (3,300)	39,544.7 (350,000)	
Engine Support Housing	489.304 (110,000)	124.550 (28,000)	98,296.7 (870,000)	44,967.9 (398,000)	13,789.5 (3,100)	14,679.1 (3,300)	39,544.7 (350,000)	--

*At forward bearing
**At aft bearing

Several static structural components on the QCGAT Engine are new or modified TFE731 components. These items include:

(a) Fan support housing
(b) Intermediate compressor housing
(c) Fan core stator
(d) Fan bypass stator
(e) Engine support housing
(f) Fan inlet housing
(g) Outer fan duct
(h) Exhaust nozzle
(i) Interturbine duct
(j) LP turbine stator assembly

With the exception of the fan-inlet housing and the outer-fan duct, the function of these items has not changed. The fan outer duct has two versions; one incorporates acoustical treatment, the other has conventional hardwall construction.

3.4 Test and Flight Configuration

There are six basic combinations of acoustically treated or hardwall engine/nacelle configurations. The inlet sections for testing were either a bellmouth for static operation, a flight-simulator lip, or the flight-nacelle lip. Inlet panels, fan duct liners, and aft-duct inner and outer panels were installed as hardwall or acoustically treated so that individual panels could be evaluated for their contribution to the overall performance and noise supression. A calibrated dual exhaust nozzle and a mixer-compound exhaust nozzle were also used in the test program with the flight configuration evaluated under ground static conditions.
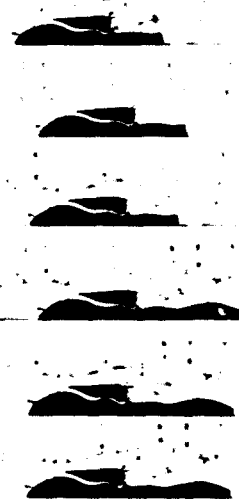
3.4.1 Test Installations

Figure 3-20 shows the various combinations that were tested during the program. Three inlets, two inlet panels, fan-duct panel, bypass-duct panel, inner- and outer- aft panels and the two different exhaust nozzles were tested.

3.5 Mixer-Compound Exhaust System

The mixer-compound exhaust system was designed with the dual objectives for obtaining an exhaust system to meet the performance and exhaust jet-noise goals of the QCGAT.

OCGAT ENGINE TEST BUILD LIST PERFORMANCE, NOISE, EMISSIONS	TEST CELL	INSTRUMENTATION LEVEL	BASIC INSTALLATION CONFIGURATION	BASIC ENGINE WITH CONTROLS & ACCESS	ENGINE BELLMOUTH	FLIGHT SIMULATOR	NACELLE LIP	(2) INLET SECTION HARDWALL	ATTENUATED	(3) FIRST INLET PANEL HARDWALL	ATTENUATED	(4) SECOND INLET PANEL HARDWALL	ATTENUATED	(5) FAN DUCT HARDWALL	ATTENUATED	(6) BYPASS DUCT HARDWALL	ATTENUATED	(7) INNER AFT PANEL HARDWALL	ATTENUATED	(8) OUTER AFT PANEL COANNULAR	MIXER COMPOUND	(9) EXHAUST NOZZLE

1 ENGINE INSTRUMENTATION AND TEST CELL CALIBRATIONS																					
A GREEN RUN	PERF	STD	I	●	●							●		●		●					●
B PRE-ENDURANCE	PERF	STD	I	●	●							●		●		●					●
2 ENGINE ENDURANCE CYCLES																					
A ENDURANCE	ENDUR	STD	I	●	●							●		●		●					●
B POST ENDURANCE CALIB	PERF	STD	I	●	●							●		●		●					●
3 REFERENCE ENGINE PERFORMANCE EMISSIONS																					
A PERFORMANCE CALIBRATION 1	PERF	PERF	I	●	●							●		●		●					●
B PERFORMANCE CALIBRATION 2	PERF	PERF	VI	●	●							●		●		●		●			●
C PERFORMANCE CALIBRATION 3	PERF	PERF	II	●		●		●		●		●		●		●					●
D PERFORMANCE CALIBRATION 4	PERF	PERF	III	●			●	●		●		●		●		●					●
E PERFORMANCE CALIBRATION 5	PERF	PERF	V	●			●	●		●		●		●		●		●			●
F PERFORMANCE CALIBRATION 6	PERF	PERF	IV	●		●		●		●		●		●		●		●			●
G PERFORMANCE CALIBRATION 7	PERF	PERF	IV	●			●	●		●		●		●		●					●
4 ENGINE NOISE																					
A NOISE CALIBRATION 1	ENDUR	STD	II	●		●															●
B NOISE CALIBRATION 2	ENDUR	STD	II	●		●															●
C NOISE CALIBRATION 3	ENDUR	STD	IV	●		●												●			●
D NOISE CALIBRATION 4	ENDUR	STD	IV	●			●		●		●		●		●		●			
E NOISE CALIBRATION 5	ENDUR	STD	IV	●				●		●		●		●		●					
F NOISE CALIBRATION 6	ENDUR	STD	V	●			●	●		●		●		●		●					
G NOISE CALIBRATION 7	ENDUR	STD	I	●			●													●
5 FINAL PERFORMANCE AND EMISSIONS CALIBRATIONS	PERF	STD	I	●	●							●		●		●					●
TASK 8 PRE-DELIVERY CALIBRATION (FOR INFORMATION ONLY)																					
A PRE-DELIVERY CALIBRATION 1	PERF	PERF	I	●	●																●
B PRE-DELIVERY CALIBRATION 2	PERF	PERF	V	●			●														●

● DENOTES HARDWALL CONFIGURATIONS

○ DENOTES ACOUSTICALLY TREATED CONFIGURATIONS

23-ART-3A

Figure 3-20.   QCGAT Engine Tests and Engine/Nacelle Build Configurations.

3.5.1 Design Procedure

A preliminary mixer nozzle optimization computer program, based on state-of-the-art techniques, defined the initial mixer configuration geometry. The initial aerodynamic contours of the mixer and fan duct were determined with a radial-equilibrium-flow analysis program. The mixer-lobe designs were analyzed with an advanced 3-D viscous compressible flow program. Several lobe modifications were studied based on the results of the flow analysis. The configurations were also analyzed in terms of relative mixing efficiency, using a turbulent mixing-model program. Based on the flow analysis, three mixer-compound configurations and a standard-compound nozzle were selected for scale-model testing.

Three mixing duct length variations were also selected. Model hardware was fabricated and tested. Performance and acoustic data from the model tests were recorded at the sea-level static takeoff and cruise design point conditions. A final mixer-exhaust system was selected and the scale-model mixer system was tested at selected off-design conditions in order to generate performance maps. The performance maps were then used in an engine-cycle-sizing analysis to obtain the optimum areas for the overall flight regime.

Since all of the mixer-compound exhaust system design information and the static rig model test data are covered under the Early Domestic Dissemination clause of the contract, all details of this design phase were published separately. The report is titled "QCGAT Mixer-Compound Exhaust System Design and Static Rig Model Test Report" and identified as NASA CR-135386 (AiResearch Report No. 21-2861). Authors are W. L. Blackmore and C. E. Thompson of the AiResearch Manufacturing Company of Arizona.

3.5.2 Full-Scale System

A reference nozzle with known flow coefficients and thrust coefficients was used for engine calibrations. Area inspections and calculated coefficients (based on the scale-model tests) were used to provide predicted data for the mixer-compound nozzle system. Agreement was obtained for the predicted performance with the actual engine take-off power setting at sea-level static conditions.

The mixer-compound exhaust system increased the thrust coefficient for the sea-level-static takeoff-power setting by 1.4 points relative to the reference-coannular exhaust system. This provides a 3.1-percent improvement in TSFC and a 10.6 K (19°F) decrease in T_{T5}. The test results exceeded the pretest status model predictions of $\Delta TSFC$ by -2.7%, and ΔT_{T5} by -7.2K (-13°F).

Since engine sea-level static test results verified the status model predictions, the cruise design point predicted improvement in thrust coefficient of 2.5 points should result in a 1.6-percent increase in cruise net thrust and a 3.2-percent improvement in cruise TSFC.

3.6 Component Hardware

3.6.1 Controls and Accessories

QCGAT performance (in terms of the control parameters) was generated and compared with the production TFE731-3 control capability. The TFE731 hydromechanical control system provides a back-up mode which results in engine thrust less than engine-rated thrust at some operating conditions and restricts power lever travel at others. Therefore, these limitations of the TFE731 control system in QCGAT engine operation makes peripheral attention necessary. The addition of peripheral electrical equipment would provide for manual bleed valve operation and an increase in the maximum fuel schedule, under certain conditions, when necessary. These functions are activated or deactivated depending on engine operating point. In addition to the close attention required, including the peripheral electrical equipment, rapid-transient operation would be unavailable.

Based on this analysis, the use of the TFE731-3 control system without a computer was not considered practical in terms of operating procedures.

Figure 3-21 is a block diagram of the system selected for the QCGAT Engine showing interfacing parameters and the functions assigned to the computer and hydromechanical control sections. QCGAT engine characteristics were compared with those of the TFE731-3 to determine the modifications necessary for the existing computer. This comparison showed the basic logic was satisfactory and the adjustment ranges are adequate. The only modification necessary would be changing component values, specifically, resistor changes.

The QCGAT control computer is a solid-state electronic unit providing engine-control features as follows:

(a) Engine condition input signals
(b) Starting control
(c) Power control and adjustments
(d) Transient operation limiting
(e) Control function selection
(f) Power output to fuel control
(g) Surge bleed valve control
(h) Computer monitoring and control mode switch
(i) Speed switch option
(j) Overspeed protection

40

FUNCTIONS:

— N$_2$ OVERSPEED GOVERNING
— N$_2$ GOVERNING; MANUAL
— OVERSPEED SHUTOFF
— FUEL SHUTOFF
— ELECTROMECHANICAL INTERFACE

P/L

HYDRO-
MECHANICAL
SECTION

FUEL FLOW

ENGINE

BLEED VALVE
SIGNAL

BLEED
VALVE

PCD

N2

PLA

CONTROL
COMPUTER

$I = (\frac{W_f}{P_3})^2$

OVERSPEED
SIGNAL

N$_1$

T$_{t2}$

P$_{t2}$

T$_{4.2}$

SUPPLY VOLTAGE

TC
COCKPIT

50%
SPEED
SWITCH

FUNCTIONS

— MAXIMUM FUEL SCHEDULE
— MINIMUM FUEL SCHEDULE
— GOVERNING
— SPEED SETTING SCHEDULE
— SURGE BLEED VALVE LOGIC
— ULTIMATE OVERSPEED SWITCH
— CLOSED LOOP T$_{4.2}$ LIMITING
— ENGINE THRUST AND FUEL VARIATION ADJUSTMENTS

Figure 3-21. QCGAT Control System.

41

The relationship between these major control features is illustrated in the functional diagram of Figure 3-22.

3.6.2 Lubrication System

The diagram in Figure 3-23 snows the major elements associated with the engine lubrication system, including the oil tank and cooling components. Oil is drawn from the tank by the pressure pump and is passed through the filter, and the air-oil cooler. From this cooler, oil flow is divided so that a portion is directed to the engine bearings and accessory gearbox, while the remainder is delivered to the fan gearbox. The air-oil cooler is equipped with a thermostatic bypass valve to maintain the oil at the desired temperature during cold-weather operation.

The oil pumps are housed in the accessory gearbox pump package, which contains four scavenge pumps and the oil-pressure pump. These pumps scavenge: (1) the fan gearbox and forward-engine bearings, (2) the aft-engine bearing, (3) the transfer gearbox and the mid-engine bearings, and (4) the accessory gearbox. The discharge side of the scavenge pumps connects to a common line that is routed to the oil tank.

The capacity of the scavenge pumps is greater than that of the pressure pump, to ensure good scavenge performance. Air is separated from the oil by the deaerator in the oil tank and is vented to the accessory gearbox. Suspended oil droplets are removed centrifugally from the air before the air is vented overboard through the breather pressurizing valve. This valve maintains a minimum pressure in the lubrication-system compartments to ensure proper oil pump operation at all altitudes within the engine operating envelope.

3.6.3 Electrical System

The engine electrical system includes dual ignition, an engine-mounted fuel control system, an interturbine-temperature thermocouple assembly, two monopole pickups for LP- and HP-spool operating speed, and a magnetic chip detector. A 24-volt dc starter-generator is provided for engine starting when supplied with sufficient electrical energy.

3.6.4 Accessories

The accessory-drive gearbox is located at the lower forward end of the engine and is driven by the HP rotor through a transfer gearbox. It provides two drives and mounting pads on the forward side for a customer-furnished alternator, hydraulic pump, or similar accessories. The total power available for extraction from the customer accessory drives varies from 14.9 kW (20 horsepower) at idle to a maximum of 29.8 kW (40 horsepower) at takeoff.

42
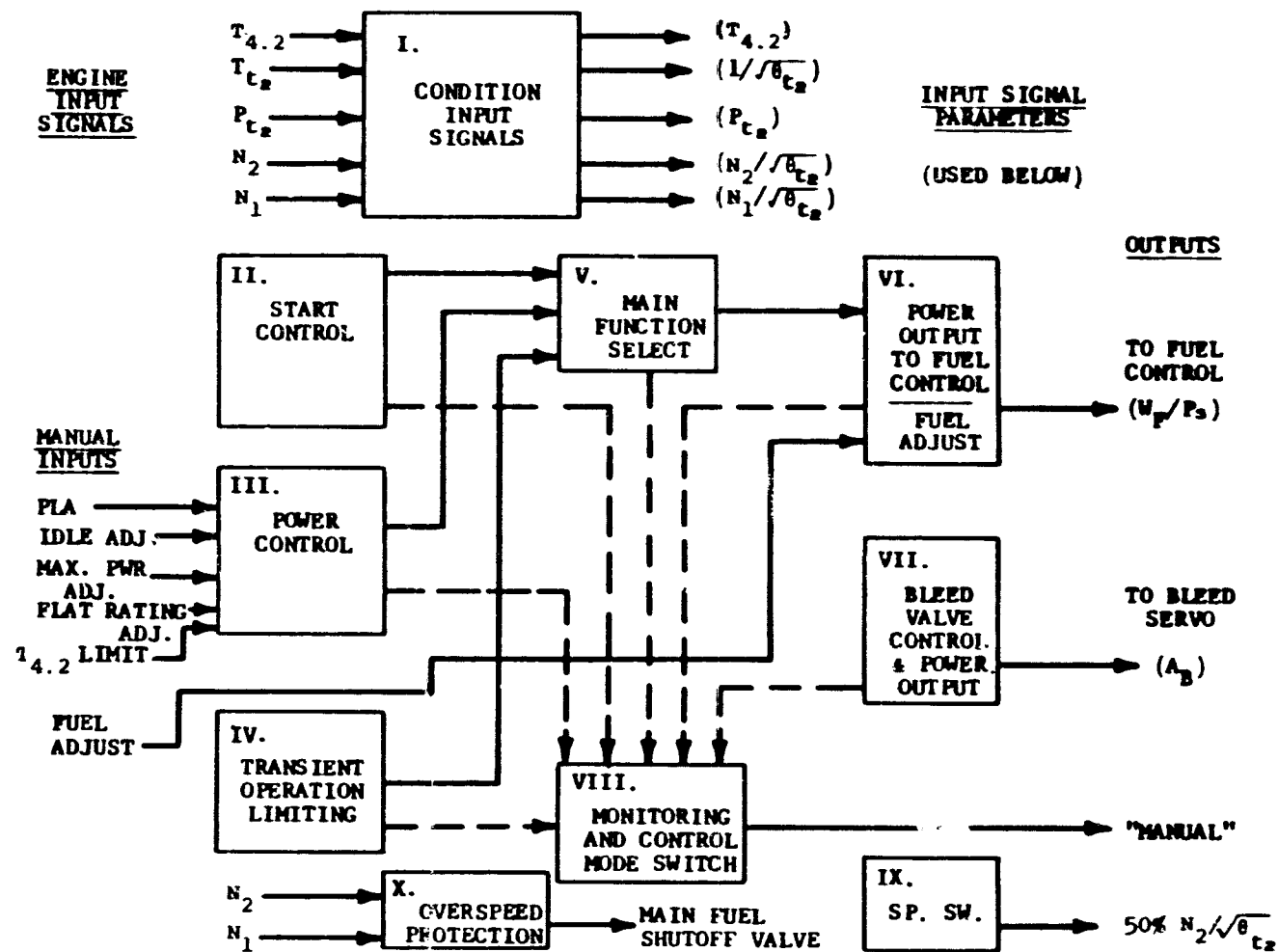
Figure 3-22. QCGAT Control Computer Functional Diagram.
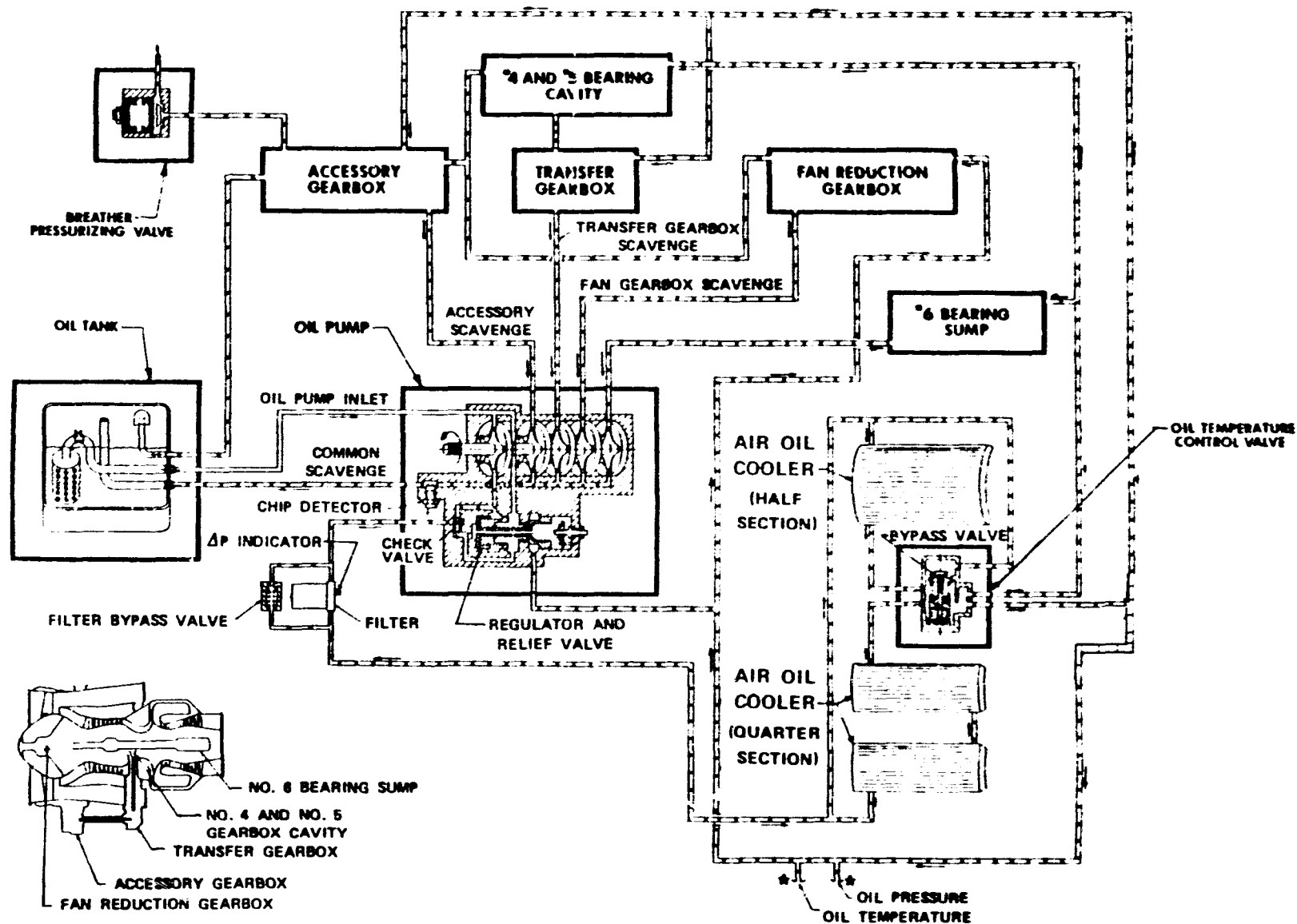
Figure 3-23. QCGAT Engine Lubrication System.

The AiResearch-furnished starter-generator is also mounted on a forward-side mounting pad.

The fuel pump supplies fuel to the hydromechanical section at the required pressure and flow. The pump is mounted on the aft end of the accessory gearbox and is driven at speeds from zero to 628.2 rad/s (6000 rpm). The two-stage fuel pump provides the mounting interface and drive for the hydromechanical section of the fuel control system.

3.7 Engine Installation

3.7.1 Engine Mounting

The basic mounting provisions are shown in Figure 3-24.

3.7.1.1 Center of Gravity

The center of gravity of the basic engine is also shown in Figure 3-24. If optional accessories are installed on the engine, the center of gravity values indicated in Table 3-8 must be used in calculating the installed center of gravity. The center of gravity location for a specific engine configuration would be shown on the applicable installation drawing. Aircraft accessories mounted on the engine should be included for calculating the installed center of gravity.

3.7.1.2 Moment of Inertia

The calculated mass moment of inertia about the center of gravity for the basic engine is tabulated as follows:

Basic Engine

$$I_{xx} = 19.6 \text{ Nm-s}^2 \ (173.5 \text{ lb-in.-sec}^2)$$

$$I_{yy} = 52.0 \text{ Nm-s}^2 \ (460.0 \text{ lb-in.-sec}^2)$$

$$I_{zz} = 46.5 \text{ Nm-s}^2 \ (411.6 \text{ lb-in.-sec}^2$$

The polar moment of inertia and direction of the major rotating masses for the QCGAT engine is as follows:

Rotating Group

High-pressure rotor	13.6 Nm-s^2 (120 cw lb-in.-sec^2)
Low-pressure rotor	0.47 Nm-s^2 (4.18 cw lb-in.-sec^2
Fan rotor	1.08 Nm-s^2 (9.60 ccw lb-in.-sec^2)
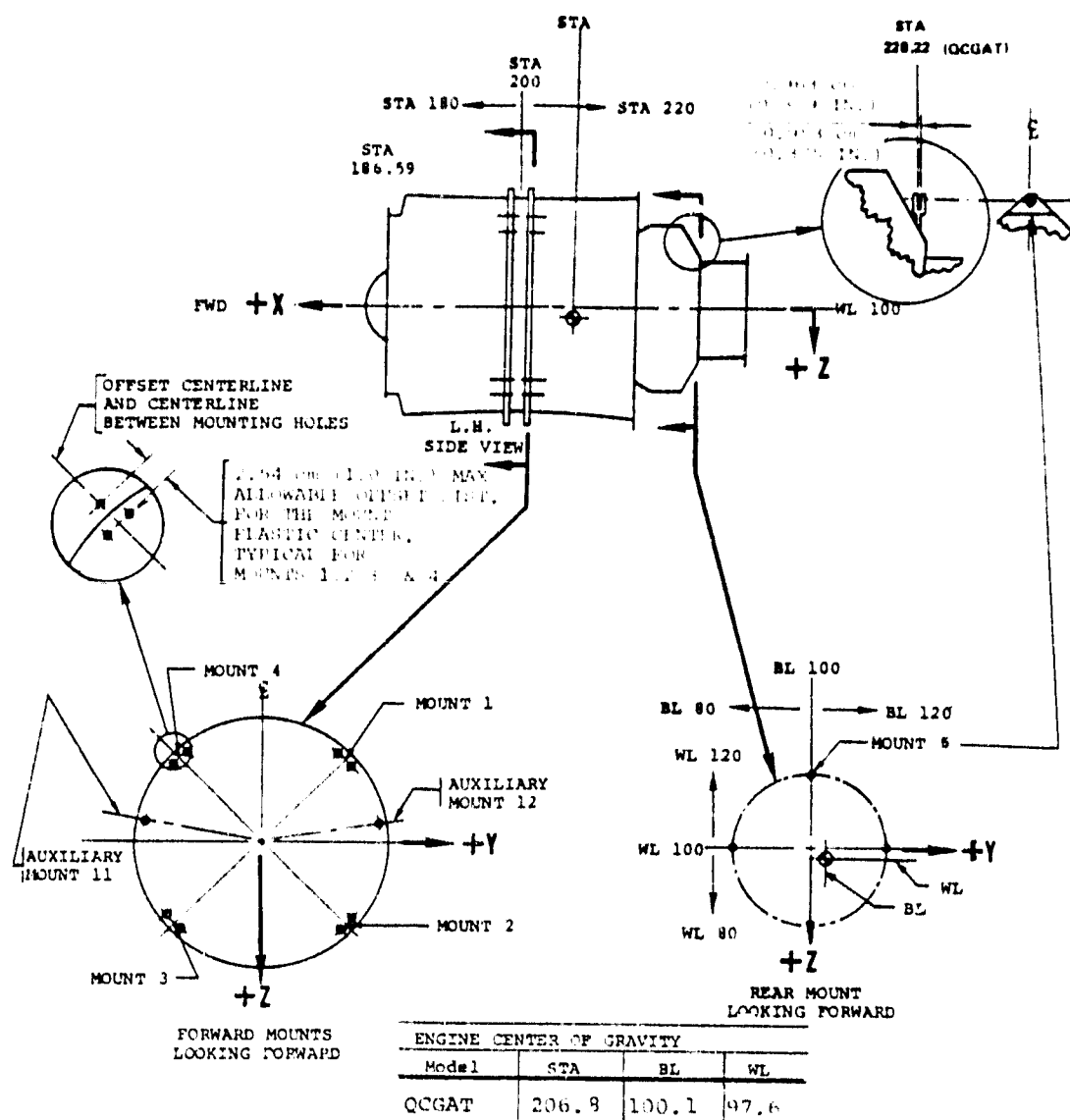
Figure 3-24.   Mounting Configuration and Basic Dry
Engine Center of Gravity.

TABLE 3-8.   ENGINE ACCESSORIES.

Item	Accessory	Maximum Weight kg (lbs)	Accessory Center of Gravity Location [1]		
			Station	Water Line	Buttock Line
1.	Air-oil cooler assembly oil-to-fuel cooler, and associated lines and valves, [2]	17.00 (37.5)	209.1	95.5	103.6
2.	Oil tank (steel) with left and right-hand fill ports, dipstick and associated plumbing [3]	5.22 (11.5)	194.4	90.2 (89.2)	112.5 (114.7)

NOTES:

[1]   To calculate the center of gravity of the final engine con-
      figuration, the incremental differences of the added acces-
      sories must be computed and algebraically added to the basic
      center of gravity shown in Table B.

[2]   If the optional air-oil cooler is not included with the
      engine, an appropriate aerodynamic fairing is required.
      This fairing is not included with the basic engine.

[3]   Note that the oil tank and plumbing weight will vary with
      installation variations, such as auxiliary fill tube length
      and other accessories that may be included. Refer to the
      applicable installation drawing.

47

3.7.2 Engine Weight

The engine weight summary is listed in Table 3-9.

3.7.2.1 Engine Dry Weight

The dry weight of the basic QCGAT engine is 380 kg (837 pounds). This weight includes the 4.67 kg (10.3 pounds) of the remotely mounted electronic computer and the weight of the standard equipment items listed in Table 3-10.

3.7.2.2 Standard Equipment

QCGAT engine standard equipment for the basic engine includes the items listed in Table 3-10.

3.7.2.3 Residual Fluids Weight

The residual fluids that remain in the engine after drainage will not exceed 1.81 kg (4 pounds) of oil and 1.36 kg (3 pounds) of fuel. Residual fluids that remain in the accessories, Items 1 and 2 of Table 3-8, after engine draining will not exceed 1.81 kg (4 pounds) for oil and 0.41 kg (2 pounds) for fuel. An installed engine filled with fluids and ready for operation will contain an additional 0.91 kg (2 pounds) of oil in the lines and sump, and 5.44 kg (12 pounds) of oil in the optional oil tank.

The accessories available for this engine, as listed in Table 3-8, must be included in calculations of the installed engine weight.

3.7.3 Nacelle Weight

3.7.3.1 QCGAT Workhorse Nacelle

The design intent of the workhorse nacelle was to provide durable and fatigue-resistant nacelle components. This was accomplished through the use of heavy-gauge sheet, plate, and bar forms that resulted in economical components. Fabrication techniques included forming, machining, and riveting. Fusion welding was not used in order to minimize distortion. The workhorse nacelle components incorporate all the aerodynamic, acoustical, and instrumentation requirements. The components also provide for easy access to the engine service areas and interchangeability of acoustic and hardwall panels with precision fits to minimize steps in the flow path. All acoustic and hardwall panels are similar in design. The difference between the hardwall panels and the acoustic panels is the substitution of a hard-face sheet for a perforated-face sheet.

48

TABLE 3-9.   ENGINE WEIGHT SUMMARY.

Component	TFE731-3 Weights kg (lbs)	QCGAT Ground Test Engine Weight kg (lbs)	QCGAT Production Flight Engine Weights kg (lbs)
Fan module	65.77 (145.0)	72.57 (160.0)	67.81 (149.5)
Star gearbox	10.88 (24.0)	14.06 (31.0)	13.15 (29.0)
Main mount and inter. case	26.35 (58.1)	31.75 (70.0)	28.12 (62.0)
Combustion system	21.77 (48.0)	39.83 (87.8*)	25.31 (55.8*)
LP turbine	25.49 (56.2)	39.00 (86.0)	39.00 (86.0)
Ring brg housing	6.94 (15.3)	10.43 (23.0)	10.43 (23.0)
Common parts	176.58 (389.3)	176.58 (389.3)	176.58 (389.3)
Total weight of power section	333.79 (735.9)	384.23 (847.1)	360.42 (794.6)
Controls and accessories	19.05 (42)	19.05 (42)	19.05 (42)
Engine Total	352.84 (777.9)	403.28 (889.1)	374.47 (836.6)

*T_1 Concept 2 System

TABLE 3-19. QCGAT STANDARD EQUIPMENT

Fuel System

    Overspeed governor

    Engine-driven pump (two-stage)

    Filter

    Metering Valve

    Shutoff valve

    Flow divider

    Nozzle manifolds

    Nozzles

    Fuel control and associated
        probes including lines

    Remotely mounted electronic fuel-
        control computer (excluding
        wiring and pressure-sense line)

Lubrication System

    Pressure pump

    Scavenge pumps

    Filter

    Pressure regulator

    Magnetic chip detector

    Oil breather pressurizing valve and vent

Ignition System, Excluding Power Source

    Dual capacitor discharge ignition
        unit capable of continuous duty

    Two ignitor plugs and shielded high-
        tension leads

Turbine Gas Temperature Sensor

    Thermocouples and an ITT $(T_{t4.3})$
        sensor harness as
        shown on the Installation
        Drawing

Instrumentation Bosses

    Oil pressure, oil temperature*, fuel
    flowmeter provisions, and fuel pump
    interstage pressure or temperature

Miscellaneous

    Spinner

    Mounting and handling provisions

    Engine inlet flane, fan duct inner
        and outer flange, and turbine
        exhaust flange connection
        points

    One high-pressure and two low-pressure
        bleed-air ports

    N_1 low-pressure rotor and N_2 high-
        pressure rotor monopole speed
        sensors

    Rotor blade containment

    Fan-tip noise attenuation

    Surge-controller system

    Gearbox and drive pads for airframe
        accessories

*Although not required for engine operation, provision for installation of fan gearbox oil-out
temperature sensing is furnished.

Figure 3-25 (Drawing 3551810) is the assembly drawing of the QCGAT engine and the Workhorse Nacelle.

3.7.3.2 Flight Nacelle

The QCGAT program required fabrication of only the workhorse nacelle. Since this assembly was for ground use, with all flight dimensions, the fabrication techniques were governed by economy rather than weight. The flight nacelle was designed in "layout" or "preliminary" form. Estimated weights of the flight nacelle and major components are listed in Table 3-11.

3.7.3.3 Total Engine/Nacelle Weight

The QCGAT Production Flight Engine and Nacelle is estimated to have a total weight of 513.27 kg (1,131.6 pounds).

Figure 3-25. QCGAT Workhorse Nacelle Assembly.

52
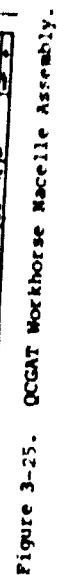
TABLE 3-11.   CCGAT PRELIMINARY FLIGHT NACELLE WEIGHT
             BREAKDOWN.

Nacelle Components	Weight kg (lbs)
Nose cowl assembly	23.1 (51)
Door assembly fan cowl	16.3 (36)
Aft fan duct	59.4 (131)

Outer barrel
    Inner
    Engine service and fount fairing	

Fan nozzle	15.4 (34)
Core mixer nozzle	19.5 (43)
Total	133.8 (295)

SECTION IV
AIRPLANE DEFINITION AND CHARACTERISTICS

4.0   AIRPLANE DEFINITION AND CHARACTERISTICS

4.1   General

The originally proposed airplane definition was based on two primary objectives: (1)   Provide for an airplane that would utilize the installed thrust of the QCGAT engine and produce a takeoff flight path that would meet the noise goals of this program; (2) Represent a viable airplane with respect to its ability to transport passengers and cargo with a fuel efficiency that would compare favorably to current business jet airplanes.

The increased thrust of the QCGAT engine, as compared with the TFE731-2 engine, was utilized to provide an airplane of the Learjet 35/36 and Falcon 10 class, and include a higher seating capacity.   The airplane definition and performance uses the QCGAT engine as described in this document.

4.2   Aircraft Performance

The airplane takeoff-gross weight and wing area have been scaled to match engine thrust changes.   Airplane parameters are shown in Table 4-1 with the engine installation losses given in Table 4-2.   The originally proposed airplane specified a total sea-level static thrust to takeoff gross weight ratio of 0.410 combined with a takeoff-gross weight to wing area ratio of 72.55. These parameters produced an acceptable acoustic takeoff flight path and good specific range cruise performance.   These ratios were retained for the March 1977 redesign.   The reduced installed-takeoff thrust of the QCGAT engine produced a reduced takeoff-gross weight as well as a smaller wing for the same takeoff flight path.

A further reduction in installed sea-level-static thrust to 16,845 N (3787 pounds) per engine (ISA 10°C), shown in Table 4-1, would necessitate a further payload reduction of 294 kg (649 pounds) in order to meet the earlier takeoff flight path. Another solution is to retain the takeoff-gross weight of 8674 kg (19,122 pounds) and reduce the takeoff thrust to weight ratio to 0.396.   This would require acceptance of reduced takeoff performance.   Table 4-3 contains the pertinent takeoff summary data. Plots of takeoff-flight paths with and without thrust cutback are given in Figure 4-1.

54

TABLE 4-1. COMPARISON OF PRESENT AIRPLANE TO PROPOSAL AIRPLANE.

Parameter	Scaled Aircraft/QCGAT Phase II (Proposal Airplane)	QCGAT Mar 77	Final QCGAT
Wing area m^2 (ft^2)	25.83 (278.0)	24.49 (263.6)	24.49 (263.6)
SLS thrust N (lb) (installed - ISA +10°C)	18,393 (4,135)	17,437 (3,920)	16,845 (3,787)
Flaps	Double-slotted	Double-slotted	Double-slotted
Flap span/wing span	0.700	0.700	0.700
SLS thrust/TOGW (ISA + 10°C)	0.410	0.410	0.396
TOGW/wing area kg m^2 (lb ft^2)	344.2 (72.55)	354.2 (72.55)	354.2 (72.55)
Capacity (crew + passengers)	2 + 14	2 + 12	2 + 12
OWE kg (lb)	4,970 (10,957)	4,790 (10,559)	4,807 (10,599)
TOGW kg (lb)	9,149 (20,170)	8,674 (19,122)	8,674 (19,122)
Max ramp wt kg (lb)	9,262 (20,420)	8,767 (19,372)	8,767 (19,372)
Max fuel wt kg (lb)	3,327 (7,335)	3,152 (6,948)	3,152 (6,948)
Max usable fuel kg (lb)	3,315 (7,309)	3,140 (6,922)	3,140 (6,922)
Max payload kg (lb)	1,413 (3,114)	1,231 (2,714)	1,231 (2,714)
Max landing wt kg (lb)	6,856 (15,115)	6,775 (14,936)	6,775 (14,936)
ZFW W/max payload kg (lb)	6,383 (14,071)	6,021 (13,273)	6,021 (13,273)
Fuel W/max payload kg (lb)	2,880 (6,349)	2,767 (6,099)	2,767 (6,099)
Payload w/max fuel kg (lb)	965 (2,128)	846 (1,865)	846 (1,865)

55

TABLE 4-2. QCGAT AIRPLANE INSTALLATION LOSSES
USED FOR TAKEOFF SEGMENT.

Parameter	Value
Inlet Ram-Pressure Recovery	0.995
High-Pressure Rotor Power Extraction	8.948 kW (12 HP)
Low-Pressure Compressor Discharge Bleed	0.0756 kg/s (10 lb/min)

TABLE 4-3. TAKEOFF PERFORMANCE OF CURRENT AIRPLANE
DEFINITION WITH MAY 1977 QCGAT ENGINE.
(SEA LEVEL RUNWAY - ISA +10°C)

Parameter	Value
Takeoff gross weight - kg(lb)	8674 (19,122)
Wing area - m^2 (ft^2)	24.49 (263.6)
Engine SLS thrust - N(lbs)	16,845 (3787)
Distance from brake release to (35 feet) in altitude km(ft)	1158 (3798)
Altitude m(ft) at a distance of 6.5km (3.5nm) from brake release	1151 (3376)
V Stall takeoff config km/hr (KIAS)	206.1 (111.3)
C_{LV2}	1.199
C_{LMAX}	1.73
V_2 + 10 KTAS km/hr (KIAS)	265.8 (143.5)

56
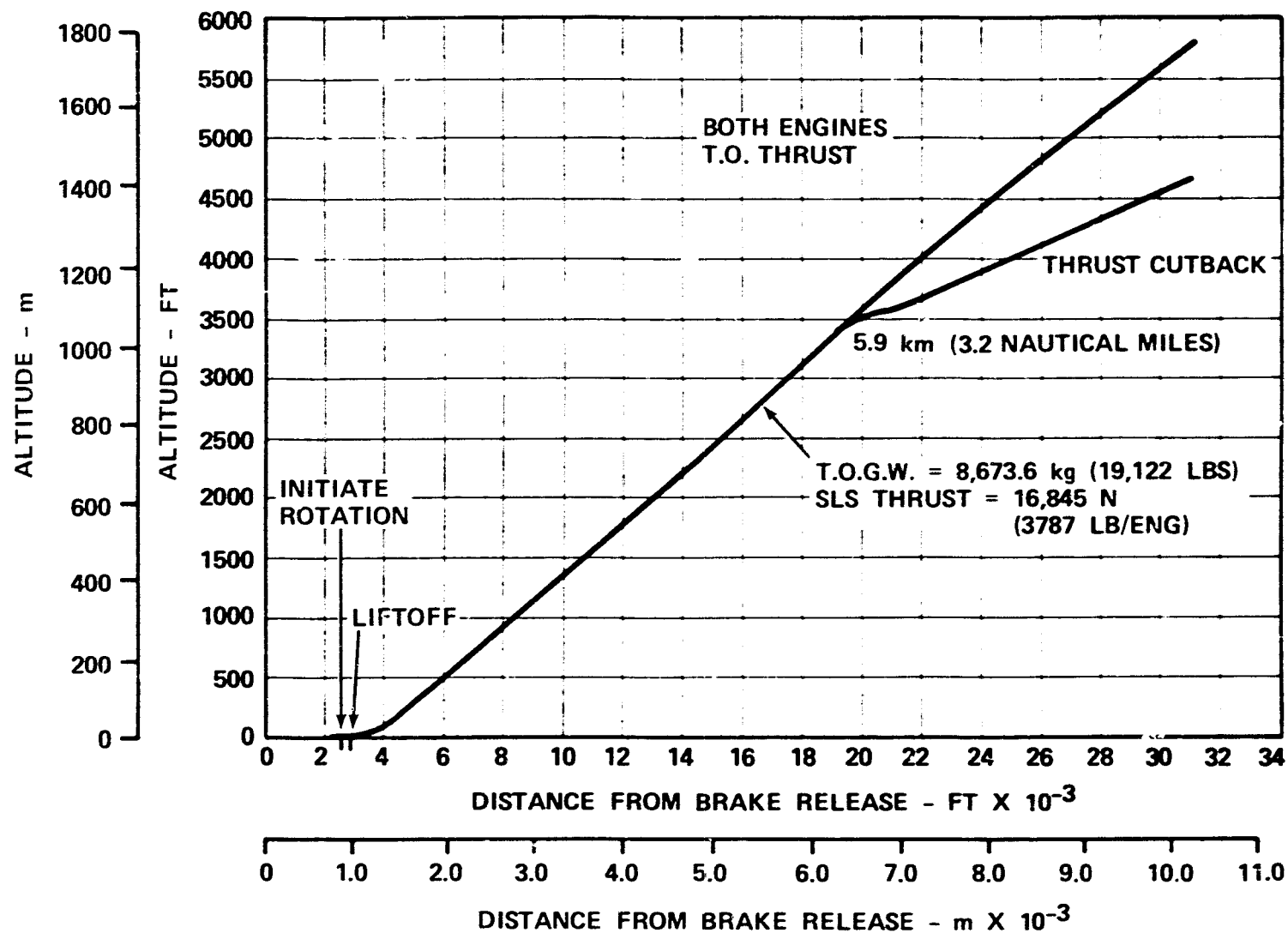
Figure 4-1. Takeoff Flight Path for Scaled Airplane/QCGAT Phase II.

The approach flight path was recalculated for a weight of 6777 kg (14,940 pounds) and the new wing area of 24.49 m² (263.6 ft²). The pertinent data is given in Table 4-4.

Specific range versus Mach number plots for several altitudes are given in Figures 4-2 through 4-9 and reflect the cruise performance of the engine with the airplane having a wing area of 24.49 m² (263.6 ft²).

The payload versus range performance of the airplane was computed and is compared with the corresponding performance of airplane/engine as given in the proposal document. This data is given in Figure 4-10 with the weight schedules given for the break points in Table 4-5.

Figure 4-11 provides a "first pass" three-view drawing of the QCGAT airplane. Further extensive improvements can also be made by increasing the wing aspect ratio and reducing the fuselage length by lowering the wing mounting relative to the fuselage so that passengers can be carried directly over the wing.

TABLE 4-4.   APPROACH FLIGHT (ISA +10°C)

Parameter	Value
Approach Flight Path rad (degrees)	-0.0524 rad (-3°)
Approach Mach Number	0.204
Approach Altitude m(ft)	112 (370)
Approach Flap Setting rad (degrees)	0.6632 rad (38°)
Approach Weight m(lb)	6777 (14,940)
Approach Thrust per Engine N(lb)	3741 (841)
Ang'e of Attach rad (degrees)	0.0227 rad (1.3)
αFRL*	0

*Angle of Attack of Fuselage Reference Line

58
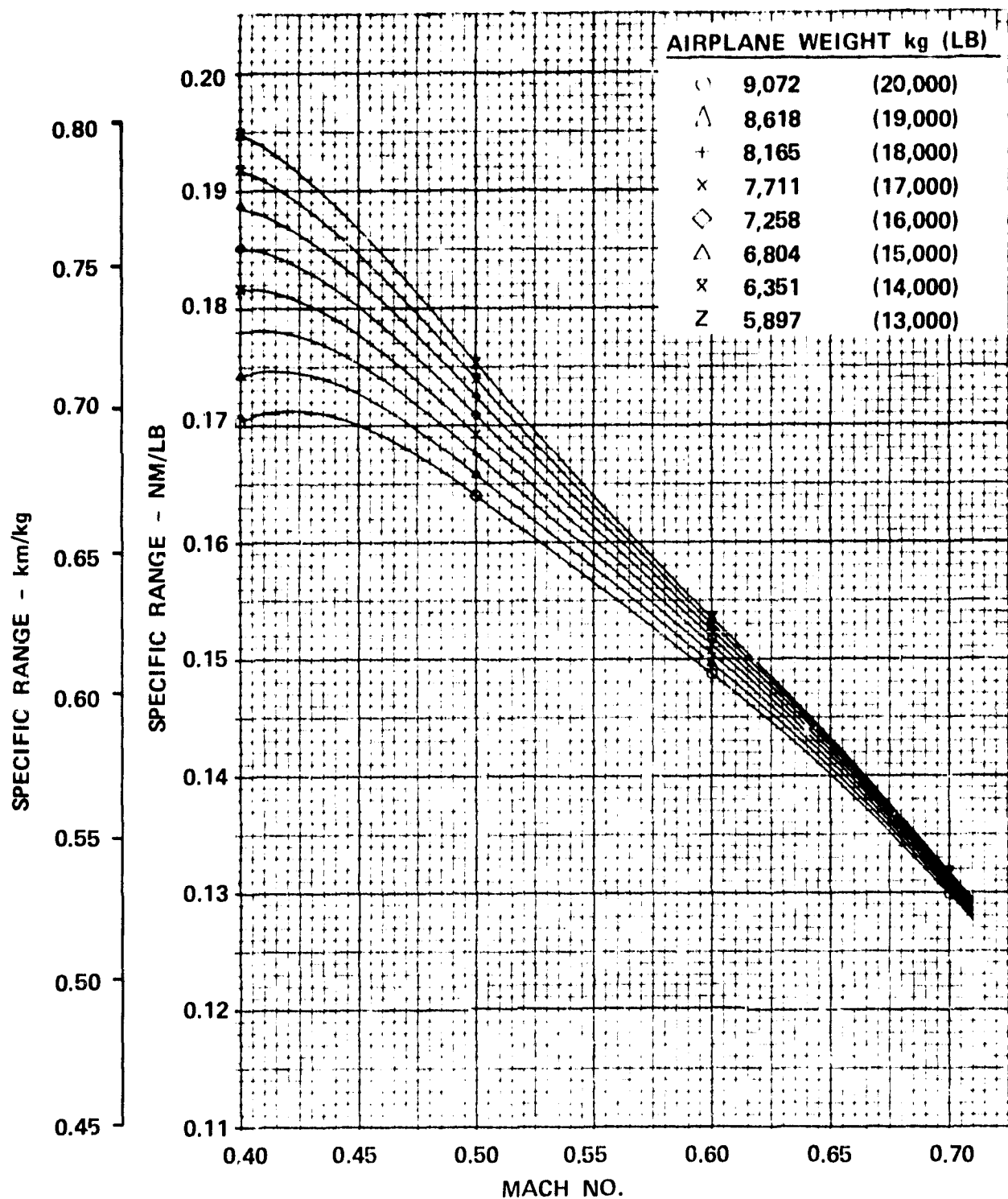
Figure 4-2. Specific Range Versus Mach No. for QCGAT-Powered
Scaled Airplane at 1,524 m (5,000 Ft) Altitude.
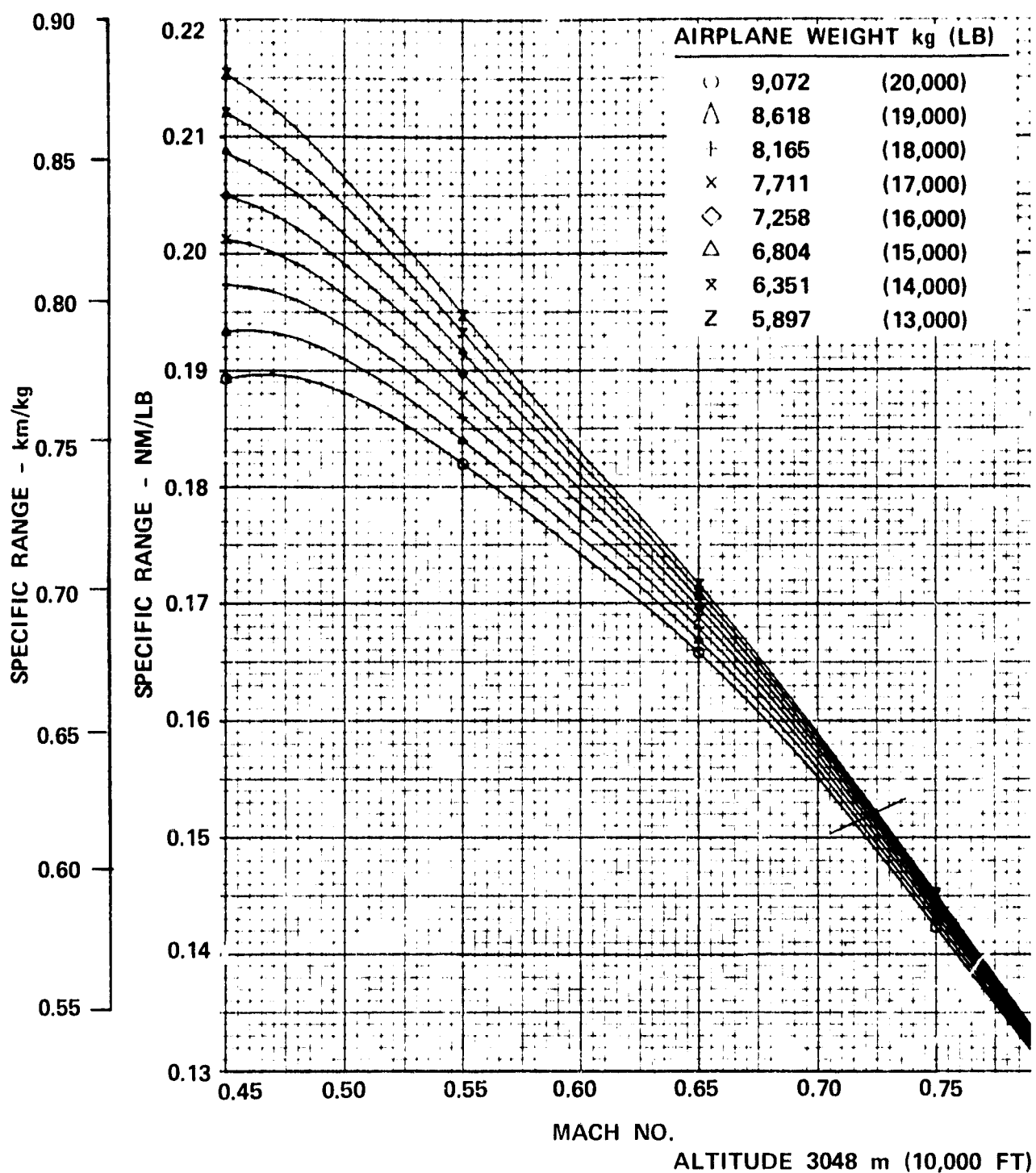
Figure 4-3. Specific Range Versus Mach No. for QCGAT-Powered
Scaled Airplane at 3,048 m (10,000 Ft) Altitude.

60
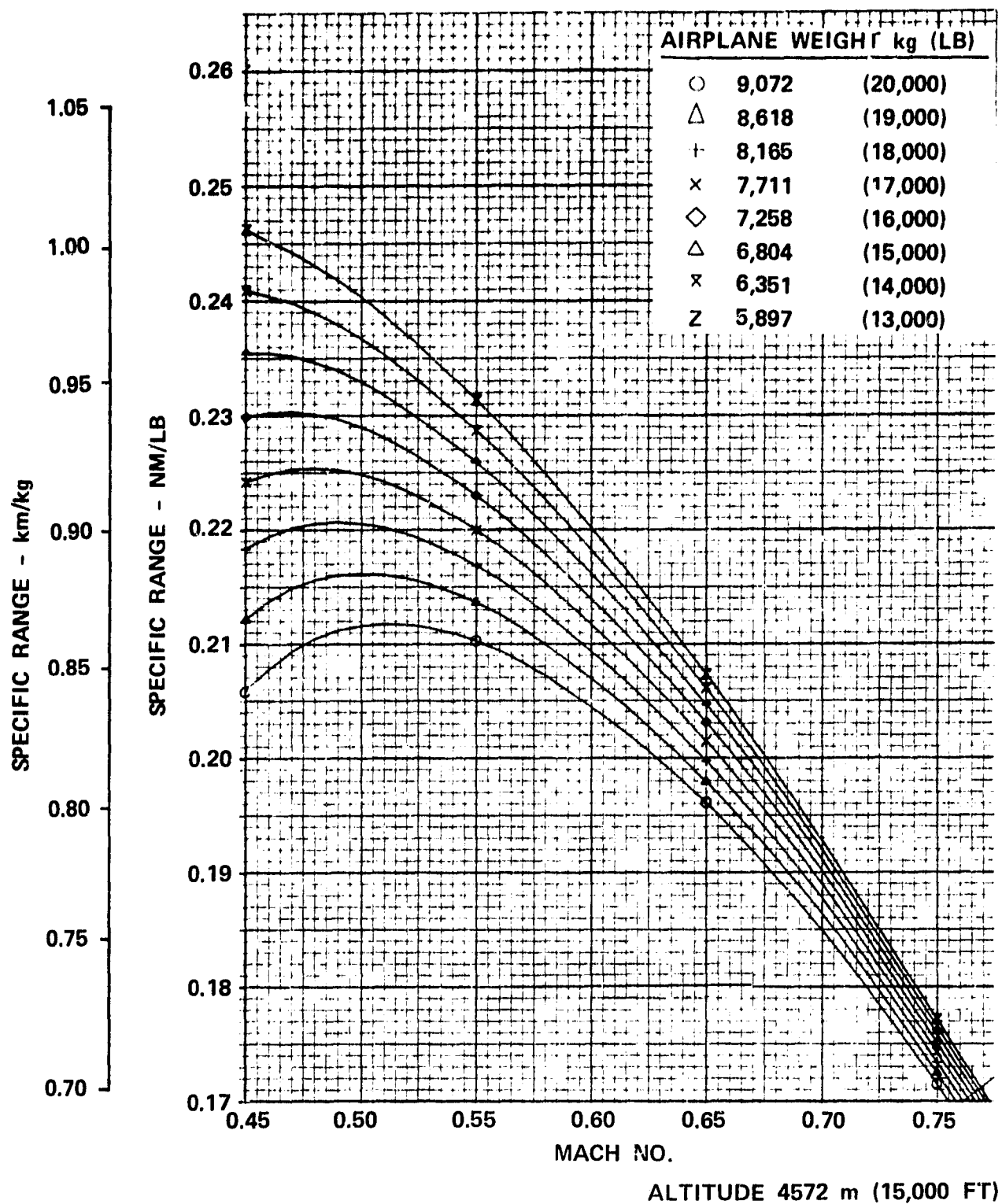
Figure 4-4. Specific Range Versus Mach No. for QCGAT-Powered Scaled Airplane at 4,570 m (15,000 Ft) Altitude.
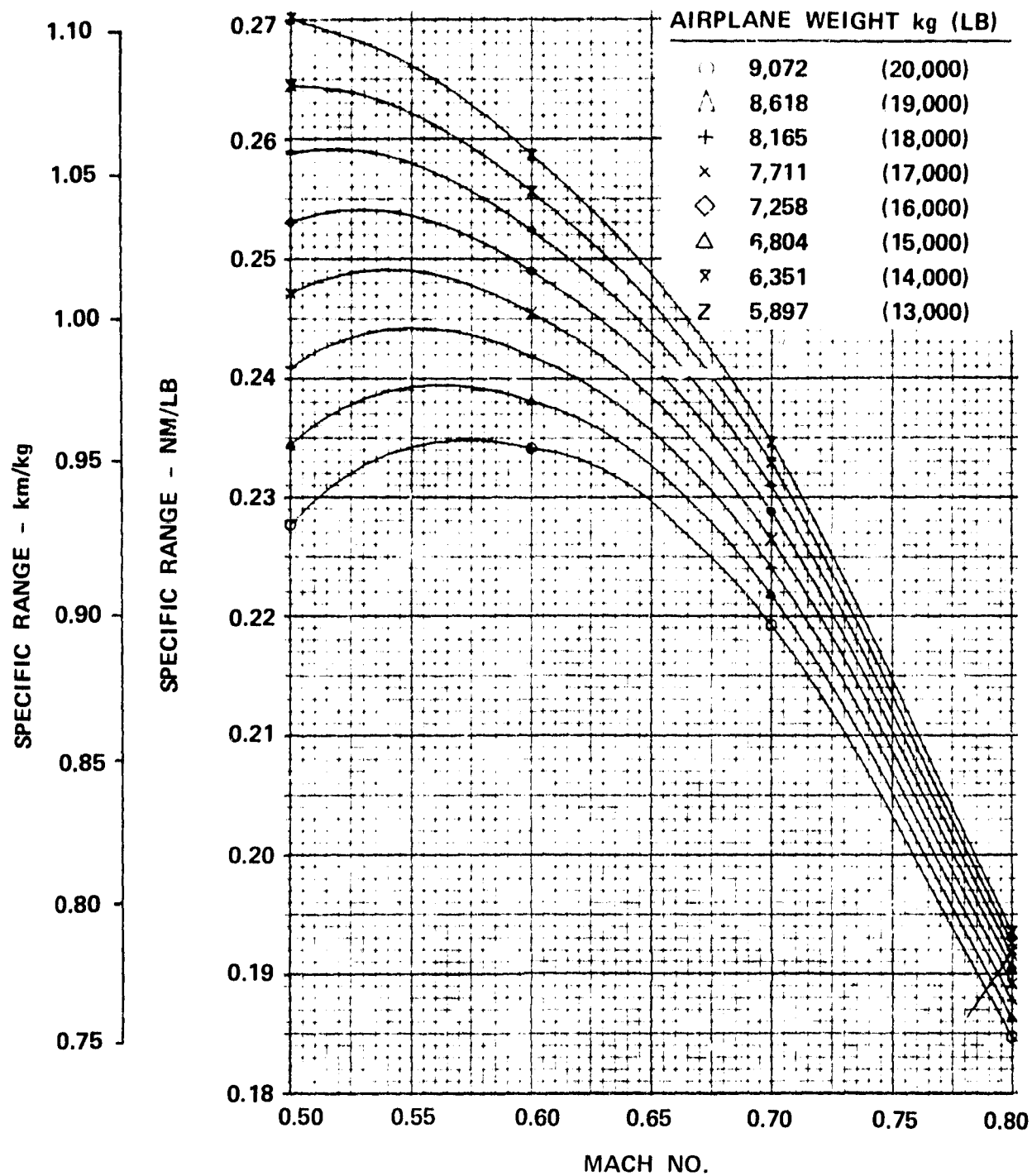
Figure 4-5. Specific Range Versus Mach No. for QCGAT-Powered
Scaled Airplane at 6,096 m (20,000 Ft) Altitude.

62
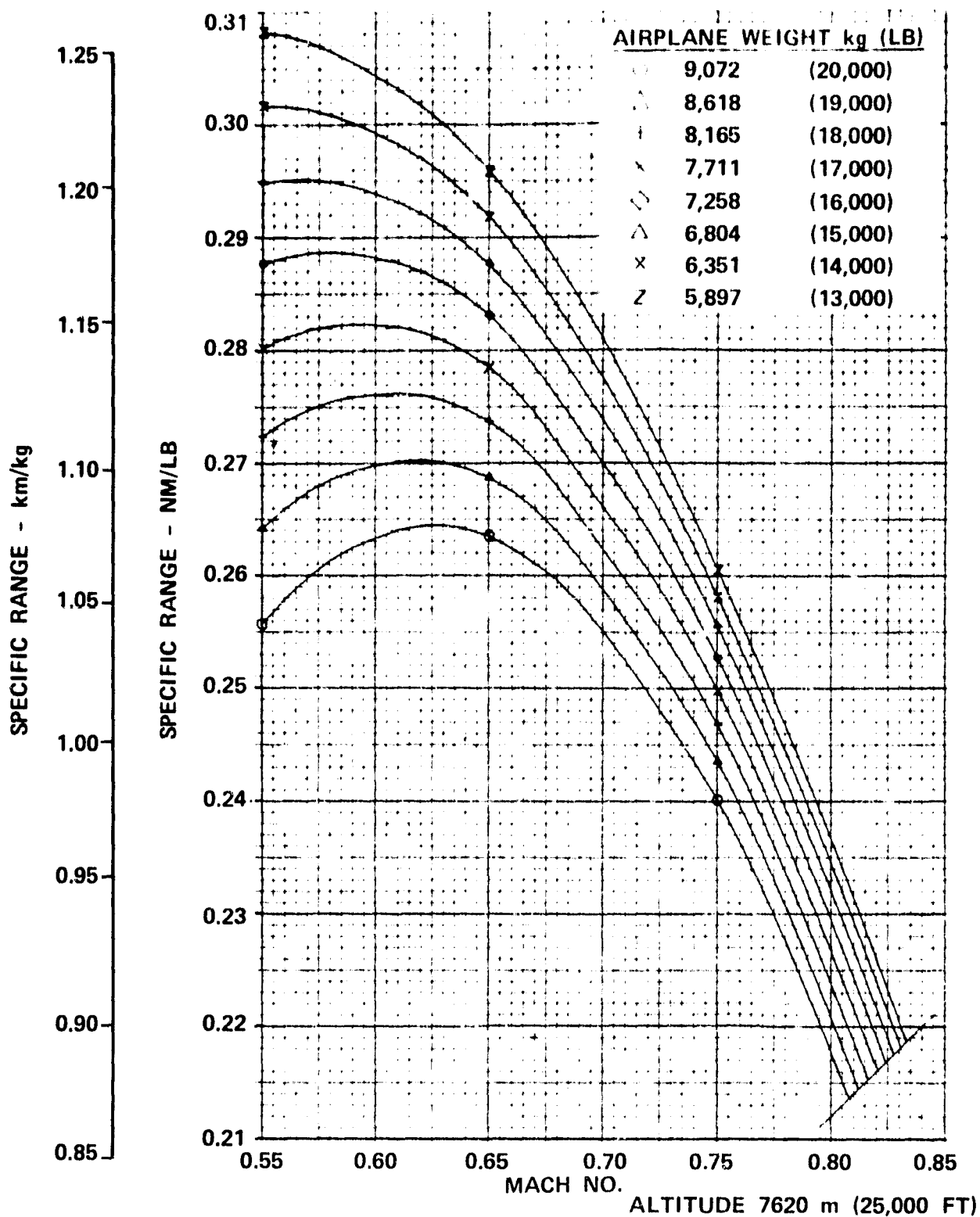
Figure 4-6. Specific Range Versus Mach No. for QCGAT-Powered Scaled Airplane at 7,620 m (25,000 Ft) Altitude.
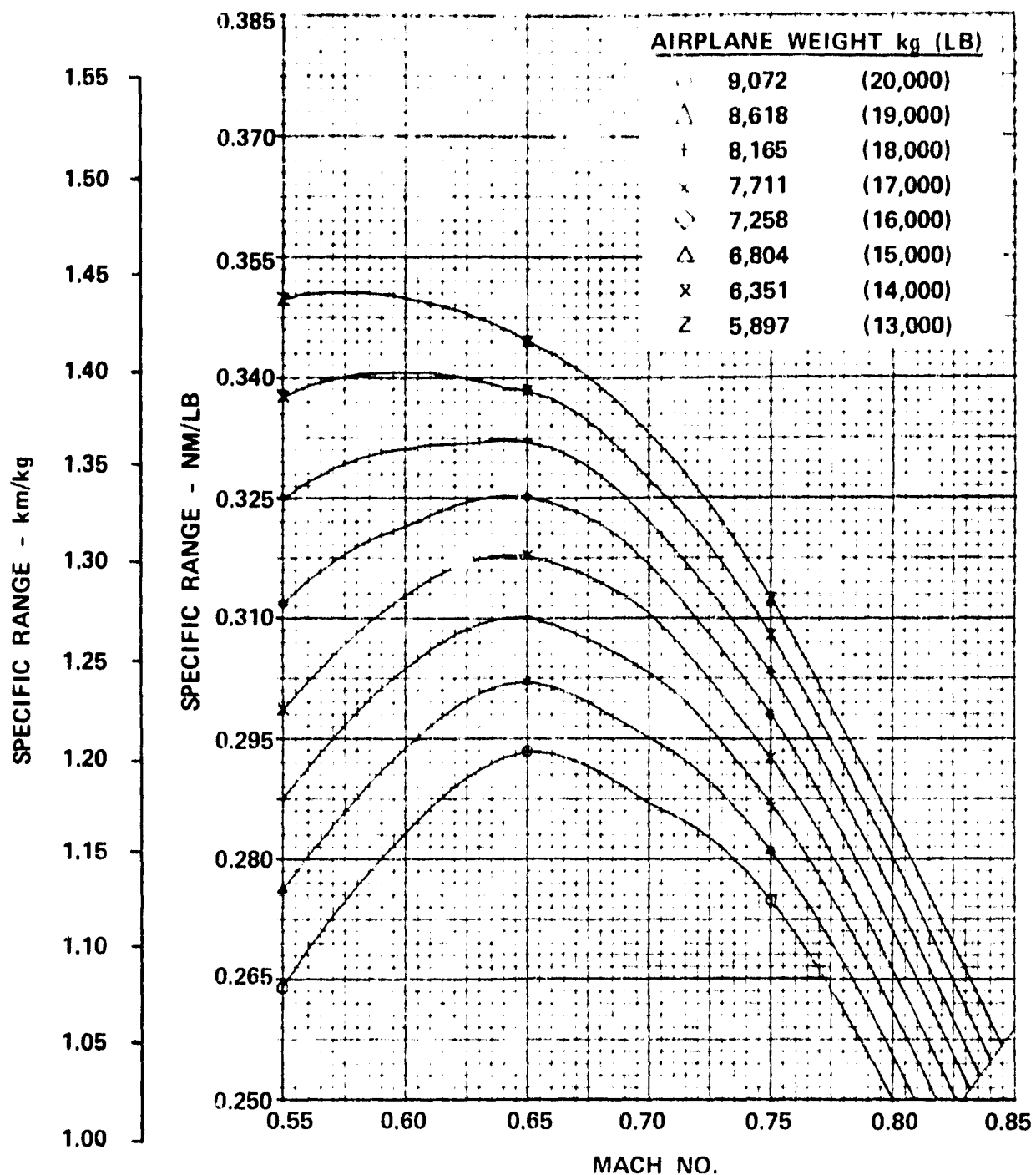
Figure 4-7. Specific Range Versus Mach No. for QCGAT-Powered Scaled Airplane at 9,144 m (30,000 Ft) Altitude.
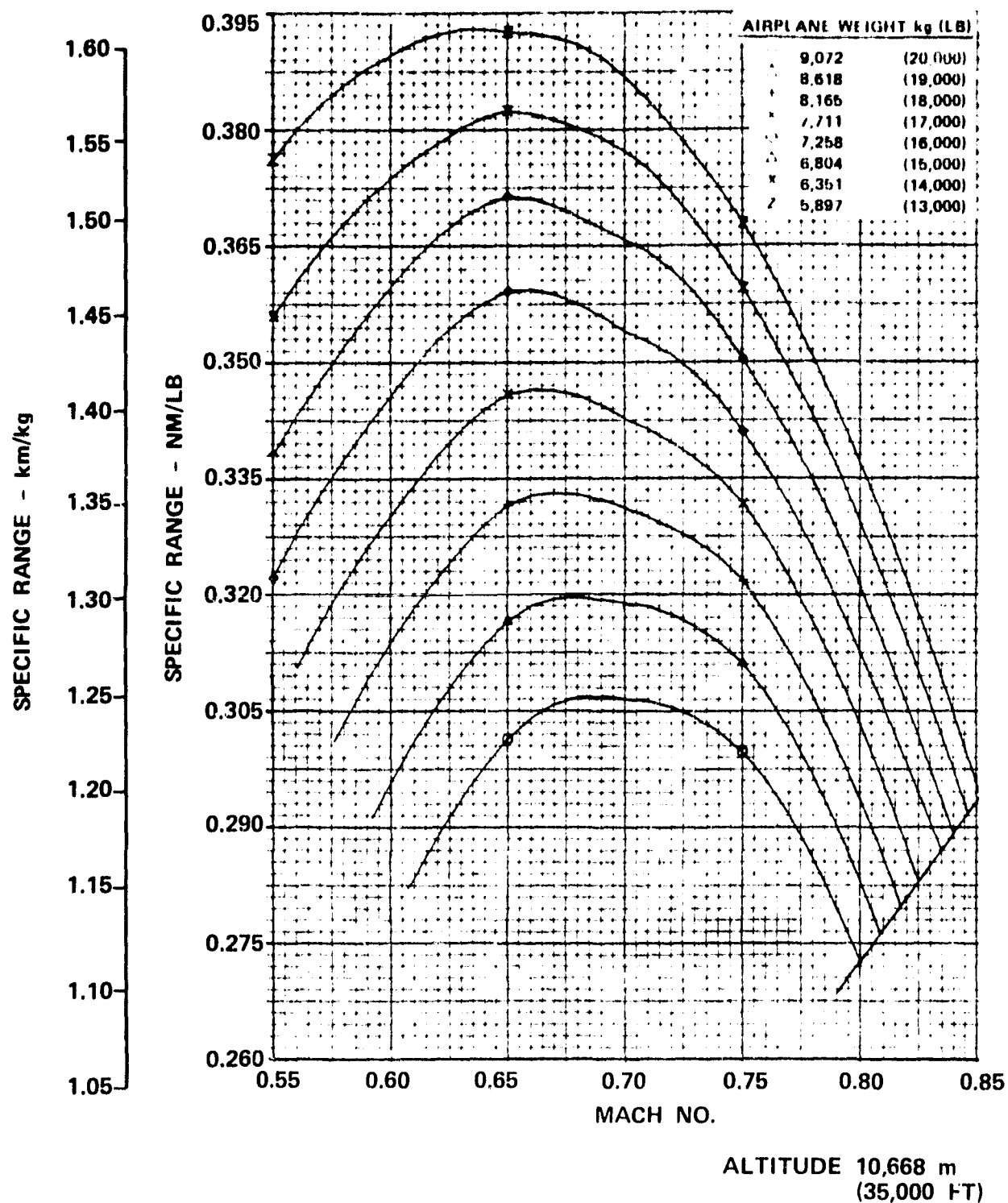
Figure 4-8.   Specific Range Versus Mach No. for QCGAT-Powered
Scaled Airplane at 10,668 m (35,000 Ft) Altitude.

65
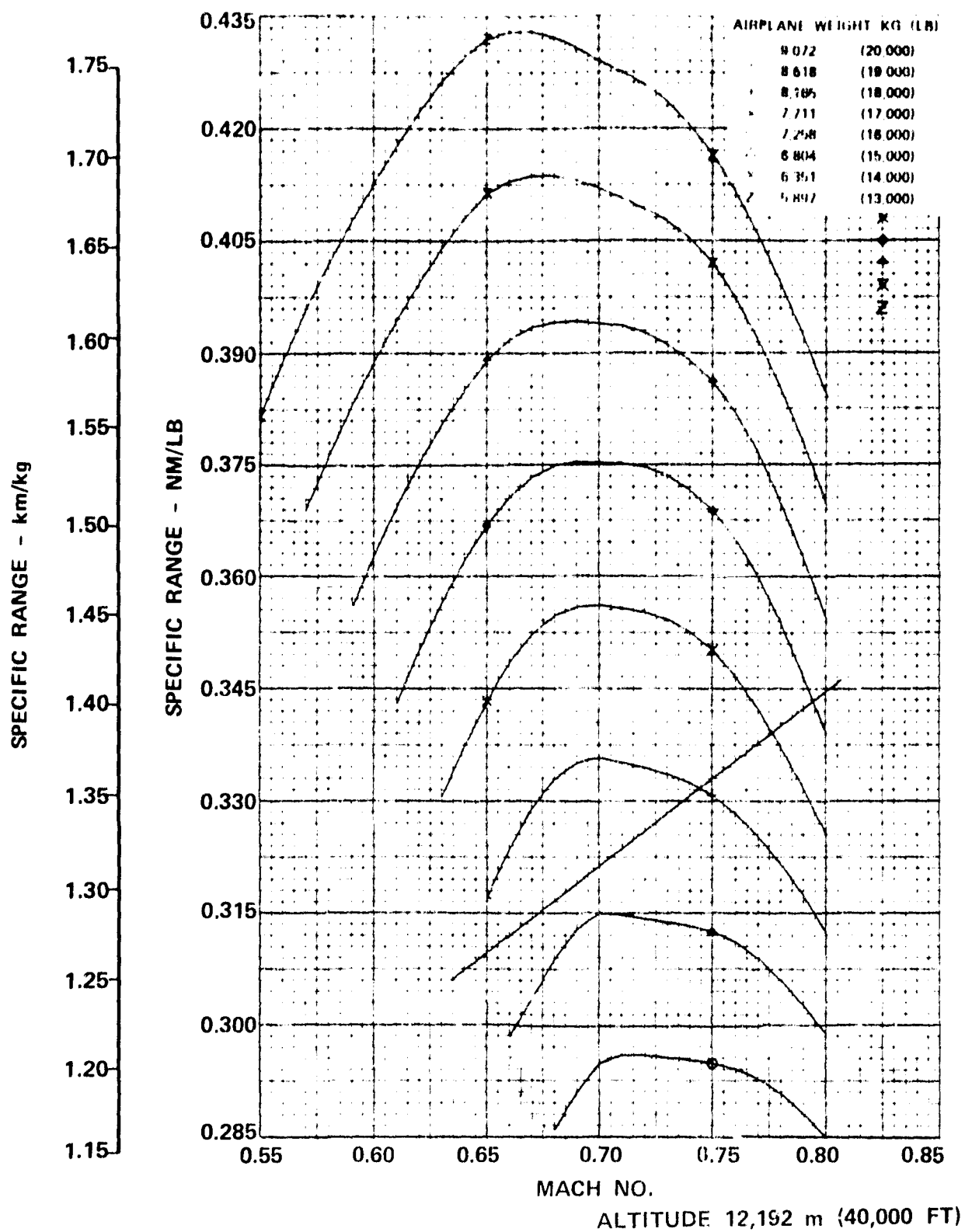
Figure 4-9. Specific Range Versus Mach No. for OCGAT-Powered
Scaled Airplane at 12,192 m (40,000 Ft) Altitude.

66
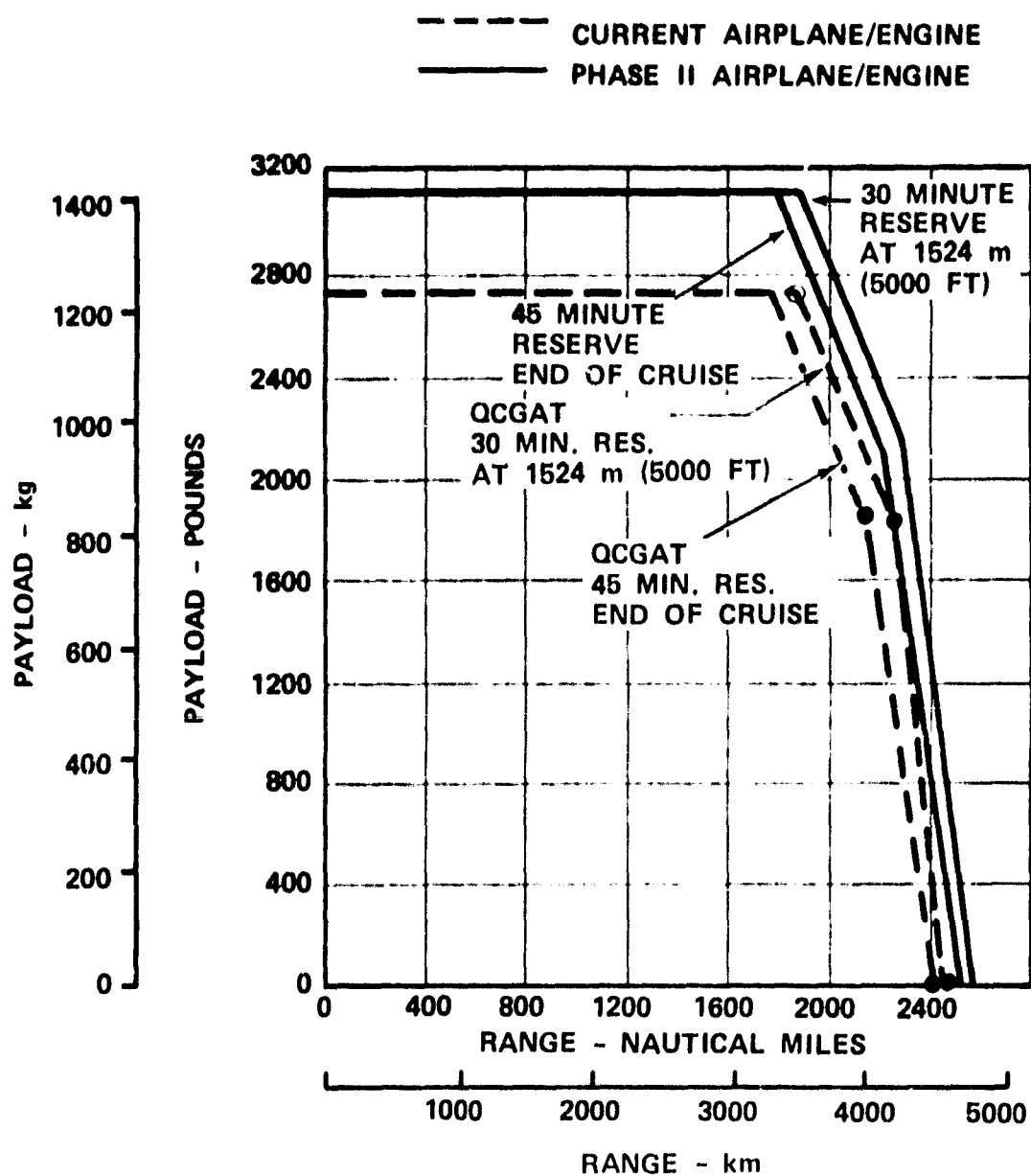
Figure 4-10. Payload Versus Range for QCGAT Powered Airplane.

TABLE 4-5. QCGAT PAYLOAD/RANGE.

Parameter	Zero Payload	Max Fuel Reduced Payload	Max P/L Reduced Fuel
Payload kg (lb)	0	850 (1865)	2714 (1231)
OWE kg (lb)	4789 (10,559)	4789 (10,559)	4789 (10,559)
ZFW kg (lb)	4789 (10,559)	5635 (12,424)	6021 (13,273)
Max fuel kg (lb)	3152 (6948)	3152 (6948)	2755 (6099)
Ramp weight kg (lb)	7941 (17,507)	8787 (19,372)	8787 (19,372)
Taxi fuel kg (lb)	113 (250)	113 (250)	113 (250)
TOGW kg (lb)	7828 (17,257)	8674 (19,122)	8674 (19,122)
Range km (NM) 30 min reserve @ 1524 m (5000 ft)	4552 (2458)	4136 (2233)	3456 (1866)
Range km (NM) 45 min reserve @ end of cruise	4463 (2410)	3993 (2156)	3295 (1779)
Cruise altitudes m (ft)	12,496/13,716 (41,000/45,000)	11,887/13,106 (39,000/43,000)	11,887/13,106 (39,000/43,000)
Cruise MACH Numbers	0.70/0.70	0.70/0.70	0.70/0.70
Beginning cruise, L/D	10.8/10.8	10.8/10.8	10.8/10.8
End cruise, L/D	10.8/10.6	10.7/10.7	10.7/10.7
Beginning of cruise, TSFC kg/N·h (lb/hr/lb)	0.073/0.075 (0.720/0.733)	0.072/0.074 (0.712/0.731)	0.072/0.074 (0.712/0.731)
End of cruise, TSFC kg/N·h (lb/hr/lb)	0.073/0.075 (0.720/0.759)	0.073/0.075 (0.717/0.740)	0.073/0.075 (0.717/0.733)

68
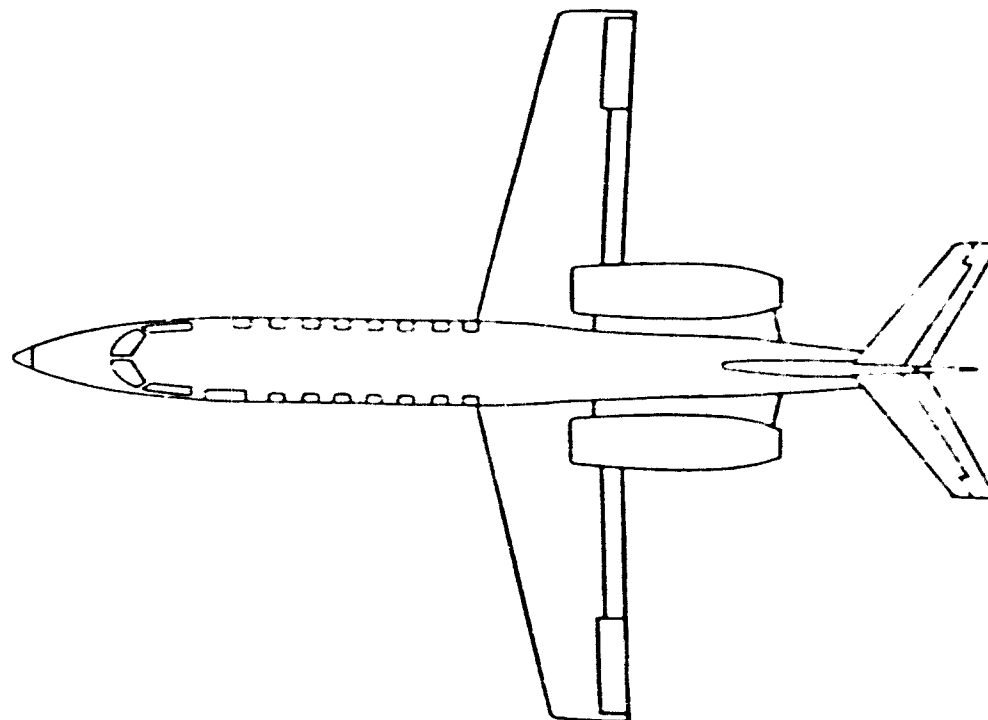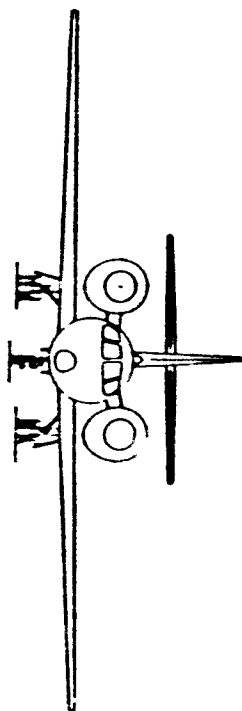
SPECIFICATIONS:

LENGTH	17.6 m (57.75 FT)
WING SPAN	12.9 m (42.5 FT)
HEIGHT	4.11 m (13.5 FT)
WING AREA	24.49 m^2 (263.6 FT^2)
MAX T.O.G.W.	8674 kg (19,122 LB)
MAX PAYLOAD	1231 kg (2714 LB)
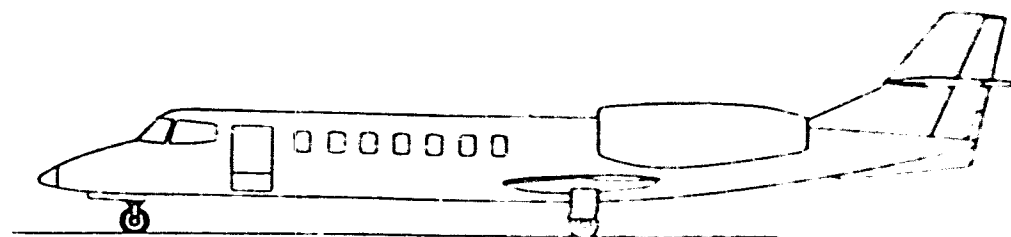
Figure 4-11. QCGAT Airplane.

5.0 COMPONENT TESTS AND RESULTS

Components of the QCGAT Engine that were tested as components included the fan blades, low-pressure turbine blade, fan gearbox and the mixer-compound exhaust nozzle.

5.1 QCGAT Fan Blades

The QCGAT fan blades are mirror images of the AiResearch Model ATF3 turbofan engine blades. Vibration frequencies and mode shapes were measured and the frequencies for the first six QCGAT-blade modes agreed with those of the ATF3 blades within three percent. Whirlpit tests and strain-gaged engine tests on the ATF3 for FAA certification have been able to verify by similarities that the QCGAT fan blades are free from harmful vibrations in the engine operating range.

5.1.1 Fan Blade Test Setup and Procedure.

Vibration tests of the QCGAT fan blades included measuring vibration frequencies and mode shapes using holographic techniques. Piezoelectric pickups were mounted on the blade at the leading-edge tip, root, and midspan. The driver was mounted at the base of the blade. The blades were maintained at room temperature for all tests.

5.1.2 Fan Blade Test Results

A summary of the results and the comparisons to the Model ATF3 blade is given in Table 5-1. A typical blade response is shown in Figure 5-1.

5.1.3 Fan Blade Test Conclusions

The frequencies for the first six QCGAT vibration modes agree with those for the Model ATF3 blades within three percent (see Table 5-1). There is also good agreement in mode shapes as shown in Figure 5-1. These results verify that the QCGAT fan blade has nearly identical vibrational characteristics to those of the Model ATF3 fan blade.

Based on the strain levels observed during the preliminary tests on the Model ATF3 fan blades and the accumulated Model ATF3 engine run time of over 1000 hours (including manned aircraft test flight hours), all evidence indicates that the blade stress levels are satisfactorily low throughout the engine operating range. The engine run time has included operation at altitude, with distorted inlet conditions, actual flight time and routine endurance running to a simulated business-jet mission profile.

TABLE 5-1. COMPARISON OF QCGAT AND MODEL ATF3
FAN BLADE VIBRATION RESULTS.

| Mode | Frequency (Hz) | | Percentage Difference |
	QCGAT	ATF3	
1	124	120	+3.0
2	446	437	+2.0
3	780	762	+2.0
4	972	996	-2.0
5	1790	1794	-0.2
6	2162	2188	-1.0

Since the QCGAT fan blades have practically the identical
vibrational characteristics when compared to the Model ATF3 fan
blades, there is a very high confidence level that the QCGAT fan
blades are also free of any harmful vibrations in the engine
operating range. Based on this information, the fan blades are
adequate for the QCGAT engine applications.

5.2 LP Turbine Blades

The QCGAT low-pressure turbine blades (LPT blades) were
designed specifically for the QCGAT application). Natural fre-
quencies and mode shapes for the three stages were evaluated for
both restrained and non-restrained tip-shroud boundary con-
ditions. Natural frequencies were determined by electronic com-
parison of blade displacement response and input drive. Measured
frequencies were verified by time-average holographic techniques
in which mode shapes were photographically recorded for comparison
with those predicted by the design analysis. Estimates of blade
frequencies at engine operating conditions were made based on the
frequencies measured and analytical corrections for temperature
and rotational speed.
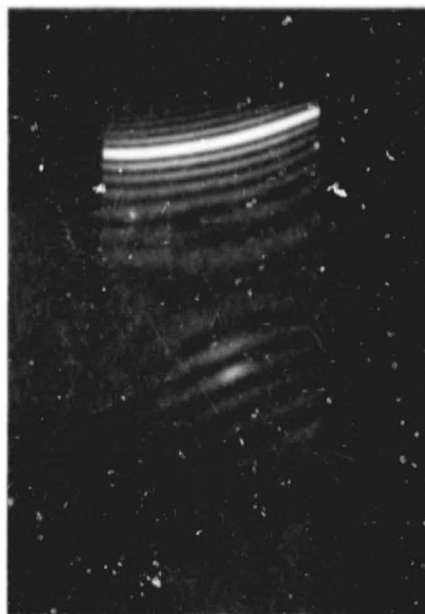
QCGAT
FAN BLADE
780 Hz
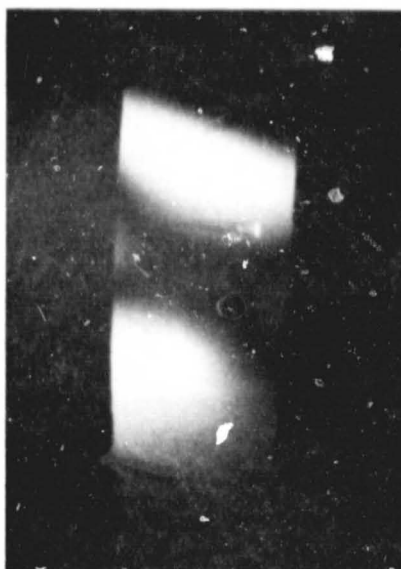
ATF3
FAN BLADE
762 Hz
1/16 AMPLITUDE

Figure 5-1.   Mode 3 Comparison of QCGAT and ATF3 Fan Blades.

MP-63916

The results of the restrained tip-shroud measurements are representative of the blades during engine operation. Contact with adjacent blades will occur at low speed even with adverse blue-print tolerance conditions. Estimated frequencies based on these measurements indicate the possibility of interference of the lower modes of the second and third stages with low-integral order excitations.

5.2.1   LPT Blade Test Setup and Procedure

The fixturing used in the testing provided restraint to the blade attachment and permitted restraint of the blade at the tip-shroud contact surfaces. The pretwist of the blade, resulting from the shroud restraint, was measured by a dial indicator at the pressure-side trailing-edge corner of the shroud. A holographic setup was used to assess mode shapes.

Drive was supplied to the blade by a crystal gauge loated on the suction side of the blade at approximately two-thirds span. Response of the blade was measured by an inductance (Bentley) probe. The probe was positioned on the suction side, trailing edge near mid span of the blade. A photograph of the typical restrained and non-restrained set-up for the blades is shown in Figure 5-2.

The blade to be tested was installed in the test fixture with only the attachment restrained. The crystal gauge was then energized and a scan of blade-displacement response from 100 to 20,000 Hz made. The input voltage to the driver and the displacement response, as measured by the Bently probe output voltage, were displayed on a dual-beam oscilloscope. Frequencies at which blade response peaked were noted. The response frequency was compared to the input frequency to assure that the response was not a harmonic of the input. Holograms were then taken at the peak response frequencies.

Restraint at the blade tip was then added by applying a pretwist type load to the tip shroud. The frequency span and hologram photography were then repeated. This procedure was employed for each of the three stages.

5.2.2   LPT Blade Test Results

Two types of data were taken during the testing; the response frequency as indicated by blade-displacement response, and photographs of the holograms taken at those frequencies.

The frequencies measured during the testing were utilized with the analytic predictions to provide an improved assessment of the vibratory characteristic of these blades under engine operating conditions. The measured mode shape, hologram, and the
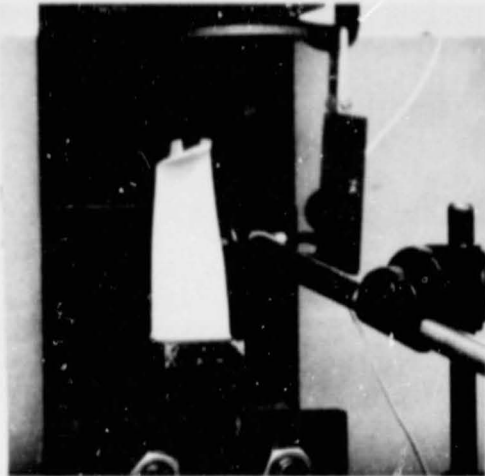
FIXTURING WITHOUT SHROUD RESTRAINT

CRYSTAL DRIVER PLACEMENT
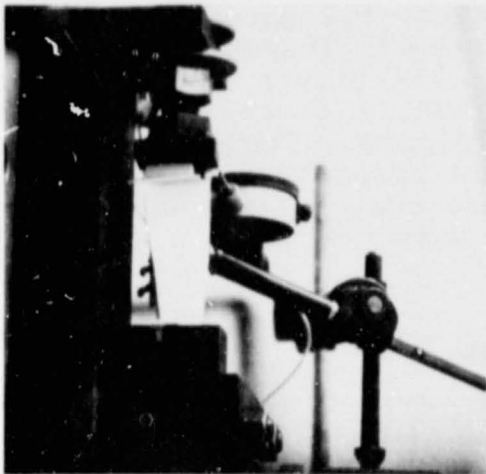
FIXTURING WITH SHROUD RESTRAINT
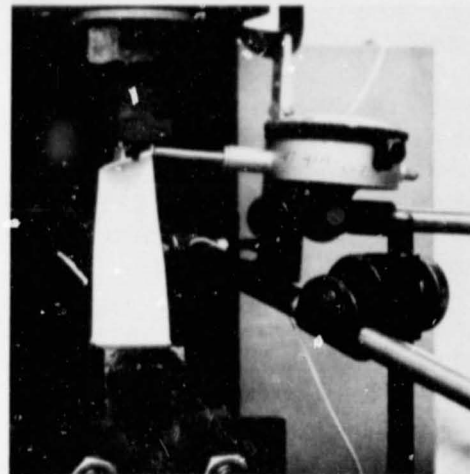
Figure 5-2. QCGAT Blade Fixturing for Frequency Testing (Second Stage LPT Blades).

MP-69429

analytic mode shape were compared to assess correlation. When a match on mode shape was obtained, the calculated centrifugal stiffening was used together with the measured frequency, adjusted for temperature, to predict the operational frequency of the blade for that mode. For measured frequencies higher than those predicted, the centrifugal stiffening was estimated from the mode shape. A typical predicted plot and photograph of actual mode conditions are shown in Figure 5-3.

The interference diagrams generated indicate possible interferences of the predicted frequencies with possible excitation sources within the operating range of the engine. Of these possible interferences, the most likely to result in problems are the lower two modes of the second and third stages with low integral order excitations.

5.2.3 LPT Blade Test

The results of these tests indicate the possibility of interference of the lower modes of the second- and third-stage LPT blades with low-integral order excitations. The engine has accumulated over 77 hours of operation at various rotor speeds including maximum power. An FOD inspection was conducted after 69 hours of operation. This inspection indicated no potential blade vibration problems. In the absence of any strain-gauge testing, careful inspection of the rotor blade should be conducted at each major engine disassembly.

5.3 Fan Gearbox

The fan gearbox tests were conducted to determine the magnitude of the heat generation and the effects that various oil flow rates, oil inlet temperatures, and gearbox speeds have on heat generation.

5.3.1 Fan Gearbox Test Setup and Procedure

The QCGAT fan gearbox and test fixture are shown schematically in Figure 5-4. The heat generation of the unloaded gearbox was measured by establishing a constant oil-flow rate through the gearbox and then increasing the speed from 0 to 20,700 rpm at given intervals. Data was taken at 0, 5,000, 10,000, 15,000, and 20,700 rpm and then repeated at the same intervals while decreasing to 0 rpm. Two oil flow ranges (3 and 5 gpm) were run at all speeds, and three oil inlet temperatures (175, 225, and 260°F) were run at the 5 gpm flow rate. A 25 horsepower U.S. varidrive system was used for the drive power.

Heat generation of the fan gearbox was calculated by two methods:
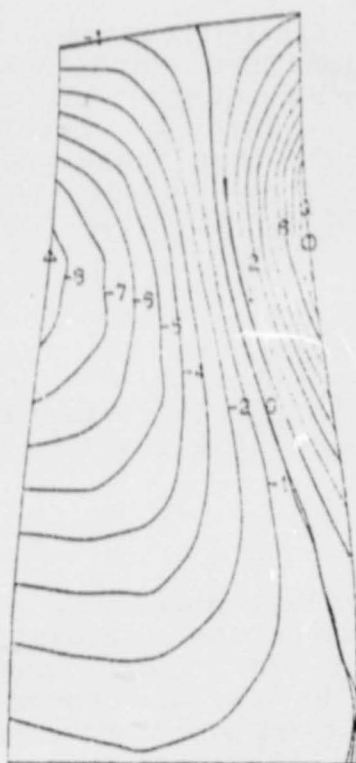
PREDICTED

MODE 2 f = 7390 Hz
NORMAL MODE SHAPE

MODE 1 f = 4910 Hz
NORMAL MODE SHAPE

ACTUAL

f = 3680 Hz   f = 4929 Hz   f = 6340 Hz   f = 6889 Hz

Figure 5-3.   QCGAT First-Stage Turbine Blade Static
               Frequencies with Shroud Restraint.

76

MP-69428
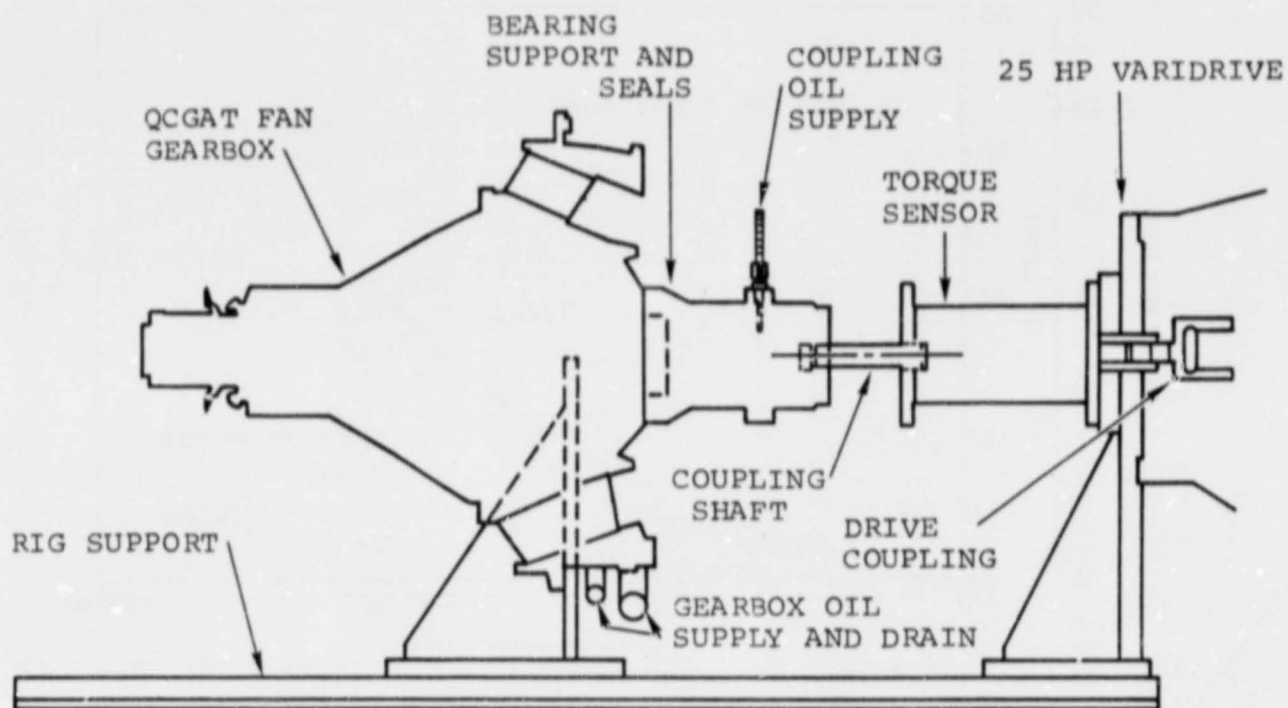
Figure 5-4. Test Rig and Gearbox Setup.

The first method used the drive torque and shaft speed to calculate the gearbox input horsepower. This value was assumed equal to the losses of the gearbox bearings, seals, and gears.

The second method used the temperature rise in the oil, supplied to the gearbox, and oil-flow rate to calculate the power loss. The gearbox was insulated to minimize the effects of heat loss from the oil system to the surrounding atmosphere. During the rig testing of the TFE731 gearbox in 1971, only this method was used because of torque meter instrumentation problems which have since been resolved. In the QCGAT test, the oil ΔT method gave lower heat generation values than the drive-torque method and was not as repeatable. Therefore, the higher and more consistent values of the drive torque and speed method were used for the QCGAT fan gearbox evaluations.

5.3.2 Fan Gearbox Test Results

Some heat generation values are shown in Figure 5-5 as a function of rig speed. Comparable values of the TFE731 fan gearbox are shown where applicable.

77
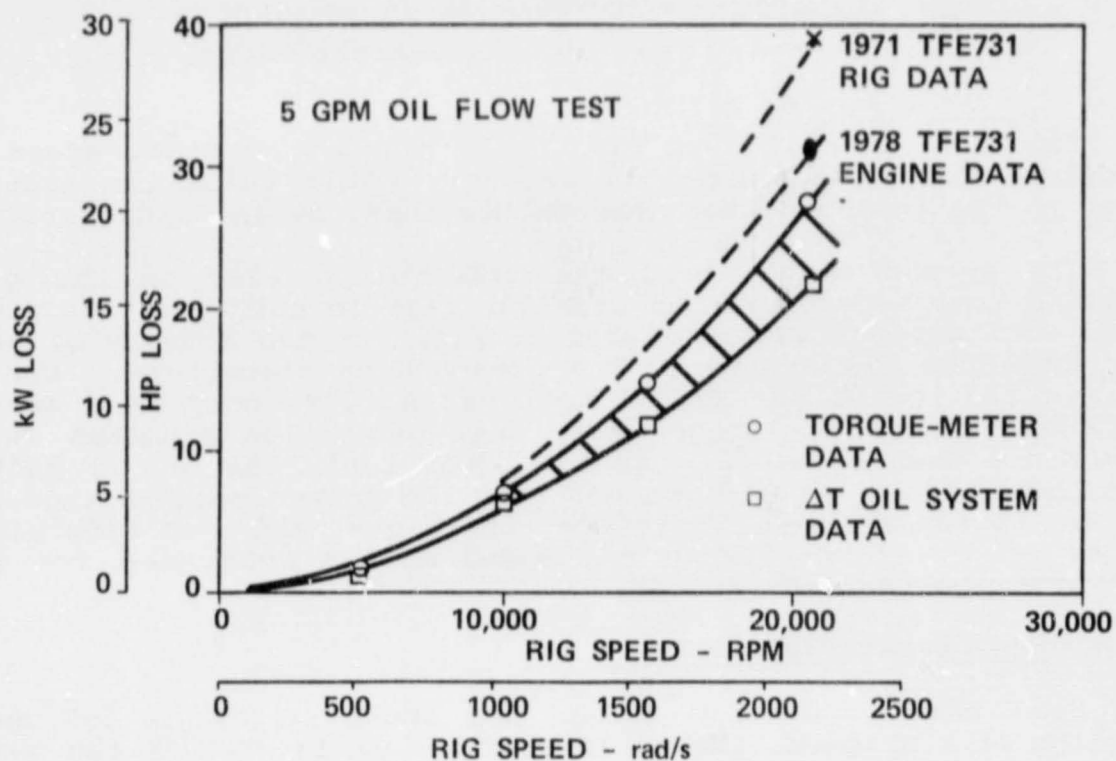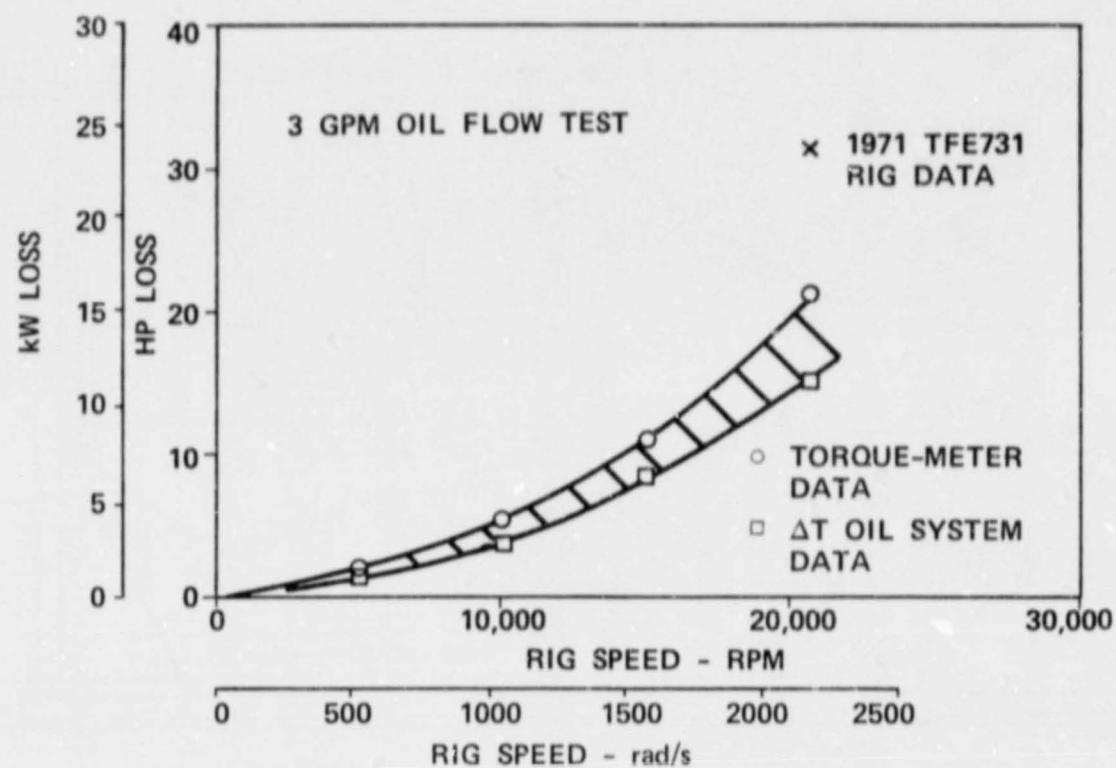
Figure 5-5. QCGAT Fan Gearbox Power Loss Comparison.

Comparison with the TFE731 fan gearbox was based on both engine data and rig data.

5.3.3 Fan Gearbox Test Conclusions

The heat generation values of the QCGAT fan gearbox assembly were lower than that of the TFE731. Variations of the heat generation with oil flow and oil temperature were as expected, and agreed with current analytical procedures and available comparable test data. These results verify that the QCGAT fan gearbox will have less heat generation than that of the TFE731 fan gearbox.

5.4 Mixer-Compound Exhaust Nozzle

The mixer-compound exhaust nozzle was tested as a 0.35 scale model. As previously mentioned, static-rig-model test data are covered under the Early Domestic Dissemination clause of the contract, all details of this test were published separately. The report is titled "QCGAT Mixer-Compound Exhaust System Design and Static Rig Model Test Report" and identified as NASA CR-135386 (AiResearch Report No. 21-2861). Authors are W. L. Blackmore and C. E. Thompson of the AiResearch Manufacturing Company of Arizona.

SUBSYSTEM TESTS AND RESULTS

6.0   SUBSYSTEM TESTS

No subsystem tests as such were conducted for the QCGAT engine. It was originally planned to bench check only the controls and accessories as subsystems prior to installation on the engine. However, it was subsequently decided to perform those tests as a part of the initial engine checkout. This decision was made because the controls and accessories were identical with TFE731-3 equipment and that is accepted procedure for the TFE731 production engines. Therefore, the control functions were checked as a part of the engine "green run" that is covered in Section 7.0 of this report. Since the only QCGAT accessory is the starter-generator, its operation was checked during later engine testing.

ENGINE/NACELLE SYSTEM TESTS

7.0   ENGINE/NACELLE SYSTEM TESTS

7.1   Engine Tests

The basic engine configuration, without acoustical treatment and without nacelle hardware, was tested to obtain a base-line performance rating. An overall schedule of the various tests performed, and a schematic drawing of the engine and system configuration used for each test was previously shown in Figure 3-20.

Builds 1 and 2 were tested as basic installation configuration I for the Green Run/Pre-endurance tests and for the endurance cycles. Performance Calibration 1 was also run with the same installation configuration.

7.1.1   Green Run

The "Green Run" and pre-endurance test was a run-in and checkout of the initial engine build. All engine instrumentation was checked out for proper operation. All engine control functions were checked.

Engine vibration signatures were well within normal operating conditions and all safety devices operated satisfactorily. After the green run, the engine was disassembled and inspected as required to investigate for any deficiencies. No engine discrepancies were found as a result of the green run.

7.1.2   Engine Endurance Cycles

The QCGAT engine was installed in the Phoenix Laboratory test cell for the endurance test. The engine was operated for 23 endurance cycles based on the duty cycle defined in Table 7-1.

7.1.3   Performance Calibration No. 1

The engine was installed with a calibrated bellmouth on the inlet. A hardwall-engine-fan duct, aft-workhorse nacelle with hardwall panels (except for the aft-barrel panel), and the coannular exhaust nozzle (Configuration I, Figure 3-20) were also installed.

The EPA LTO-Cycle (gaseous) Emissions measurements were recorded. The engine, with the fuel-flow divider connected, was accelerated to takeoff power after a brief warmup period at idle. Gaseous emission data were taken at 100-percent rated power,

TABLE 7-1. QCGAT ENDURANCE TEST CYCLE.

Condition	Cycle Time, (Min)
Start	--
Idle	5
Takeoff	5
Max. continuous	10
Max. cruise	45
Idle	5
75% max. cruise	5
Idle	5
Approach	5
Idle	5
Shutdown	15

75-percent, 50-percent, 30-percent, 25-percent, and taxi idle. The engine was then shutdown and the air-assist hardware installed. The engine was restarted and accelerated to the 1112 N (250-pounds) thrust taxi-idle point. The assist-airflow rate was adjusted to produce the desired HC and CO results. These data are recorded in Figures 7-1 and 7-2.

An engine tear-down inspection was not accomplished at the completion of the post-endurance calibration test. Turbine stages were inspected by boroscope equipment and the condition was judged to be excellent and not requiring disassembly for inspection. The post-endurance calibration test, therefore, was considered to be Performance Calibration 1 for the test program. Performance data was recorded and the thrust versus specific fuel consumption is plotted and shown in Figure 7-3.

7.1.4 Engine Performance

The QCGAT engine performance testing consisted of seven different combinations of inlet and exhaust nozzle configurations. These various configurations were previously defined in Figure 3-20 and are listed in Table 7-2.

7.1.5 Engine Configuration Performance Comparisons

A comparison of performance for the above listed configurations for certain parameters at a low-pressure rotor speed of 1938 rad/s (18,510 rpm) is presented in Table 7-3. This speed was selected since it is the highest speed common to all the tested configurations.

82
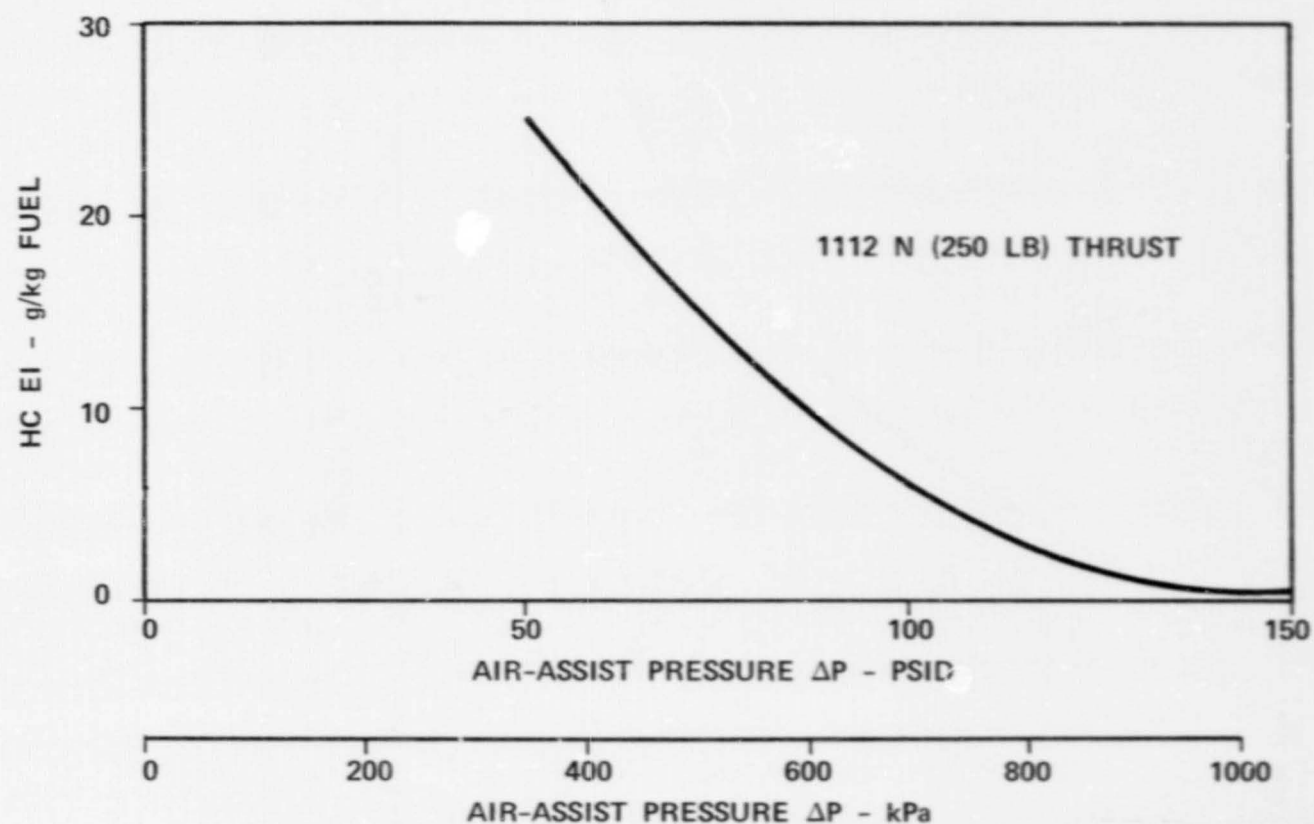
Figure 7-1.   QCGAT Taxi-Idle HC Emission Indices
as a Function of Air Assist Pressure.
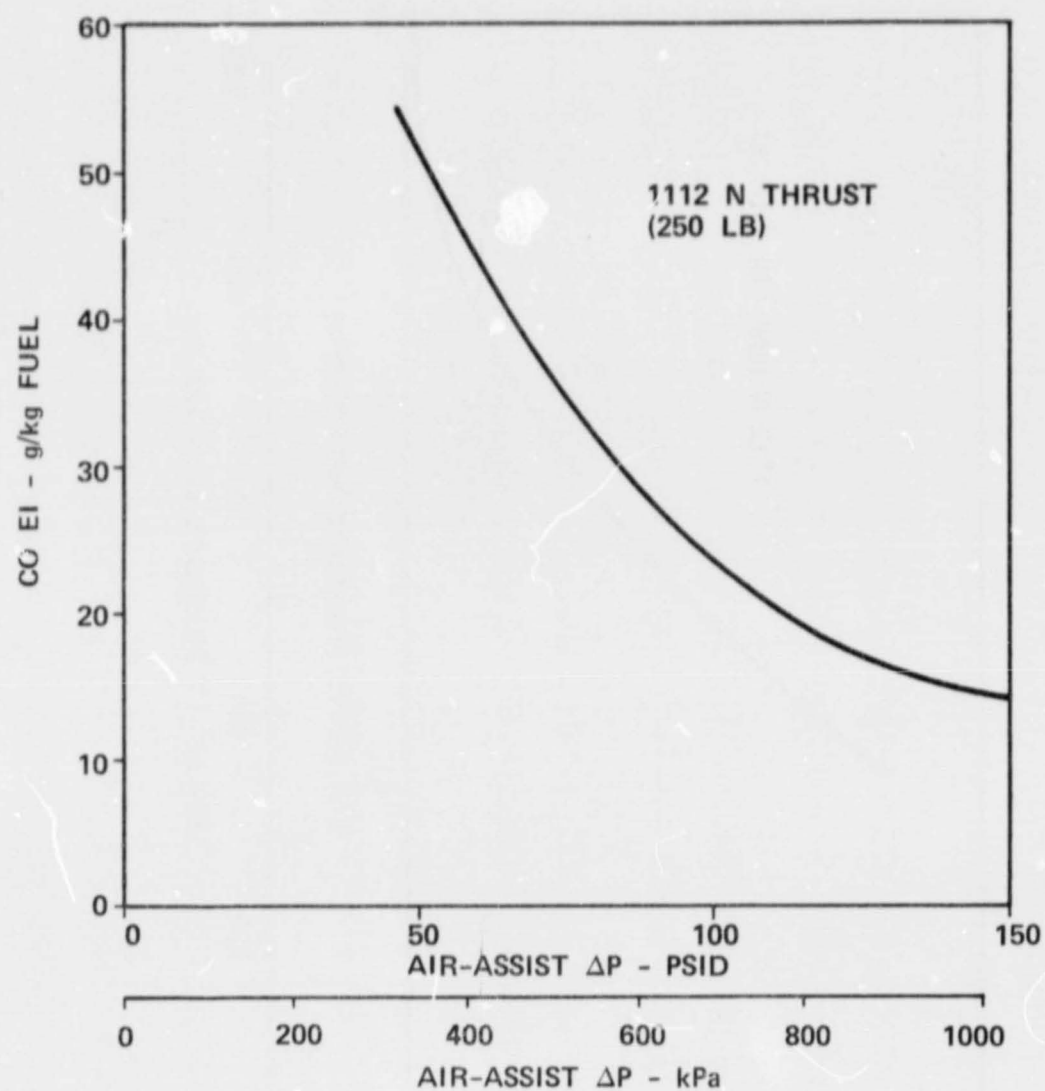
Figure 7-2. QCGAT Taxi-Idle CO Emission Indices as a Function of Air-Assist Pressure.

C-2
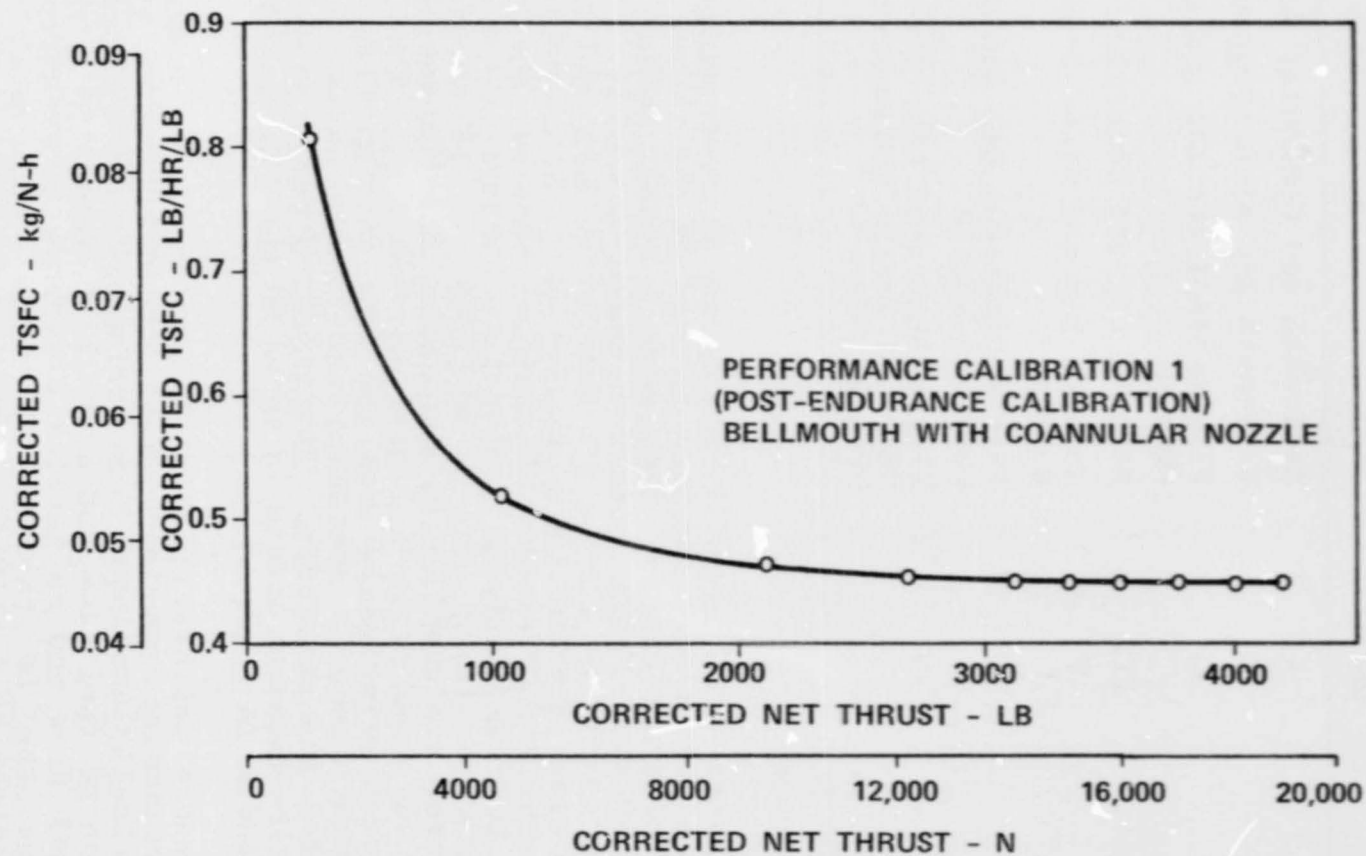
Figure 7-3.   Engine Calibration No. 1 (Post Endurance) –
TSFC Versus Thrust.

TABLE 7-2. PERFORMANCE CALIBRATIONS AND ENGINE CONFIGURATIONS.

Calibration No.	Configuration No.*	Description
1	I	Bellmouth and Coannular Nozzle
2	VI	Bellmouth and Mixer-Compound Nozzle
3	II	Flight-Simulator Lip and Coannular Nozzle
4	III	Nacelle Lip and Coannular Nozzle
5	V	Nacelle Lip and Mixer-Compound Nozzle
6	IV	Flight-Simulator Lip and Mixer-Compound Nozzle
7	IV	Flight-Simulator Lip, Mixer-Compound Nozzle and Acoustically Treated Ducts

*See Figure 3-20.

Performance calibration 2, using the mixer-compound nozzle, resulted in a significant increase in airflow and thrust at a constant N_1. The mixer-compound nozzle has a bypass stream area that is effectively much larger than the coannular nozzle. This provides a rematch of the fan to a higher efficiency and flow. The core stream area is effectively smaller than the coannular nozzle and causes a higher LP turbine discharge pressure. The engine has a higher HP turbine discharge temperature because of the increased total airflow requiring more power from the LP turbine. The increased power was supplied by increasing the turbine-inlet temperature which results in a higher N_2 and P_{t3}. The increased thrust resulted principally from the increased airflow, with the increased core stream temperature and nozzle thrust efficiency accounting for the remainder. The improved performance achieved with the mixer-compound nozzle is shown on the comparison of calibrations 1 and 2 in Figure 7-4.

Performance calibration 3 utilized the flight simulator lip with the coannular nozzle. The internal engine parameters remained virtually unchanged from performance calibration 1, with the exception of fuel flow and HP turbine discharge temperature. Both the fuel flow and HP turbine discharge temperature were up slightly but the LP turbine discharge temperature remained unchanged indicating a slight increase in LP turbine work output. The increased LP turbine work was necessary because of an apparent small increase in total flow as evidenced by the increase in engine thrust.

86

TABLE 7-3. QCGAT ENGINE PERFORMANCE COMPARISON AT LOW-PRESSURE ROTOR SPEED OF 1938 RAD/S (18,510 RPM).

Configuration	I	VI		II		III		V		IV Hardwall		IV Acoustic	
Parameter	Perf Cal 1	Perf Cal 2	Δ%	Perf Cal 3	Δ%	Perf Cal 4	Δ%	Perf Cal 5	Δ%	Perf Cal 6	Δ%	Perf Cal 7	Δ%
Thrust N (lbs)	15,413 (3465)	16,225 (3715)	+7.2	15,569 (3500)	+1.0	15,560 (3507)	+1.2	16,903 (3800)	+9.7	16,770 (3770)	+8.8	16,792 (3775)	+8.9
Fuel Flow kg/h (lbs/hr)	704 (1553)	732 (1613)	+3.9	705 (1555)	+0.1	709 (1562)	+0.6	739 (1630)	+5.0	738 (1628)	+4.8	737 (1625)	+4.6
N_1 rad/s (rpm)	1938 (18,510)	1938 (18,510)	0	1938 (18,510)	0	1938 (18,510)	0	1938 (18,510)	0	1938 (18,510)	0	1938 (18,510)	0
N_2 rad/s (rpm)	3011 (28,760)	3024 (28,880)	+0.4	3014 (28,790)	+0.1	3011 (28,760)	0	3033 (28,970)	+0.7	3030 (28,940)	+0.6	3035 (28,990)	+0.8
$T_{t4.2}$ K (°F)	1105 (1530)	1119 (1555)	+1.6	1112 (1543)	+0.8	1121 (1558)	+1.8	1125 (1566)	+2.3	1126 (1567)	+2.4	1119 (1554)	+1.6
$T_{t7.0}$ K (°F)	794 (969)	806 (991)	+2.3	794 (969)	0	794 (969)	0	807 (994)	+2.6	805 (989)	+2.0	809 (996)	+2.7
$T_{t11.0}$ K (°F)	326 (128.1)	324 (124.2)	-3.0	326 (127.5)	-0.5	326 (127.5)	-0.5	325 (125.5)	-2.0	325 (124.8)	-2.5	326 (128.1)	0
$P_{t3.0}$ kPa (psig)	1215 (176.2)	1234 (179.0)	+1.6	1215 (176.2)	0	1215 (176.2)	0	1234 (179.0)	+1.6	1227 (177.9)	+1.0	1233 (178.8)	+1.5
$P_{t7.0}$ kPa (psig)	1340 (19.43)	1376 (19.96)	+2.7	1340 (19.43)	0	1339 (19.42)	-0.1	1379 (20.00)	+2.9	1373 (19.92)	+2.5	1374 (19.93)	+2.6
$P_{t11.0}$ kPa (psig)	1404 (20.36)	1410 (20.45)	+0.4	1400 (20.31)	-0.2	1404 (20.36)	0	1413 (20.46)	+0.5	1409 (20.43)	+0.3	1402 (20.33)	-0.1
TOTAL AIRFLOW kg/s (lbs/sec)	60.87 (134.2)	63.55 (140.1)	+4.4										

NOTE:

$$\Delta\% = \frac{\text{Test } \# - \text{Test 1}}{\text{Test 1}} \times 100$$
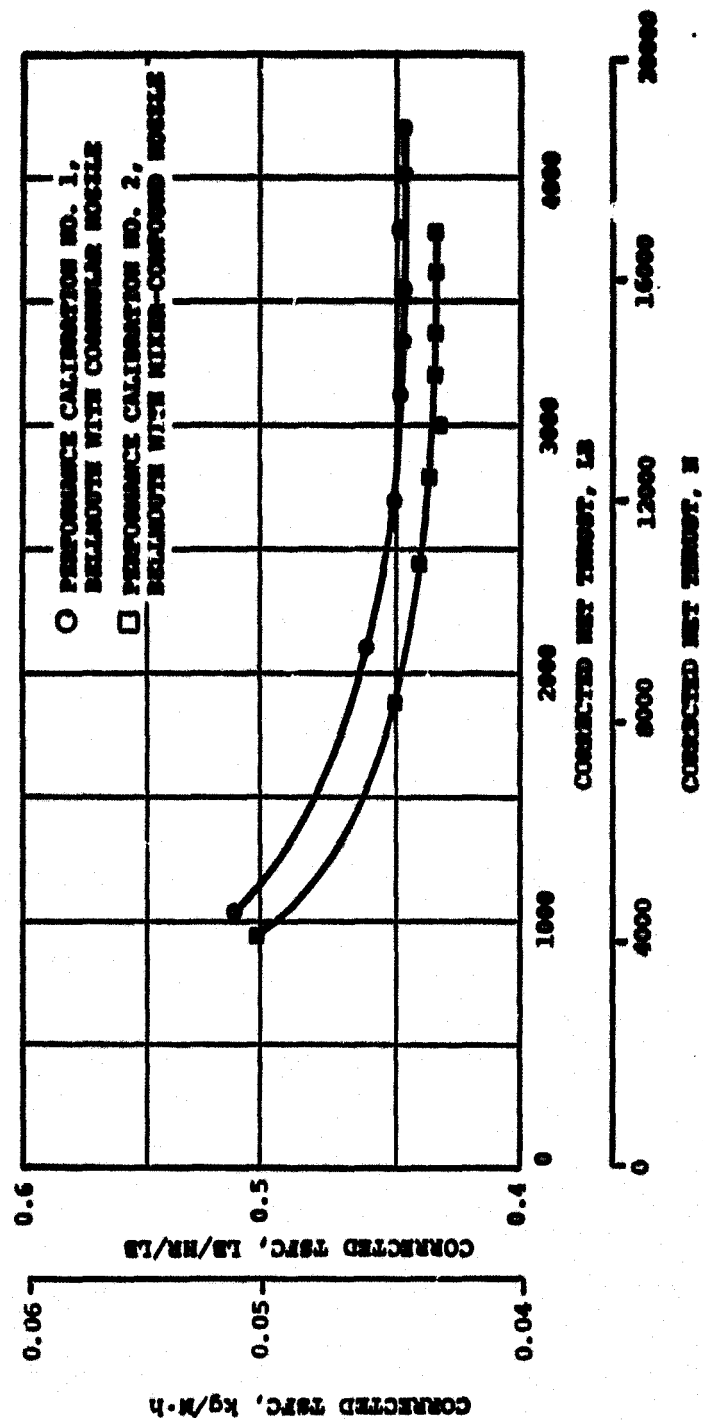
Figure 7-4. Comparison of TSFC for Coannular and Mixer-Compound Configurations.

Performance calibration 4 used the nacelle-lip inlet with the coannular nozzles. The engine parameters behaved in a manner similar to calibration 3 although the magnitudes were slightly larger. Again, fuel flow and HP turbine discharge temperature were up while LP turbine discharge temperature remained the same. Thrust was increased, indicating an increase in total flow. This would account for the increased LP turbine work.

Performance calibration 5 used the nacelle-lip inlet with the mixer-compound nozzle. The engine performance was similar to performance calibration 2, which also had the mixer-compound nozzle. The nacelle lip had the same effect with mixer-compound nozzle as it had with the coannular nozzles.

Performance calibration 6 used the flight-simulator inlet with the mixer-compound nozzle. The engine behavior was similar to performance calibration 2 and the flight-simulator lip had the same effect with the mixer-compound nozzle as it had with the coannular nozzles.

Performance calibration 7 was run using the flight simulator lip inlet, the mixer-compound nozzle, and full acoustic treatment in the bypass duct. The acoustic treatment had little effect on the performance of the engine relative to performance calibration 6. Calibration 6 had an identical configuration without acoustic treatment. Thrust, fuel flow, HP turbine discharge temperature and bypass-stream nozzle inlet pressure were all reduced slightly while bypass stream temperature was increased relative to calibration 6. The reduced bypass stream pressure indicates that the bypass airflow has been reduced slightly and this is supported by the reduced thrust and fuel flow. The reduced airflow is apparently attributable to an increased pressure drop in the bypass stream.

7.1.6 Performance Comparisons to the Pretest Model

A comparison of the QCGAT engine pre-endurance calibration with the pretest model, including coannular nozzles, is shown in Table 7-4. Table 7-4 shows that thrust, airflow, P_{t7}, P_{t17}, and high-rotor speed are in reasonable agreement with the model. Fuel flow, however, and $T_{t4.2}$, T_{t7}, T_{t17}, and P_{t3} are discrepant. Analysis of the data shows that the fan is lower in efficiency than was predicted by the pretest analytical model and lower than predicted in airflow at maximum power. The discrepancy in airflow is about 0.5 percent low at maximum power and changes to a higher value of 3.9 percent as speed is decreased to 17,000 rpm.

The airflow versus speed discrepancy of the fan in the model is the primary reason for the increasing differences between the tested data and the analytical model.

TABLE 7-4. QCGAT TEST TO PRETEST MODEL COMPARISON.

Parameter	$N_1 = 19,500$ Coannular Nozzles			$N = 18,500$ Mixer Nozzle		
	Model	Test	Δ	Model	Test	Δ
Thrust F_N – N – (lbs)	18,055 (4059)	18,038 (4055)	-0.1%	15,813 (3555)	16,503 (3710)	+4.4%
Fuel Flow W_f – kg/h – (lbs/hr)	800.7 (1764)	823.9 (1815)	+2.9%	684.1 (1507)	730.8 (1610)	+6.8%
High-Rotor Speed N_2 – rad/s – (rpm)	3025 (28,887)	3061 (29,240)	+1.2%	2970 (28,354)	3024 (28,880)	+1.8%
HP Turbine Discharge Temperature, $T_{t4.2}$ – K – (°F)	1123.0 (1562)	1140.3 (1594)	+2.0%	1043.0 (1490)	1118.6 (1554)	+4.1%
LP Turbine Discharge Temperature, T_{t7} – K – (°F)	791.9 (966)	806.3 (992)	+2.7%	778.0 (941)	805.2 (990)	+5.1%
Fan Nozzle Inlet Temperature, T_{t17} – K – (°F)	327.1 (129.6)	330.2 (135.0)	+3.2%	321.6 (119.6)	324.1 (124.0)	+3.4%
HP Compressor Discharge Pressure, P_{t3} – kPa – (psig)	1357 (196.8)	1389 (201.5)	+2.4%	1184 (171.7)	1231 (178.5)	+4.0%
Core Nozzle Total Pressure, P_{t7} – kPa – (psig)	141.5 (20.52)	142.3 (20.64)	+0.6%	134.5 (19.51)	137.4 (19.93)	+2.2%
Fan Nozzle Total Pressure, P_{t17} – kPa – (psig)	145.8 (21.15)	146.0 (21.18)	+0.1%	143.8 (20.85)	140.8 (20.42)	-2.1%
Engine Inlet Total Airflow, W_{AT} – kg/s – (lb/sec)	66.6 (144.6)	65.3 (143.9)	-0.5%	62.3 (137.4)	63.6 (140.1)	+2.0%

NOTES: (1) Coannular Nozzles – Pre-endurance Calibration
(2) Mixer Nozzles – Performance Calibration No. 2

Table 7-4 also provides a comparison of the pretest QCGAT engine with the mixer-compound nozzle. This comparison shows that the model does not compare with the mixer-compound nozzle as favorably as it did with the coannular nozzles. The disagreement between the model and the engine is the difference in the predicted fan performance versus actual fan performance. The predicted fan map, in addition to having higher efficiencies, is also in error in the shape and spacing of the speed lines. The incorrect shapes of the speed lines prevent the model from predicting the correct rematch that occurs when the mixer-compound nozzles are installed.

Analysis of internal engine instrumentation indicates that the levels of efficiency of the LP compressor and LP turbine in the model are only slightly in error. The shape are correct and the efficiency errors offset each other, but the model LP compressor efficiency is low and the model LP turbine is slightly high. The HP compressor and the HP turbine in the model are correct. The principle factor in the comparison of the model to test data is the incorrectly estimated fan map. This map was prepared from early ATF3 fan-component data. The map was subsequently corrected based on more recent rig tests for the ATF3 fan configurations.

7.1.7 Performance Comparisons to Contract Goals

Presented in Table 7-5 is a comparison of the engine with the contract performance goals. Comparison of the performance model at the goal conditions with the engine test data shows that the engine fan is down in efficiency and that the engine coannular nozzles also are down in thrust coefficient by 1-percent. These differences account for the fuel flow (TSFC) discrepancy with the coannular nozzle. Comparison of the performance model at the goal conditions to the engine test data for the mixer-compound nozzle configuration shows that a significant rematch occurred on the fan, moving it towards peak efficiency. The goal analytical model showed virtually no rematch on the fan; therefore, the engine fan performance (although down in efficiency) is not reduced as much relative to the goal with the mixer-compound nozzles as it was with coannular nozzles. In addition, the mixer-compound nozzles achieved a 1-percent better thrust coefficient than had been predicted, and this, combined with the fan rematch, accounts for the improvement in the engine TSFC relative to the coannular nozzle. When extrapolated to the design-point cruise, the combined effects on the fan reduce the TSFC significantly and results in meeting the installed design-point TSFC goal.

TABLE 7-5. QCGAT TEST TO PERFORMANCE GOALS COMPARISON.

Flight Condition	Thrust N (lbs)			TSFC kg/Nh (lb/hr/lb)		
	Goal	Test	Δ%	Goal	Test	Δ%
SEA-LEVEL STATIC						
STANDARD DAY						
UNINSTALLED*	17,513 (3937)	17,513 (3937)	0	0.0426 (0.418)	0.0459 (0.450)	+7.7
INSTALLED**	17,313 (3892)	17,313 (3892)	0	0.0431 (0.423)	0.0437 (0.429)	+1.4
DESIGN CRUISE						
12,192 M (40,000 FT.) ALTITUDE 0.3M						
UNINSTALLED*	3,955 (889)	3,955 (889)	0	0.0775 (0.760)	0.0797 (0.782)	+2.8
INSTALLED**	4017 (903)	4017 (903)	0	0.0759 (0.744)	0.0755 (0.741)	-0.1

*Reference Bellmouth, Hardwall bypass duct,
 Reference Coannular Nozzle.

**Ground Test Nacelle with Nacelle Lip,
  Acoustic Treatment and Mixer Nozzle.

7.2 Emissions Performance

7.2.1 Engine Exhaust Emission Goals

The emissions goals for the QCGAT engine are identical to the proposed 1979 EPA standards for T1 Class engines. These standards have since been abandoned by EPA. For gaseous emissions, the standards are expressed in terms of the EPA Parameter (EPAP) for each of the three pollutants. To determine the EPAPs, emissions measurements were made at four power settings (100-percent rated power, 90 percent, 30 percent and taxi-idle). At each of the four power settings, the emission rate (pound of pollutant per hour) for each pollutant is determined and multiplied by a time weighting factor, then divided by a work output term which involves the engine thrust for that specific power setting. The four terms, one for each power setting, are then added together to arrive at the EPAP. The time weighting factor used in the calculation is a function of an engine operation cycle established by the EPA as being the typical time spent in each operating mode for an aircraft with T1 Class engines.

For the QCGAT Engine, this T1 Class cycle is defined in Table 7-6.

TABLE 7-6.   EPAP T1 CLASS CYCLE

Mode	% Rated Power	Time Minutes
Taxi-Out	Taxi-Idle	19.0
Takeoff	100	0.5
Climbout	90	2.5
Approach	30	4.5
Taxi-In	Taxi-Idle	7.0

The smoke standard is established as a function of rated engine power and represents, approximately, the threshold for visible smoke from an engine exhaust. The standard is expressed as Smoke Number (SN). This value is a function of the amount of light reflected from a sample of particulate collected on a piece of filter paper that has been exposed to the engine exhaust. The higher the SN, the greater the amount of particulate, and hence, the greater the smoke visibility. Smoke measurements are made at the same four power settings as the gaseous emission test. The highest SN of the four power settings is considered the smoke number for the engine.

The EPA pollutant standards for T1 Class engines, and also the program goals for the QCGAT Engine are listed in Table 7-7.

TABLE 7-7.   EPA POLLUTANT STANDARDS

Pollutant	Program Goal	
Unburned Hydrocarbon (HC)	0.726 (1.6)	
Carbon Monoxide (CO)	4.26 (9.4)	kg/4448 N thrust-hr/cycle (lb/1000 lb thrust-hr/
Oxides of Nitorgen (NO_x)	1.68 (3.7)	cycle)
Smoke	38 SN	

7.2.2 Combustor Liner Test Configuration

The combustor liner used in the QCGAT engine was a modified version of Part 3072674, improved durability burner, which was placed in production for the TFE731-3 production during the first part of 1979. The QCGAT combustor, Part P.#234342, had a row of orifices added to the dome for the purpose of smoke reduction. The fuel nozzles were production TFE731-3 dual orifice assemblies, Part 3071101-14.

When gaseous emissions were being sampled at taxi-idle, the secondary side of the fuel-flow divider was capped and an air line was connected to the secondary fuel manifold. This air line supplied high-pressure air to the nozzle tips to aid in the atomization process. The air was supplied from a laboratory compressed air source with a supply pressure of 2.068 kPa (300 psig). After passing through a 20-micron filter, the laboratory compressed air was heated by an electric heat exchanger to between 366 and 422K (200° and 300°F) and passed through an air-flow measuring section. This was to simulate an air assist system where the discharge temperature from the heat of compression for the assist air would be similar to air extracted from the boost compressor. At all other power settings and for smoke measurement tests, the flow divider was reconnected to the secondary circuit and the air assist system was not used. For the emission measurement tests, the engine was equipped with a coannular-exhaust nozzle.

7.2.3 Emissions Test Results

The emissions tests were run during Calibration 1 (Post Endurance Calibration) and was previously discussed in Section 6.0, Paragraph 6.3. The EPAPs and the smoke number for the QCGAT engine are listed in Table 7-8 with the program goals.

TABLE 7-8. QCGAT EPAPS AND SMOKE NUMBER VALUES.

Pollutant	QCGAT EPAPS	Program Goals
HC	0.726 (1.6)	0.726 (1.6)
kg/4448 N Thrust-hr cycle		
CO (lb/1000 lb Thrust-hr/cycle	3.36 (8.0)	4.26 (9.4)
NO$_x$	2.09 (4.6)	1.68 (3.7)
Smoke Number (SN)	42	38

94

In order to meet the HC and CO goals, air-assist at an inlet pressure of 724 kPa (105 psid) at the taxi-idle power setting was used. Lower air-assist pressure would have resulted in higher emission index values (EI, g/kg fuel) for both HC and CO. This relationship was previously shown in Figures 6-2 and 6-3. Since more than 90 percent of the HC and CO EPAPs values are contributed by the taxi-idle terms, small changes in HC and CO emission index values at that power setting result in significant changes in the overall EPAPs for the two pollutants. Test data and corrected EI values are shown in Table 7-9.

TABLE 7-9. QCGAT EMISSION INDICES.

	HCEI	COEI	NO$_x$EI	Smoke Number
Uncorrected Engine Values (g/kg)*				
Takeoff	0.18	2.2	16.6	41
Climbout	0.15	2.5	12.8	42
Approach	1.64	12.5	6.6	28
Taxi-Idle	5.00	22.0	3.1	10
Corrected Engine Values for Model Pressure and Temperature				
Takeoff	0.18	2.2	17.0	41
Climbout	0.14	2.3	14.2	42
Approach	1.70	13.0	6.3	28
Taxi-Idle	5.62	24.7	2.9	10

*Measured at the Model f/A ratios for the individual power settings.

7.2.4 Emissions Test Conclusions

From the test results, the following can be concluded:

1. The engine met the program goals for HC and CO with the use of air assist at taxi-idle.

2. There was a significant reduction in the engine NO$_x$ level over the production TFE731-3, but it did not meet the program goal.

3. The smoke number of 42 is in excess of the program goal of 38, however, the engine was visually judged to be smokeless.

7.3 Acoustic Characteristics

The acoustic design effort for the QCGAT engine/nacelle system directed noise reduction technology toward minimizing noise generation at the source, and maximizing the attenuation achieved through judicious application of nacelle acoustic treatment in the fan inlet and exhaust ducts. The acoustical duct liner configurations were designed to balance the noise suppression at takeoff, sideline, and approach conditions. This provides the broadest possible attenuation bandwidth without sacrificing significant attenuation from optimum at any of the three operating conditions.

The major acoustic features of the QCGAT engine are illustrated in Figure 7-5. Noise reduction technology was applied to three major noise sources: fan, jet, and core. The fan-noise source reduction features include: elimination of inlet guide vanes, single-stage fan, low fan-tip speed, low pressure ratio, large fan rotor-stator spacing, and optimum fan-blade/stator-vane number ratio. The jet-noise reduction features include low jet-exhaust velocity, and a mixer-compound exhaust system. Core noise is minimized by the use of a reverse-flow annular combustor, and a highly loaded three-stage low-pressure turbine.
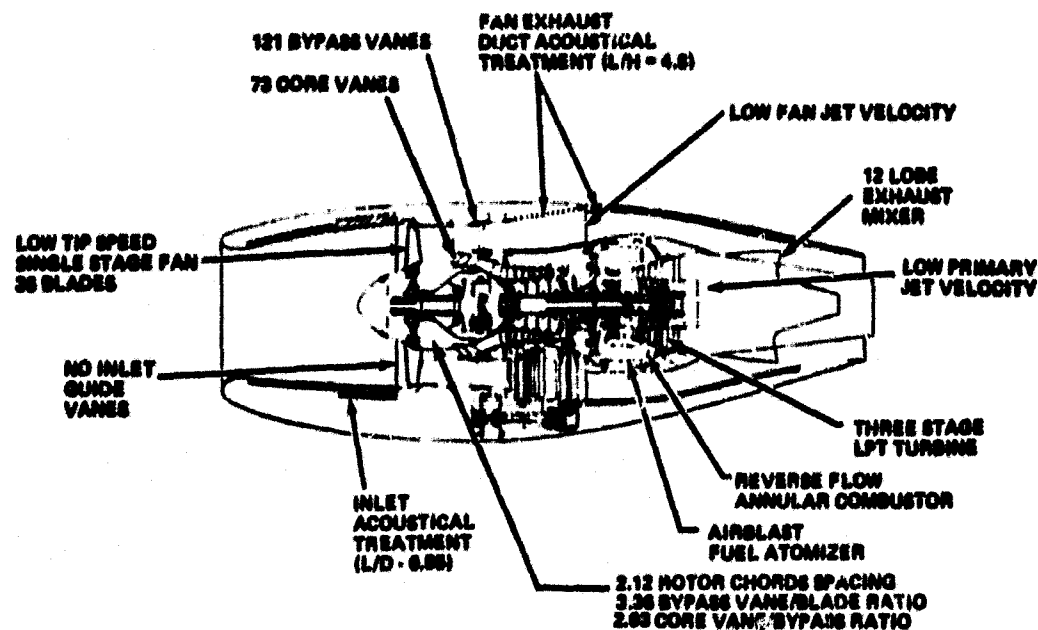
Figure 7-5. Acoustical Features of the QCGAT Engine/Nacelle.

7.3.1 Nacelle Acoustic Treatment Design

The nacelle acoustic treatment design selected for the QCGAT engine consisted of a single-cavity system used in series, with different cavity depths in the axial direction and equivalent depths on opposing walls, where possible. Because of its structural ruggedness, lower cost, and proven acoustical performance in the above configuration, a perforated-plate, broadband-resonator was constructed from aluminum perforated sheet, bonded to 3/8-inch cell aluminum honeycomb backing.

The acoustic liner installations are shown schematically in Figure 7-6. The design parameters of the three inlet sections and the three exhaust sections are given in Table 7-10. The inlet wall treatment has a length equal to 0.85 mean inlet diameters, and was tuned to provide primary suppression at the FAR Part 36 sideline condition. The fan discharge duct wall treatment has an effective length equal to 5.4 times the average duct height and is tuned to provide balanced attenuation between the FAR Part 36 sideline and approach conditions.

Final optimization of the engine and nacelle exhaust liner design was completed using a computer program based on axisymmetric mode theory of Minner and Rice (Reference 1). The cavity depths and face sheet open areas required to achieve optimum attenuation were computed. A summary of the exhaust liner design methodology is shown in Figure 7-7.

The design procedure for the inlet nacelle liners was based upon the recent multimodal analysis developed by Rice (References 2 through 5). A simplified general description of the optimization procedure is shown in Figure 7-8. The optimization criteria was determined by comparing the liner impedance map and the optimum impedance map as illustrated schematically in Figure 7-9. By selecting a liner-cavity depth and face-sheet open area so that the liner impedance is in a region where a large number of modes cluster, a broad acoustic power attenuation should be obtained. A map for each liner section for modes having cut-off ratios of 1 to 4 with one-third octave center frequencies of 1600, 2000, 2500, 3150, and 5000 Hz was constructed. A typical map is shown in Figure 7-10. The inlet liners were tuned for modes with moderate to small cut-off ratios that radiate energy at larger angles from the inlet axis in order to minimize the sideline noise radiation.

7.3.2 Engine Noise Tests

The QCGAT engine was installed at the San Tan Test Facility for acoustical measurements. Noise data at the specified engine load conditons were taken to determine the untreated engine noise levels, the effect of various combinations of acoustic treatments,
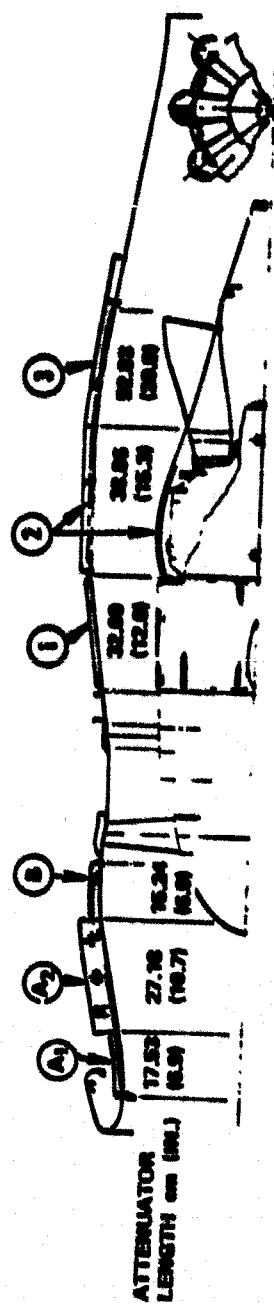
Figure 7-6. Nacelle Acoustical Treatment.

TABLE 7-10. QCSEE NACELLE ATTENUATION DESIGN PARAMETERS.

	Inlet Duct						Fan Exhaust					
	Section A		Section B		Section 1		Section 1		Section 2		Section 3	
Parameter	Pre-liminary	Final	Pre-liminary	Final	Pre-liminary	Final	Pre-liminary	Final	Pre-liminary	Final	Pre-liminary	Final
Average Duct Height, h - cm - (in.)[1]	35.05 (13.8)	35.05 (13.8)	38.80 (15.3)	38.35 (15.1)	14.48 (5.7)	14.48 (5.7)	24.22 (5.6)	14.22 (5.6)	24.22 (5.6)	14.22 (5.6)	17.02 (6.7)	17.02 (6.7)
Treatment (A_1 x A_2) Length - cm - (in.)	46.48 (18.3)	44.70 (17.6)	16.51 (6.5)	15.24 (6.0)	32.00 (12.6)	32.00 (12.6)	38.86 (15.3)	38.86 (15.3)	38.86 (15.3)	38.86 (15.3)	52.83 (20.8)	52.83 (20.8)
Tuned Center Frequency, Hz	2500 1000	1000 1000	5000	2500	2500	2500	5000	5000	5000	5000	2000	2000
Cavity Depth - cm - (in.) - cm - (in.)	1.52 (0.6) 3.43 (1.35)	2.79 (1.1) 1.83 (0.72)	0.76 (0.3)	1.32 (0.52)	1.42 (0.56)	1.42 (0.56)	0.69 (0.27)	0.91 (0.36)	0.69 (0.27)	0.91 (0.36)	1.91 (0.75)	1.95 (0.77)
Percent Open Area - %	7.1 10.1	8.6 5.8	18.2	14.2	8.0	7.0	10.3	8.6	10.3	8.6	7.1	6.8
Frequency Parameter[2], ηw/c	5.19 2.07	2.131 1.99	5.71	5.644	2.85	2.85	1.93	1.59	1.93	1.59	1.92	1.92
Condition Tuned For:	Sideline	Sideline	Sideline	Approach	Approach	Approach	Takeoff	Approach	Approach	Approach	Approach	Approach

[1] For Inlet h = D/2

[2] For one wall treated, h = 2h
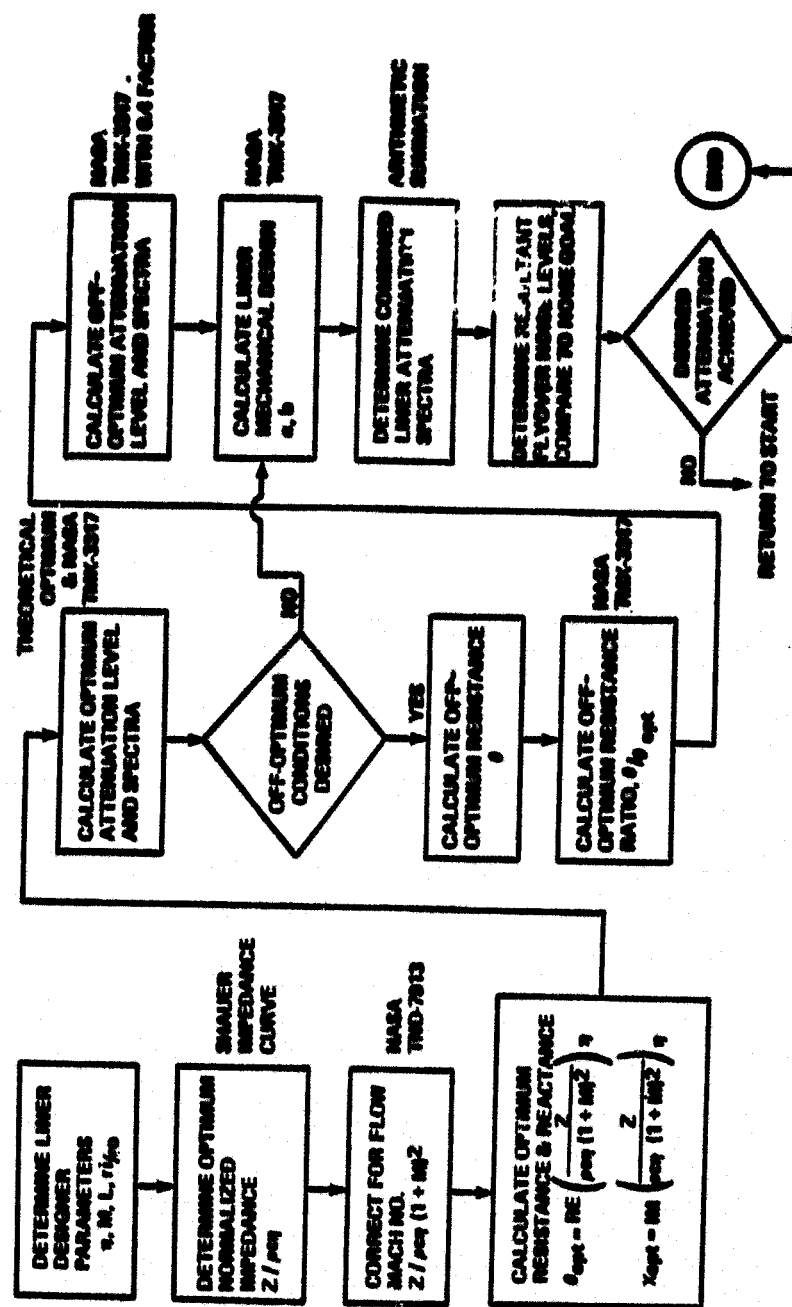
Figure 7-7. Fan-Exhaust-Duct Liner Design Methodology.
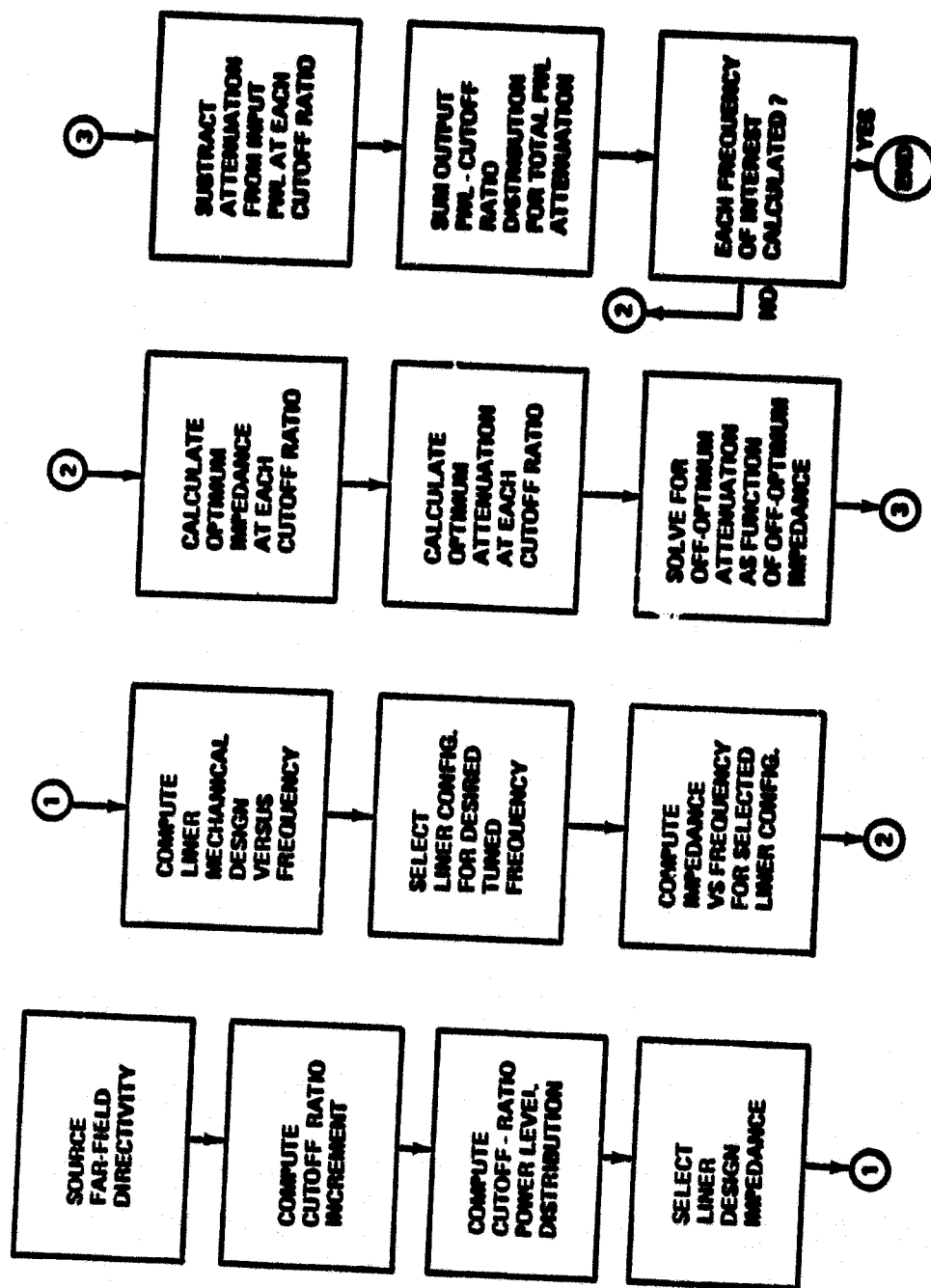
Figure 7-8. Multimode Attenuator Design Optimization.
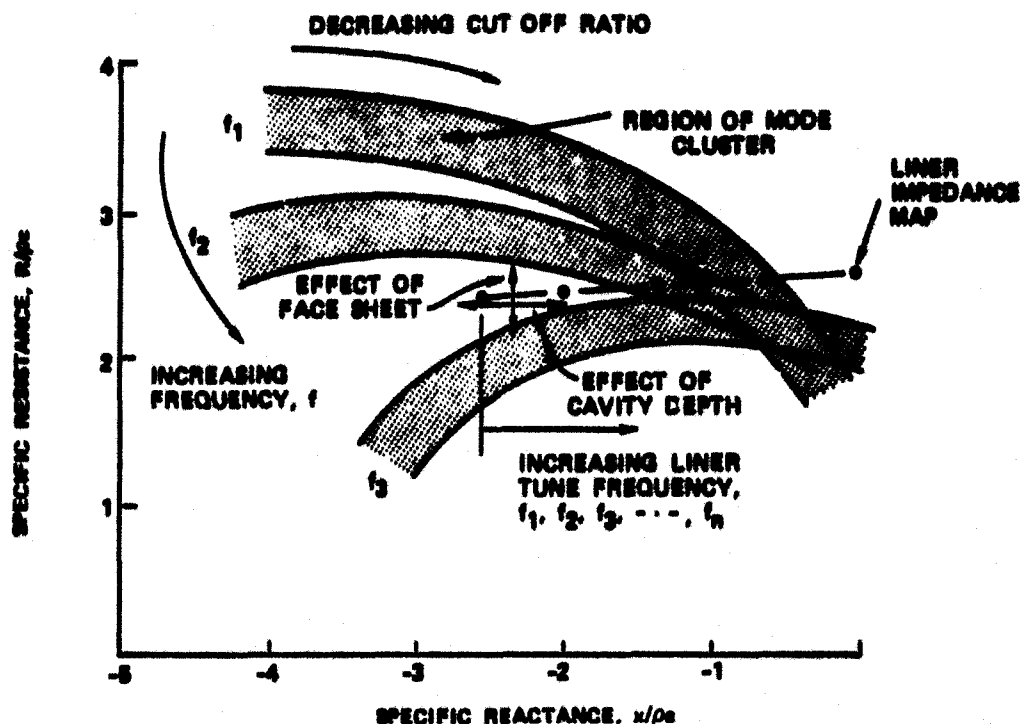
Figure 7-9. Optimum Impedance.

and to determine the effect of the mixer-compound nozzle on the
treated engine signature. The data from this test series was used
to determine the minimum attenuation configuration required to
meet QCGAT noise goals, and to determine the static noise levels
for use in predicting flyover noise levels.

Figure 7-11 shows the installation of the QCGAT engine with
the 16 microphone positions utilized for the engine far-field
noise directivity measurements. A schematic of the noise test
setup is shown in Figure 7-12.

In addition to the 16 far field microphone locations, six
internal noise measurements were made on selected engine test con-
figurations. The internal noise measurements were conducted using
three 0.3175-cm (1/8-inch) condenser microphones and three
0.635-cm (1/4-inch) condenser microphone infinite-tube systems.
The locations of the internal acoustic probes are given in
Table 7-11.

The acoustic data were recorded on two fourteen-channel
analog tape recorders providing twenty-eight channels of data plus
a voice track. The six internal microphone outputs were split and
recorded on both tape recorders.

102
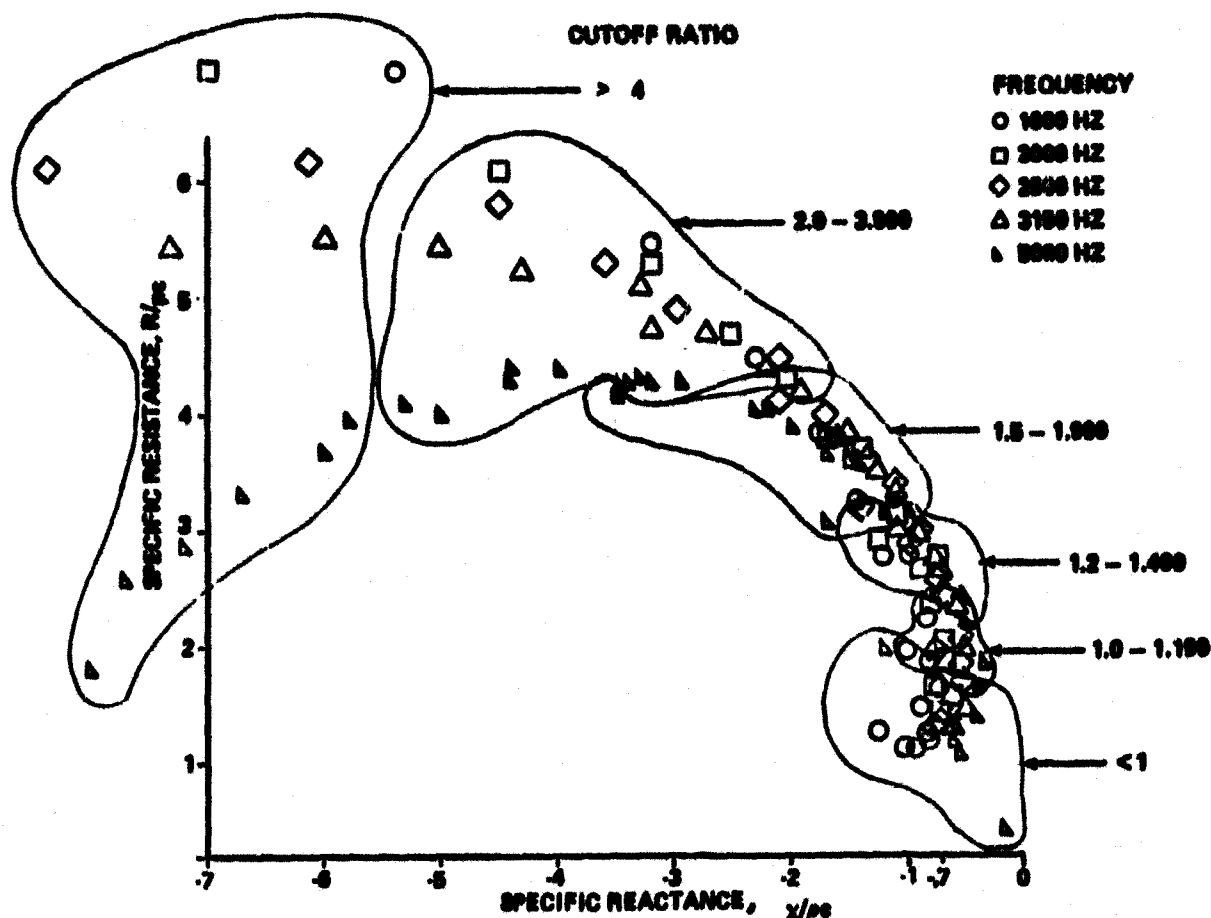
Figure 7-10. Single-Mode Analysis, Section B Inlet Nacelle, Takeoff Static Conditions.

Prior to acoustic testing, all microphones were calibrated according to ANSI SI-11-1971. Before each test sequence, a piston phone calibration of each microphone was recorded, as well as a measurement of the ambient noise level with the engine shut down. Individual measurements of ambient temperature, relative humidity, wind velocity and direction were made immediately prior to testing, or at least each 1/2 hour, whichever was less. All tests were conducted within the specified limits of: wind speed no more than 9.66 km/hr (6 miles/hour); relative humidity no less than 10 percent or more than 90 percent; and ambient temperature no less than 5° or more than 30°C (41°F or more than 86°F).

The far-field acoustic data for all seven configurations listed in Table 7-12 were taken with the B&K 4133 microphones mounted for normal incidence of the direct sound field at a height of 1.52 meters (five feet) above the ground. The first configuration tested, Configuration 2, was run at takeoff and approach power settings and acoustic data recorded at three individual

103
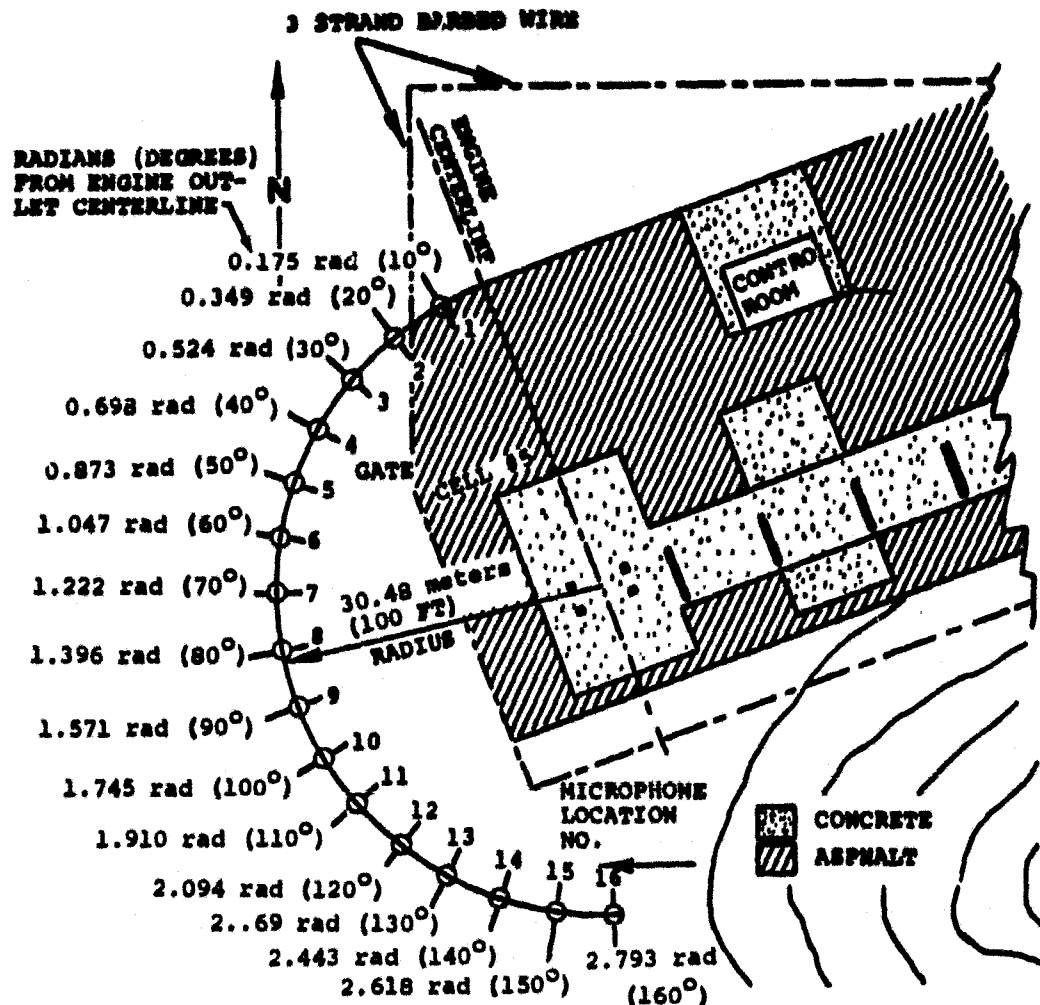
Figure 7-12. QCGAT Noise Test Setup at San Tan.

microphone heights: 1.52 meters, 0.762 meters, and ground level - 10.16 cm (5-feet, 2.5 feet, and ground level - 4 inches). This data was used to determine a ground reflection correction which was applied to the 1.52-meter (5-foot) microphone data taken for all configurations.

A 3.66-meter by 3.66-meter (12-foot by 12-foot) movable noise shield (barrier) was utilized for Configurations 1 and 5 to aid in isolating the inlet (forward) and exhaust (aft) radiated noise sources. For these configurations a three-fold test was conducted: with the barrier shielding the inlet, with the barrier shielding the exhaust; and without the barrier. (See Figure 7-13.)

A schematic of the seven test configurations, showing the various combinations of acoustic treatments, exhaust nozzles, and

104

Figure 7-11. QCGAT Engine Installed at San Tan Test Facility with Far-Field Acoustic Test Microphones and Engine Radiated Noise Barrier.

TABLE 7-11. QCGAT ENGINE/NACELLE ACOUSTIC INSTRUMENTATION

Item	Description	Location	Qty
1	Microphone, B&K4133	Free field	16
2	Microphone 0.3175-cm (1/8-in.) condenser	Fan inlet	2
3	Microphone, 0.3175-cm (1/8-in.) condenser	Exhaust nozzle	1
4	Microphone, 0.635-cm (1/4-in.) condenser infinite tube	LP turbine rear bearing support	1
5	Microphone, 0.635-cm (1/4-in.) condenser infinite tube	Exhaust nozzle	2
6	Temperature, dry bulb	Ambient	1
7	Temperature, wet bulb	Ambient	1
8	Wind velocity and direction	Ambient	1
9	Pistonphone	Microphone calibration	

TABLE 7-12. ACOUSTIC CALIBRATIONS AND ENGINE CONFIGURATIONS.

Acoustic Calibration No.	Acoustic Configuration No.	Engine Configuration No.	Description
1	1	IV	Flight Simulator Lip, Mixer-Compound Nozzle, Full Acoustic Treatment
2	2	II	Flight Simulator Lip Coannular Nozzle, Full Acoustic Treatment (except for hard aft panel)
3	3	IV	Flight Simulator Lip, Mixer-Compound Nozzle Hardwall Outer Aft Panel
4	4	IV	Flight Simulator Lip, Mixer-Compound Nozzle, Hardwall Outer, Inner Aft Panel, Bypass Duct, Inlet Duct Panel
5	5	IV	Flight Simulator Lip, Mixer-Compound Nozzle, Full Hardwall Nacelle
6	6	V	Nacelle Lip, Mixer-Compound Nozzle, Full Hardwall Nacelle
7	7	II	Flight Simulator Lip, Coannular Nozzle, Full Hardwall Nacelle
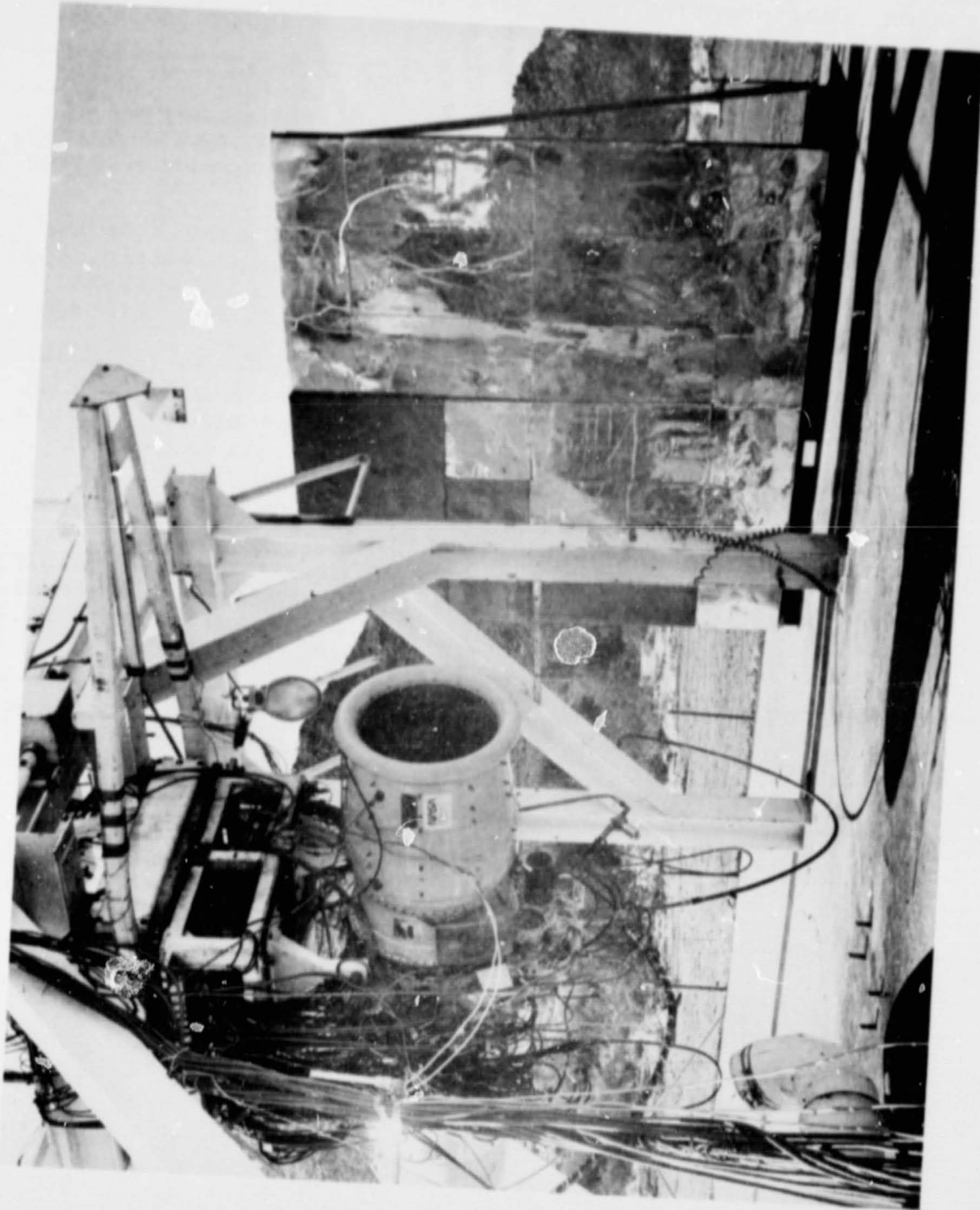
Figure 7-13. QCGAT Engine with Barrier Shielding Inlet.

108

inlet lips is shown in Figure 7-14. A series of test points were designed to provide: core-noise definition (points 1, 2 and 3), FAR Part 36 simulated noise-certification conditions of approach, cutback, and takeoff (points 5, 7, and 8). and intermediate power points (points 4, and 6). Simultaneous two-minute recordings of internal-probe data and far-field microphones were made for Configurations 1 and 5. Copies of these tapes were sent to NASA-Lewis for cross-correlation analysis to separate core and jet noise sources.

The acoustic data for each test configuration were analyzed using the instrumentation system shown in Figure 7-15. The resultant one-third octave sound pressure level spectra were transmitted to the CYBER 174 computer to be corrected for atmospheric absorption and ground reflection. This automated data analysis system is outlined in Figure 7-16.

7.3.3 Ground-Reflection Analysis

To correct the measured acoustic data to free-field conditions, the contribution of the acoustic ground-reflection wave must be removed from the measured value. A major factor in the analytical determination of the ground-reflection contribution is the acoustic impedance of the ground (soil) boundary. The type of desert soil at the San Tan test site consists of a random combination of hard-packed clay, sand, and decomposed granite particles. No known data exists on the impedance of this type of soil. Thus, it was decided to estimate the impedance of the San Tan soil boundary by recording the QCGAT acoustic data at three pre-selected microphone heights: 1.52m, 0.76m and 10.16cm (5 ft., 2.5 ft, and 0.33 ft.) for certain operating conditions and correlating the data to obtain a reasonable prediction for the surface impedance.

The terrain around San Tan Cell No. 5 slopes downward from the engine pad so that the ground locations upon which the microphones were placed are at an average elevation of 1.13 meters (3.7-ft.) below that of the engine pad. Although QCGAT engine centerline was 2.29 meters (7.5-ft.) above the pad, the difference in elevation placed it an average of 3.41 meters (11.2-ft.) above the ground at the microphone locations.

The ground reflection geometry model used in the analysis is shown in Figure 7-17. For the distances associated with the QCGAT tests, the angle ϕ is sufficiently small (0.1148 to 0.1606 radians) that near-grazing incidence should be assumed. At these conditions, and assuming the ground to be locally reacting, the velocity potential at the microphones can be given as:

CALIBRATION 1
CONFIGURATION IV

CALIBRATION 4
CONFIGURATION IV

CALIBRATION 7
CONFIGURATION II

CALIBRATION 2
CONFIGURATION II

CALIBRATION 5
CONFIGURATION IV

CALIBRATION 3
CONFIGURATION IV

CALIBRATION 6
CONFIGURATION V

KEY

1   BASIC ENGINE CONFIGURATION
2   FLIGHT SIMULATOR OR NACELLE LIP

ATTENUATED PANELS

3   FIRST INLET PANEL
4   SECOND INLET PANEL
5   FAN DUCT PANEL
6   BYPASS DUCT PANEL
7   INNER-AFT PANEL
8   OUTER-AFT PANEL
9   MIXER-COMPOUND NOZZLE

●   DENOTES HARDWALL PANEL OR COANNULAR NOZZLE

CONFIGURATION II – FLIGHT SIMULATOR LIP, COANNULAR NOZZLE

CONFIGURATION IV – FLIGHT SIMULATOR LIP, MIXER-COMPOUND NOZZLE

CONFIGURATION V – NACELLE LIP, MIXER-COMPOUND NOZZLE

Figure 7-14.   QCGAT Acoustic Test Configurations.
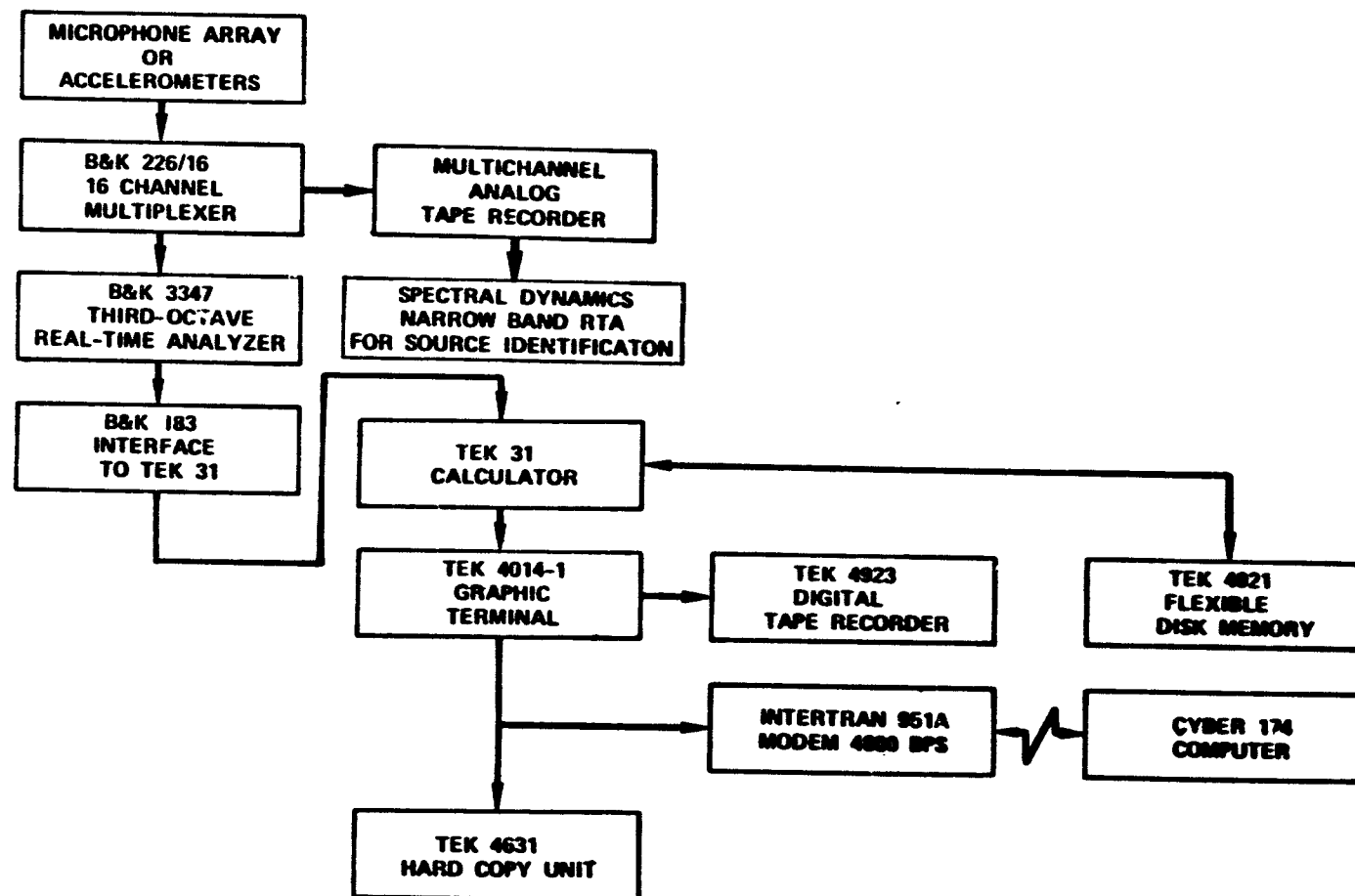
Figure 7-15.   Acoustic Data Acquisition, Analysis, and Software System.

```
┌────────────────────────────┐        ┌──────────────┐
│Program DRIVER              │   ─/─  │    TEK 31    │
│ (Interactive)             │        │    SYSTEM    │
│ .Transmits SPL Data Files │        └──────────────┘
│ ..Measured SPL data       │
│ ..Text                    │   ─/─  ┌──────────────┐       ┌──────────────────┐
│ ..Test conditions         │        │     CDC      │       │ Temporary Storage │
└────────────────────────────┘        │  CYBER 174   │       └──────────────────┘
                                      └──────────────┘       ┌──────────────────┐
                                                             │ Acoustic Data Base│
                ┌──────────────────────────┐                │   .Disk Storage   │
                │    Program ALAB          │                │   .Tape Storage   │
                │    (Interactive)         │                └──────────────────┘
                │  .Translates SPL Data Files │
                │  .Stores File in Acoustic Data Base │
                └──────────────────────────┘
```

Program SEARCH
(Interactive)

.Retrieves requested SPL data files from data base
.Performs Data Base Audit
.Performs ΔdB calculations between 2 files
.Generates system commands for plots and microfiche
.Generates execution commands for Program SPL

Program SPL
(Interactive)

.Uses SPL Data Files retrieved by SEARCH
.Produces corrected SPL spectra, computes PWL and Directivity
    Indices
.User Options include:
 ..Atmospheric absorption correction
   ...
 ..Ground reflection correction
    ..?Boeing procedure
    ...SAE 1327
    ...QCGAT procedure
 ..Create a combined SPL spectra from ground and pole microphones
    ...used only with Boeing ground reflection correction procedure
 ..Surface area selection for PWL calculations
 ...Input surface areas
 ...Areas calculated for Cell 76 using mike height, source height,
    radius, and mike angles.
 ..Output selection
  ...Printer and microfiche
      -1/3 octave bands and octave bands
      -Linear and A-scale
      -Space-averaged SPL spectra
      -Directivity indices
      - ΔdB's between 2 PWL spectra 1/3 octave bands
      - PWL and PNLT
  ...Calcomp plots
      -1/3 octave band SPL spectra
      -Single mike or 2 mike comparison
      -Linear and/or A-scale
      -Directivity patterns, multi-mike capability
  ...Disk
      -Storage of corrected/combined spectra on Acoustic Data Base

Figure 7-16.   Automated Data Analysis System Flow Chart.

112

$$R_1 = [r^2 + (h_s - h_r)^2]^{1/2} \qquad R_2 = [r^2 + (h_s + h_r)^2]^{1/2}$$

$$\Delta r = R_2 - R_1 \qquad\qquad R' = R_2/R_1$$

Figure 7-17.   Ground Reflection Correction Model.

$$\Phi = \frac{e^{ikR_1}}{R_1} + \frac{e^{ikR_2}}{R_2} \; [R_p + F \; (1-R_p)]$$

The plane wave reflection coefficient, R_p, is defined as:

$$R_p = \frac{\sin\phi - Z_1/Z_2}{\sin\phi + Z_1/Z_2}$$

and the impedances are:

$$Z_1 = \rho_o C_o \text{ for air, and}$$

$$Z_2 = R + iX \text{ for the ground.}$$

The boundary-loss factor, F, is a part of the ground wave representation and is a complex function of a complex argument, w, i.e.:

$$F(w) = 1 + 2 \; i \; \bar{w} \; e^{-w} \int_{-i\sqrt{w}}^{\infty} e^{-u^2} du$$

For the locally reacting case, w, the "numerical distance" is assumed to be:

113

$$w = \frac{ikR_2}{2} \frac{(Z_1/Z_2 + \sin\phi)^2}{(1+Z_1/Z_2 \sin\phi)}$$

From , the source strength of the image, or reflected wave, is:

$$Q = R_p + F (1-R_p)$$

The velocity potential can be approximated by:

$$\Phi \cong \frac{e^{ikR_1}}{R_1} [1 + \frac{R_1}{R_2} Q e^{ik\Delta R}]$$

Thus, setting $Q = |Q|e^{i\theta}$, the excess attenuation due to ground reflection, in one-third octave bands, is:

$$Ae_i = 10 \log_{10} \left[1 + \frac{|Q_i|^2}{R'^2} + \frac{|Q_i|}{R'} \frac{\sin(\mu\Delta R/\lambda_i)\cos(\eta\Delta R/\lambda_i + \theta_i)}{\mu\Delta R/\lambda_i} \right]$$

where:

$$\eta = 2 \pi 1 + (\Delta f_i/2f_i)^2 {}^{1/2}$$

$$\mu = 2\pi\Delta f_i/2f_i$$

$$\lambda_i = c/f_i$$

f_i = center frequency of ith 1/3-octave band

Δf_i = frequency range of ith 1/3-octave band

R' = R_2/R_1

The above methodology for predicting the excess attenuation of ground reflections is contained in an AiResearch computer program and was used to establish the average ground impedance at San Tan and the ground-reflection corrections to be applied to the measured data. References 6 through 13 were reviewed extensively in the preparation of this methodology.

The impedance correlation procedure used is outlined as follows:

1. Measured data for test CF208 at all three microphone heights and all 16 array angles were used to obtain final San Tan soil impedance estimates.

114

2. From previously published data, an initial normalized impedance array was assumed ($R/\rho c$ and $X/\rho c$ versus frequency)

3. The excess attenuation, A_e, was computed for each microphone height and corrected SPL (SPL_c) spectra were determined.

4. A 3-way difference scheme was used to calculate the differences between the 3 corrected spectra at each 1/3-octave band.

5. Iterations were performed on the values of $R/\rho c$ and $X/\rho c$ until all differences approached zero (steps 3 and 4, above). The convergence criteria was based upon the values of average differences at each 1/3-octave band. When reasonable values of impedance failed to provide convergence at a 1/3-octave band, the two microphone heights furthest away from a null frequency were used and convergence was then obtained.

6. Inasmuch as the convergence criteria was based only upon average differences, observations of individual differences were then made, and minor adjustments to the normalized impedance were performed to establish the final impedance values given in Figure 7-18.

7. Excess attenuation 1/3-octave band spectra were computed for the 3 microphone heights, based upon the final ground impedance estimates. See Figure 7-19.

8. These A_e spectra then were applied to the CF208 measured data for all 3 microphone heights and comparison plots were prepared at representative array angles, as shown in Figures 7-20 through 7-23.

9. Acoustic measurements were also made at the 3 microphone heights for another QCGAT operating condition, CF205. To check the relative validity of the ground reflection correction procedure, the A_e spectra were applied to the CF205 data and comparison plots of the corrected data again were made. The correlation of the CF205 corrected data was shown to be consistent with that of the CF208 corrected data.

The ground correction procedure was used to correct all of the data taken with the microphones located 1.52m (5 ft.) above the ground. Figures 7-24 through 7-31 are plots of the raw and corrected spectra for acoustic configuration 5, (hardwall mixer configuration) at takeoff and approach conditions at the 0.873-, 1.571-, 2.269-, and 2.618-radian (50-, 90-, 120-, and 150-degree) far-field locations.

115
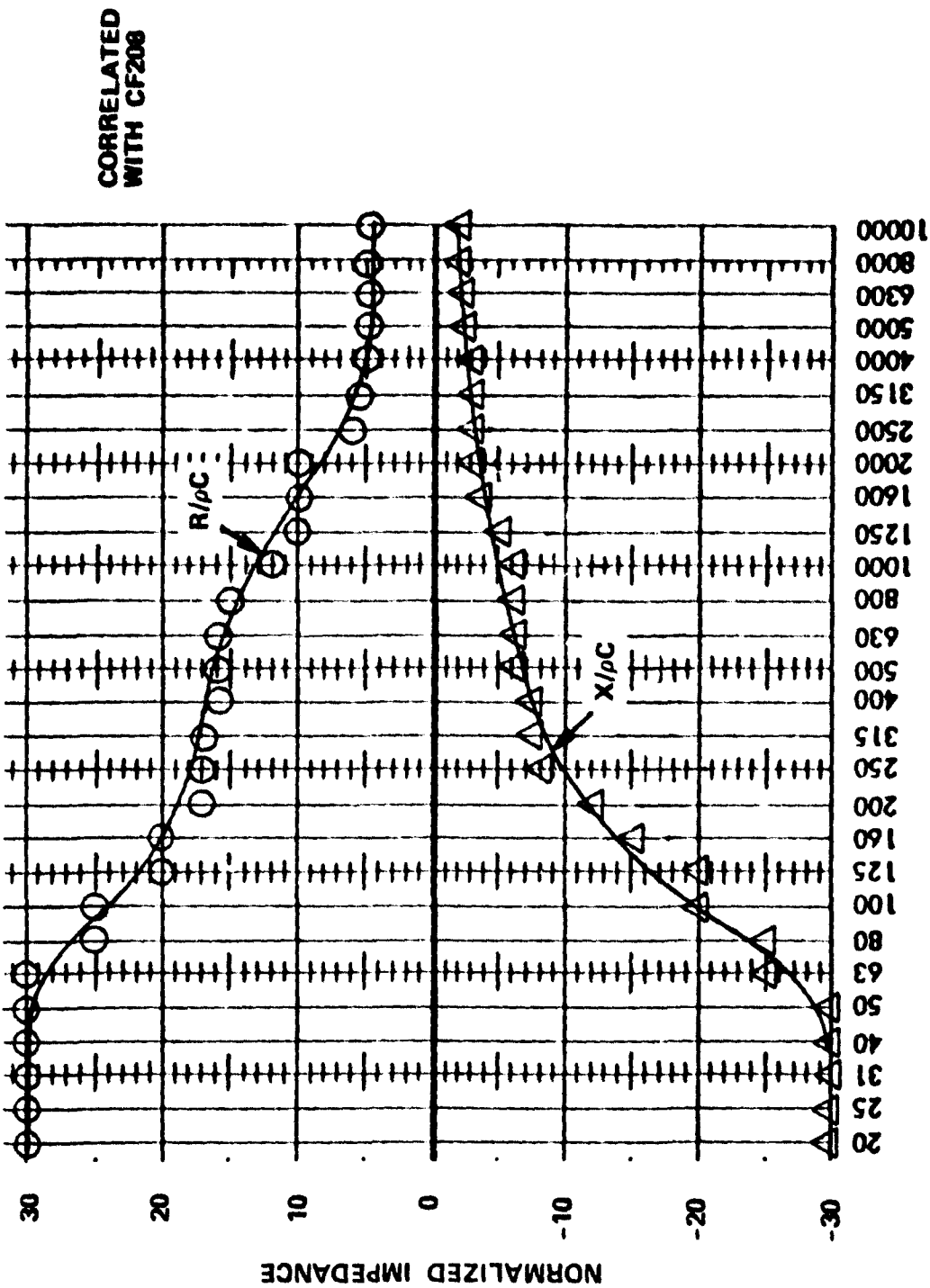
Figure 7-18. Correlated Acoustic Impedance for Desert Soil at San Tan.

116
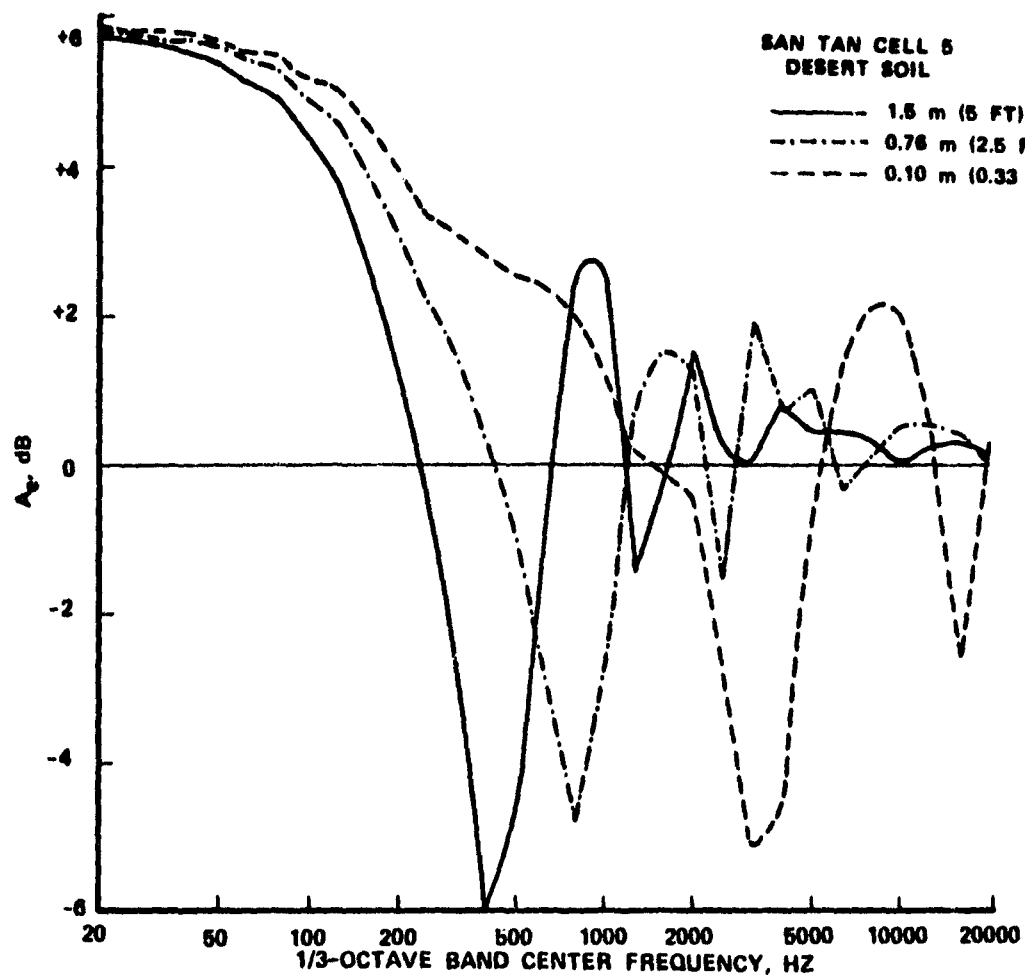
Figure 7-19. Ground Reflection Excess Attenuation, A_e.
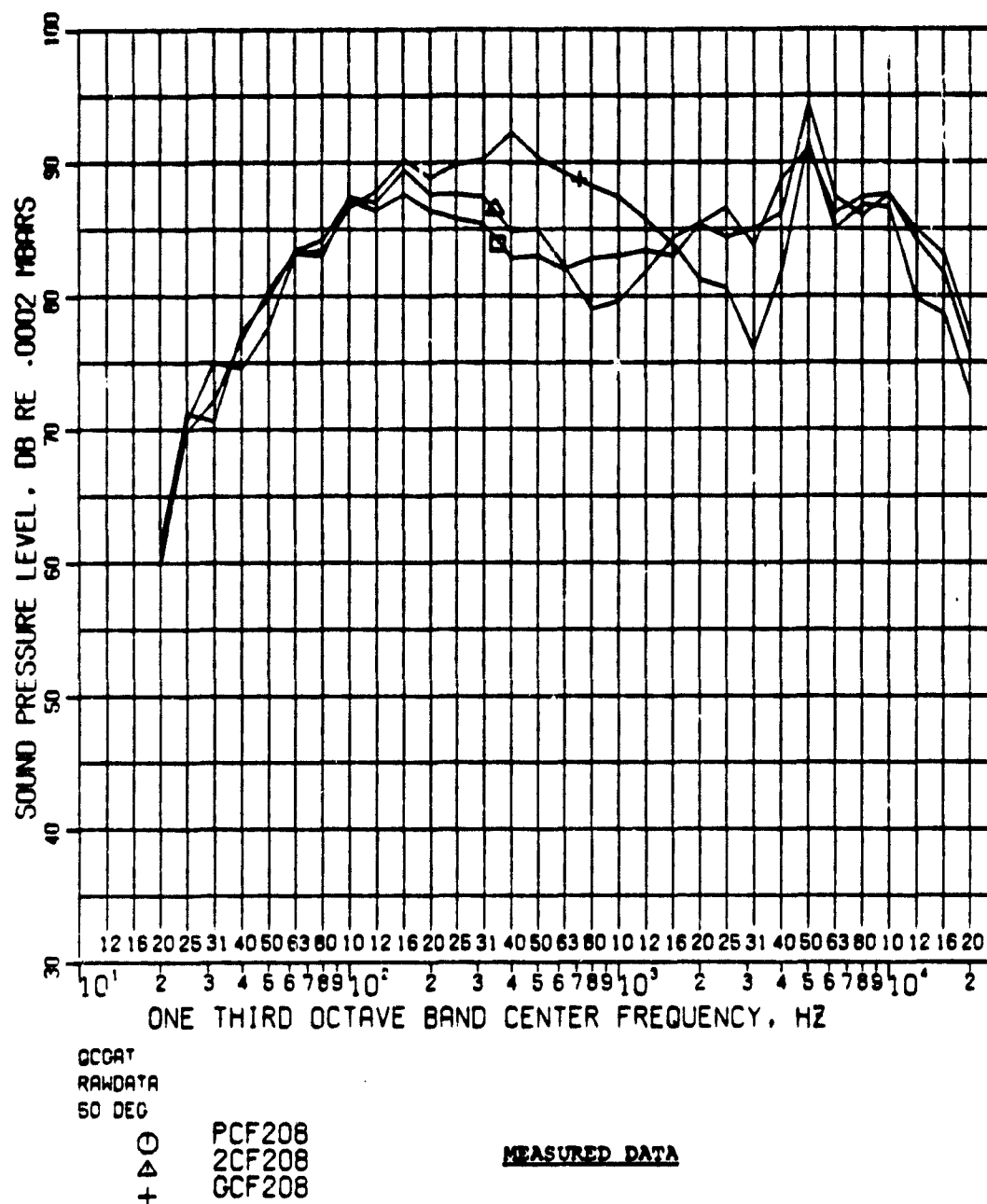
Figure 7-20. Measured Data Acoustic Configuration No. 2, 0.873 Radian (50-Degree) Position.

Figure 7-21. Corrected Data, 18,630 Rpm N_1, 0.873 Radian (50-Degree) Position.

119
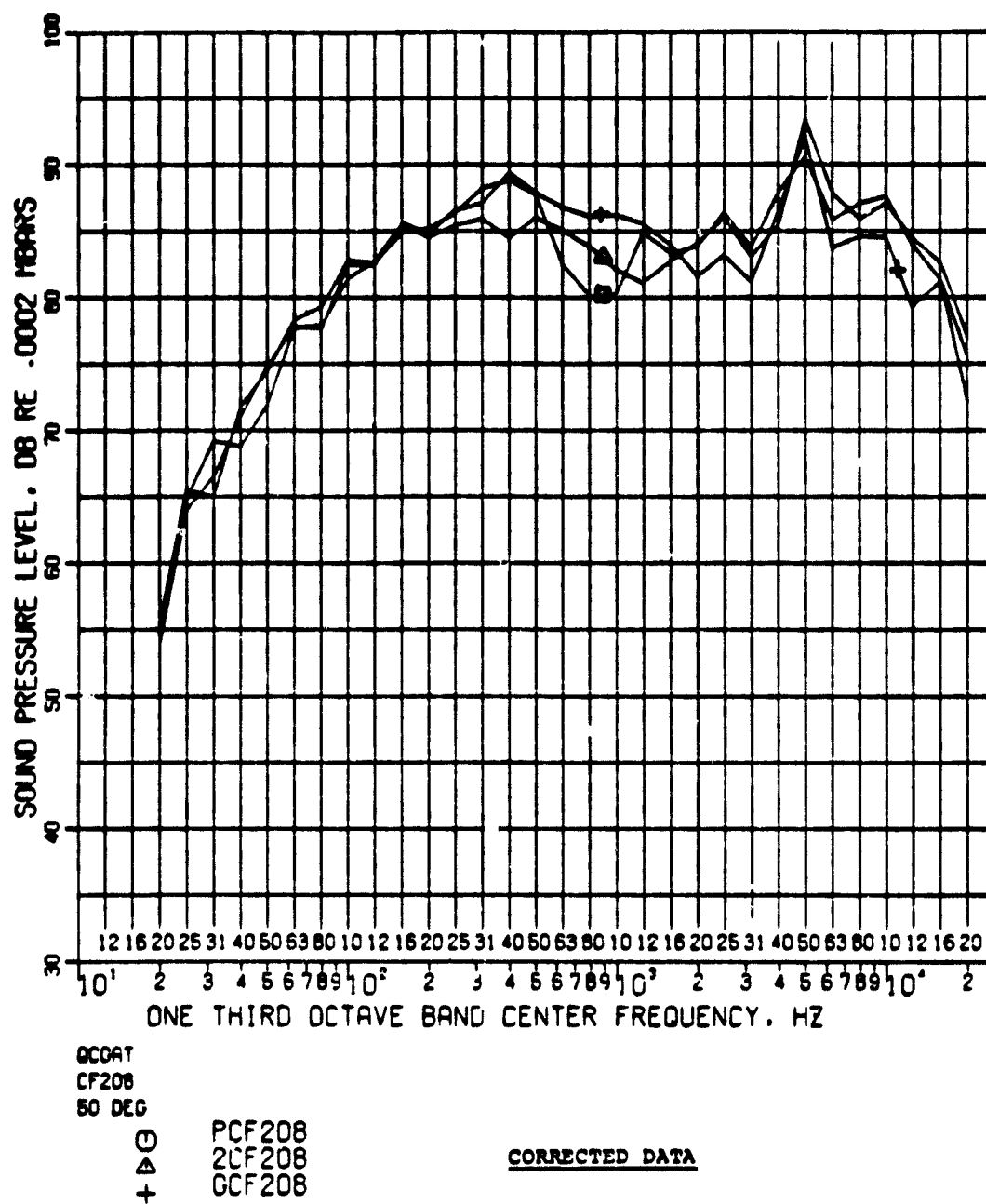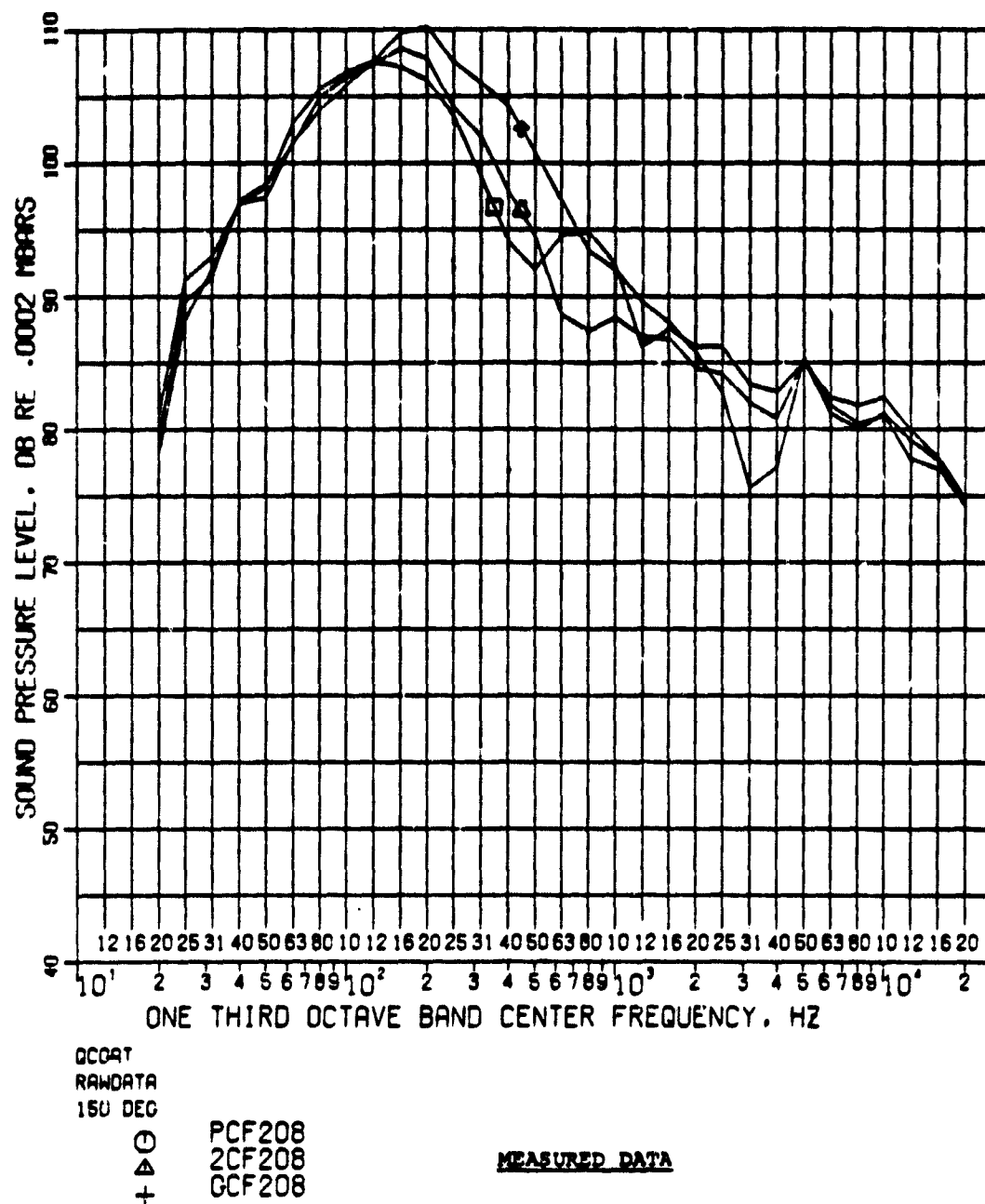
Figure 7-22.   Measured Data, Acoustic Configuration No. 2, 2.618
Radian (150-Degree) Position.

120
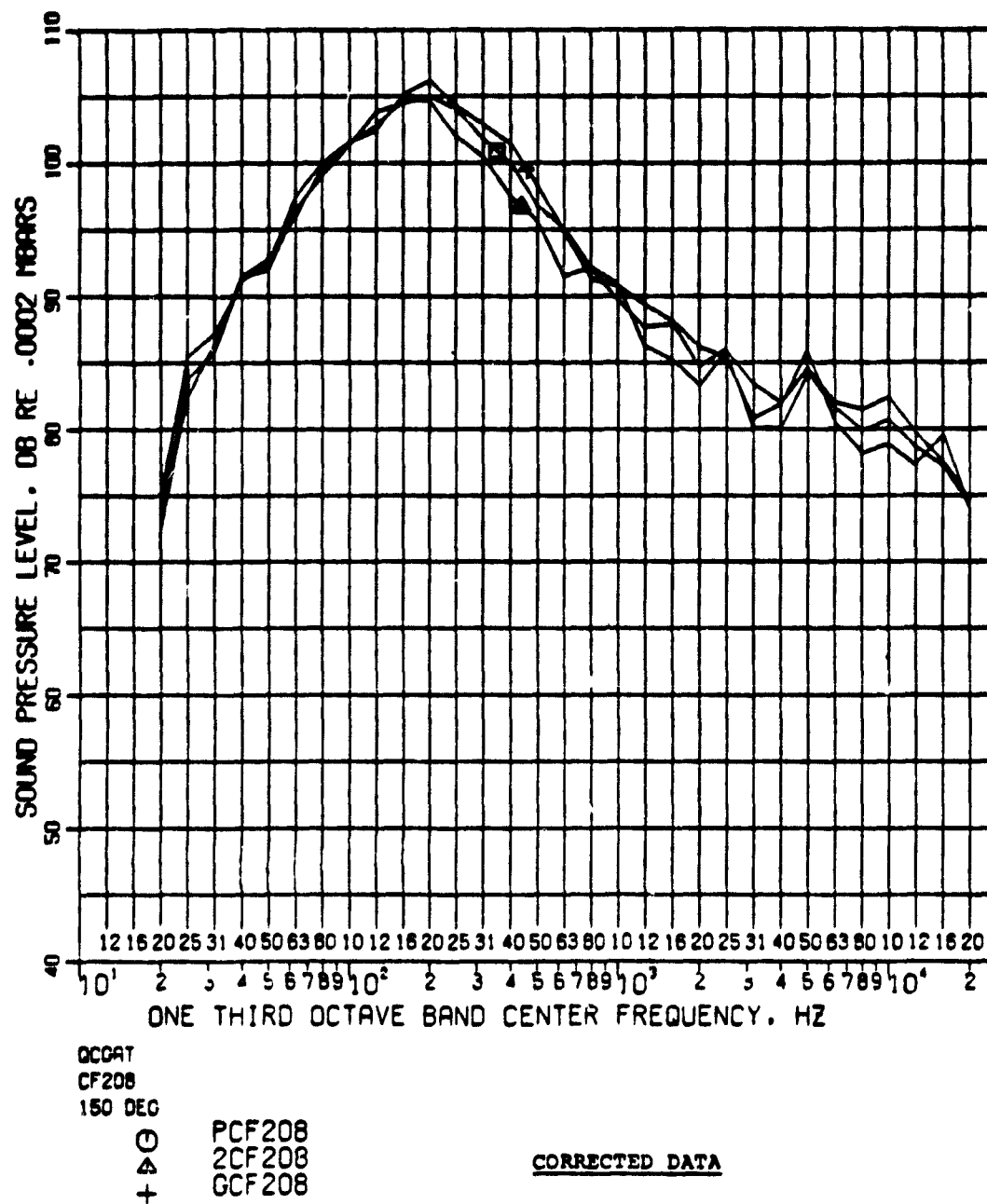
Figure 7-23.   Corrected Data, 18,630 Rpm N_1, 2.618 Radian (150-Degree) Position.
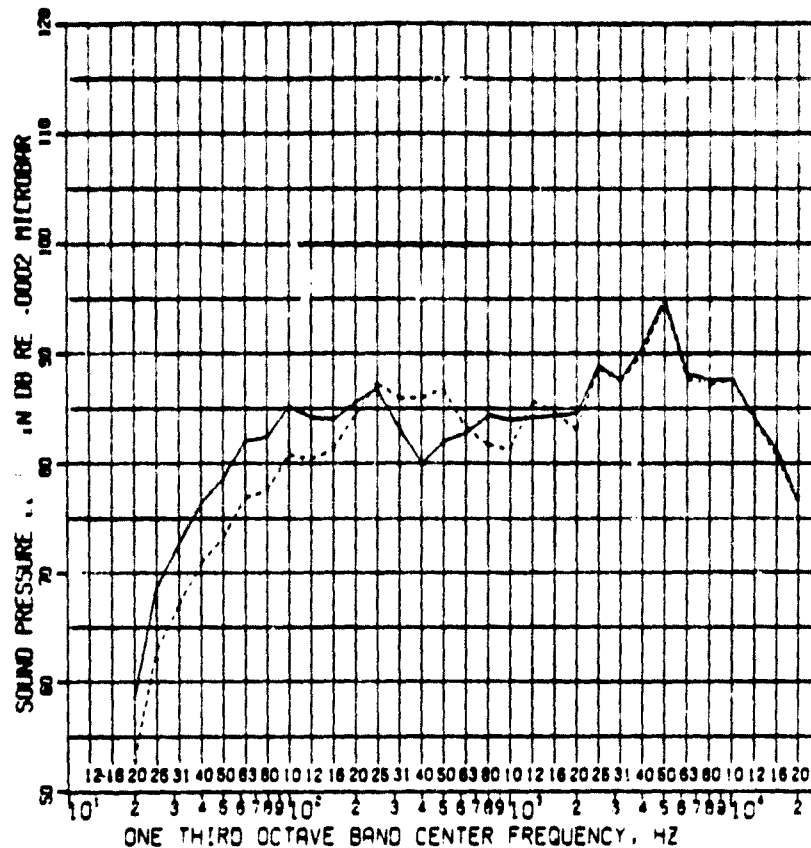
Far-Field 16-Mike Array, 30.48 m (100 ft) Radius,
Mike Height 1.5 m (6 ft) 0.873 rad (50°)
————— Raw Data
— — — — — Corrected Data

Figure 7-24.   Corrected Versus Raw Data, Code Point CF508, 0.873
Radian Position.
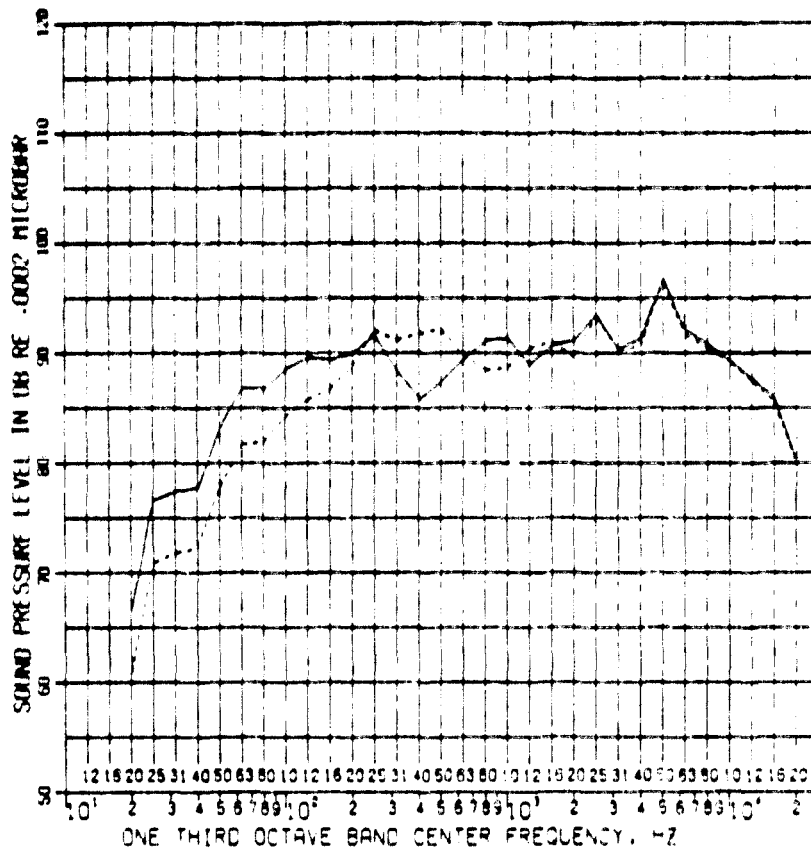
Far-Field 16-Mike Array, 30.48 m (100 ft) Radius,
Mike Height 1.5 m (6 ft) 1.571 rad (90°)
———— Raw Data
— — — — - Corrected Data

Figure 7-25.   Corrected Versus Raw Data, Code Point CF508, 1.571
               Radian Position.

123
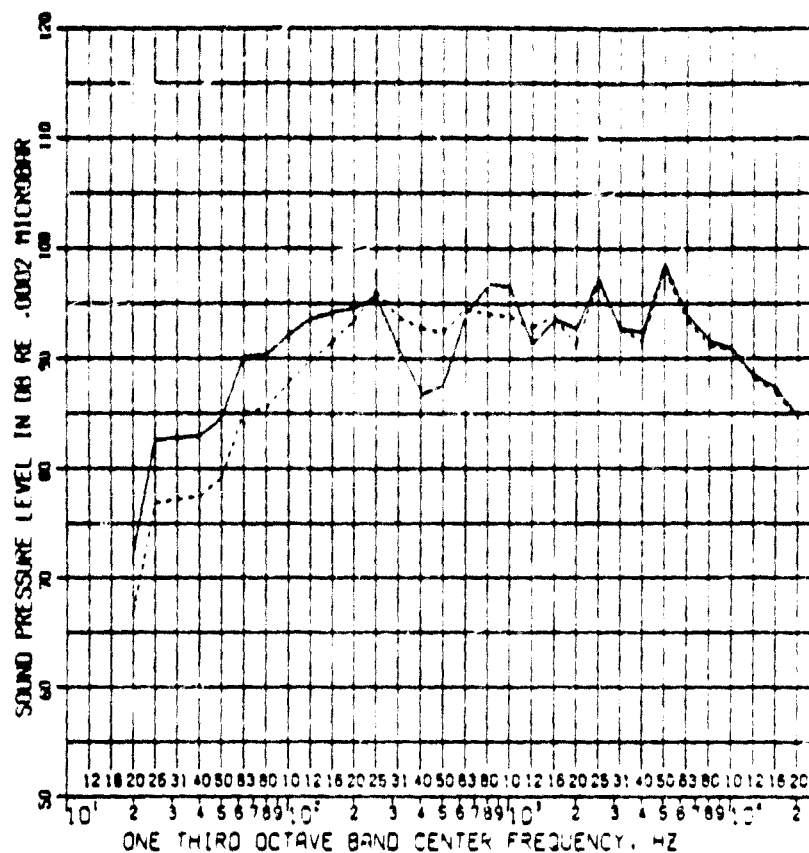
Far-Field 16-Mike Array, 30.48 m (100 ft) Radius,
Mike Height 1.5 m (6 ft) 2.094 rad (120°)
——————— Raw Data
— — — — Corrected Data

Figure 7-26 Corrected Versus Raw Data, Code Point CF508, 2.094
Radian Position.

124
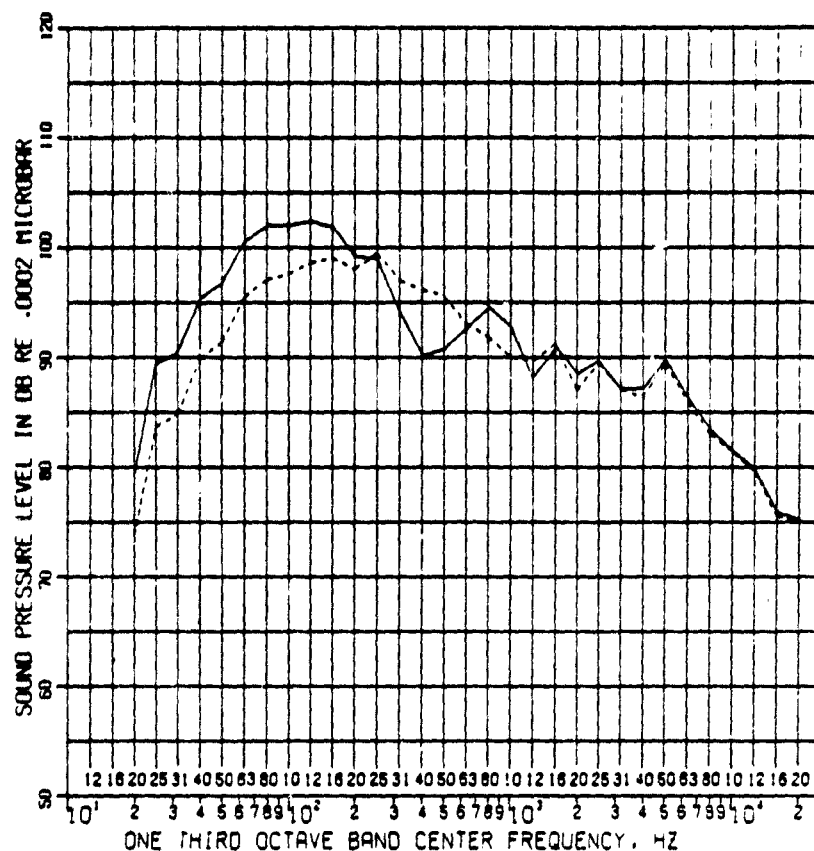
Far-Field 16-Mike Array, 30.48 m (100 ft) Radius,
Mike Height 1.5 m (6 ft) 2.618 rad (150°)
——————— Raw Data
— — — — — Corrected Data

Figure 7-27. Corrected Versus Raw Data, Code Point CF508, 2.618
Radian Position.
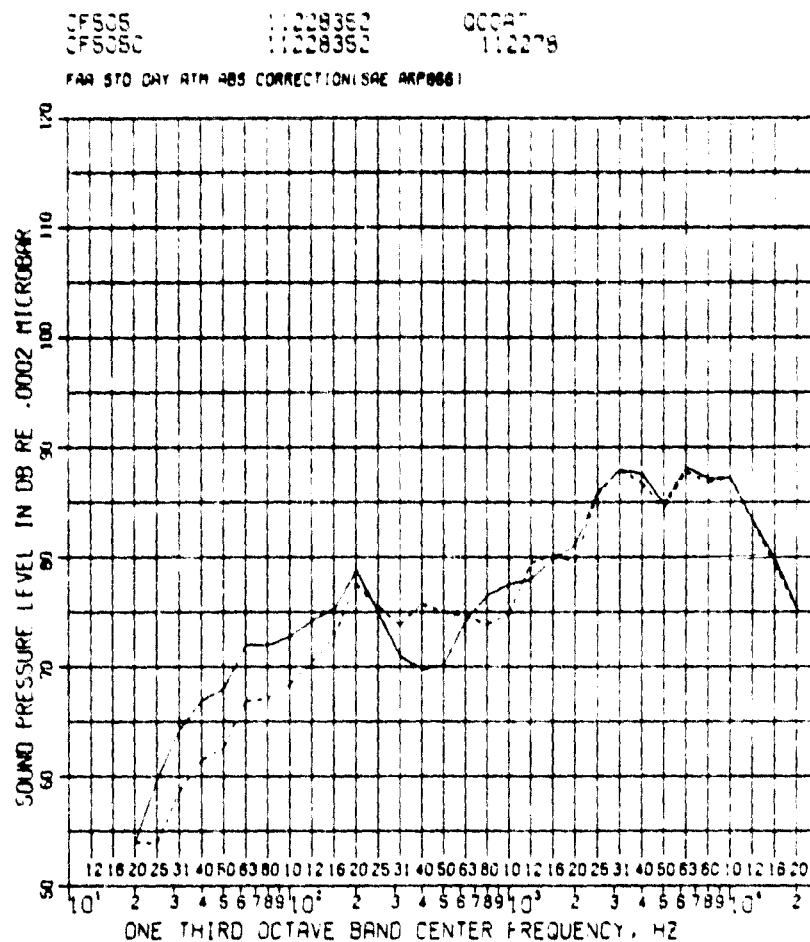
Far-Field 16-Mike Array, 30.48 m (100 ft) Radius,
Mike Height 1.5 m (6 ft) 0.873 rad (50°)
——————— Raw Data
— — — — — Corrected Data

Figure 7-28. Corrected Versus Raw Data, Code Point CF505, 0.873
Radian Position.

126

Far-Field 16-Mike Array, 30.48 m (100 ft) Radius,
Mike Height 1.5 m (6 ft) 1.571 rad (90°)
──────── Raw Data
── ── ── ── ── Corrected Data
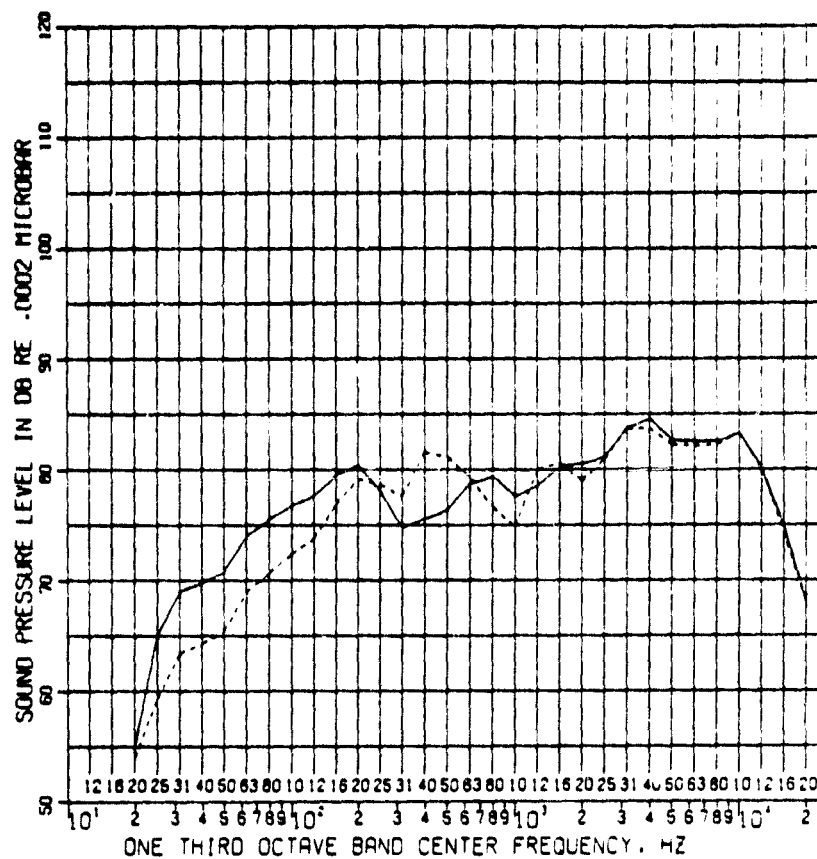
Figure 7-29.   Corrected Versus Raw Data, Code Point CF505, 1.571
Radian Position.
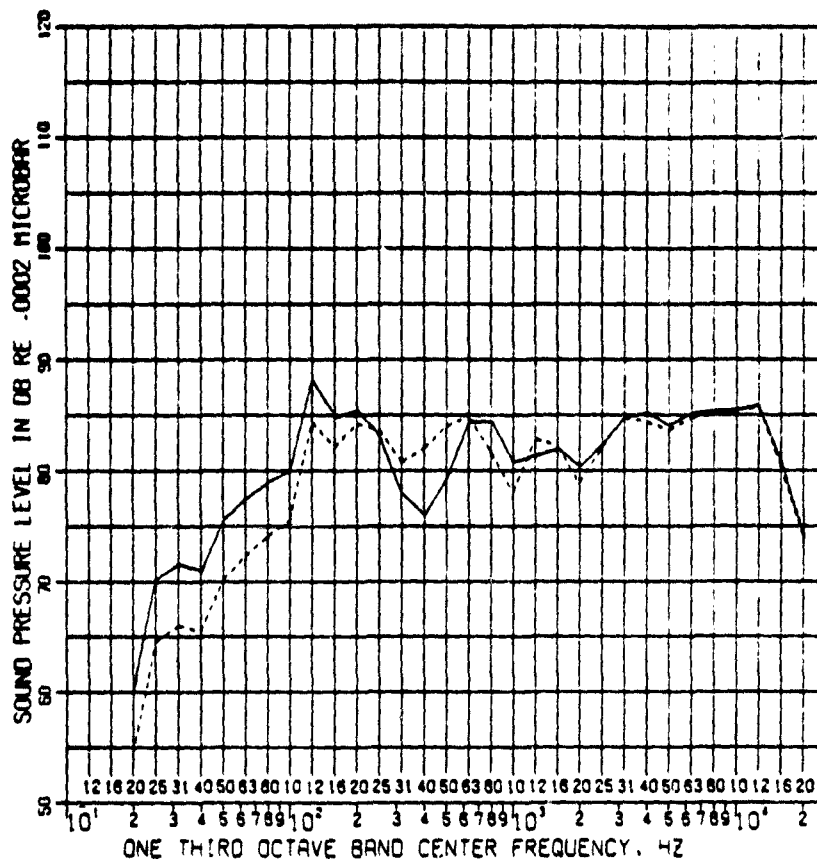
Far-Field 16-Mike Array, 30.48 m (100 ft) Radius,
Mike Height 1.5 m (6 ft) 2.094 rad (120°)
———————— Raw Data
— — — — — Corrected Data

Figure 7-30.   Corrected Versus Raw Data, Code Point CF505, 2.094
Radian Position.

128

Far-Field 16-Mike Array, 30.48 m (100 ft) Radius,
Mike Height 1.5 m (6 ft) 2.618 rad (150°)
─────── Raw Data
── ── ── Corrected Data

Figure 7-31.   Corrected Versus Raw Data, Code Point CF505, 2.618
                Radian Position.
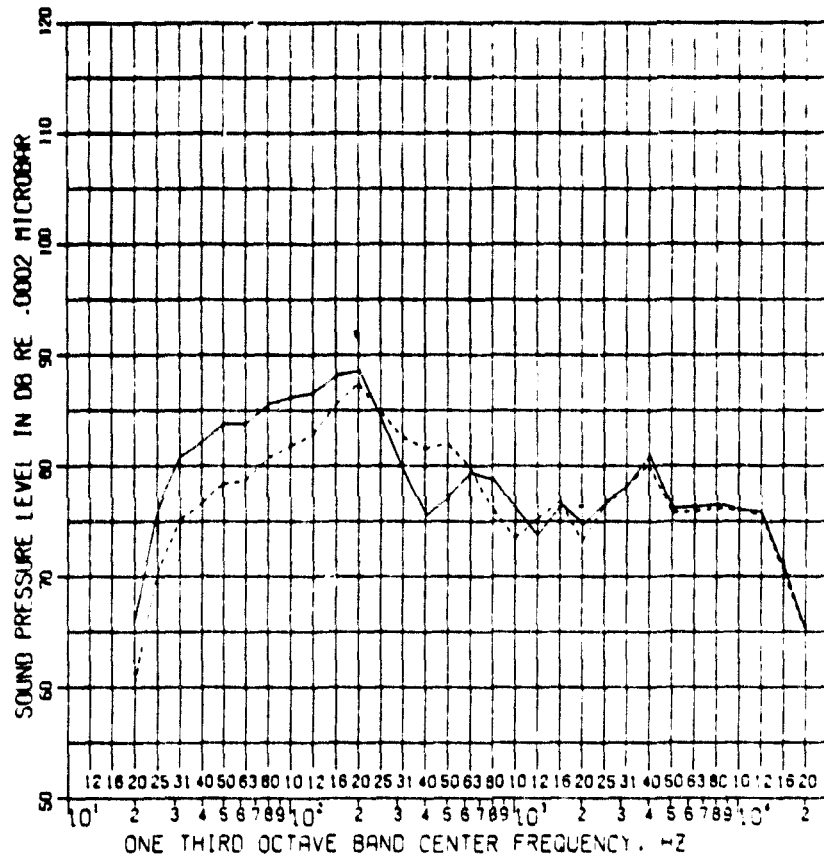
Because of the relative nonuniformity of the ground conditions at the San Tan QCGAT test site, it is highly probable that the actual ground impedance was different at each microphone location. Improved ground reflection correction spectra might have been obtained by determining a separate ground impedance at each microphone location. However, this would entail the use of a large amount of additional test data and appeared to be beyond the scope of the work statement. It was also felt that the overall benefits of establishing individual impedance models at each microphone location would be minimal when projected to flyover conditions.

It is recommended, however, that statistical methods be applied to any future determination of ground impedance when the acoustic data has been obtained over nonuniform ground conditions.

7.3.4 Noise Source Correlations

A primary objective of the QCGAT acoustic program is to determine flyover noise levels based on static engine data, and to demonstrate that these noise levels meet the program goals that have been set well below current technology aircraft levels. To accomplish the above objectives, a methodology was derived to: predict major component noise sources; adjust the individual sources based on static data; and project these sources to the flight condition.

The analytical tools used by AiResearch to predict the QCGAT noise sources are presented in Table 7-13. The prediction procedures for fan noise, core noise, and jet noise are based upon the NASA ANOPP recommended procedures, with empirical modifications based upon TFE731 acoustic data. The turbine noise is predicted using a method developed by General Electric.

A comparison of predicted noise sources based upon these prediction procedures and measured data is shown in Figure 7-32. The fan noise prediction agrees well with the measured data with a slight overprediction of the blade passing harmonic. However, the measured low-frequency noise, particularly from 160 Hz to 2500 Hz, is higher than predicted jet and core noise. In order to account for this, it is necessary to make assumptions for the apportionment of the jet and core to the total noise signature. Two approaches were used and are shown in Table 7-14: The first model attributed the difference between predicted and measured noise in the 50- to 2500-Hz frequency range to the jet. Jet noise was adjusted accordingly on an average delta basis. The second model assumed jet noise predictions were valid, and adjusted the core noise to exactly match the measured data. Both models adjusted the fan and turbine noise to exactly match the measured levels in the appropriate frequency range.

130

TABLE 7-13. QCGAT ENGINE NOISE PREDICTION PROCEDURE.

Major Component Noise Sources Predicted	Prediction Method
o Fan Inlet Noise - Discrete, Broadband, Buzz Saw	NASA TMX-71763* FAA-RD-71-73*
o Fan Discharge Noise - Discrete, Broadband	NASA TMX-71763*
o Jet Noise	NASA TMX-73552
o Combustion Noise	NASA TMS-71627
o Turbine Noise	AIAA 75-449
o Total Noise	Sum of Individual Component Noise Levels

NOTE:

One-third octave spectra from 50 to 16,000 Hertz

Directivity angles from 10 to 160 degrees from inlet C_1

*Modified by AiResearch
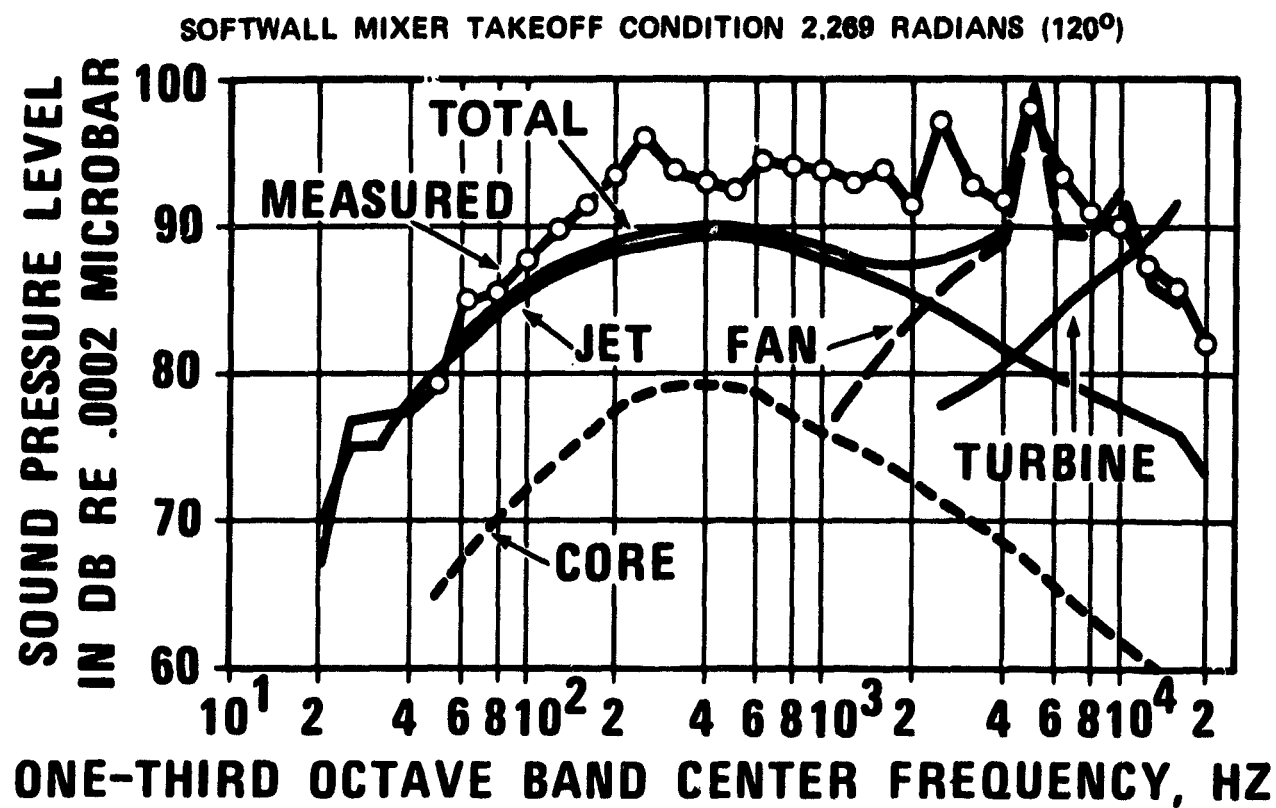
Figure 7-32. Comparison of Measured and Predicted Noise Levels Before Correlation.

TABLE 7-14.   NOISE PREDICTION METHODOLOGY COMPARISON.

Excess Jet Model	Excess Core Model
o TFE731-3 Acoustic Baseline	o TFE731-3 Acoustic Baseline
o Jet Noise Based on NASA Method Adjusted to Fair Through Low-Frequency Data	o Jet Noise Based on NASA Method
o Core Noise Based on NASA Method	o Core Noise Defined as Difference Between Measured and Predicted Sum of Jet, Fan, Turbine in 50-2500 Hz Frequency Bands
o Fan Discrete, Broadband, and Buzz Saw Adjusted to 731 Data	o Fan Inlet and Fan Discharge Defined as Difference Between Measured and Predicted Sum of Jet, Core, Turbine in 3150-10,000 Hz Bands
o GE Turbine Noise Method	o GE Turbine Noise Method

o The same flight profile, static-to-flight corrections, and wing shielding model was used for both cases. The ground correction models were compared and found to be in good agreement.

A schematic of the acoustic analysis system is shown in Figure 7-33. The measured data were shipped to the CDC CYBER 174 computer from the noise lab and processed through program ALAB. A general purpose data reduction program (SPL) corrected the data files for ground reflection and FAA 25°C (77°F) day conditions. Using the actual cycle performance for each acoustic data point, (see Table 7-15) the free-field noise source levels were predicted using program GTEN5. A new program called NASADELTA was written to compare the predicted and measured noise levels and generate delta spectra for each source. Two versions of this program were written based upon the two methodologies discussed previously. Program GTEN5 was used a second time to predict the noise sources for the flight condition. For comparative purposes, the initial Definition and Characteristics (DaC) values for the cycle parameters are listed with the final program results in Table 7-16. These predictions were then adjusted in program NASADELTA with the delta spectra determined from the ground static data.

An example of the jet noise dominated correlation is shown in Figure 7-34, for the softwall mixer at 2.09 radians (120 degrees) at takeoff condition. The average delta from 50 to 2000 Hz is applied to each frequency to produce a modified jet noise prediction that fits the low frequency data. Core noise is predicted to be well below the jet noise at both takeoff and approach conditions with this model. Above 2000 Hz, the fan noise discrete and broadband noise is adjusted to exactly fit the data. Turbine noise contributions were unimportant except in the high-frequency range above 12,500 Hz, out of the range of interest for perceived noise level calculations. Correlations of this sort were made for each far field angle from 0.17 to 2.79 radians (10 to 160 degrees).

The same set of acoustic data is shown in Figure 7-35, with the core noise dominated source correlation. The jet noise prediction is considerably below the measured data from 200 to 2000 Hz. The excess noise was attributed to the core as shown. The fan noise was determined as the difference between the measured total and the predicted sum of jet, core, and turbine in the 3150 to 10,000-Hz bands.

7.3.5 Acoustic Comparisons of Static Data

The corrected data for each acoustic configuration tested were compared on a tone-corrected perceived noise level (PNLT) basis. This established trends and illustrates the level comparisons with equivalent TFE731-3 takeoff- and approach-static data. The results of these comparisons are tabulated in Tables 7-17 and 7-18.

134
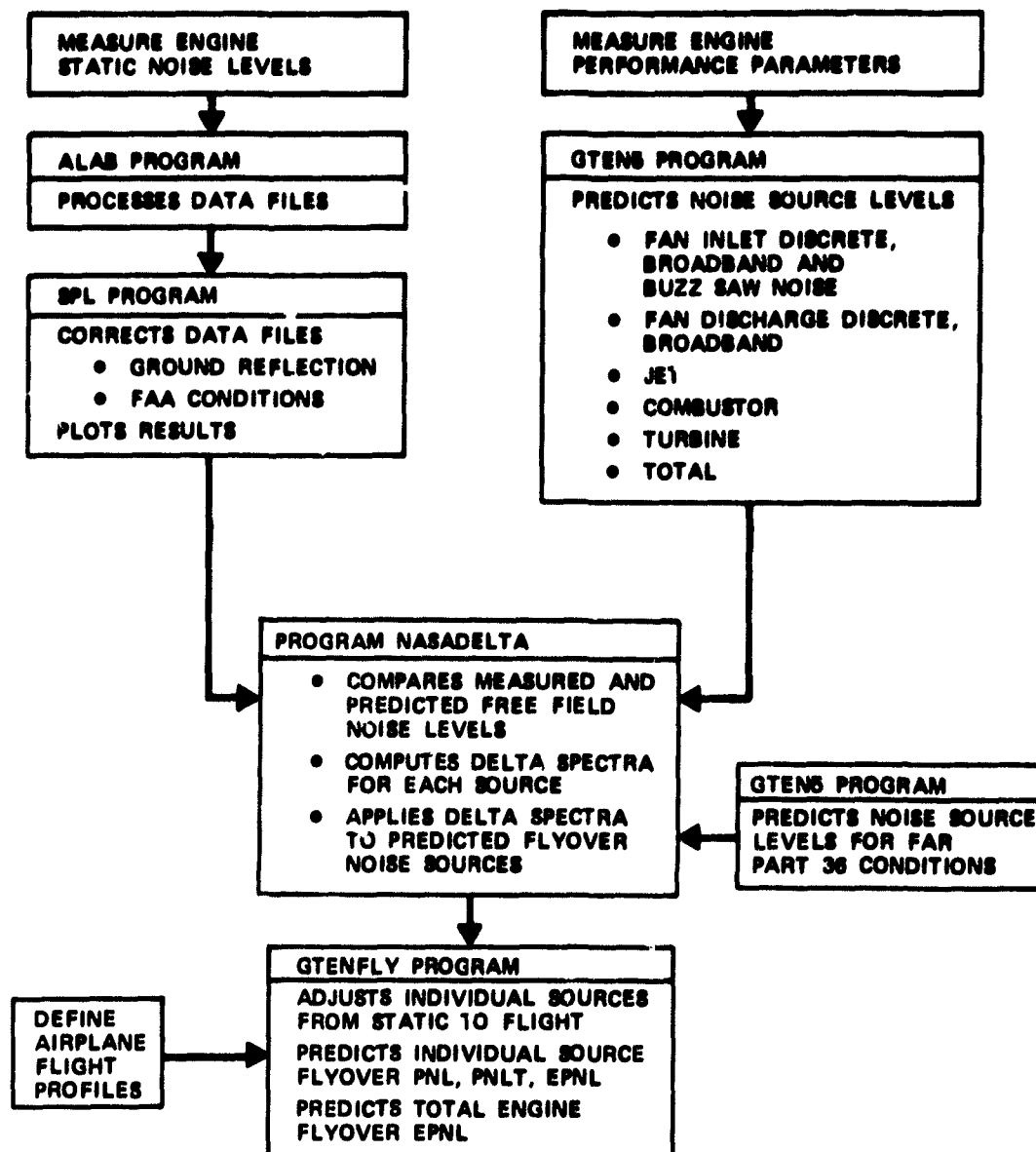
Figure 7-33. AiResearch Acoustic Analysis System.

TABLE 7-15. QCGAT ENGINE KEY ACOUSTIC PARAMETERS.

Engine Parameter	Simulated Static Test Condition, 48°F	
	Takeoff	Approach
Engine Net Thrust, N (lbs)	16,098 (3619.0)	7019.0 (1578.0)
Fan Rotor Speed, rad/s (rpm)	913.6 (8726.0)	634.8 (6063.0)
Fan Pressure Ratio, Tip	1.41	1.18
Fan Tip Relative Mach Number	1.17	0.79
Fan Blade Passage Frequency, Hz	5236.0	3638.0
Fan Weight Flow, kg/s (lbs/sec)	61.7 (136.1)	42.4 (93.5)
Core Weight Flow, kg/s (lbs/sec)	11.6 (25.5)	6.2 (13.6)
Mixer Exhaust Velocity, m/s (ft/sec)	257.9 (846.0)	166.1 (545.0)
Mixer Exhaust Total Temperature, K (°R)	406.0 (732.3)	366.0 (658.6)
LP Turbine Rotor Speed, rad/s (rpm)	1941.5 (18543.0)	1348.9 (12883.0)
Turbine Last Stage Rel. Tip Mach No.	0.472	0.349
Turbine Last Stage Pressure Ratio, T-S	1.61	1.22

TABLE 7-16. QCGAT ENGINE KEY ACOUSTIC PARAMETERS.

Engine Parameter	FAR Part 36 Certification Condition					
	Takeoff		Sideline		Approach	
	Final	DAC	Final	DAC	Final	DAC
Engine net thrust, N (lbs)	12,869.7 (2,893.0)	12,868.7 (2,893.0)	13,317.9 (2,994.0)	13,269.0 (2,983.0)	4,639.5 (1,043.0)	4,639.5 (1,043.0)
Fan rotor speed, rad/s (rpm)	958.9 (9159.0)	943.8 (9014.0)	954.8 (9119.0)	936.5 (8945.0)	641.4 (6126.0)	651.1 (6219.0)
Fan pressure ratio, tip	1.44	1.47	1.43	1.45	1.16	1.17
Fan tip relative Mach number	1.22	1.20	1.20	1.18	0.78	0.79
Fan blade passage Frequency, Hz	5495.0	5408.0	5471.0	5367.0	3677.0	3731.0
Fan weightflow, kg/s (lbs/sec)	60.1 (132.4)	59.5 (131.1)	62.4 (137.6)	62.4 (137.6)	44.8 (98.7)	43.1 (94.9)
Core weightflow, kg/s (lbs/sec)	11.4 (25.2)	11.5 (25.4)	11.9 (26.3)	11.9 (26.3)	6.0 (13.7)	6.3 (13.9)
Mixer exhaust velocity, m/s (ft/sec)	285.3 (936.0)	287.1 (942.0)	284.4 (933.0)	282.9 (928.0)	175.9 (577.0)	173.4 (569.0)
Mixer exhaust total temperature, K (°R)	430.3 (772.3)	428.3 (771.3)	434.8 (780.8)	430.8 (776.3)	381.2 (686.7)	381.7 (688.3)
LP turbine rotor speed, rad/s (rpm)	2,037.7 (19,463.0)	2,005.4 (19,154.0)	2,028.9 (19,378.0)	1,990.1 (19,007.0)	1,363.3 (13,021.0)	1,383.7 (13,216.0)
Turbine last stage rel tip Mach no.	0.467	---	0.465	---	0.356	---
Turbine last stage pressure ratio, T-S	1.70	---	1.69	---	1.26	---

137
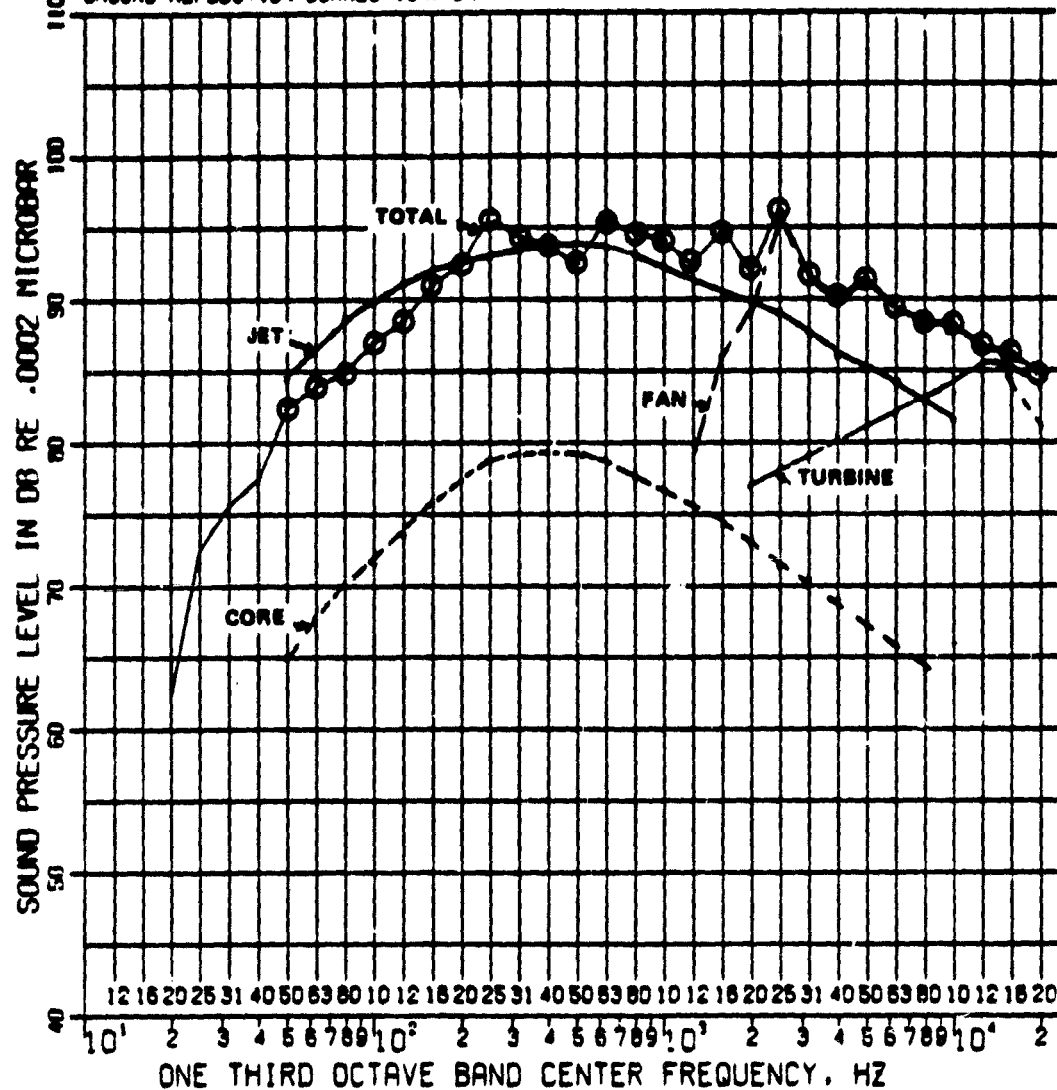
Figure 7-34. Jet Noise Dominated Correlation, Softwall Mixer, 2.269-Radian (120-Degree) Position.
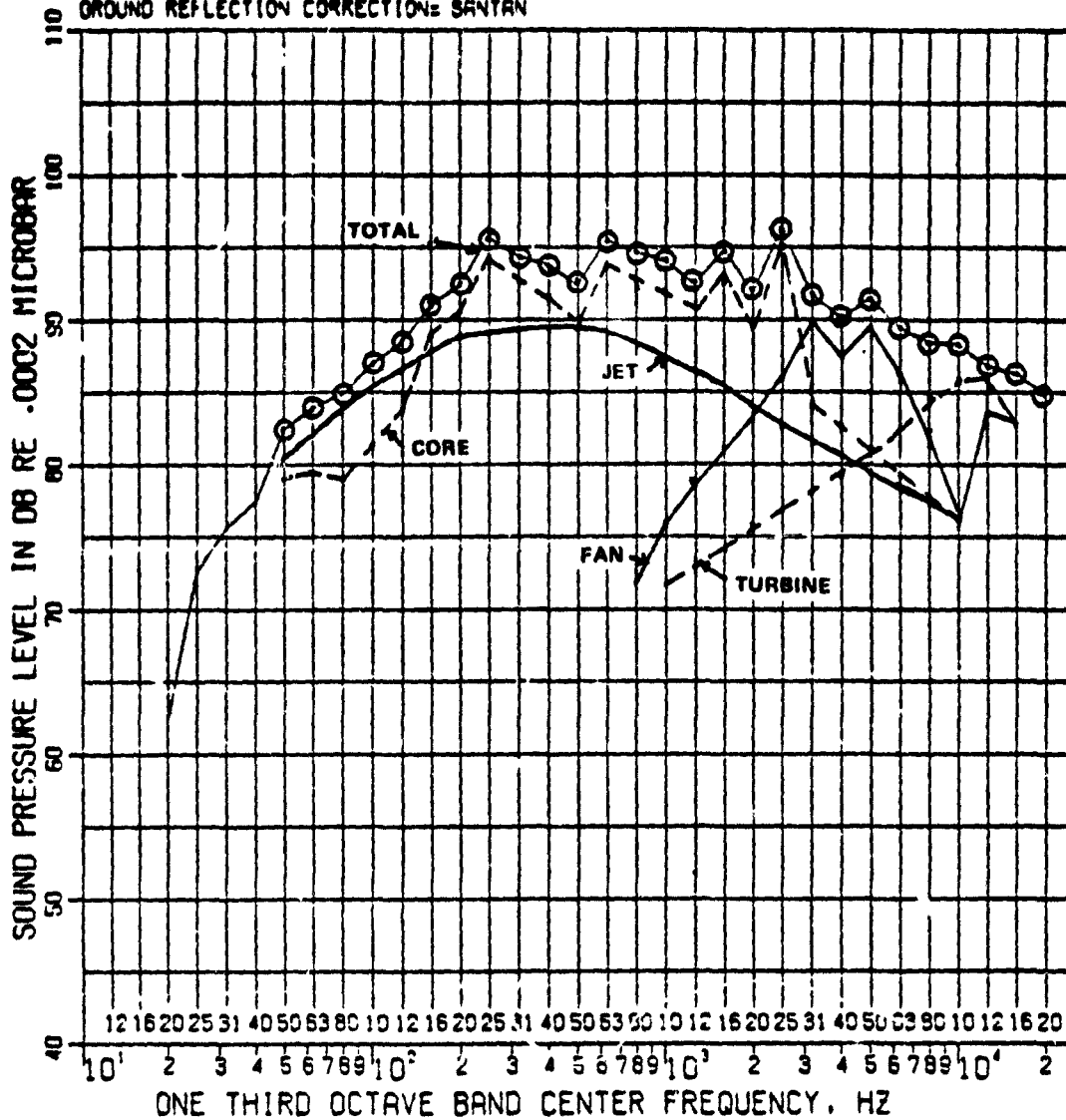
Figure 7-35.   Core Noise Dominated Correlation, Softwall
Mixer, 2.269-Radian (120-Degree) Position.

TABLE 7-17.   ACOUSTIC COMPARISONS - TAKEOFF PNLT.

Angle Radian(°)	QCGAT Configuration No.							Run 9 TFE731-3
	1	2	3	4	5	6	7	
0.175(10°)	115.0	118.7	113.7	117.6	116.5	116.3	118.8	120.3
0.349(20°)	117.0	115.8	113.0	115.8	114.7	116.0	118.3	118.3
0.524(30°)	114.2	116.6	115.2	116.6	115.6	115.0	117.2	121.5
0.698(40°)	112.1	113.5	113.1	114.7	116.1	114.5	118.0	121.7
0.873(50°)	113.2	114.1	115.4	117.9	116.9	116.7	117.3	121.7
1.047(60°)	114.7	114.9	114.8	117.7	115.8	116.3	120.5	121.5
1.222(70°)	112.4	116.5	114.1	117.5	118.3	117.0	118.9	122.5
1.396(80°)	113.0	116.8	115.5	119.3	117.7	117.0	119.8	122.1
1.571(90°)	116.4	115.2	117.3	119.1	119.9	11 .	117.2	121.8
1.745(100°)	116.4	117.6	116.9	120.2	123.3	122.3	122.0	121.9
1.920(110°)	118.2	118.8	120.1	121.5	121.0	122.4	121.2	123.3
2.094(120°)	120.5	119.4	121.2	121.4	122.3	121.7	122.9	125.0
2.269(130°)	117.1	118.8	117.7	119.0	119.7	118.7	119.8	123.7
2.4.43(140°)	115.9	118.7	117.7	117.7	118.4	117.4	118.4	124.4
2.618(150°)	115.9	118.0	116.3	115.9	117.7	117.0	119.2	127.0
2.743(160°)	112.5	119.2	115.9	--	117.3	116.2	118.3	127.6

TABLE 7-18.   ACOUSTIC COMPARISONS - TAKEOFF PNLT.

Angle Radian(°)	QCGAT Configuration No.							Run 14 TFE731-3
	1	2	3	4	5	6	7	
0.175 (10°)	107.5	107.8	107.0	107.9	109.3	108.7	109.9	111.5
0.349 (20°)	107.4	107.9	107.0	107.9	109.8	110.8	110.0	113.1
0.524 (30°)	105.3	107.5	105.4	110.6	108.1	108.1	108.2	110.7
0.698 (40°)	105.1	106.0	105.4	109.0	107.5	109.1	109.7	111.7
0.873 (50°)	106.3	107.0	105.7	110.5	109.7	110.6	109.4	112.4
1.047 (60°)	104.8	104.8	103.3	107.3	108.3	109.3	109.2	111.7
1.222 (70°)	105.5	103.9	103.2	107.4	108.0	109.3	110.6	114.2
1.396 (80°)	103.1	104.1	103.4	108.1	109.3	109.5	109.6	115.3
1.571 (90°)	103.8	103.3	104.8	110.3	107.3	108.4	110.0	114.7
1.745 (100°)	104.8	106.6	105.7	110.4	109.4	109.1	114.5	114.5
1.920 (110°)	105.1	107.3	107.1	108.0	109.4	109.9	110.3	113.4
2.094 (120°)	105.7	107.5	107.9	109.0	109.3	110.0	111.0	113.5
2.269 (130°)	105.5	107.0	105.6	110.3	111.6	112.2	110.2	113.2
2.443 (140°)	102.8	104.0	103.4	107.1	107.9	108.4	107.4	112.2
2.618 (150°)	102.4	102.6	103.7	104.2	106.2	104.9	107.5	112.6
2.793 (160°)	98.6	101.9	100.8	--	105.4	105.0	105.3	113.5

Comparison of configurations 1, 3, 4, and 5 shows the effect of successively replacing softwall nacelle panels with hardwall panels. Configurations 2 and 7 are coannular nozzle exhaust systems and are significantly louder (particularly at takeoff power) at angles near the jet-exhaust centerline.

As previously noted, the aft barrel with the outer-aft panel is removed when the coannular nozzle system is installed. Thus the final acoustic-treatment panel is not used with Calibrations 2 and 7 (Configurations II and III). A comparison of configuration 5 and 6 shows that the inlet-nacelle lip and flight-simulator lip noise levels are quite similar on a PNLT basis.

Note that all the QCGAT configurations are significantly quieter than the TFE731-3 Engine, a current quiet business-jet engine. A comparative plot of the hardwall coannular configuration versus the TFE731-3 at takeoff condition is shown in Figure 7-36. A similar plot for the approach static condition is presented in Figure 7-37. A one-third octave spectral comparison at the 2.618-radian position (150°) from the inlet axis is presented in Figure 7-38.

A spectral comparison of the QCGAT mixer versus the QCGAT coannular nozzle for the hardwall nacelle configuration at the 2.618-radian position (150°), takeoff static condition is shown in Figure 7-39. At 200 Hz, the mixer is about 7 dB quieter than the coannular nozzle. Note, however, that there are peaks at 1600 and 2500 Hz with the mixer being 2- to 3-dB higher at these frequencies. Note that the mixer nozzle is about 7 dB higher at these frequencies. The source of these tones were investigated in detail, including some cross-correlation analysis at NASA. The results of this investigation revealed a high correlation between internal core noise and the far-field noise levels at certain discrete frequencies, primarily centered around 250 Hz and 2500 Hz. This led to the development of a new noise-source correlation attributing this excess noise to core noise.

Comparisons of treated versus hardwall spectra for the mixer nozzle and coannular nozzle configurations at approach static are shown in Figures 7-40 and 7-41. A broad attenuation was achieved, particularly at angles from 0.873 to 1.571 radians (50 to 90°) indicating attenuation of the desired low cut-off ratio modes.

7.3.6 Flyover Prediction Procedure

Calculated flyover noise levels for the QCGAT engine were based upon the adjusted noise sources obtained from correlating the predicted noise source levels with the measured corrected noise levels. The comparisons yielded a set of correction spectra for each noise source at all the engine operating conditions. Each spectrum was identified by two characteristic aeroacoustic parameters as listed in Table 7-19.

142
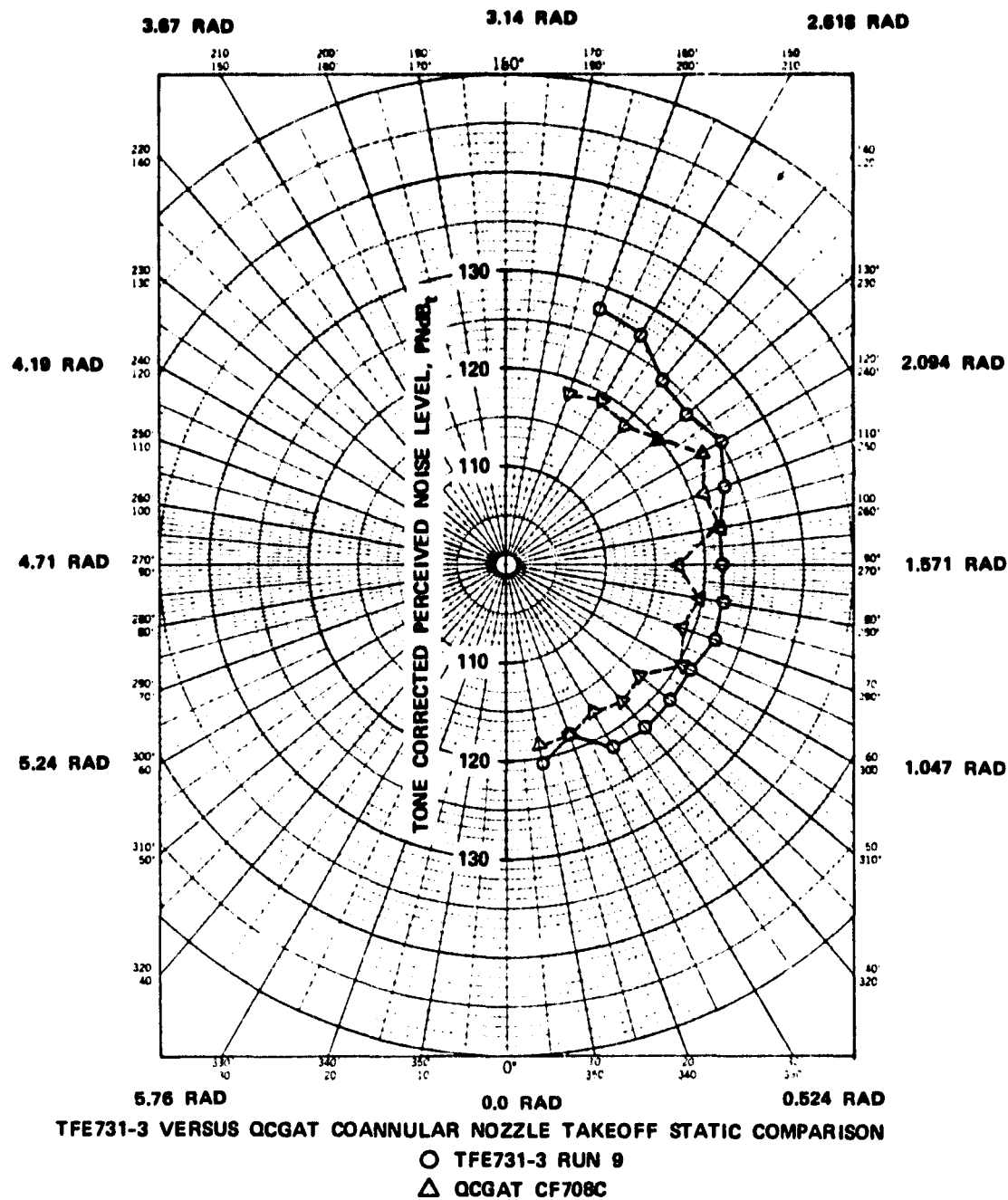
Figure 7-36. TFE731-3 Versus QCGAT Coannular Nozzle Takeoff Static Comparison.

O TFE731-3 RUN 14
△ QCGAT CF705C

Figure 7-37.   TFE731-3 Versus QCGAT Coannular Nozzle Approach
Static Comparison.
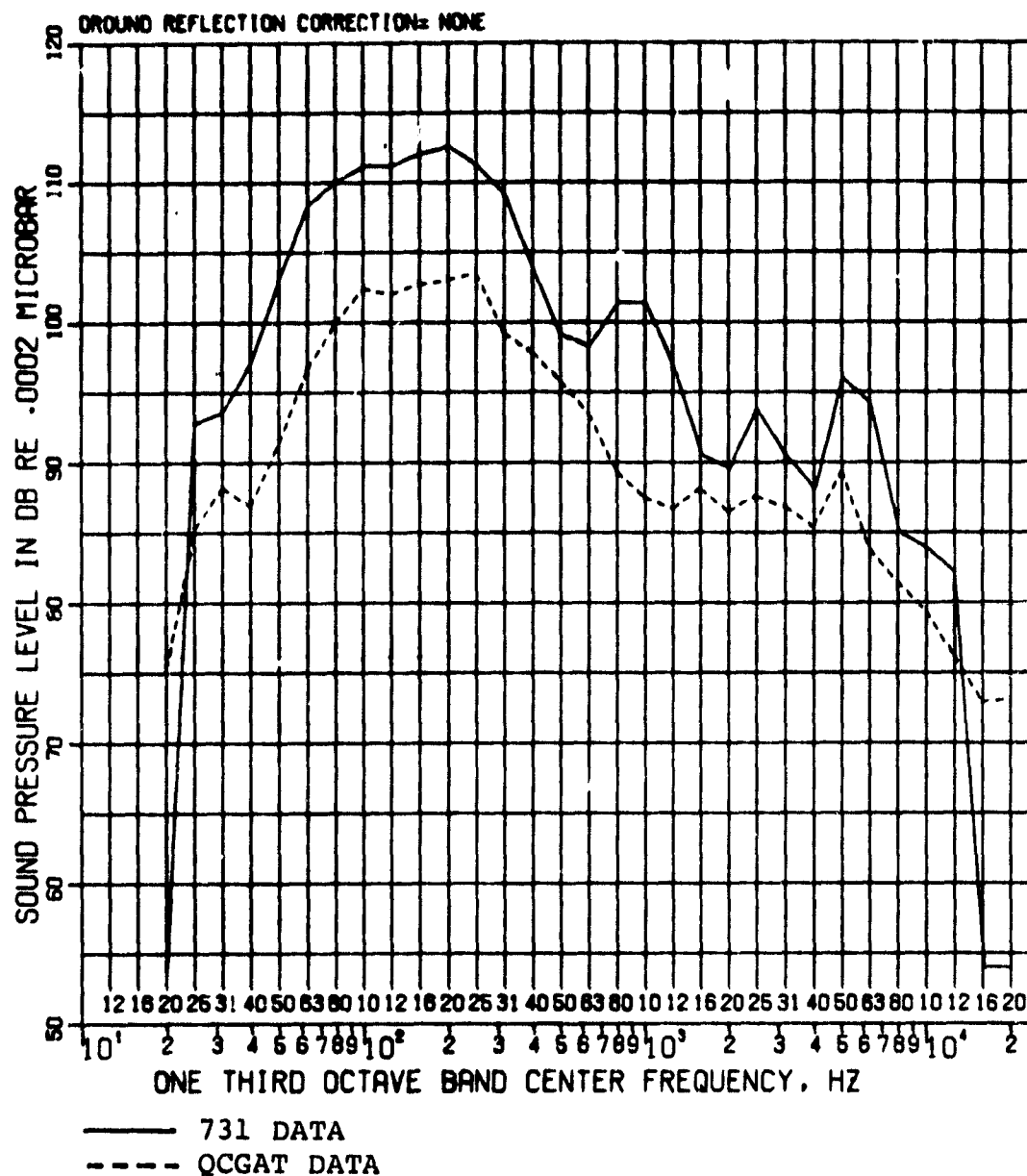
Figure 7-38. TFE731-3 Acoustic Data Compared to QCGAT Untreated Coannular Nozzle Configuration.
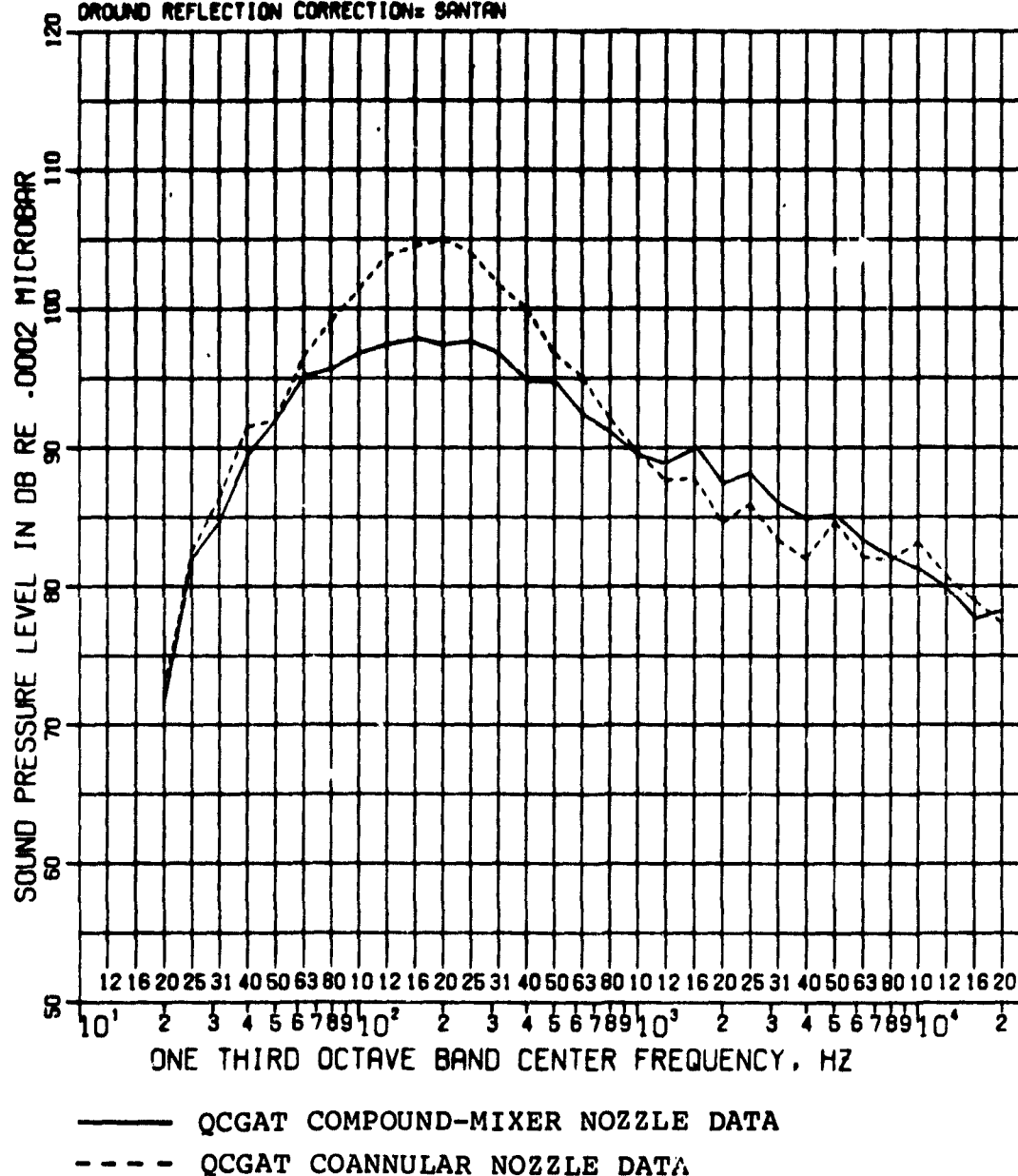
Figure 7-39. Compound-Mixer Nozzle Acoustic Data Compared to Coannular Data.

146

Figure 7-40. QCGAT Untreated Mixer-Compound Nozzle Data Compared to Treated Mixer-Compound Data.
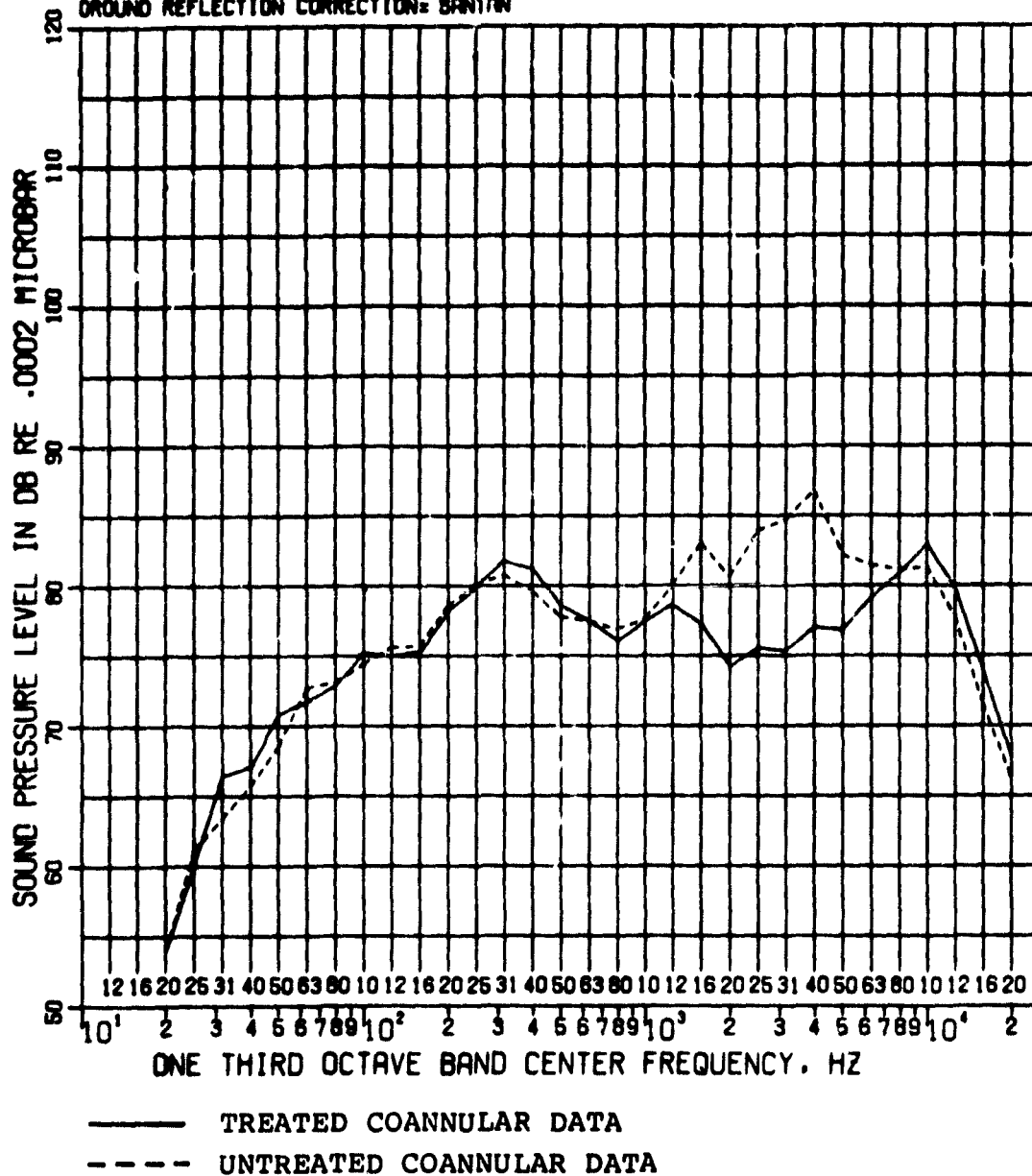
Figure 7-41. QCGAT Treated Coannular Nozzle Data Compared to Untreated Coannular Data.

148

TABLE 19. CHARACTERISTIC AEROACOUSTIC PARAMETERS.

Noise Source	Aeroacoustic Parameters
Fan Inlet and Exit	Fan blade passage frequency, pressure ratio
Combustor	Max flow rate, temperature rise
Turbine	Turbine blade passage frequency, temperature ratio
Jet	T_{jet}/T_{amb}, $V_{effective}$*

$$*V_{eff} = V_{jet} (1-V_{amb}/V_{jet})^{3/4}$$

The component noise sources for the flyover conditions were analogically predicted, and the appropriate correction spectra for each noise source, based upon the key aeroacoustic parameters, were applied to the predicted flyover-noise levels. The result was a static-data-flyover noise prediction at the given FAR Part 36 condition. The resultant noise sources were "flown" using the GTENFLY program. A block diagram of this program is given in Figure 7-42. The locations for the takeoff, approach, and sideline noise prediction, as well as the QCGAT noise goals for each condition are presented in Figure 7-43.

7.3.7 Flyover Calibration with Measured Learjet Data

The adjusted noise sources were taken to flight conditions with corrections for distance, atmospheric attenuation, jet relative velocity and dynamic amplification effects, fan inlet cleanup, doppler effects, wing shielding, and ground effects as detailed in the flyover prediction procedure.

For each flyover condition, takeoff, sideline, and approach, the SPL, PNL, and PNLT were calculated for each 1/2 second of the flight trajectory. The duration time, duration correction and EPNL for each source and the total EPNL were calculated in accordance to FAR Part 36 procedures.

Based upon static data comparisons, the QCGAT engine demonstrated substantial reductions in noise compared to the quiet TFE731-3 engine, which powers the Learjet 35/36 aircraft certified to be 5 EPNdB below the FAR Part 36 Stage 3 noise limits. However, the initial QCGAT flyover predictions based upon the previously described methodology yielded noise levels comparable to the measured Learjet flyover noise levels. A flyover noise calibration procedure was thus developed, and is outlined in Figure 7-44.

Figure 7-42. QCGAT Flyover Noise Prediction Procedure.

Figure 7-43. QCGAT Flyover Noise Goals at Specified Noise Points.

Figure 7-44. Flyover Noise Prediction Calibration Procedure.

A comparison of the predicted and measured in-flight spectra for the Learjet 35/36 based upon the jet dominated model is shown in Figure 7-45. Although the static noise predictions are adjusted to agree with the static noise levels, when taken to flight the predictions are higher than the measured certification noise levels. The overprediction is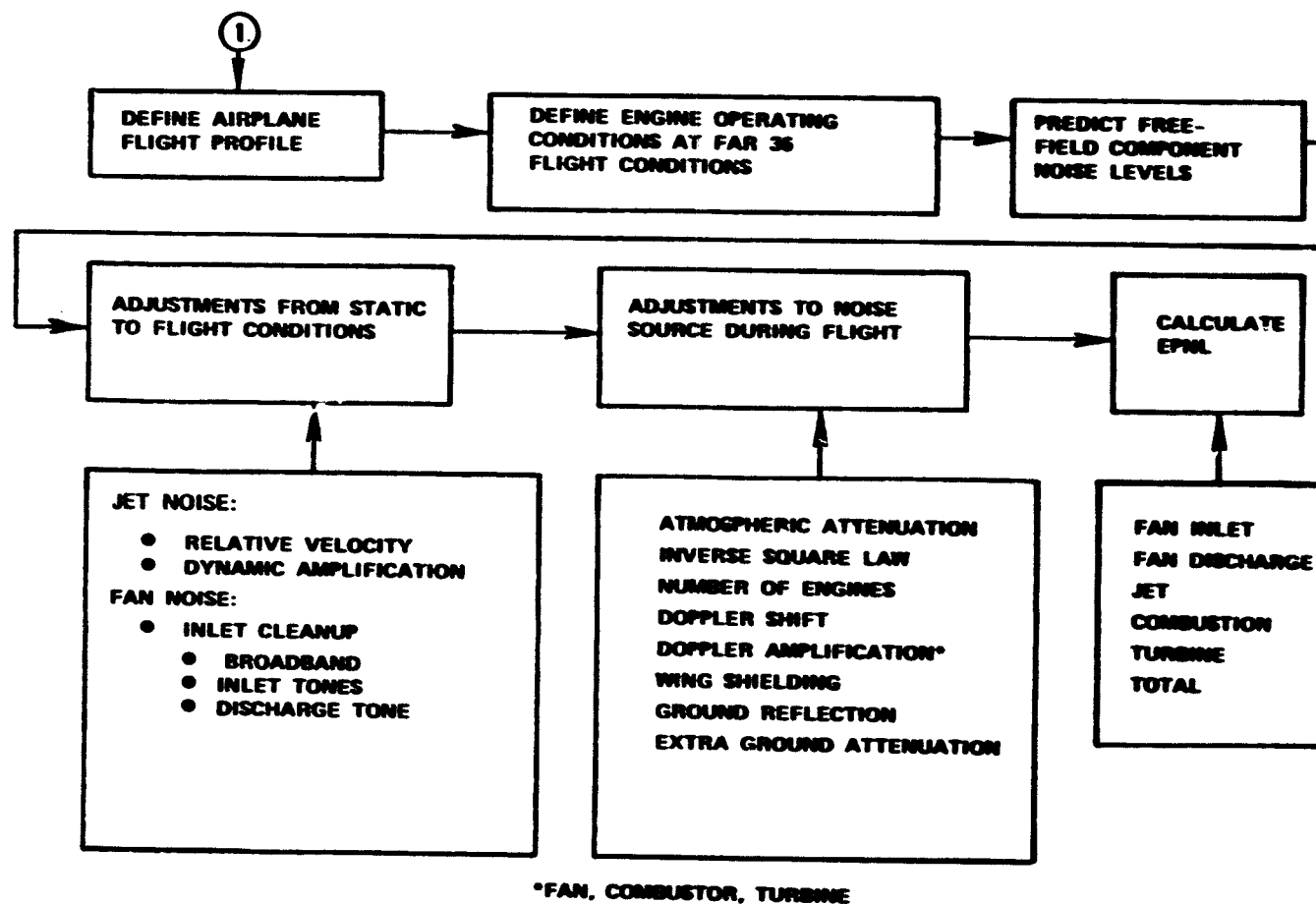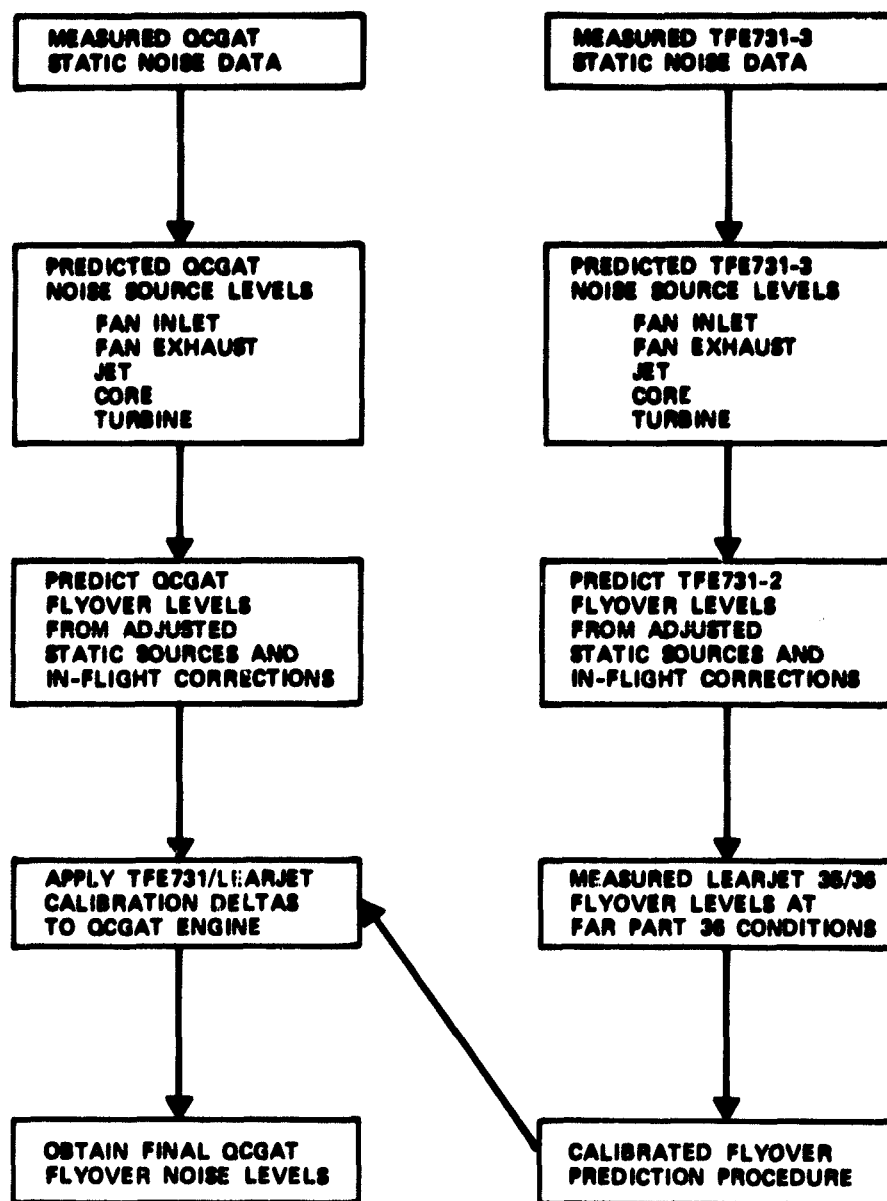 primarily in the low frequency, jet dominated range. At the takeoff condition, the predicted flyover EPNL is 88.7 EPNdB compared to a measured value of 84.0 EPNdB. Similar deltas between predicted and measured flyover noise levels were observed for approach and sideline conditions. Adjusted QCGAT flyover noise predictions were made by applying the Learjet deltas discussed above.

A second set of flyover noise predictions for the Learjet certification tests was made based upon the core noise dominated model. The static TFE731-3 data correlation at takeoff condition at 2.094 radian (120 degrees) is shown in Figure 7-46. The resultant flyover predictions at takeoff condition based upon this method are also shown in Figure 7-46. The predicted levels are even higher than those based upon the previous model; this is primarily due to the assumed dominance of core noise for which beneficial in-flight reductions are not applied.

Table 7-20 and 7-21 compare the predicted component noise sources and the predicted total with the measured flyover levels for the takeoff and approach conditions for both methods. The individual noise sources cannot be compared directly because the flight-path position for which the maximum tone corrected perceived noise level occurs is not the same, resulting in a different composition of noise sources. This shift in location of the maximum PNLT prevents the use of an inflight spectral delta array to match the measured data as shown in Figure 7-47. The jet and core noise spectra were reduced so that the total predicted spectra matched the measured spectra at the point of maximum PNLT. However, when the adjusted predictions were flown over the EPNL was still 1.6 EPNdB higher than the measured takeoff EPNL. The spectral correction approach was thus abandoned in favor of a single EPNdB delta applied to the QCGAT predictions.

A comparison of the unadjusted QCGAT coannular nozzle hard-wall nacelle configuration predictions with the TFE731-2 predictions is shown in Table 7-22 at takeoff conditions. The unadjusted and adjusted flyover noise predictions based on the NASA core noise dominated model are given in Table 7-23. The QCGAT mixer flyover predictions at takeoff, approach, and sideline are presented in Table 7-24 for both the excess jet noise and excess core noise models. Each method, with its appropriate adjustment for the difference between predicted and measured Learjet level yields similar results, indicating the QCGAT engine to be 2.0 EPNdB below the sideline noise goal, 4.6-5.4 EPNdB below the approach noise goal, and from 0.2 EPNdB below to 1.4 EPNdB above the takeoff noise goal.

153
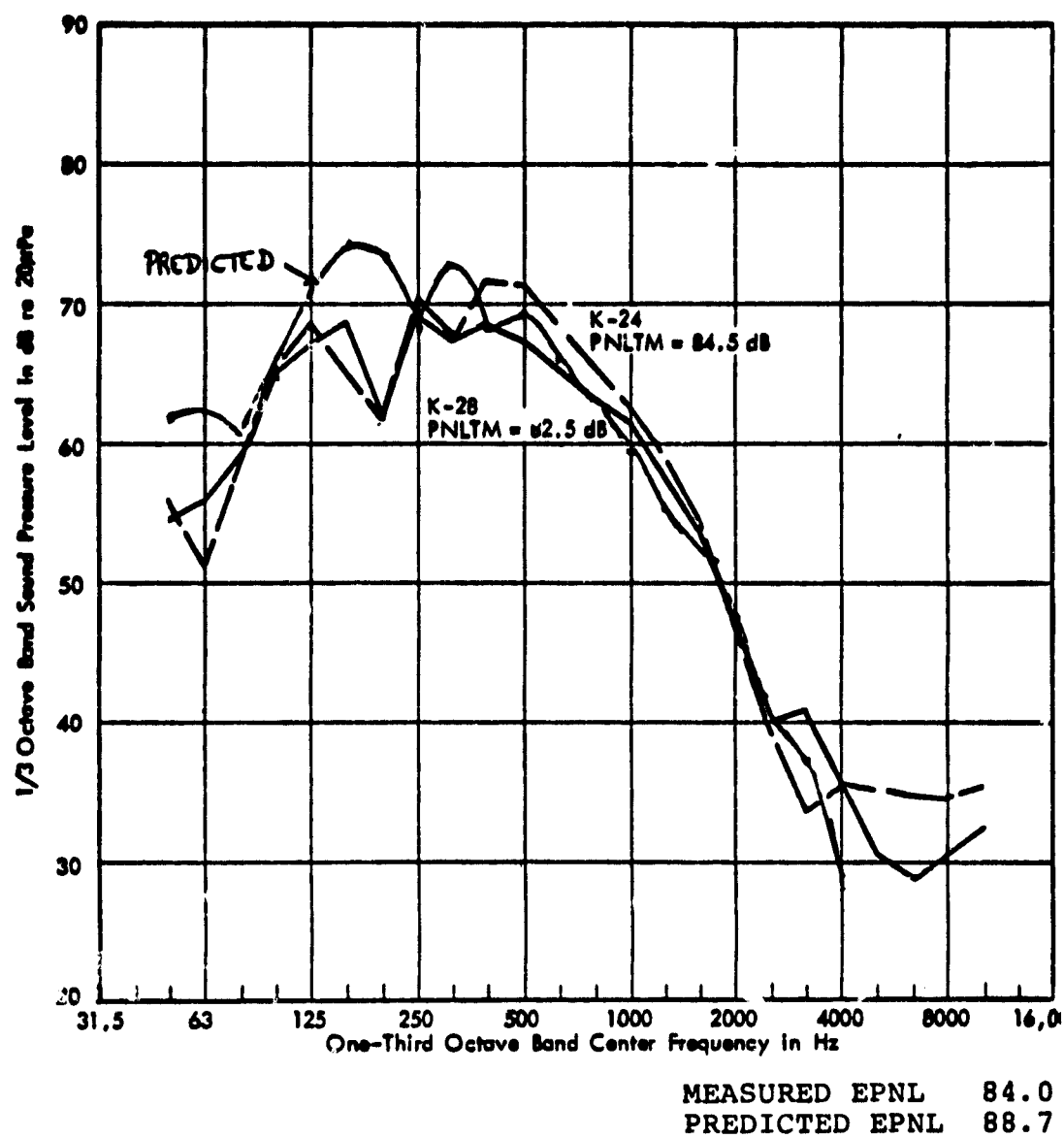
Figure 7-45. Comparison of Predicted Spectra Using Jet Noise
Dominated Correlation Method with Measured Spectra
at the Point of Maximum PNLT for the Learjet 35/36
at Takeoff Conditions.
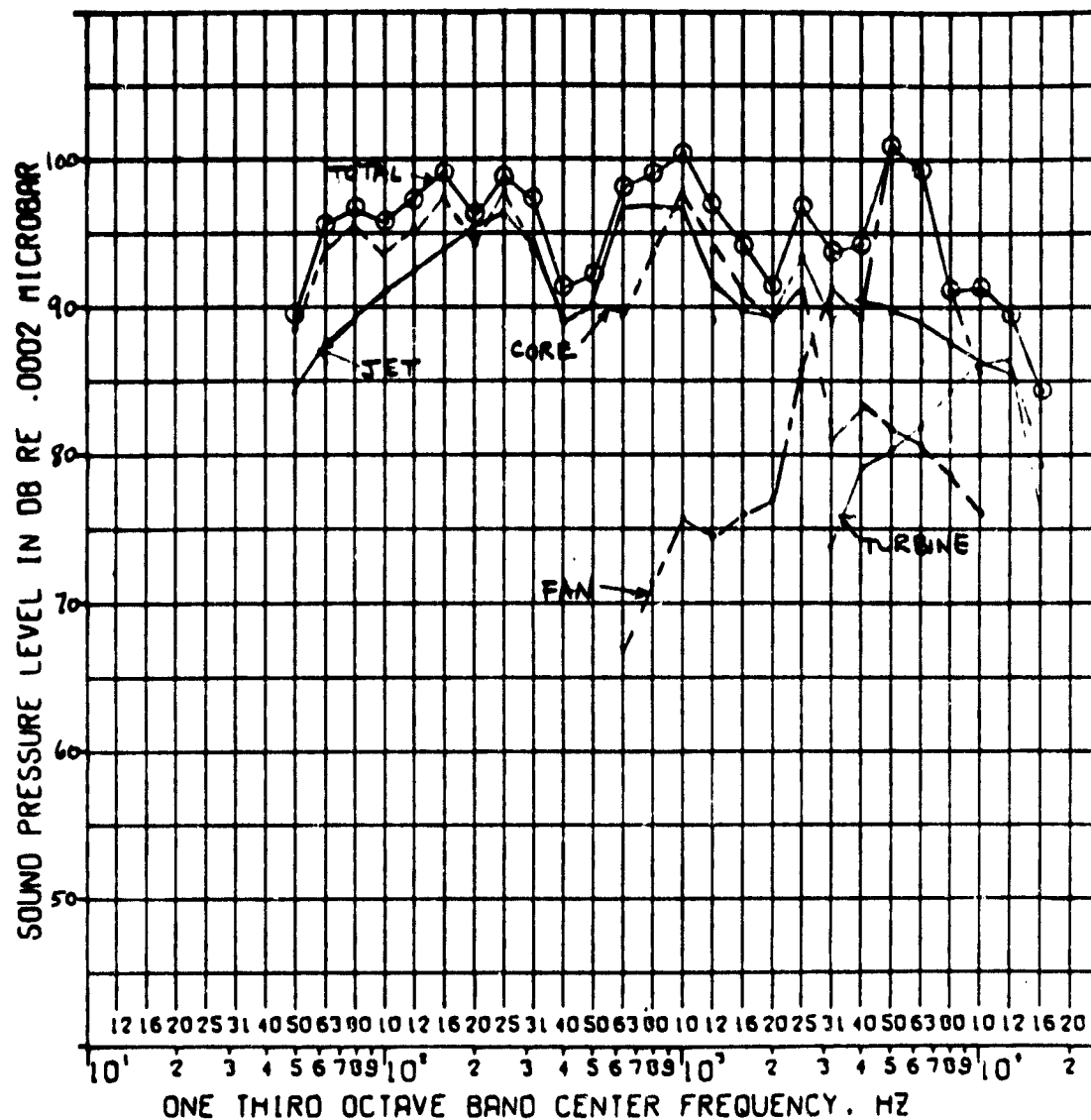
Figure 7-46. TFE731-3 Takeoff Static Comparison at 2.094 Radians
(120°) Using Core Noise Dominated Correlation Method.

155

TABLE 7-20. TFE731-2/LEAR 36 FLYOVER NOISE COMPARISON.

	EPNL, EPNdB	
Noise Source	Jet Noise Dominated Prediction	Core Noise Dominated Prediction
Fan Inlet	78.8	56.5
Fan Discharge	66.1	63.5
Combustion	67.6	89.9
Jet	86.4	85.4
Turbine	42.3	54.2
Total	88.7	90.8
Predicted-Measured	+4.7	+6.8

Takeoff at 990.6m (3250 Ft.) Altitude

TABLE 7-21. TFE731-2/LEAR 36 FLYOVER NOISE COMPARISON.

	EPNL, EPNdB	
Noise Source	Jet Noise Dominated Prediction	Core Noise Dominated Prediction
Fan Inlet	73.5	89.8
Fan Discharge	93.9	92.4
Combustion	79.1	94.0
Jet	81.0	91.8
Turbine	81.7	79.7
Total	95.9	98.6
Predicted-Measured (92.2)	+3.7	+6.4

Approach At 120.1m (394 Ft.) Altitude

ONE-THIRD OCTAVE SPECTRA AT POINT OF MAXIMUM PNLT
TOTAL
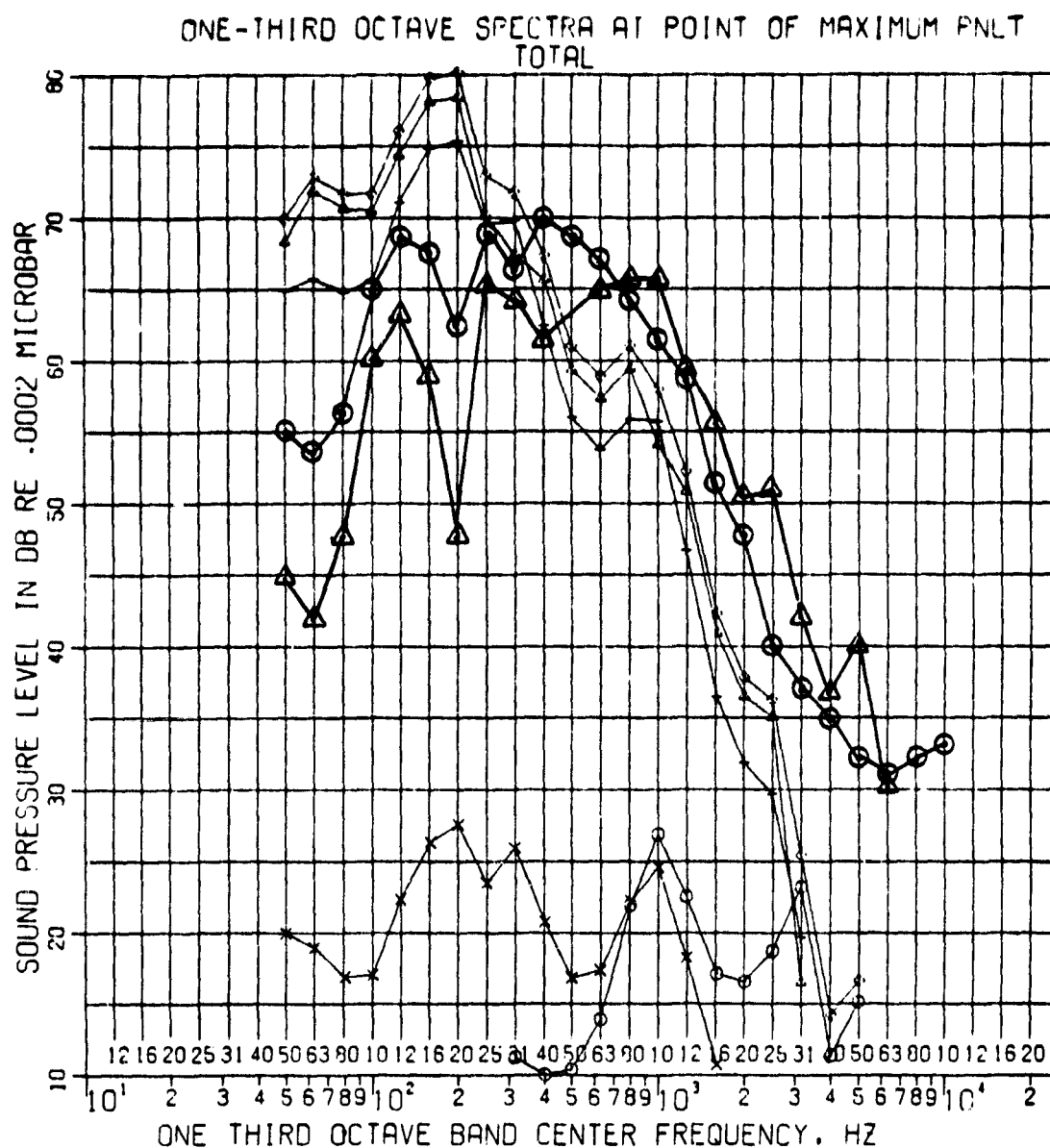
SOURCE	SYMBOL	PNL	PNLTT	EPNL
FAN INLET	⊡	0.00	0.00	
FAN EXIT	⊙	42.92	45.77	
COMBUSTION	△	84.74	86.63	
JET	+	81.75	83.20	
TURBINE	×	38.42	39.87	
TOTAL	◇	86.71	88.69	90.8

△ PREDICTED DATA

⊙ MEASURED DATA

Figure 7-47.   Comparison of Predicted and Flyover Noise Levels
for Learjet 35/36 Using Core Noise Dominated
Method.

157

TABLE 7-22. QCGAT COANNULAR NOZZLE VERSUS TFE731-2
FLYOVER NOISE AT TAKEOFF CONDITIONS.

Noise Source	EPNL, EPNdB		
	QCGAT	TFE731-2	Δ(QCGAT-TFE731-2)
Fan Inlet	62.0	56.5	+5.5
Fan Discharge	62.7	63.5	-0.8
Combustion	83.9	89.9	-6.0
Jet	83.5	85.4	-1.9
Turbine	57.8	54.2	+3.6
Total	86.6	90.8	-4.2

NOTE: Predictions made with core noise correlation.
QCGAT levels based on hardwall coannular nozzle
configuration.

TABLE 7-23. QCGAT EPNL PREDICTIONS.

Final QCGAT flyover predictions based on the core noise correlation
procedure.

Configuration	FAA Part36 Condition	EPNL, EPNdB	
		Unadjusted	Adjusted
Hardwall Mixer	Takeoff	83.1	76.0
	Sideline	89.0	81.7
	Approach	91.0	84.5
Softwall Mixer	Takeoff	81.7	74.7
	Sideline	87.6	80.3
	Approach	88.5	81.9
Hardwall Coannular	Takeoff	86.6	79.8
	Sideline	92.0	85.2
	Approach	95.3	88.9
Softwall Coannular	Takeoff	87.6	80.8
	Sideline	92.7	85.9
	Approach	92.0	85.6

TABLE 7-24. QCGAT FLYOVER NOISE SUMMARY.

Configuration	EPNL, EPNdB					QCGAT Goal
	Jet Noise Dominated Prediction Method		Core Noise Dominated Prediction Method			
	With Lear Δ		With Lear Δ			
Hardwall Mixer Takeoff	79.3	74.6	83.1	76.3		
Softwall Mixer Takeoff	77.8	73.1 (-0.2)	81.7	74.9 (+1.6)		73.3
Hardwall Mixer Approach	88.2	84.5	91.0	84.6		
Softwall Mixer Approach	86.4	82.7 (-4.6)	88.5	82.1 (-5.2)		87.3
Hardwall Mixer Sideline	85.7	81.7	89.0	82.2		
Softwall Mixer Sideline	84.3	80.3 (-2.0)	87.6	80.8 (-1.5)		82.3

7.3.8 Final Flyover Predictions for the QCGAT Engine

The predicted flyover-noise levels for the QCGAT powered air-craft at the FAR Part 36 conditions of takeoff (no cutback), side-line, and approach for each separate noise source and the total noise for both the hardwall and acoustically treated mixer nozzle configurations are shown in Tables 7-25 through 7-30. In addition to the effective perceived noise levels (EPNL) for each source, the maximum PNL, maximum PNLT, slant distance, aircraft altitude, angle of radiation from the inlet centerline, and duration correc-tion are given. The flyover levels are based upon measured static data, with in-flight corrections applied, determined from the pre-dicted and measured TFE731/Learjet noise data using the core noise dominated model.

The noise levels for the above conditions are presented in bar-chart form in Figures 7-48 through 7-50. The effects of the acoustic treatment on the fan inlet, fan exit, and total noise levels are shown.

One-third octave spectral plots for each condition at the point of maximum PNLT are shown in Figures 7-51 through 7-56.

Flyover-noise parametric curves were generated by predicting level flyover EPNL for various engine thrust settings at various altitudes. A carpet plot for the total EPNL of the acoustically treated nacelle mixer nozzle configuration is shown in Figure 7-57.

7.3.9 Conclusions

The noise levels of the QCGAT engine were markedly lcwer than those of the TFE731, which is a recognized quiet engine. The QCGAT engine/nacelle system met or bettered the contract noise goals based on the jet noise dominated correlation analysis of measured static acoustic data. Based on the core noise dominated correlation analysis, the engine/nacelle system bettered the sideline and approach goals and was only 1.4 EPNdB above the goal at takeoff. It should be noted that a detailed analysis of the component noise characteristics of the engine showed that if it were possible to fully suppress the fan com-ponent noise, it would have a nearly insignificant effect on the total noise level, with the result that meeting the takeoff noise goal would still be difficult or impossible.

Based upon the core noise dominated model prediction, the following conclusions were made:

o   The QCGAT softwall nacelle/mixer configuration demon-strated a 9.1 EPNdB reduction in flyover noise at take-off condition, a 10.1 EPNdB reduction at approach, and a

160

TABLE 7-25. FLYOVER NOISE PREDICTION - TAKEOFF, HARDWALL.

Noise Source	Slant Dist.- Meters (Feet)	Aircraft Alt.- Meters (Feet)	Angle From Inlet ξ Radians (Deg.)	PNL Max PNdB	PNLT Max PNdB	Time Dur. Sec.	Dur. Corr. dB	EPNL EPNdB	QCGAT Goal EPNdB
Fan Inlet	1168.7 (3834.3	924.7 (3033.8)	1.04 (59.5)	41.0	46.0	39.0	2.4	48.5	
Fan Discharge	1080.8 (3546)	1070.7 (3512.7)	1.56 (89.4)	55.0	58.0	14.5	-2.5	55.5	
Combustion	1281.9 (4205.7)	1193.5 (3925.8)	2.09 (119.5)	70.1	73.6	37.0	1.9	75.6	
Jet	1281.9 (4205.7)	1193.5 (3915.8)	2.09 (119.5)	62.0	62.0	40.0	3.0	65.0	
Turbine	1201.1 (3940.7)	1162.9 (3815.2)	1.95 (111.7)	48.2	48.2	34.5	2.3	50.5	
Total	1118.7 (3670.3)	1116.7 (3663.8)	1.77 (101.4)	71.2	74.0	35.5	1.9	76.0	73.3

QCGAT mixer-coupound exhaust system

TABLE 7-26. FLYOVER NOISE PREDICTION - HARDWALL, APPROACH..

Noise Source	Slant Dist.- Meters (Feet)	Aircraft Alt.- Meters (Feet)	Angle From Inlet ξ Radians (Deg.)	PNL Max PNdB	PNLT Max PNdB	Time Dur. Sec.	Dur. Corr. dB	EPNL EPNdB	QCGAT Goal EPNdB
Fan Inlet	423.1 (1388.0)	130.0 (426.6)	0.34 19.2)	75.8	77.9	9.0	-4.1	73.7	
Fan Discharge	112.0 (367.3)	111.6 (366.0)	1.68 (96.2)	86.3	87.6	2.5	-8.9	78.7	
Combustion	112.0 (367.3)	111.6 (366.0)	1.68 (96.2)	86.7	87.9	5.0	-6.3	81.5	
Jet	112.0 (367.3)	111.6 (366.0)	1.68 (96.2)	65.9	67.6	6.0	-5.8	61.8	
Turbine	116.4 (382.0)	113.4 (372.1)	1.36 (78.2)	77.8	79.1	5.5	-5.4	73.1	
Total	112.0 (367.3)	111.6 (366.0)	1.68 (96.2)	91.2	91.2	5.0	-6.0	84.5	87.3

QCGAT mixer-compound exhaust system

TABLE 7-27. FLYOVER NOISE PREDICTION - HARDWALL, SIDELINE.

Noise Source	Slant Dist.- Meters (Feet)	Aircraft Alt.- Meters (Feet)	Angle From Inlet ξ Radians (Deg.)	PWL Max PWdB	PWLT Max PWdB	Time Dur. Sec.	Dur. Corr. dB	EPNL EPNdB	QCGAT Goal EPNdB
Fan Inlet	92.3 (302.9)	72.4 (237.4)	0.98 (55.9)	61.7	66.9	9.0	-4.0	62.9	
Fan Discharge	161.0 (528.1)	160.5 (526.5)	1.76 (101.0)	69.9	72.5	7.0	-4.8	67.7	
Combustion	219.0 (718.7)	200.1 (656.6	2.10 (120.2)	79.8	83.3	13.0	-2.4	80.9	
Jet	205.3 (673.7	192.2 (630.6)	2.04 (116.8)	70.9	70.9	16.0	-0.8	70.1	
Turbine	192.6 (631.9	184.3 (604.6)	1.97 (113.0)	60.7	60.7	13.0	-1.5	59.2	
Total	161.0 (528.1)	160.5 (526.5)	1.76 (101.0	81.5	83.9	13.5	-2.2	81.7	82.3

GCGAT mixer-compound exhaust system

TABLE 7-28. FLYOVER NOISE PREDICTION - SOFTWALL, TAKEOFF.

Noise Source	Slant Dist.- Meters (Feet)	Aircraft Alt.- Meters (Feet)	Angle From Inlet ξ Radians (Deg.)	PWL Max PWdB	PWLT Max PWdB	Time Dur. Sec.	Dur. Corr. dB	EPNL EPNdB	QCGAT Goal EPNdB
Fan Inlet	1079.5 (3541.5)	1032.3 (3386.8)	1.4 (80.3)	40.0	44.1	44.5	3.6	47.7	
Fan Discharge	1080.9 (3546.4)	1070.7 (3512.7)	1.6 (89.4)	54.2	56.6	14.0	-4.0	52.6	
Combustion	1281.9 (4205.8)	1193.5 (3915.8)	2.09 (119.5)	69.9	72.9	35.0	1.3	74.2	
Jet	1281.9 (4205.8)	1193.5 (3915.8)	2.09 (119.5)	62.0	62.0	38.5	2.8	64.8	
Turbine	1281.9 (4205.8	1193.5 (3925.8)	2.09 (119.5)	48.2	48.2	33.5	2.0	50.3	
Total	1281.9 (4205.8)	1193.5 (3915.8)	2.09 (119.5)	70.7	73.0	36.0	1.7	74.7	73.3

QCGAT mixer-compound exhaust system

Noise Source	Slant Dist.- Meters (Feet)	Aircraft Alt.- Meters (Feet)	Angle From Inlet ξ Radians (Deg.)	PNL Max PNdB	PNLT Max PNdB	Time Dur. Sec.	Dur. Corr. dB	EPNL EPNdB	QCGAT Goal EPNdB
Fan Inlet	423.06 (1388.0)	130.0 (426.6)	0.335 (19.2)	73.8	75.8	8.5	-4.6	71.3	
Fan Discharge	111.9 (367.3)	111.6 (366.0)	1.77 (96.2)	78.9	79.6	3.5	-7.3	72.3	
Combustion	111.9 (367.3)	111.6 (366.0)	1.67 (96.2)	85.0	86.5	6.5	-6.5	79.9	
Jet	118.3 (388.3)	109.7 (360.0)	1.97 (113.2)	64.4	66.2	6.5	-5.6	68.6	
Turbine	111.9 (367.3)	111.6 (366.0)	1.67 (96.2)	77.0	78.6	5.0	-6.5	72.2	
Total	111.9 (367.3)	111.6 (366.0)	1.67 (96.2)	87.2	87.2	9.0	-5.2	81.9	87.3

QCGAT mixer-compound exhaust system

Noise Source	Slant Dist.- Meters (Feet)	Aircraft Alt.- Meters (Feet)	Angle From Inlet ξ Radians (Deg.)	PNL Max PNdB	PNLT Max PNdB	Time Dur. Sec.	Dur. Corr. dB	EPNL EPNdB	QCGAT Goal EPNdB
Fan Inlet	99.7 (327.1)	80.7 (264.6)	1.03 (59.5)	60.2	61.7	9.0	-3.8	59.8	
Fan Discharge	144.9 (475.6)	144.6 (474.5)	1.60 (92.0)	67.2	68.5	8.0	-4.8	63.7	
Combustion	219.0 (718.7)	200.1 (656.6)	2.09 (120.2)	79.4	82.4	12.0	-2.7	79.6	
Jet	219.0 (718.7)	200.1 (656.6)	2.09 (120.2)	70.8	70.8	15.5	-1.0	69.8	
Turbine	192.6 (631.9)	184.3 (604.6)	1.97 (113.0)	60.7	60.7	13.5	-1.5	59.2	
Total	219.0 (718.7)	200.1 (656.6)	2.09 (120.2)	80.4	82.6	13.5	-2.3	80.3	82.3

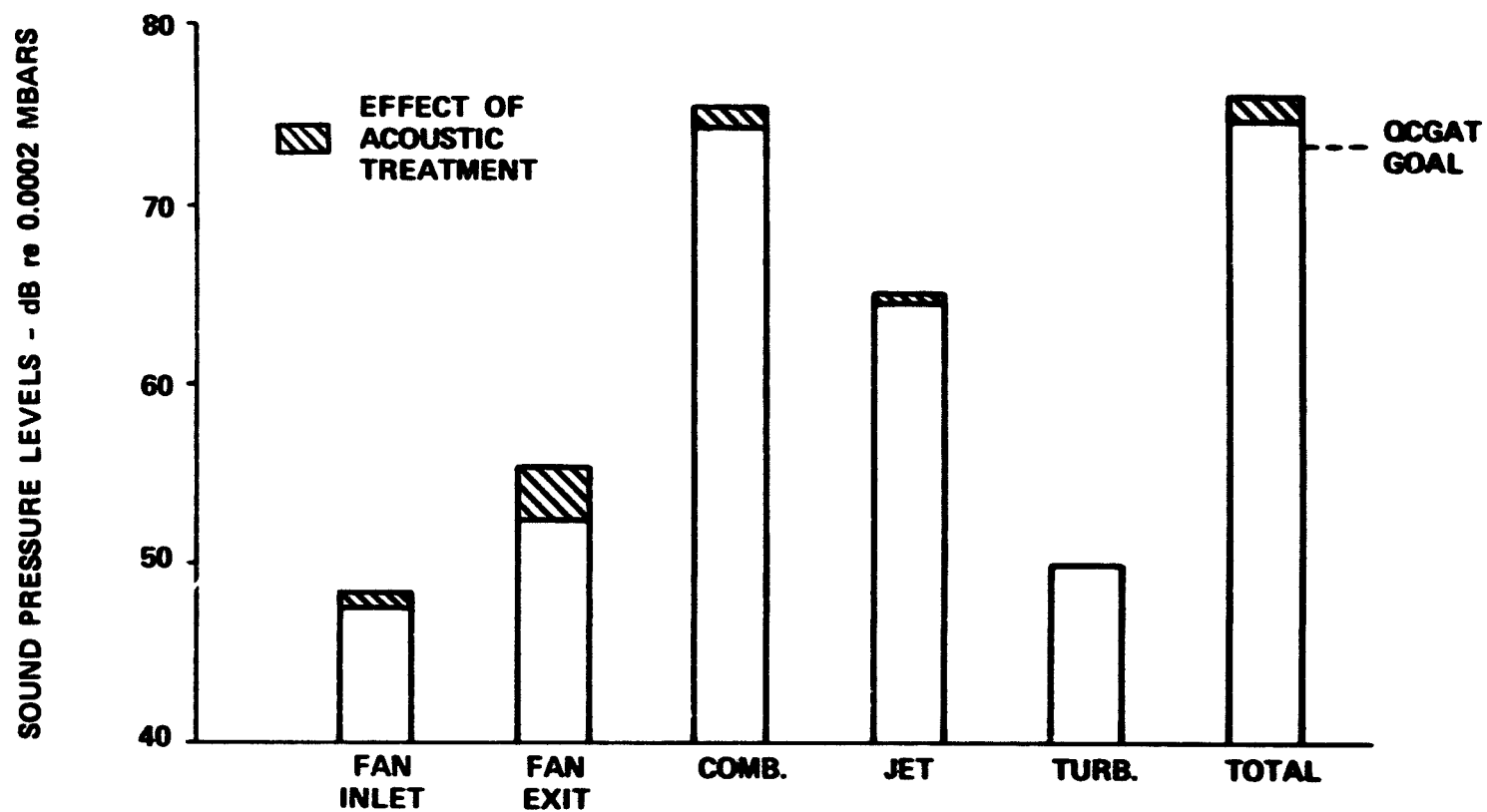QCGAT mixer-compound exhaust system

Figure 7-48. QCGAT Takeoff Noise Levels.
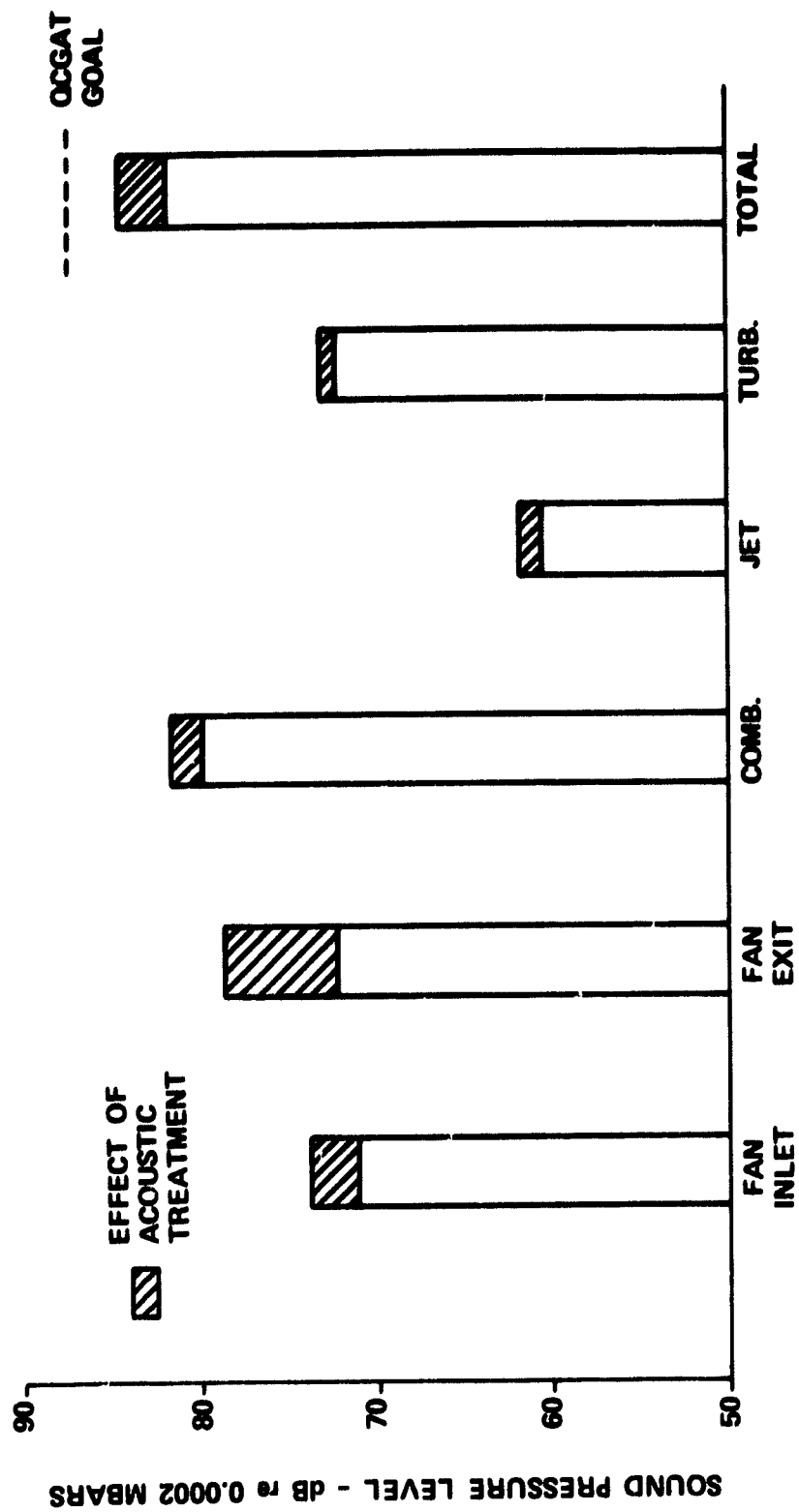
Figure 7-49. QCGAT Approach Noise Levels.

165
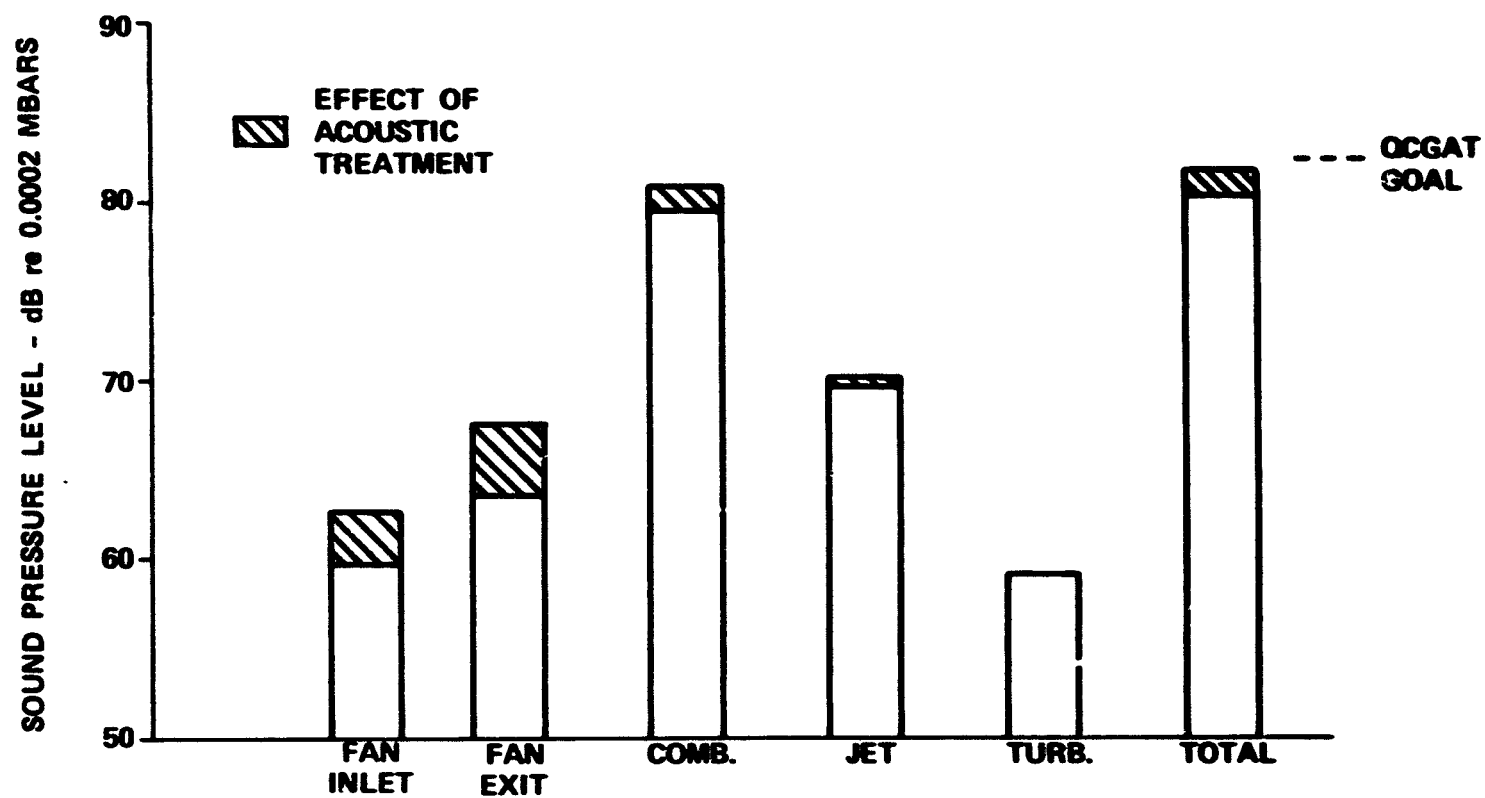
Figure 7-50. QCGAT Sideline Noise Levels.
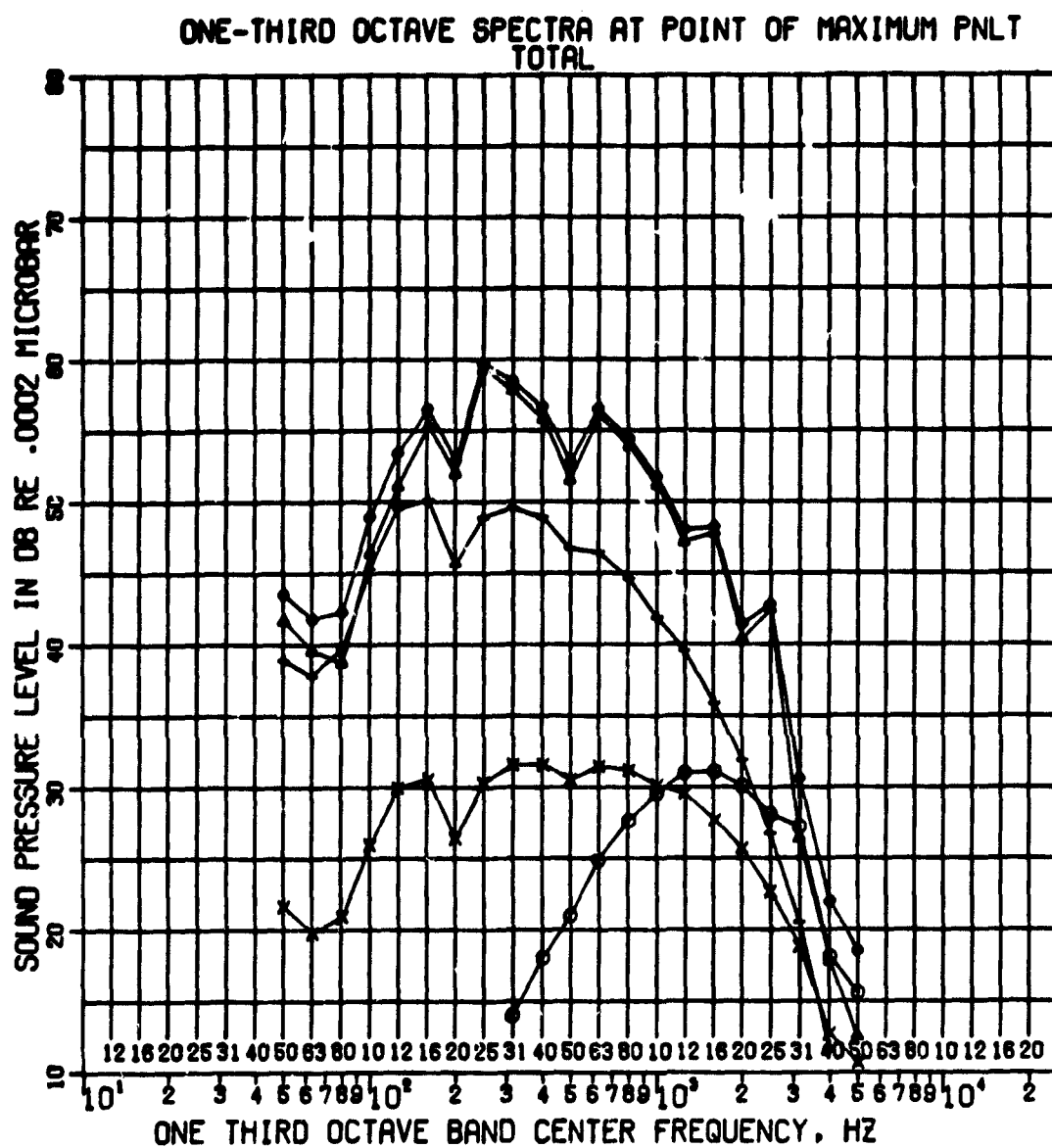
Figure 7-51. QCGAT Takeoff Noise Predictions for Treated Mixer-Compound Configurations Using Core-Noise Method.

ONE-THIRD OCTAVE SPECTRA AT POINT OF MAXIMUM PNLT
TOTAL
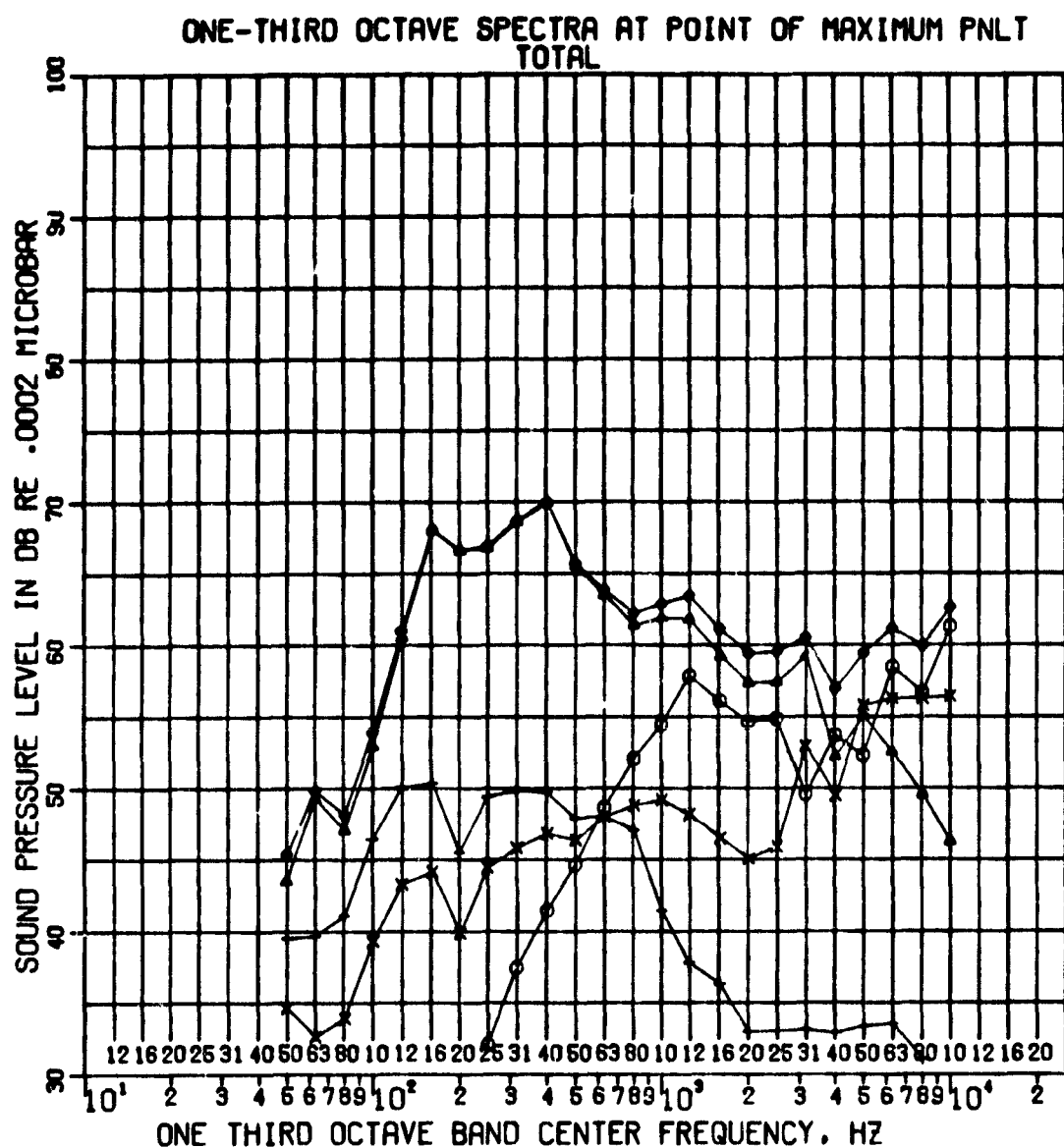
SOURCE	SYMBOL	PNL	PNLTT	EPNL
FAN INLET	▣	42.22	43.64	
FAN EXIT	◉	78.94	79.60	
COMBUSTION	▲	85.02	86.49	
JET	+	64.69	64.69	
TURBINE	✕	77.04	78.79	
TOTAL	◈	87.18	87.18	81.9

Figure 7-52. QCGAT Approach Noise Prediction for Treated Mixer-Compound Configuration Using Core-Noise Method.

168

ONE-THIRD OCTAVE SPECTRA AT POINT OF MAXIMUM PNLT
TOTAL
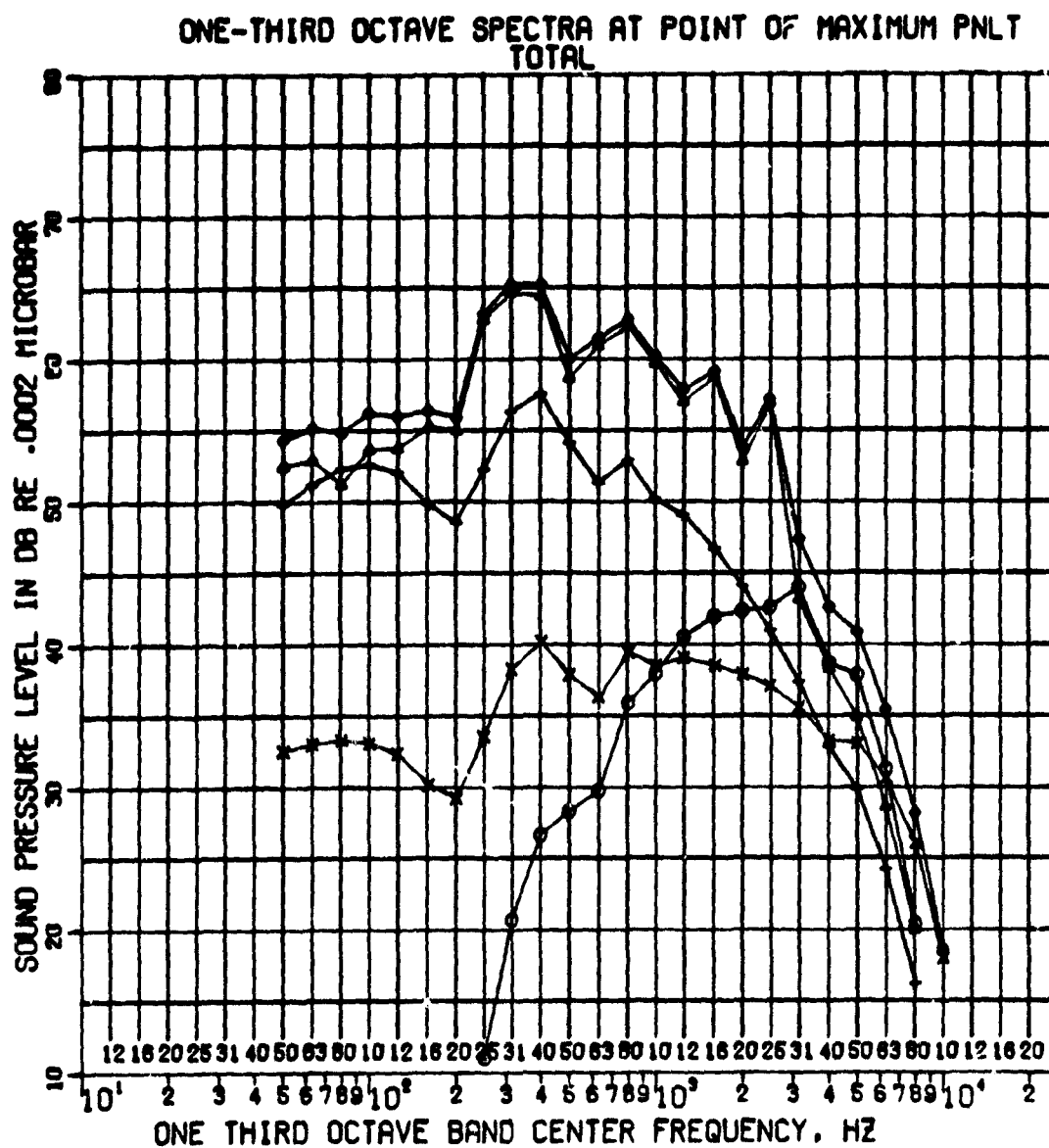
SOURCE	SYMBOL	PNL	PNLTT	EPNL
FAN INLET	⊡	0.00	0.00	
FAN EXIT	⊙	63.70	64.82	
COMBUSTION	▲	79.36	82.36	
JET	+	70.80	70.80	
TURBINE	×	60.42	60.42	
TOTAL	◆	80.39	82.60	80.3

Figure 7-53. QCGAT Sideline Noise Prediction for Treated Mixer-
Compound Configuration Using Core-Noise Method.

ONE-THIRD OCTAVE SPECTRA AT POINT OF MAXIMUM PNLT
TOTAL

SOURCE	SYMBOL	PNL	PNLT	EPNL
FAN INLET	◨	31.55	36.09	
FAN EXIT	◔	52.14	55.31	
COMBUSTION	▲	70.18	73.14	
JET	+	60.93	60.93	
TURBINE	✕	46.99	46.99	
TOTAL	◈	71.19	74.03	76.0

Figure 7-54. QCGAT Takeoff Noise Predictions for Untreated Mixer-Compound Configuration Using Core-Noise Method.

170

ONE-THIRD OCTAVE SPECTRA AT POINT OF MAXIMUM PNLT
TOTAL
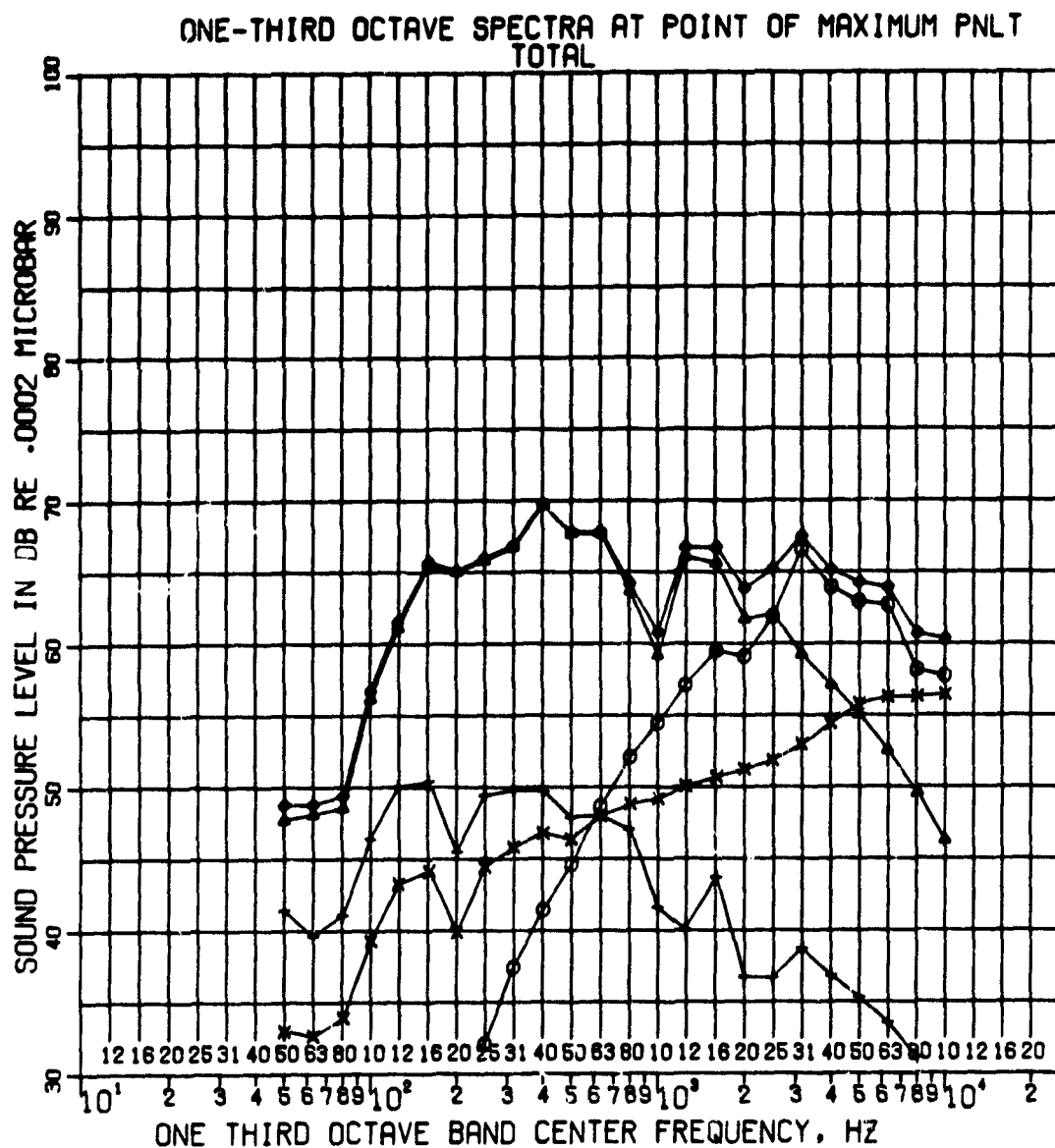
SOURCE	SYMBOL	PNL	PNLT	EPNL
FAN INLET	▣	44.57	44.57	
FAN EXIT	◐	86.33	87.55	
COMBUSTION	▲	86.66	87.88	
JET	+	65.87	67.64	
TURBINE	×	77.93	77.93	
TOTAL	◇	91.25	91.25	84.5

Figure 7-55.   QCGAT Approach Noise Predictions for Untreated Mixer-
Compound Configuration Using Core-Noise Method.

171

ONE-THIRD OCTAVE SPECTRA AT POINT OF MAXIMUM PNLT
TOTAL

SOURCE	SYMBOL	PNL	PNLT	EPNL
FAN INLET	▣	37.87	43.03	
FAN EXIT	◉	69.85	72.47	
COMBUSTION	▲	80.03	82.90	
JET	+	70.25	70.25	
TURBINE	×	59.58	59.58	
TOTAL	◆	81.53	83.86	81.7

Figure 7-56.   QCGAT Sideline Noise Predictions for Untreated Mixer-Compound Configuration Using Core-Noise Method.
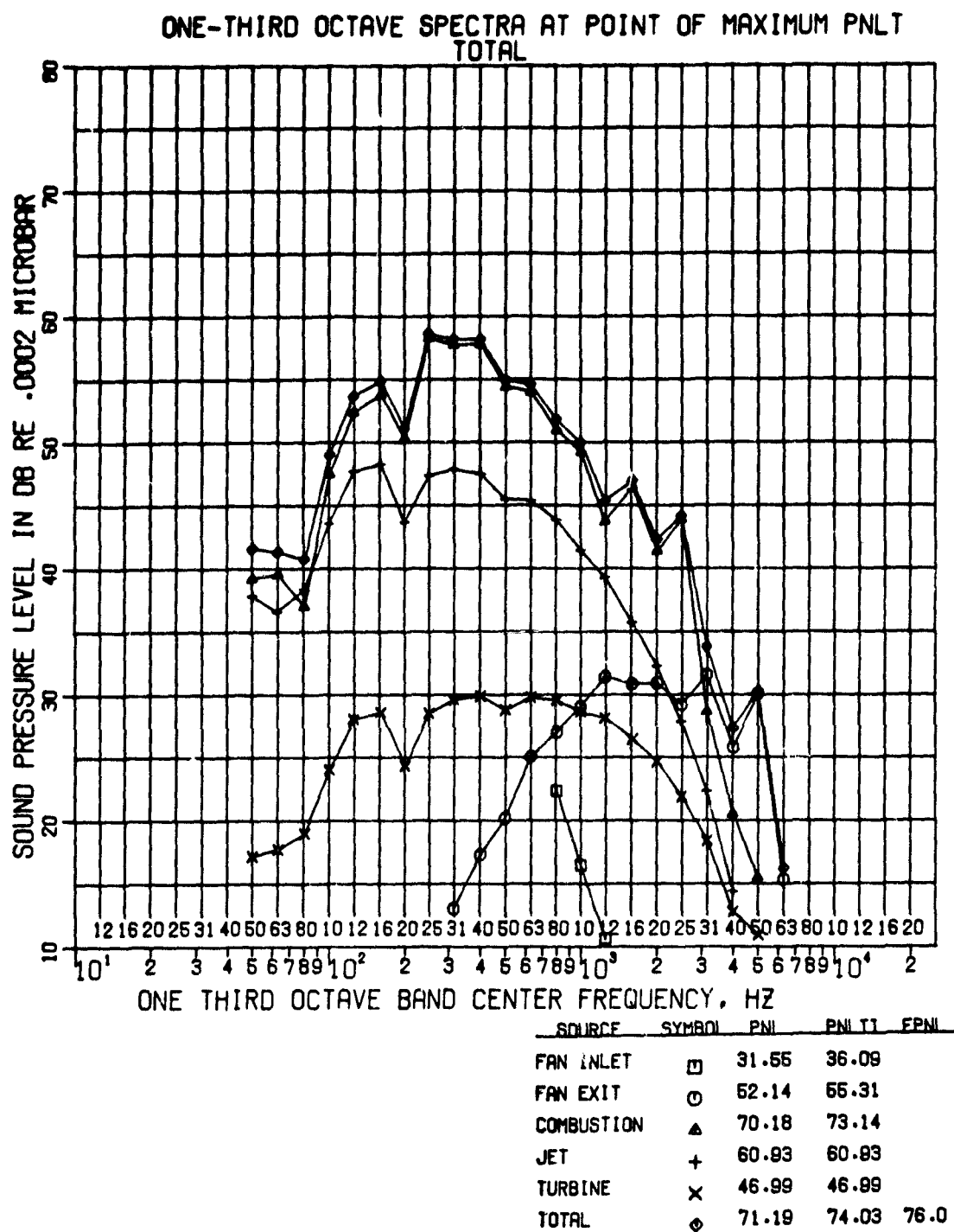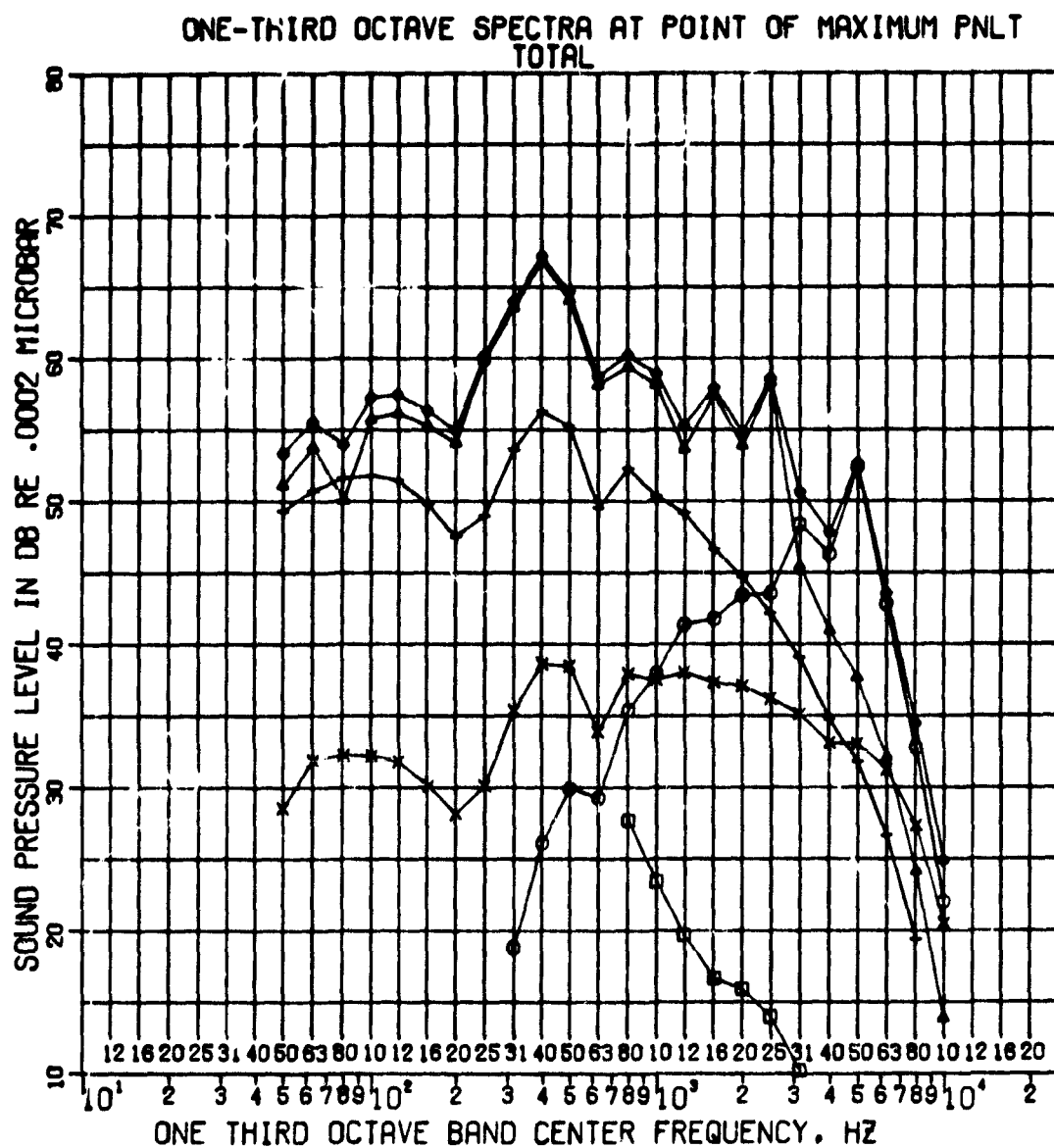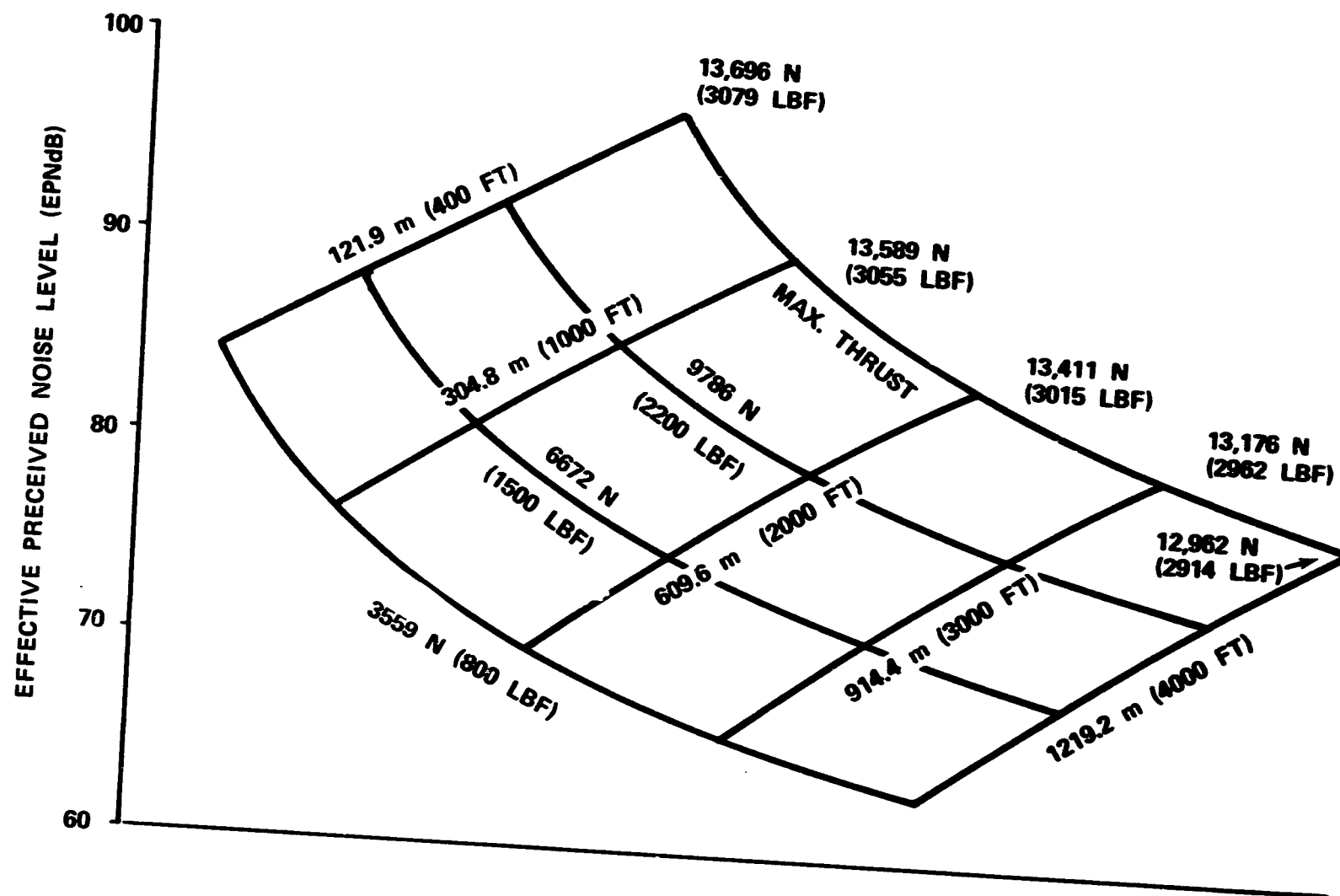
172

Figure 7-57.   Predicted QCGAT Flyover Noise at Mach 0.21.

6.9 EPNdB reduction at sideline condition compared to the TFE731-2 powered Learjet.

o The QCGAT hardwall nacelle coannular nozzle configuration was shown to be 4.2 EPNdB quieter than the Learjet at takeoff condition although the QCGAT airplane takeoff gross weight is 2122 pounds greater than the Learjet airplane.

o The QCGAT hardwall nacelle/mixer was 3.5 EPNdB quieter at takeoff and 4.3 EPNdB quieter at approach than the QCGAT hardwall nacelle/coannular nozzle.

o The QCGAT softwall nacelle/mixer was quieter than the QCGAT hardwall nacelle/mixer by 2.5 EPNdB and 1.4 EPNdB at approach and takeoff conditions, respectively.

7.3.10 Recommendations

Uncertainty exists with regard to the noise source correlation method that will best match static data to predictions. It is recommended that additional internal engine to far-field noise-coherence measurements be made in order to better define a correlation method that will yield accurate flyover predictions. It is further recommended that additional in-flight spectral data for small general aviation turbofan engines be made available so that the static-to-flight prediction methods can be refined.

174

SECTION VIII

SUMMARY OF RESULTS AND CONCLUSIONS

8.0 SUMMARY OF RESULTS AND CONCLUSIONS

8.1 Engine and Nacelle Design

The design of the QCGAT engine was based on the core of the AiResearch TFE731-3 engine and incorporated several unique components specifically for reduced noise and emissions. The core consisted of the TFE731-3 low-pressure compressor, high-pressure compressor, and high-pressure turbine, with the TFE731 accessory gearbox. The unique components includes a low-speed fan, a fan gearbox, associated ducts and structure, a reduced-emissions combustion system, and low-pressure turbine.

Two nacelles were designed -- a production flight-weight nacelle and a "workhorse" nacelle. Only the workhorse nacelle was fabricated for the program; the flight nacelle was used primarily to evaluate airplane characteristics and for weight estimates. Both nacelle designs incorporate acoustic treatment forward and aft of the fan and a mixer-compound nozzle. However, the workhorse nacelle also featured replaceable inlet lips and interchangeable acoustic and hardwall duct liners. In addition, the nacelle inlet barrel could be replaced with a bellmouth, and the mixer-compound nozzle could be replaced with a coannular nozzle system to obtain reference performance data.

8.2 Engine Performance

Performance of the QCGAT engine was excellent throughout all testing. No serious mechanical problems were encountered and no significant test time was lost due to engine related problems. The uninstalled thermodynamic performance of the engine differed from the contract goals in that the TSFC was slightly higher than the TSFC goal at rated thrust points (7.7 percent). The installed performance was very close to the goal (1.4 percent). These differences are attributed to lower than predicted fan efficiency and coannular nozzle thrust coefficient, higher than predicted mixer-compound nozzle thrust coefficient, and the resultant matching of the engine with these components.

An estimate of the engine's performance at the cruise condition was made with the engine model. Comparison of this performance with the contract goals at cruise shows that the engine meets the thrust goals for both the uninstalled and the installed conditions, and betters the TSFC goal at the installed condition.

175

8.3 Noise

The noise levels of the QCGAT engine were markedly lower than those of the TFE731, which is a demonstrably quiet engine. The QCGAT engine/nacelle system met or bettered the contract noise goals based on the jet noise dominated correlation analysis of measured static acoustic data. Based on the core noise dominated correlation analysis, the engine/nacelle system bettered the sideline and approach goals and was only 1.4 EPNdb above the goal at takeoff. It should be noted that a detailed analysis of the component noise characteristics of the engine showed that if it were possible to fully suppress the fan component noise, it would have a nearly insignificant effect on the total noise level, with the result that meeting the takeoff noise goal would still be difficult or impossible.

8.4 Emissions

With the engine configured to use air assist at the taxi-idle condition, the goals for HC and CO were met. The engine exhibited a significant reduction in NO_x level from that of a production TFE731-3, but it exceeded the program goal by an EPAP value of 0.9. The measured smoke number exceeded the program goal of 38 by 4 points, however, the engine was visually judged to be smokeless.

SECTION IX

RECOMMENDATIONS

9.0 RECOMMENDATIONS

9.1 Performance

Considerable ground-level testing was conducted to define the QCGAT engine performance at low altitude. However, it is recommended that additional tests be conducted at simulated flight conditions in order to refine the engine computer model and to permit comparison of the engine performance at the cruise design point with the program goals. It is also recommended that tests be conducted with nacelle hardwall and acoustical panels to define the duct pressure loss attributable to the acoustical panels and the effect of that loss (if any) on engine performance.

9.2 Noise

Uncertainty exists with regard to the noise source correlation method that will best match static data to predictions. It is recommended that internal engine to far-field noise-coherence measurements be used in order to better define a correlation method that will yield accurate flyover predictions. It is further recommended that additional in-flight spectral data for small general aviation turbofan engines be made available so that the static-to-flight prediction methods can be refined.

APPENDIX I

# REFERENCES

PAGE 178 INTENTIONALLY BLANK

APPENDIX I

REFERENCES

1. Minner, G. L. and Rice, E. J., "Computer Method for Design of Acoustic Liners for Turbofan Engines," NASA TM X-3317, 1976.

2. Rice, E. J., "Acoustic Liner Optimum Impedance for Spinning Modes with Mode Cut-Off Ratio as the Design Criterion," AIA Paper 76-516, Palo Alto, CA., 1976.

3. Rice, E. J., "Inlet Noise Suppressor Design Method Based Upon the Distribution of Acoustic Power with Mode Cut-Off RAtic " Paper Presented at the Thirteenth Annual Meeting of the Society of Engineering Science, Inc., George Washington Univeristy, 1976.

4. Rice, E. J., "Multimodal Far-Field Acoustic Radiation Pattern - An approximate Equation," AIAA Paper 77-1281, presented in Atlanta, Georgia, October, 1977.

5. Rice, E. J., "Attenuation of Sound in Ducts with Acoustic Treatment - A generalized Approximate Equation," NASA TMX-71830.

6. Pao, S. P., A. R. Wenzel, and P. B. Oncely: Prediction of Ground Effects on Aircraft Noise, NASA-TP-1104, 1978.

7. Zorumski, W. E.: Prediction of Aircraft Sideline Noise Attenuation, NASA-TM-78717, 1978.

8. Chessell, C. I.: Propagation of Noise along a Finite Impedance Boundary, J. Acoust. Soc. America, Vol. 62, No. 4, Oct. 1977, pp. 825-834.

9. Chessell, C. I.: Meteorological and Ground Effects on the Propagation of Aircraft Noise Close to the Earth's Surface, Jl. of Sound and Vib., Vol. 60, No. 2, 1978, pp. 251-266.

10. Embleton, T. F. W., J. E. Piercy, and N. Olson: Outdoor Sound Propagation over Ground of Finite Impedance, J. Acoust. Soc. Am., Vol. 59, No. 2, Feb. 1976, pp. 267-277.

11. Daigle, G. A., Effects of Atmospheric Turbulence on the Interface of Sound Waves above a Finite Impedance Boundary, J. Acoust. Soc. Am., Vol. 65, No. 1, Jan. 1979, pp. 45-49.

12. Putnam, T. W.: Review of Aircraft Noise Propagation. NASA-TMX-56033, Sept. 197 .

13. Oncely, P. B.: Propagation of Jet Engine Noise Near a Porous Surface, J. Sound Vib., Vol. 13, No. 1, 1970, pp. 27-35.

APPENDIX II

LIST OF SYMBOLS AND ABBREVIATIONS

Dual Nozzle Configuration Station Location.
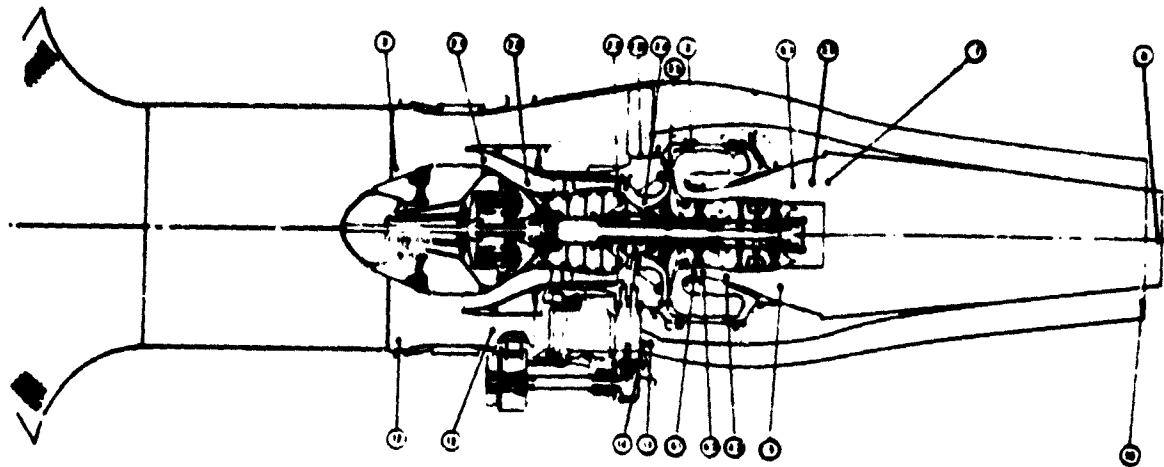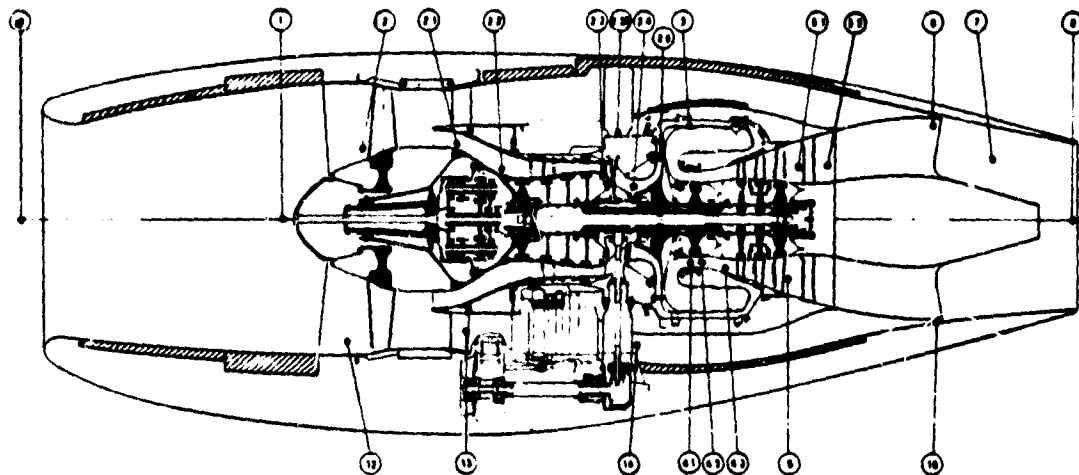

Mixer-Compound Nozzle Configuration Station Locations.

Figure II-A.   Axial Locations of Instrumentation.

184

APPENDIX II

LIST OF SYMBOLS AND ABBREVIATIONS

A_B	Surge bleed area
A_e	Excess attenuation
BL	Buttock line
C_{LV2}	Coefficient of lift at V_2
C_{LMAX}	Maximum coefficient of left
CO	Carbon monodixde
COMB.	Combustor
EPNdB	Effective perceived noise in decibels
EPNL	Effective perceived noise level
fi	Center frequency
F	Thrust
F_N	Thrust at a given power setting, net thrust
HPC	High-pressure compressor
HPT	High-pressure turbine
I_{xx}	X-axis location of center of gravity
I_{YY}	Y-axis location of center of gravity
I_{ZZ}	Z-axis location of center of gravity
ISA	International standards association
LPT	Low-pressure turbine
L/D	Lift-to-drag ratio
M	Mach Number
N	Rotor speed
N_1	Low-pressure compressor and turbine speed

APPENDIX II (CONTD)

LIST OF SYMBOLS AND ABBREVIATIONS

N_2	High-pressure compressor and turbine speed
N_{CR}	Critical speed
NOX	Oxides of Nitrogen
P_{t2}	Total pressure
P_3	HP compressor discharge pressure
P/P	Pressure ratio
PLA	Power lever angle
PR	Pressure ratio
$P_{T4.3}/P_{T5.0}$	Low-pressure turbine overall pressure ratio
QCGAT	Quiet Clean General Aviation Turbofan
R_1	Plug radius [cm (IN.)]
R_2	Duct radius [cm (IN.)]
$R/\rho c$	Specific Resistance
SLS	Sea-level static
STA	Station identification
T1	Combustion design concept
T_{t2}	Fan inlet temperature
$T_{t4.2}$	LP turbine inlet temperature
TO	Take Off
TSFC	Thrust specific fuel consumption
TOGW	Take-of gross weight
TURB	Turbine
U/A_{CR}	Wheel speed critical velocity ratio

LIST OF SYMBOLS AND ABBREVIATIONS

U	Turbine blade tip velocity
UHC	Unburned hydrocarbons
V/A'_{CR}	Absolute critical velocity ratio
W	Maximum takeoff gross weight (in pounds)
W/A''_{CR}	Relative critical velocity ratio
w	Complex argument
$\dfrac{W/\sqrt{\theta}_{CR}}{\delta_{4.3}}$	Mass flow rate (kg/s)[lbm/sec]
z_1	Impedance
z_2	Impedance
3D	Three-dimensional
α	Absolute flow angle (deg)
β	Relative flow angle (deg)
ΔP	Differential pressure
ΔH	Differential enthalpy
$\Delta H/\sqrt{\theta}_{CR}$	Specific Work [J/kg (Btu/lbm)]
δ	Pressure divided by Standard Sea Level Static Day Pressure
λ_1	Pressure Ratio
$\lambda = \Delta H/V_n^2$	Mean work coefficient
$\phi = V_X/V_M$	Mean flow coefficient
ϕ	Flow coefficient
$X/\rho c$	Specific reactance